RUNNING ALPS ACROSS SCALES

Effective Field Theories and Phenomenology of Axion-Like Particles

Anne Mareike Galda
born in Mainz, Germany

Dissertation submitted for the award of the title

Doctor of Natural Sciences

to the Faculty of Physics, Mathematics and Computer Science
Johannes Gutenberg University Mainz

August 14, 2025

Betreuer und erster Gutachter:	*Removed for privacy reasons.*
Zweiter Gutachter:	*Removed for privacy reasons.*
Prüfungskommission:	*Removed for privacy reasons.*
Tag der mündlichen Prüfung:	16. Dezember 2025

Ich versichere, dass ich die Arbeit selbstständig verfasst und keine anderen als die angegebenen Quellen und Hilfsmittel benutzt, sowie Zitate kenntlich gemacht habe. Diese Arbeit wurde weder als Ganzes noch in Teilen als Dissertation oder Prüfungsarbeit bei einer anderen Fakultät oder einem anderen Fachbereich eingereicht.

Verwendung von KI-Tools: Das KI-Tool ChatGPT wurde als Schreibhilfe und zur Unterstützung bei der Überarbeitung des Manuskripts verwendet.

I hereby declare that this thesis has been written my myself and is based on my own research, unless stated otherwise. No other than the indicated sources have been used. This work has not been submitted, either in whole or in part, as a dissertation or examination paper to any other faculty or department.

Use of AI tools: The AI tool ChatGPT was utilized as a writing aid and to support the refinement of the manuscript.

Mainz, den 14. August 2025

Anne Mareike Galda
Mainz Institute for Theoretical Physics (MITP)
Staudingerweg 7
Johannes Gutenberg-Universität D-55099 Mainz
agalda@uni-mainz.de

List of Publications

This thesis is based on the publications listed below. The author's contributions and the main findings are briefly summarized.

(1) **"ALP–SMEFT Interference"**
A. M. Galda, M. Neubert and S. Renner
JHEP **06** (2021), 135, [arXiv:2105.01078]

In this work, we showed that axion-like particles generate nearly the whole dimension-six basis of SMEFT operators at one-loop level via inhomogeneous source terms contributing to the renormalization group evolution equations of the SMEFT Wilson coefficients. The research was carried out as part of the author's Master's thesis, and the findings of this paper laid the foundations for the results presented in (2) and (3). All results were derived independently by all authors of the paper.

(2) **"A global analysis of axion-like particle interactions using SMEFT fits"**
A. Biekötter, J. Fuentes-Martín, A. M. Galda and M. Neubert
JHEP **09** (2023), 120, [arXiv:2307.10372]

In this paper, we used the *ALP–SMEFT interference* to derive indirect, model-independent bounds on the dimension-five ALP couplings to the SM particles. Specifically, we translated experimental constraints on dimension-six SMEFT Wilson coefficients, obtained from Higgs, top-quark, and low-energy data, into constraints on ALP couplings. This analysis was performed for a generic ALP without assuming a specific UV model, as well as for the DFSZ and KSVZ scenarios. The resulting indirect bounds are competitive with, or even more stringent than, direct experimental limits for ALP masses in the GeV to TeV range. All authors contributed equally to the paper.

(3) **"ALP–LEFT Interference and the Muon ($g-2$)"**
A. M. Galda and M. Neubert
JHEP **11** (2023), 15, [arXiv:2308.01338]

Below the scale of electroweak symmetry breaking, the appropriate effective field theory to describe the interactions of particles is the low-energy effective field theory (LEFT). We extended the concept of *ALP–SMEFT interference* to these energy scales by computing the full set of one-loop ALP-induced source terms that modify the renormalization-group evolution equations of the LEFT Wilson coefficients up to dimension-six order and applied our results to the case of the anomalous magnetic moment of the muon. All computations were done by both authors independently; the Feynman graphs were created by the author of this thesis.

(4) **"$K^{\pm} \to \pi^{\pm} a$ at Next-to-Leading Order in Chiral Perturbation Theory and Updated Bounds on ALP Couplings"**
C. Cornella, A. M. Galda, M. Neubert and D. Wyler
JHEP **06** (2024), 29, [arXiv:2308.16903]

The processes $K^{\pm} \to \pi^{\pm} a$ offer powerful probes of axion-like particles. In this work, we extended the current LO prediction in chiral perturbation theory by the corresponding NLO results and also included isospin-breaking corrections at first order in $(m_u - m_d)$. We showed that in the presence of the ALP, the operator basis at NLO needs to be extended. We furthermore consistently included the so-called "weak mass term" in our calculation, which we showed to be non-redundant already at LO when the SM is extended by an ALP. As a phenomenological application, we updated the bounds on the ALP–SM couplings as obtained from the full NLO computations, which remained the strongest constraints from particle-physics for ALP masses below 300 MeV. Finally, we translated to bounds on the ALP–SM couplings to bounds on ALP-nucleon couplings. All authors contributed to the text and the derivation of the complete operator basis necessary for incorporating the ALP into chiral perturbation theory. C.C. and the author of this thesis were responsible for computing the amplitudes, deriving the bounds, and creating the figures presented in the paper. The comment on the η' was authored by D.W.

(5) **"Saving or Destroying the Universe with Axion-Like Particles"**
A. M. Galda and M. Neubert
[arXiv:2506.06426]

This paper is based on the observation made in the *ALP–SMEFT interference* that the presence of the ALP contributes an additional, inhomogeneous term to the β-function of the Higgs quartic coupling, thus having an impact on the instability scale of the electroweak vacuum. Furthermore, also the ALP-generated SMEFT Wilson coefficients influence the scale evolution of this coupling. Requiring that the Universe remains in a meta-stable state when the ALP is present thus allowed us to deduce bounds on ALP couplings to the Standard Model fields. We also showed that the modification of the β-functions of the gauge couplings by the ALP can lead to a unification below the Planck scale. The computation of the β-function of C_{HH}, the text and figures were produced by the author of this thesis.

Unless explicitly specified otherwise, the figures presented in this thesis were created by the author. They closely correspond to those published in the aforementioned works, with minor adjustments made to align with the layout and formatting of this thesis. Parts of this thesis contain verbatim or slightly modified text of the above mentioned articles. All reused material was originally written by the author of this thesis, unless indicated differently.

Units and Notation

In this work, *natural units* are employed, which means that one sets

$$\hbar = c = k_B = G = 1\,.$$

This implies that masses, temperatures and energies have the same units and that length and time both carry inverse energy units, which are measured in eV where $1\,\mathrm{eV} \approx 1.6 \times 10^{-19}\,\mathrm{J}$. Unless explicitly stated otherwise, Einstein's summation-convention is imposed, where double indices are contracted. Vector components provided with latin indices run from one to three, while greek indices are used for spacetime vectors and extend from one to four. Indices are raised and lowered with the metric tensor $g_{\mu\nu}$ of the Minkowski metric via $k_\mu = g_{\mu\nu}k^\nu$, where the signature $(+,-,-,-)$ is used. For the contraction of a four-vector k^μ with a gamma matrix γ_μ the Feynman-slash notation, $\not{k} \equiv k^\mu\gamma_\mu$, is applied. For the Levi-Civita symbol $\epsilon^{\mu\nu\alpha\beta}$ the convention $\epsilon^{0123} = 1$ is chosen.
Throughout this thesis, red dashed lines in Feynman diagrams correspond to axions or ALPs, while black dashed lines denote the Higgs. Solid lines with (without) arrows symbolize leptons and quarks (hadrons). Wavy lines show photons or heavy gauge bosons, and curly lines are used for gluons.

Abstract

The Standard Model of particle physics (SM) is an astonishingly successful theory that describes nature with almost inconceivable accuracy. Yet, it is incomplete, as several hints point toward the existence of additional particles outside its field content. One of the most promising candidate for such a new state is the axion-like particle (ALP), a generalization of the axion, initially proposed to solve the strong CP problem. This thesis explores ALP effective theories and their phenomenological implications across different energy scales, divided into four parts. The first part is based on the *ALP–SMEFT interference*, where one-loop ALP exchange generates dimension-six SMEFT operators. By running these effects down to experimental scales and using existing bounds on SMEFT Wilson coefficients, strong model-independent constraints on ALP–SM couplings are derived that are compatible with or even surpass direct searches. In the second part, this concept is systematically extended to the low-energy effective field theory (LEFT), showing how ALPs can contribute to the $(g-2)_\mu$ via the *ALP–LEFT interference*. Moving down to even lower energies at and below the scale of chiral symmetry breaking, a consistent ALP extension of chiral perturbation theory at next-to-leading order is constructed. Applying this framework to the flavor-violating decays $K^\pm \to \pi^\pm a$ provides the strongest constraints on ALP–SM couplings for $m_a \lesssim 300$ MeV. Finally, by running the modified RG equation of the quartic Higgs coupling up to the Planck scale, ALP influences on the electroweak stability are analyzed, as well as a possible gauge coupling unification scenario in the presence of this new particle.

Kurzzusammenfassung

Das Standardmodell der Teilchenphysik (SM) stellt vermutlich einen der bedeutendsten Durchbrüche der Physik dar und erlaubt es, die Natur mit fast unvorstellbarer Genauigkeit zu beschreiben. Dennoch wissen wir, dass es ein unvollständiges Modell ist, da eine Vielzahl von direkten und indirekten Hinweisen auf die Existenz von Teilchen hindeuten, die über das Spektrum des SM hinausgehen. Einer der vielversprechendsten Kandidaten für solch neue Felder ist das axionartige Teilchen (ALP), eine Verallgemeinerung des Axions, das ursprünglich vorgeschlagen wurde, um das starke CP Problem zu lösen. Diese Dissertation untersucht effektive Theorien für ALPs auf verschiedenen Energieskalen, sowie die daraus resultierenden phänomenologischen Implikationen. Dazu ist diese Arbeit in vier Teile gegliedert. Der erste Teil basiert auf dem Konzept der *ALP–SMEFT-Interferenz*, der Beobachtung, dass Ein-Schleifen-Diagramme mit virtuellem ALP-Austausch Dimension-sechs SMEFT-Operatoren erzeugen. Durch das Lösen der Renormierungsgruppen (RG)-Gleichungen von der ALP-Skala bis hinunter zur experimentellen Skala und der Verwendung bestehender Grenzen an die SMEFT-Wilson-Koeffizienten werden starke, modellagnostische Grenzen für die ALP–SM-Kopplungen abgeleitet, die mit direkten Suchergebnissen übereinstimmen oder diese sogar übertreffen. Im zweiten Teil wird dieses Konzept systematisch auf die effektive Feldtheorie niedriger Energien (LEFT) ausgeweitet. Nach systematischer Konstruktion der *ALP–LEFT-Interferenz* wird gezeigt, wie bisher nicht eingeschränkter ALP-Parameterraum zum Wert des prominenten $(g-2)_\mu$ beitragen kann. Bei noch niedrigeren Energien, an und unterhalb der Skala der chiralen Symmetriebrechung, wird die erste konsistente, nicht-triviale Erweiterung der bekannten Operatorbasen der chiralen Störungstheorie in Anwesenheit von ALPs in führender und nächstführender Ordnung konstruiert. Als Anwendung werden die flavorverletzenden Zerfälle $K^\pm \to \pi^\pm a$ betrachtet, die die stärksten Teilchenphysik-Limits für ALP–SM-Kopplungen für $m_a \lesssim 300$ MeV liefern. Im abschließenden Kapitel wird durch das Lösen der modifizierten RG-Gleichung der quartischen Higgs-Kopplung gezeigt, welchen Einfluss ALPs auf die Stabilität des elektroschwachen Vakuums haben können, sowie ein mögliches Szenario der Vereinheitlichung der Eichkopplungen in Anwesenheit dieses neuen Teilchens untersucht.

Contents

Preface: An ALPine Journey Through Energy Scales

When we run or hike through mountains, the landscape around us changes constantly, and new perspectives emerge with each step. Beginning our journey at the foothills, we can observe the smallest details of our starting point, such as the leaves on the trees or the structure of the buildings. But once we start climbing higher, these features eventually fade and become unrecognizable to us. As we reach the summit, however, a broader perspective unfolds, revealing a magnificent view that was hidden from sight below. Similarly, when we describe physical processes at very low energy scales, we get a different view from that at very high energies, and the laws of nature that describe phenomena at these levels even seem, at first glance, to be completely decoupled from each other. Yet, we can traverse and describe all energy scales smoothly and consistently, as long as we adjust our perspective accordingly. For a physicist, this "perspective" is provided by the relevant degrees of freedom and the corresponding effective (field) theory at a given scale. While we can apply Newton's laws to macroscopic objects to describe their motion, moving down to the level of nucleons requires chiral perturbation theory for a consistent treatment of their interactions. The most fundamental degrees of freedom known today are those used to calculate processes at the highest energies reachable at colliders: the particles of the Standard Model of Particle Physics (SM), with the discovery of its last missing piece, the Higgs boson, announced by the ATLAS and CMS collaborations at CERN on July 4, 2012 [1, 2]. It is more than astounding with what accuracy this theory allows us to compute physical quantities. For instance, the experimentally measured value of the electron anomalous magnetic moment agrees with the theoretical prediction to a precision of $\Delta a_e = a_{e,\text{exp}} - a_{e,\text{theo}} = (4.8 \pm 3.0) \times 10^{-13}$ [3, 4]. Yet, even tiny differences like this one make physicists wonder if there is a deeper explanation to it. But there is even more striking evidence for physics beyond the particle spectrum of the SM: A plethora of independent observations points toward the fact that "ordinary" matter contributes only 5% to the total energy density of the Universe, while the *dark matter*, an unknown form of matter that interacts gravitationally but has no or very weak interactions with light, accounts for roughly 27% [5]. Moreover, there are inconsistencies within the SM that remain to be explained. For instance, although neutrinos are theoretically predicted to be massless, the discovery of neutrino oscillations, recognized with the 2015 Nobel Prize in Physics [6], demonstrates that they must possess a nonzero mass. Also in the Higgs sector, mysteries remain to be explained, such as the so-called instability problem, which refers to the fact that the measured value of the Higgs mass indicates that the electroweak vacuum is only meta-stable [7–11]. Another notable problem arises from the observation that CP is conserved in strong interactions, even though no symmetry of the SM prohibits such an interaction. The last conundrum was elegantly addressed by Roberto Peccei and Helen Quinn who proposed an additional global $U(1)_{\text{PQ}}$ symmetry, whose spon-

taneous breaking gives rise to a pseudo Nambu–Goldstone boson, called the *axion*[1]. When it acquires a vacuum expectation value, the axion dynamically cancels the CP-violating term of quantum chromodynamics (QCD), providing a natural solution to the problem. A generalization of axions are axion-like particles (ALPs), which refer to any light, gauge-singlet pseudo Nambu–Goldstone boson arising from the spontaneous breaking of a new, global $U(1)$ symmetry at a high UV-scale Λ, but they do not necessarily solve the strong CP problem. ALPs spanning a wide range of masses and couplings naturally arise in many extensions of the SM, such as composite-Higgs models [13, 14] or supersymmetric extensions [15–17], and can potentially solve many more questions apart from the strong CP problem. They have, for instance, been suggested as candidates for dark matter [18], but can also solve discrepancies between theoretical prediction and experimental measurement, with examples being the anomalous magnetic dipole moments of the electron and the muon [19], although recent developments have resolved these anomalies within the SM. Due to their classical shift-symmetric interactions, ALP–SM couplings are of dimension-five order or higher, yielding a suppression by at least one factor of $1/\Lambda$. Search strategies for these elusive particles involve a diverse range of approaches, including cosmological observations [20, 21], astrophysical measurements [22, 23], collider probes [24–29], and precision studies of flavor-violating transitions in the quark and lepton sectors [19, 30–34].
In this thesis, we will go on a journey through the theoretical and phenomenological landscape of ALPs. As we cross different scales, we will encounter various effective field theories with different degrees of freedom that provide complementary perspectives on ALP searches. Beginning at the scale where it is generated from the breaking of the global $U(1)$ symmetry, we will see in Chapter 1 that its appearance as a virtual particle in one-loop diagrams generates dimension-six operators of the Standard Model Effective Field Theory (SMEFT), an effect called the *ALP–SMEFT interference* [35]. Chapter 2 of this work will explore how renormalization group (RG) running of this phenomenon from the ALP scale down to the experimental scale, together with existing bounds on SMEFT Wilson coefficients, can be used to put strong constraints on the dimension-five ALP–SM couplings. Moving further down to even lower energies, below the scale of electroweak symmetry breaking, the effective degrees of freedom of the SM change, and also the heavy particles are no longer present as external states. The appropriate theory in this regime is the Low-Energy Effective Field Theory (LEFT), and Chapter 3 systematically extends the previously described concept to the *ALP–LEFT interference*. We will see how this framework and so far unconstrained ALP parameter space contributes to the prominent value of $(g-2)_\mu$. Continuing our journey below the scale of chiral symmetry breaking in Chapter 4, the effective degrees of freedom will change once more and are then given by the pseudoscalar mesons and baryons instead of free quarks. Here, the first consistent, non-trivial extension of the known operator bases of chiral perturbation theory in the presence of ALPs at leading and next-to-leading order will be constructed. As an application, the flavor-violating decays $K^\pm \to \pi^\pm a$ will be considered that provide the strongest particle-physics constraints on ALP–SM couplings for $m_a \lesssim 300$ MeV. In addition, these limits will be translated to ALP-nucleon couplings, which, so far, were

[1] The name "axion" was coined by Frank Wilczek after a brand of detergent, as the particle "cleans up" the strong CP problem [12].

only constrained by astrophysical measurements and non-accelerator experiments. In the final chapter, Chapter 5, we will run the energy scales back up and continue even further, all the way to the Planck scale around $\mathcal{O}(10^{19}\,\mathrm{GeV})$. From the highest energy scale where the known laws of physics apply, we will review the problem of the metastability of the electroweak vacuum in the SM. We will see how the presence of the ALP, by modifying the RG equations of the quartic Higgs coupling, can either tighten or worsen this scenario, and what effect it can have on the scale evolution of the three gauge couplings of the SM. To begin with, however, we need a few theoretical basics about the SM, its symmetries and particles, as well as ALPs, which will be described in the next chapter.

Chapter 1: Theoretical Foundations

This chapter provides a general overview of the fundamental concepts underlying this thesis. It begins with an introduction to the Standard Model of Particle Physics based on [36, 37], followed by a brief discussion of effective field theories. Next, various unresolved phenomena and conceptual challenges within the Standard Model are outlined, leading to an introduction to axions and ALPs. In addition to the introduction provided here, each subsequent chapter starts with an explanation of the specific theoretical foundations relevant to its subject.

1.1. The Standard Model of Particle Physics

The Standard Model of Particle Physics (SM) provides a unified description of three of the four fundamental forces, the strong, the weak and the electromagnetic force, and offers a mathematically consistent framework for the description of particle interactions. It is based on the local symmetry group

$$SU(3)_c \times SU(2)_L \times U(1)_Y \,, \tag{1.1}$$

where the special unitary group $SU(3)_c$ corresponds to the strong interactions whose spin-one force carriers are called gluons. The symmetry groups $SU(2)_L$ and $U(1)_Y$ describe the weak and the electromagnetic interactions, mediated by the W- and the B-bosons, respectively. Schematically, the physical particle content of the SM Lagrangian and the interactions among those fields can be written as

$$\mathcal{L}_{\text{SM}} = \mathcal{L}_{\text{gauge}} + \mathcal{L}_{\text{fermion}} + \mathcal{L}_{\text{Higgs}} + \mathcal{L}_{\text{Yukawa}} \,. \tag{1.2}$$

In more detail, the first term, $\mathcal{L}_{\text{gauge}}$, contains the kinetic terms of the gauge bosons, as well as their self-interactions, and is given by

$$\mathcal{L}_{\text{gauge}} = -\frac{1}{4} \left(G^a_{\mu\nu} G^{a,\mu\nu} + W^I_{\mu\nu} W^{I,\mu\nu} + B_{\mu\nu} B^{\mu\nu} \right) \,, \tag{1.3}$$

where $G^a_{\mu\nu}$, $W^I_{\mu\nu}$ and $B_{\mu\nu}$ are the field-strength tensors of $SU(3)_c$, $SU(2)_L$ and $U(1)$, respectively. Correspondingly, a runs from 1 to 8, while the $SU(2)_L$ index is $I \in \{1, 2, 3\}$. The second term in (1.2) contains the kinetic term of the fermions, as well as the interactions with the gauge bosons. It is given by

$$\mathcal{L}_{\text{fermion}} = \bar{\psi}_F \, i \not{D} \, \psi_F \,, \tag{1.4}$$

where the sum extends over the chiral fermion multiplets $F = \{q, l, u_R, d_R, e_R\}$ and the covariant derivative reads

$$D_\mu = \partial_\mu - i g_1 \mathcal{Y} B_\mu - i g_2 \tau_j W^j_\mu - i g_s t_a G^a_\mu \,. \tag{1.5}$$

The set of fermions can be subdivided into two groups, the quarks, that transform as triplets under $SU(3)_c$, and leptons, that are $SU(3)_c$ singlets. No explicit mass

Field	Representation	Isospin T_3	Electric Charge
$q = \begin{pmatrix} u_L \\ d_L \end{pmatrix}$	$(\mathbf{3}, \mathbf{2}, 1/6)$	$\begin{pmatrix} 1/2 \\ -1/2 \end{pmatrix}$	$\begin{pmatrix} 2/3 \\ -1/3 \end{pmatrix}$
u_R	$(\mathbf{3}, \mathbf{1}, 2/3)$	0	2/3
d_R	$(\mathbf{3}, \mathbf{1}, -1/3)$	0	$-1/3$
$l = \begin{pmatrix} \nu_L \\ e_L \end{pmatrix}$	$(\mathbf{1}, \mathbf{2}, -1/2)$	$\begin{pmatrix} 1/2 \\ -1/2 \end{pmatrix}$	$\begin{pmatrix} 0 \\ -1 \end{pmatrix}$
e_R	$(\mathbf{1}, \mathbf{1}, -1)$	0	-1
H	$(\mathbf{1}, \mathbf{2}, 1/2)$	-1/2	0

Table 1.1.: Representations of the fermions and the Higgs boson under the SM gauge groups, as well as their isospin and electric charge. The hypercharge $\mathcal{Y}$, the isospin T_3 and the electric charge are related via the Gell–Mann–Nishijima equation $Q = T_3 + \mathcal{Y}$ [38, 39].

terms are present for the fermions in the SM. The full transformation properties of the fermion fields under the SM gauge groups are summarized in Table 1.1. Next, $\mathcal{L}_{\text{Higgs}}$ contains the Higgs potential, as well as its kinetic term and reads

$$\mathcal{L}_{\text{Higgs}} = (D_\mu H)^\dagger (D^\mu H) + m_H^2 H^\dagger H - \frac{\lambda}{2} (H^\dagger H)^2 \,, \tag{1.6}$$

where the Higgs-doublet is given by $H = (H^+, H^0)^T$ and m_H is the Higgs mass parameter. Finally, the Higgs-fermion interactions are parametrized by

$$\mathcal{L}_{\text{Yukawa}} = -\left(\bar{q}\, \boldsymbol{Y}_d\, H\, d_R + \bar{q}\, \boldsymbol{Y}_u\, \tilde{H}\, u_R + \bar{l}\, \boldsymbol{Y}_e\, H\, e_R + \text{h.c.} \right) , \tag{1.7}$$

where the $\boldsymbol{Y}_i$ with $i = u,\, d,\, e$ denote the Yukawa matrices and $\tilde{H} = i\sigma_2 H$.

1.2. Electroweak Symmetry Breaking

Even though it may appear to contradict the statement made in the preceding section, fermions are not massless particles and the observed mass spectrum even spans over several orders of magnitude. This apparent contradiction is resolved by the Higgs mechanism, which leads to a spontaneous breaking of the full SM symmetry down to

$$SU(3)_c \times SU(2)_L \times U(1)_Y \overset{\text{EWSB}}{\longrightarrow} SU(3)_c \times U(1)_{\text{EM}} \,. \tag{1.8}$$

In more detail, the potential in (1.6) is minimized when the Higgs doublet acquires a vacuum expectation value (vev) of the form

$$\langle 0|H|0\rangle = \frac{1}{\sqrt{2}} \begin{pmatrix} 0 \\ v \end{pmatrix} , \tag{1.9}$$

with $v = \sqrt{2\, m_H^2/\lambda} \approx 246$ GeV [40]. Applying a unitary gauge transformation, the Higgs field can then be written as

$$H = \frac{1}{\sqrt{2}} \begin{pmatrix} 0 \\ v + h \end{pmatrix} , \tag{1.10}$$

where h denotes the physical Higgs field with $\langle h \rangle = 0$. Expanding around the vev in the Lagrangian yields the massive gauge bosons as a linear combination of W_μ and B_μ as

$$\begin{aligned} W_\mu^\pm &= \frac{1}{\sqrt{2}}(W_\mu^1 \mp i W_\mu^2) \quad \text{with} \quad m_W = \frac{g_2\, v}{2}\,, \\ Z_\mu^0 &= \frac{1}{\sqrt{g_2^2 + g_1^2}}\,(g W_\mu^3 - g' B_\mu) \quad \text{with} \quad m_Z = \sqrt{g_2^2 + g_1^2}\,\frac{v}{2}\,. \end{aligned} \tag{1.11}$$

In addition, there is one vector boson, the *photon*, that does not acquire a mass,

$$A_\mu = \frac{1}{\sqrt{g_1^2 + g_2^2}}\,(g_1 W_\mu^3 + g_2 B_\mu) \quad \text{with} \quad m_A = 0\,. \tag{1.12}$$

Analogously, inserting the Higgs-field expansion in the Yukawa-terms of the Lagrangian (1.6) yields

$$\mathcal{L}_{\text{Yukawa}} = -\boldsymbol{Y}_u^{ij}\,\bar{u}_{L_i}\frac{(v+h)}{\sqrt{2}}u_{R_j} - \boldsymbol{Y}_d^{ij}\,\bar{d}_{L_i}\frac{(v+h)}{\sqrt{2}}d_{R_j} - \boldsymbol{Y}_e^{ij}\,\bar{e}_{L_i}\frac{(v+h)}{\sqrt{2}}e_{R_j} + \text{h.c.} \tag{1.13}$$

In order to find the physical fermion masses, the mass matrices

$$\mathcal{M}_a^{ij} = \frac{v}{\sqrt{2}}\,\boldsymbol{Y}_a^{ij}\,, \tag{1.14}$$

remain to be diagonalized by means of a unitary transformation,

$$\begin{aligned} U_R^{-1}\,\mathcal{M}_u\,U_L &= \text{diag}(m_u, m_c, m_t)\,, \\ D_R^{-1}\,\mathcal{M}_d\,D_L &= \text{diag}(m_d, m_s, m_b)\,, \\ E_R^{-1}\,\mathcal{M}_e\,E_L &= \text{diag}(m_e, m_\mu, m_\tau)\,. \end{aligned} \tag{1.15}$$

1.3. Effective Field Theories

Although one might without doubt call the SM one of the most important achievements of mankind, it is a relatively recent theory. Many outstanding discoveries, such as electromagnetism, thermodynamics, and general relativity, were successfully explained long before the development of today's most fundamental description of nature. This raises the question of how a consistent theory can be constructed without complete knowledge of its underlying elementary constituents. The key concept addressing this issue is *effective field theory (EFT)*, and is based on three pillars [41]: the expansion in a small parameter, the identification of the relevant degrees of freedom, and symmetries. To illustrate this based on the review [42], consider the computation of a scattering amplitude at an energy scale $\mu \ll \Lambda$, where Λ corresponds to the mass scale of a heavy, elementary state in the full theory. Since this state can appear as a virtual, but not as an external degree of freedom at the low energy scale μ, it can be removed from the Lagrangian by replacing the couplings of the remaining fields with an effective interaction that accounts for the virtual effects of the heavy particle. The effective Lagrangian is constructed by systematically including all operators that

respect the symmetries of the underlying theory, ordered in an expansion in $1/\Lambda$. This approach, known as the *operator product expansion*, is given by

$$\mathcal{L}_{\text{EFT}} = \sum_d \sum_i^{n_d} \frac{C_i^{(d)}(\mu)}{\Lambda^{d-4}} Q_i^{(d)}(\mu)\,, \tag{1.16}$$

where μ is called the factorization- or renormalization-scale and d denotes the mass-dimension. In essence, by writing down (1.16), the full theory is simplified by retaining only the relevant degrees of freedom at the expense of introducing an infinite tower of local operators. They are multiplied by a-priori unknown couplings C_i that are referred to as *Wilson coefficients* and implicitly contain information about the underlying ultra-violet (UV) physics. Returning to the historical examples mentioned earlier, such as the formulation of electromagnetism, it becomes clear that not all fundamental degrees of freedom are necessary for describing a given process, as long as those that contribute directly are correctly identified and accounted for.

Today, it is often assumed that the SM is the low-energy effective theory of a more complete theory, which includes additional, yet-unknown heavy degrees of freedom that lie beyond the energy scales accessible to current particle colliders. In this scenario, one can write down an expansion as in 1.16, to include the effective higher dimensional operators generated by the new heavy fields as

$$\mathcal{L} = \mathcal{L}_{\text{SM}} + \frac{1}{\Lambda}\mathcal{L}_5 + \frac{1}{\Lambda^2}\mathcal{L}_6 + \dots\,, \tag{1.17}$$

and the framework that systematically organizes these additional operators is called the Standard Model Effective Field Theory (SMEFT). At dimension five in the SMEFT, there is only one operator, and it generates masses for the neutrinos. It reads [43][1]

$$\mathcal{L}_5 = (\tilde{H}^\dagger l_p)^T\, C\, (\tilde{H}^\dagger l_r)\,, \tag{1.18}$$

with charge-conjugation matrix $C = i\gamma^2\gamma^0$. At dimension six, on the other hand, the number of independent operators that can be built out of SM fields while respecting the SM symmetries increases to 2499 (59 when omitting flavor indices)[2]. Since the full list of non-redundant operators was found by four physicists affiliated with the University of Warsaw, the dimension-six minimal SMEFT basis is commonly referred to as the *Warsaw basis* [46].

Concerning the C_i's in (1.16), there are in general two procedures via which they can be determined: in a *top-down* EFT, one can calculate a physical process in both theories, the full and the effective one, and require the two results to be equal, i.e.

$$\langle f \,|\, \mathcal{L}_{\text{full}} \,|i\rangle \overset{!}{=} \sum_d \sum_{i=1}^{n_d} \frac{C_i^{(d)}(\mu)}{\Lambda^{d-4}} \langle f \,|\, Q_i^{(d)}(\mu) \,|i\rangle\,. \tag{1.19}$$

[1] This operator is sometimes referred to as the "Weinberg operator". In this thesis, this name is used for the dimension-six three-gauge-boson operators. To avoid confusion, no specific name is assigned to the dimension-five operator here.

[2] At higher mass dimensions, the number of effective operators increases and can be found using the Hilbert series technique, as done in [44, 45].

Truncating the sum at a fixed mass dimension then determines the Wilson coefficients up to higher-order power corrections. On the other hand, if the full theory is unknown, a *bottom-up* approach still allows for a systematic parametrization of the effects of heavy, unknown states. In this case, however, the Wilson coefficients need to be fixed by experiment. An important observation is the fact that the scale μ in (1.16), which separates UV contributions between the operators Q_i and the Wilson coefficients C_i, is arbitrary. As a result, any physical amplitude must remain independent of μ. In other words, the equation

$$\frac{d}{d\ln\mu}\, C_i(\mu)\,\langle Q_i(\mu)\rangle \stackrel{!}{=} 0 \tag{1.20}$$

must hold, where a summation over the double index is implied. If the operators are linearly independent and defining the *anomalous dimension* matrix via

$$\frac{d}{d\ln\mu}\langle Q_i(\mu)\rangle \equiv -\gamma_{ij}(\mu)\langle Q_j(\mu)\rangle\,, \tag{1.21}$$

this automatically implies that

$$\frac{d}{d\ln\mu}\, C_j(\mu) = \gamma_{ij}(\mu)\, C_i(\mu)\,. \tag{1.22}$$

This important equation captures the scale dependence of the Wilson coefficients and is called the renormalization group (RG) equation, while the right-hand side of (1.22) is often called the β-function of $C_j(\mu)$. The concept of EFTs is a central one in this thesis. In particular, the effects of ALPs in the SMEFT, the LEFT and χPT will be examined, and details on the respective EFT and the impacts on the RG equations will be given in the beginning of each corresponding chapter.

1.4. Physics Beyond the Standard Model

Despite its remarkable success in accurately predicting fundamental particle physics processes, the SM is confronted with a variety of observations, of both experimental and theoretical nature, that cannot be adequately explained within this framework. Of particular importance to this thesis is the so-called *strong CP problem*, which is reviewed in the following, based on [37]. In essence, it consists of the question of why a CP-violating term of the form

$$\frac{\bar\theta}{16\pi^2}\, g_s^2\, G^a_{\mu\nu}\tilde G^{a,\mu\nu}\,, \tag{1.23}$$

which could, in principle, be included in the SM Lagrangian, has a coupling $\bar\theta$ that is unnaturally small or even exactly zero[3]. Naively, the presence of such a term may

[3]The parameter $\bar\theta \equiv \theta_{\rm QCD} - \arg\det(Y_u Y_d)$ is a combination of the Lagrangian parameter $\theta_{\rm QCD}$ and a phase induced by chiral rotations on the quarks. As such, it is basis independent and cannot be removed from the theory. The situation is different for equivalent $SU(2)$ and $U(1)$ expressions, where the angle can be removed by chiral rotations and is therefore unphysical.

not seem problematic, as it can be rewritten as the total derivative of the so-called *Chern-Simons current* K_μ [37],

$$\partial^\mu K_\mu = \epsilon^{\mu\nu\alpha\beta} G^a_{\mu\nu} G^a_{\alpha\beta}\,, \text{ with } K_\mu = \epsilon_{\mu\nu\alpha\beta}\left(A^a_\nu G^a_{\alpha\beta} - \frac{g_s}{3} f^{abc} A^a_\nu A^b_\alpha A^c_\beta\right)\,, \tag{1.24}$$

and one would therefore expect it to give zero contribution to physical quantities. When considering non-perturbative Quantum Chromodynamics (QCD) effects, however, the situation changes. Indeed, below the QCD confinement scale, instanton effects generate a coupling between pions and the isospin doublet ψ containing the proton p and the neutron n, of the form [37]

$$\mathcal{L}_{\pi NN} = \pi^a \bar{\psi}\,\left(i\gamma_5\, g_{\pi NN} + \bar{g}_{\pi NN}\right)\,\tau^a \psi\,, \tag{1.25}$$

where $\bar{g}_{\pi NN}$ ($g_{\pi NN}$) is a CP-violating (conserving) coupling. In more detail [37],

$$\bar{g}_{\pi NN} \propto \frac{\bar{\theta}}{f_\pi}\,\frac{m_u m_d}{m_u + m_d}\,. \tag{1.26}$$

The presence of such a term generates an electric dipole moment (EDM) of the neutron d_n from loop-diagrams such as [37, 47]

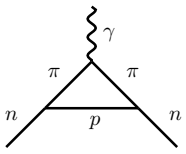

$$\text{with} \qquad d_{n,\,\text{theo}} \sim 10^{-16}\, e\,\text{cm}\,\bar{\theta}\,. \tag{1.27}$$

In contrast, experimental measurements tightly constrain the neutron EDM [48],

$$|d_{n,\,\text{exp}}| < 1.8 \times 10^{-26}\, e\,\text{cm} \quad (90\ \%\ \text{C.L.})\,, \tag{1.28}$$

which can be translated into an upper bound on $\bar{\theta}$, yielding

$$|\bar{\theta}| \lesssim 10^{-10}\,. \tag{1.29}$$

In principle a small but radiatively stable parameter does not directly pose a problem. Comparing it to the remaining parameters of the SM, however, would rather suggest a value of $\bar{\theta} \sim \mathcal{O}(1)$ and one can question the *naturalness* of this coupling. A dynamical process, that automatically relaxes $\bar{\theta}$ to zero, would be much more elegant. For this purpose, the QCD axion has been proposed and the mechanism by which it cancels the QCD $\bar{\theta}$ term from the Lagrangian will be explained in Section 1.5. While the strong CP problem provides one of the main motivations to search for axions, it is not the only unsolved question regarding the SM. In fact, unexplained phenomena and conceptual problems are encountered across multiple energy scales:

- Most evidently, the SM unifies only three of the four fundamental forces, leaving the description of gravity unaccounted for. At very high energies above the so-called Planck scale at $\mathcal{O}(10^{19}$ GeV), quantum effects of gravity become sizable and therefore cannot be neglected.

- Remaining at very high energies, the experimentally measured value of the Higgs mass of $m_h \sim 125$ GeV indicates that the electroweak vacuum is meta-stable. At large scales, around 10^{11} GeV, the Higgs quartic coupling λ becomes negative, resulting in an instability as the potential is then unbounded from below. The electroweak vacuum we live in, however, has a lifetime that is longer than the age of the Universe. While in principle this is not an inconsistency, it would be much more elegant to avoid the scenario of a spontaneous vacuum decay. Any kind of new physics model that has an influence on the RG equations of the Higgs quartic coupling can, however, modify this situation.

- Moving down to slightly lower energies, around $\mathcal{O}(10^{16}$ GeV), another indication of physics beyond the SM emerges. Solving the RG evolution equations for the three gauge couplings reveals that they converge to nearly identical values at this energy scale. While one can certainly argue that this behavior is a coincidence, the presence of yet unknown new particles could potentially modify the scale evolution of the gauge couplings and indeed yield a *Grand Unified Theory (GUT)*. The SM in this scenario could then be the subgroup of a broken larger symmetry group. While the simplest form of such a unification, a $SU(5)$ gauge symmetry known as the Georgi-Glashow model [49], is experimentally excluded [50], modifications to this scenario could potentially still be realized in nature.

- The next challenge arises from the only fundamental physical scale in the SM, the Higgs mass $m_h \sim 125$ GeV. While its value alone does not pose an issue in the absence of additional new physics, the situation changes when considering any new physics coupled to the Higgs with a cutoff scale Λ. In this case, m_h receives radiative loop corrections that are of the order of Λ. To arrive at the experimentally measured Higgs mass, that is 17 orders of magnitude below the Planck scale, extreme cancellations between the terms need to occur, which can be considered *unnatural* and is therefore often referred to as the *hierarchy problem*.

- In the SM, the masses of the fermions are generated via the Higgs mechanism. In more detail, the mass terms are given by the diagonalized mass matrices, that are proportional to the Yukawa matrices and the Higgs vev. A naive expectation would therefore be that the resulting fermion masses are roughly of the same order of magnitude. Experimentally, however, one finds strong hierarchies: In the quark sector, the mass gap between the heaviest quark, the top quark, and the lightest one, the up quark, spans five orders of magnitude and the neutrinos, which are massless in the SM, are found to have a tiny mass, with $m_\nu/m_e \lesssim 10^{-6}$.
  Another central question in the flavor sector concerns the structure of the mixing matrices: while the mixing angles between the neutrinos, parametrized in the so-called Pontecorvo–Maki–Nakagawa–Sakata (PMNS) matrix are large, the Cabibbo–Kobayashi–Maskawa (CKM) matrix describing the mixing between the quark flavors, exhibits an almost diagonal pattern.
  The fact that there is no dynamic mechanism within the SM that could explain these behaviors is referred to as the *flavor problem*.

- Apart from the challenges within the SM, a variety of observational hints point toward the existence of at least one more type of matter beyond the known particle spectrum, that interacts gravitationally but has no or very weak interactions with light and is therefore referred to as *dark matter*. In fact, today it is believed that this unknown form of matter makes up approximately 27% of the Universe's energy density, while "ordinary" matter only contributes 5% [5]. The first observations pointing toward this assumption have been made as early as 1933, when F. Zwicky applied the virial theorem to the Coma cluster and noticed a lack of luminous matter to explain the average velocity of about 1000 km/s, which would require about 400 times the observed average matter density [51]. Since then, a plethora of independent observations have been made that also suggest this conclusion: To name a few, they range from V. Rubin's observation of almost flat rotation curves of galaxies (instead of a $1/\sqrt{r}$ behavior, as expected for instance outside a spherical symmetric matter distribution) [52] to anisotropies in the cosmic microwave background (CMB) power spectrum that are compatible with the Lambda cold dark matter model, Λ_{CDM} [5].

While this list is by no means exhaustive, it provides clear evidence that searches for physics beyond the SM are crucial to find a consistent model that accurately describes nature. Axions and axion-like particles, introduced in the following section, have the potential to address several of these key challenges of the SM, as this thesis will show.

1.5. Axions and Axion-Like Particles

An elegant solution to the strong CP problem that dynamically relaxes the parameter $\bar{\theta}$ to zero has first been proposed by R. Peccei and H. Quinn in [53]. It consists of extending the SM by a new $U(1)_{\mathrm{PQ}}$ symmetry that is spontaneously broken at a high scale Λ. The resulting pseudoscalar Goldstone boson is called the *QCD axion*. This mechanism generates a coupling of the axion a to gluons of the form

$$\mathcal{L} \supset \frac{a}{f} \frac{g_s^2}{16\pi^2} G^a_{\mu\nu} \tilde{G}^{a,\mu\nu} \,, \tag{1.30}$$

where f is the axion decay constant, related to the scale of spontaneous symmetry breaking via $\Lambda = 4\pi f$. Most importantly for the solution of the strong CP problem is that non-perturbative instanton effects below the QCD confinement scale generate a potential for the axion [54]. It can, for instance, be obtained from the chiral effective Lagrangian including the axion and reads [55]

$$V(a) = -m_\pi^2 f_\pi^2 \sqrt{1 - \frac{4 m_u m_d}{(m_u + m_d)^2} \sin^2\left(\frac{a}{2f} + \frac{\bar{\theta}}{2}\right)} \,, \tag{1.31}$$

with a minimum at $\langle a \rangle = -\bar{\theta} f$. In that way, the axion now provides a solution to the strong CP problem, as the sum

$$\left(\bar{\theta} + \frac{\langle a \rangle}{f}\right) \frac{\alpha_s}{4\pi} G^a_{\mu\nu} \tilde{G}^{a,\mu\nu} = 0 \tag{1.32}$$

dynamically vanishes. In addition, a mass term is generated for the axion, even in the case $m_{a,0} = 0$. Denoting the axion–gluon coupling by c_{GG}, it is, up to higher-order corrections in the chiral expansion and for $m_{a,0} = 0$, given by [56]

$$m_a^2 = c_{GG}^2 \, \frac{f_\pi^2 m_\pi^2}{f^2} \, \frac{2 m_u m_d}{(m_u + m_d)^2} \,, \tag{1.33}$$

with m_u and m_d the up- and down-quark mass, respectively, and f_π denotes the pion decay constant.

Axion-Like Particles

As a generalization of the QCD axion, an axion-like particle (ALP) arises as generic pseudo Nambu–Goldstone boson from a spontaneously broken global $U(1)_{\mathrm{PQ}}$ symmetry[4], but does not necessarily solve the strong CP problem. As ALPs are shift invariant under $a \to a + \text{const.}$, the Lagrangian contains only derivative couplings as well as anomalous couplings to gauge bosons. Including an additional bare mass term[5] $m_{a,0}$ that explicitly breaks the shift symmetry, the most general Lagrangian up to dimension-six order can be written as [59]

$$\begin{aligned} \mathcal{L}_{\text{eff}}^{D\leq 6} = & \frac{1}{2} (\partial_\mu a)(\partial^\mu a) - \frac{m_{a,0}^2}{2} a^2 + \frac{\partial^\mu a}{f} \sum_F \bar{\Psi}_F \, \boldsymbol{c}_F \, \gamma_\mu \, \Psi_F + c_\phi \, \frac{\partial^\mu a}{f} \, (H^\dagger \, i \overleftrightarrow{D_\mu} \, H) \\ & + c_{GG} \, \frac{\alpha_s}{4\pi} \frac{a}{f} G_{\mu\nu}^a \, \tilde{G}^{\mu\nu,a} + c_{BB} \frac{\alpha_1}{4\pi} \frac{a}{f} B_{\mu\nu} \, \tilde{B}^{\mu\nu} \; + c_{WW} \frac{\alpha_2}{4\pi} \frac{a}{f} W_{\mu\nu}^A \, \tilde{W}^{\mu\nu,A} \\ & + \frac{C_{HH}}{f^2} \, (\partial^\mu a)(\partial_\mu a) \, H^\dagger H \,. \end{aligned} \tag{1.34}$$

As for the axion, the ALP decay constant f is related to the new-physics scale via $\Lambda = 4\pi f$ and it is assumed that $\Lambda \gg \mu_w$, with μ_w denoting the scale of electroweak symmetry breaking. The sum in the first line extends over the SM chiral fermion multiplets F and the $\boldsymbol{c}_F$ denote 3×3 hermitian matrices in generation space. The second line of the Lagrangian includes the ALP couplings to $G_{\mu\nu}^a$, $W_{\mu\nu}^A$ and $B_{\mu\nu}$, i.e. the field-strength tensors of $SU(3)_c$, $SU(2)_L$ and $U(1)_Y$, respectively. The corresponding dual field strength tensors are defined as $\tilde{B}^{\mu\nu} = \frac{1}{2}\epsilon^{\mu\nu\alpha\beta} B_{\alpha\beta}$, where $\epsilon^{0123} = 1$ and equivalently for $\tilde{W}^{\mu\nu,A}$ and $\tilde{G}^{\mu\nu,a}$.
The Lagrangian as given in (1.34) contains several redundant operators: The single-ALP coupling to the two Higgs-fields in the first line can be written as a sum of an operator that vanishes by the equations of motion plus a term that contains the derivative coupling to fermions [60]. In addition, baryon number, as well as individual lepton number conservation remove four redundant degrees of freedom, such that all in all, the Lagrangian contains 46 free parameters. The bosonic couplings can, for

[4] To avoid confusion with the notation in following chapters, the global symmetry that generates ALPs upon its breaking is also referred to as $U(1)_{\mathrm{PQ}}$, as it is in the case of the QCD axion.

[5] If this explicit mass term is absent, non-perturbative QCD effects nevertheless dynamically generate a mass for the ALP, see (1.33) [57, 58].

instance, be chosen as [34, 60]

$$\begin{aligned}
\tilde{c}_{GG} &= c_{GG} + \frac{1}{2}\,\mathrm{Tr}[\boldsymbol{c}_u + \boldsymbol{c}_d - N_L\,\boldsymbol{c}_Q]\,,\\
\tilde{c}_{WW} &= c_{WW} - \frac{1}{2}\,\mathrm{Tr}[N_c\,\boldsymbol{c}_Q + \boldsymbol{c}_L]\,,\\
\tilde{c}_{BB} &= c_{BB} + \frac{1}{2}\,\mathrm{Tr}[N_c\,(\mathcal{Y}_u^2\boldsymbol{c}_u + \mathcal{Y}_d^2\boldsymbol{c}_d - N_L\,\mathcal{Y}_Q^2\,\boldsymbol{c}_Q) + \mathcal{Y}_e^2\,\boldsymbol{c}_e - N_L\,\mathcal{Y}_L^2\,\boldsymbol{c}_L]\,,
\end{aligned} \tag{1.35}$$

where the number of colors is $N_c = 3$, the number of weak isospin components is $N_L = 2$ and the hypercharges are denoted as $\mathcal{Y}_u = 2/3$, $\mathcal{Y}_d = -1/3$, $\mathcal{Y}_q = 1/6$, $\mathcal{Y}_e = -1$, $\mathcal{Y}_L = -1/2$. While in Lagrangian (1.34), the shift symmetry is explicit due to the derivative interactions, it can be rewritten by applying the field redefinition $\Psi_F \to \Psi_F + i\,\frac{a}{f}\,\boldsymbol{c}_F\,\Psi_F$, yielding the equivalent form

$$\begin{aligned}
\mathcal{L}^{D\leq 6}_{\text{SM+ALP}} = {}& \frac{1}{2}\,(\partial_\mu a)(\partial^\mu a) - \frac{m_{a,0}^2}{2}\,a^2\\
&+ C_{GG}\,\frac{a}{f}\,G^A_{\mu\nu}\,\tilde{G}^{\mu\nu\,A} + C_{WW}\,\frac{a}{f}\,W^I_{\mu\nu}\,\tilde{W}^{\mu\nu\,I} + C_{BB}\,\frac{a}{f}\,B_{\mu\nu}\,\tilde{B}^{\mu\nu}\\
&- \frac{a}{f}\,\Big(\bar{q}\,\tilde{H}\,\tilde{\boldsymbol{Y}}_u\,u_R + \bar{q}\,H\,\tilde{\boldsymbol{Y}}_d\,d_R + \bar{l}\,H\,\tilde{\boldsymbol{Y}}_e\,e_R + \text{h.c.}\Big)\\
&+ \frac{1}{2}\,\frac{a^2}{f^2}\,\Big(\bar{q}\,\tilde{H}\,\boldsymbol{Y}'_u\,u_R + \bar{q}\,H\,\boldsymbol{Y}'_d\,d_R + \bar{l}\,H\,\boldsymbol{Y}'_e\,e_R + \text{h.c.}\Big)\\
&+ \frac{C_{HH}}{f^2}\,(\partial^\mu a)(\partial_\mu a)\,H^\dagger H\,,
\end{aligned} \tag{1.36}$$

where

$$\tilde{\boldsymbol{Y}}_d = i\,(\boldsymbol{Y}_d\,\boldsymbol{c}_d - \boldsymbol{c}_Q\boldsymbol{Y}_d)\,,\quad \tilde{\boldsymbol{Y}}_u = i\,(\boldsymbol{Y}_u\,\boldsymbol{c}_u - \boldsymbol{c}_Q\boldsymbol{Y}_u)\,,\quad \tilde{\boldsymbol{Y}}_e = i\,(\boldsymbol{Y}_e\,\boldsymbol{c}_e - \boldsymbol{c}_L\boldsymbol{Y}_e)\,, \tag{1.37}$$

and

$$\begin{aligned}
\boldsymbol{Y}'_d = \boldsymbol{c}_Q^2\,\boldsymbol{Y}_d - 2\,\boldsymbol{c}_Q\,\boldsymbol{Y}_d\,\boldsymbol{c}_d + \boldsymbol{Y}_d\,\boldsymbol{c}_d^2\,,\quad \boldsymbol{Y}'_u = \boldsymbol{c}_Q^2\,\boldsymbol{Y}_u - 2\,\boldsymbol{c}_Q\,\boldsymbol{Y}_u\,\boldsymbol{c}_u + \boldsymbol{Y}_u\,\boldsymbol{c}_u^2\,,\\
\boldsymbol{Y}'_e = \boldsymbol{c}_L^2\,\boldsymbol{Y}_e - 2\,\boldsymbol{c}_L\,\boldsymbol{Y}_e\,\boldsymbol{c}_e + \boldsymbol{Y}_e\,\boldsymbol{c}_e^2\,.
\end{aligned} \tag{1.38}$$

The axial anomaly generates additional contributions to the ALP-gauge boson couplings of the form [60]

$$\begin{aligned}
C_{GG} &= \frac{\alpha_s}{4\pi}\,\left[c_{GG} + \frac{1}{2}\,\mathrm{Tr}(\boldsymbol{c}_d + \boldsymbol{c}_u - 2\boldsymbol{c}_q)\right] \equiv \frac{\alpha_s}{4\pi}\,\tilde{c}_{GG},\\
C_{WW} &= \frac{\alpha_2}{4\pi}\,\left[c_{WW} - \frac{1}{2}\,\mathrm{Tr}(N_c\,\boldsymbol{c}_q + \boldsymbol{c}_l)\right] \equiv \frac{\alpha_2}{4\pi}\,\tilde{c}_{WW},\\
C_{BB} &= \frac{\alpha_1}{4\pi}\,\left[c_{BB} + \mathrm{Tr}\Big(N_c\,(\mathcal{Y}_d^2\,\boldsymbol{c}_d + \mathcal{Y}_u^2\,\boldsymbol{c}_u - 2\,\mathcal{Y}_q^2\,\boldsymbol{c}_q) + \mathcal{Y}_e^2\,\boldsymbol{c}_e - 2\,\mathcal{Y}_l^2\,\boldsymbol{c}_L\Big)\right]\\
&\equiv \frac{\alpha_1}{4\pi}\,\tilde{c}_{BB}.
\end{aligned} \tag{1.39}$$

The full set of RG evolution equations of the ALP–SM couplings in (1.34) and (1.36) has been computed in [60, 61], and the matching corrections at the weak scale μ_w in [60]. While most couplings evolve non-trivially under a scale variation, factoring

out the SM gauge couplings α_i in the c_{VV} as introduced in (1.34) yields a scale independence up to two-loop order, i.e.

$$\frac{d}{d\ln\mu}\, c_{VV}(\mu) = 0 \quad \text{for} \quad V = G,\, W,\, B\,. \tag{1.40}$$

In this work it is assumed that the ALP is the only degree of freedom beyond the SM fields below the scale Λ of global $U(1)_{\text{PQ}}$ symmetry breaking. In the case with new-physics particles beyond the ALP, matching corrections at the corresponding thresholds would need to be taken into account, and further contributions to the RG evolution equations could arise.

1.6. UV-Complete Axion and ALP Models

While the ALP Lagrangian in (1.34) comprises all terms that can, in general, appear for a shift symmetric pseudo Nambu–Goldstone boson up to dimension-six order, concrete UV-complete models for the classical QCD axion typically only generate a subset of these terms. The two most prominent UV-complete frameworks that generate the QCD anomaly term via the presence of an axion are the Kim-Shifman-Vainshtein-Zakharov (KSVZ) [62, 63] and the Dine-Fischler-Srednicki-Zhitnitsky (DFSZ) [64, 65] models, that have also been proposed as benchmark models for ALPs in [66]. They are introduced in greater detail below, following [67].

1.6.1. KSVZ Model

In the KSVZ model, the SM is extended by two fermions, a left- (Q_L) and a right-handed one (Q_R), as well as a heavy scalar S. All new particles are charged under a $U(1)_{\text{PQ}}$ symmetry, but while the heavy scalar is a singlet under the SM gauge groups, the heavy fermions transform non-trivially under $SU(3)_c$. With this setup, the Lagrangian takes the form

$$\mathcal{L}_{\text{KSVZ}} = \mathcal{L}_{\text{SM}} + |\partial_\mu S|^2 + \bar{Q}\, i\not{D}\, Q - y_Q \left(S\, \bar{Q}_L Q_R + \text{h.c.}\right) - V(S) + \mathcal{L}_{Qq}\,, \tag{1.41}$$

where y_Q, μ_S, λ_S, and λ_{SH} are real parameters. The term $\mathcal{L}_{Qq}$ denotes a portal coupling between Q and a SM fermion that vanishes in the original description of the model, where $Q_{L,R} \sim (\mathbf{3}, \mathbf{1}, 0)$. In this case, however, the extra fermions become stable. This problem can be circumvented, when for instance instead $Q_{L,R} \sim (\mathbf{3}, \mathbf{1}, -1/3)$ with $U(1)_{\text{PQ}}$ charges $X_S = 1$, $X_{Q_L} = 1$ and $X_{Q_R} = 0$, such that a possible portal term reads

$$\mathcal{L}_{Qq} = -y_q^p\, \bar{q}_L^p\, H\, Q_R + \text{h.c.}\,. \tag{1.42}$$

In order to solve the strong CP problem, the scalar potential $V(S)$ in (1.41) can be chosen as

$$V(S) = \frac{\lambda_S}{2}\left(|S|^2 - \frac{f^2}{2}\right)^2\,, \tag{1.43}$$

such that the $U(1)_{\text{PQ}}$ is spontaneously broken. In order to explicitly break the symmetry and generate a mass term for the Goldstone boson, one can modify the above potential to

$$\begin{aligned} V'(S) &= -\mu_S^2|S|^2 + \frac{\lambda_S}{2}|S|^4 + \lambda_{SH}|S|^2(H^\dagger H) - \frac{\kappa^2}{2}\left(S^2 + (S^*)^2\right), \\ &= V(S) - \frac{\lambda_S f^4}{8} + \lambda_{SH}|S|^2(H^\dagger H) - \frac{\kappa^2}{2}\left(S^2 + (S^*)^2\right), \end{aligned} \tag{1.44}$$

where $\mu_s^2 = \lambda_S f^2/2$. The parameters in this form of the potential will be examined in Chapter 2. In the broken phase, it is convenient to parametrize the scalar in terms of a heavy radial component, ρ, and the axion or ALP a as

$$S(x) = \frac{1}{\sqrt{2}}\left[f + \rho(x)\right] e^{\frac{ia(x)}{f}}, \tag{1.45}$$

where f denotes the vev of S. The additional fermions receive a mass term with $m_Q = y_Q\, f/\sqrt{2}$, which can be seen when replacing the scalar in the Yukawa-like term in the first line of (1.41) by the form in polar coordinates in (1.45) and performing the rotation

$$Q_L \to e^{\frac{ia(x)}{f}}\, Q_L\,. \tag{1.46}$$

Applying this fermion redefinition and focusing on the potential in (1.44), integrating out the heavy fields ρ and $Q_{L,R}$ at tree-level using `Matchete` [68] yields in the broken phase

$$\begin{aligned} \mathcal{L}_{\text{EFT}} = \mathcal{L}_{\text{SM}} &- \frac{\lambda_{SH} f^2}{2}(H^\dagger H) + \frac{1}{2}\frac{f^2\,\lambda_{SH}^2}{M_\rho^2}(H^\dagger H)^2 + \frac{1}{2}(\partial_\mu a)^2 - \frac{1}{2}m_a^2\, a^2 \\ &- \frac{a}{f}\,\frac{\alpha_s}{8\pi}\, G^A_{\mu\nu}\tilde{G}^{\mu\nu\, A} - \frac{1}{3}\,\frac{a}{f}\,\frac{\alpha_Y}{4\pi}\, B_{\mu\nu}\tilde{B}^{\mu\nu} \\ &+ 4\,\frac{m_a^2}{f^2}\,\frac{a^4}{4!} + \lambda_{SH}\,\frac{m_a^2}{M_\rho^2}\, a^2(H^\dagger H) - \frac{\lambda_{SH}}{M_\rho^2}\,(\partial_\mu a)^2(H^\dagger H) \\ &- \frac{\lambda_{SH}^2 f^2}{2M_\rho^4} Q_{H\Box} + \frac{y_q^p y_q^{r\,*}}{2M_Q^2}\left(\boldsymbol{Y}_d^{rs}\,[Q_{dH}]_{ps} - \frac{1}{2}\,[Q_{Hq}^{(1)}]_{pr} - \frac{1}{2}\,[Q_{Hq}^{(3)}]_{pr} + \text{h.c.}\right), \end{aligned} \tag{1.47}$$

where $m_a^2 = 2\kappa^2$ and the last line contains dimension-six operators in the Warsaw basis [46]. Certainly, in order to remove the double appearance of the quadratic and quartic Higgs interactions in the first line, the SM parameters μ and λ need to be redefined via

$$\mu^2 \to \tilde{\mu}^2 = \mu^2 - \frac{\lambda_{SH} f^2}{2}, \quad \text{and} \quad \lambda \to \tilde{\lambda} = \lambda - \frac{f^2\,\lambda_{SH}^2}{2M_\rho^2}\,. \tag{1.48}$$

From the Lagrangian in (1.47), it is possible to deduce the dimension-five ALP parameters of the model as $c_{GG} = -1/2$, $c_{BB} = -1/3$ and all other couplings are zero at the scale Λ. This is also summarized in Table 1.2.

1.6.2. DFSZ Model

The DFSZ model is based on a two-Higgs scenario in combination with an additional heavy SM-singlet scalar S. The additional fields are assigned to the representation $H_1 \sim (\mathbf{1}, \mathbf{2}, 1/2)$, $H_2 \sim (\mathbf{1}, \mathbf{2}, -1/2)$ and $S \sim (\mathbf{1}, \mathbf{1}, 0)$. In general, there are two types of the DFSZ model, distinguished by which of the two Higgs fields couples to the SM leptons. For the DFSZ-I model, the Yukawa term reads

$$\mathcal{L}_{\text{DFSZ-I}} = -Y_u\, \bar{q}_L\, u_R\, \tilde{H}_1 - Y_d\, \bar{q}_L\, d_R\, H_2 - Y_e\, \bar{l}_L\, e_R\, H_1 + \text{h.c.}\,, \tag{1.49}$$

while for the DFSZ-II model,

$$\mathcal{L}_{\text{DFSZ-II}} = -Y_u\, \bar{q}_L\, u_R\, \tilde{H}_1 - Y_d\, \bar{q}_L\, d_R\, H_2 - Y_e\, \bar{l}_L\, e_R\, H_2 + \text{h.c.}\,. \tag{1.50}$$

Therefore, in the Lagrangian

$$\begin{aligned}
\mathcal{L}_{\text{DFSZ}} \supset\ & |D_\mu H_1|^2 + |D_\mu H_2|^2 + |\partial_\mu S|^2 \\
& - (\bar{q}\, \tilde{H}_1\, \mathbf{\Gamma}_u\, u_R + \bar{q}\, H_2\, \mathbf{\Gamma}_d\, d_R + \bar{l}\, H_i\, \mathbf{\Gamma}_e\, e_R + \text{h.c.}) \\
& - m_1^2\, |H_1|^2 - m_2^2\, |H_2|^2 - \frac{\lambda_1}{2}\, |H_1|^4 - \frac{\lambda_2}{2}\, |H_2|^4 - \lambda_3\, |H_1|^2 |H_2|^2 \\
& - \lambda_4\, |H_1^\dagger H_2|^2 + \mu_S^2\, |S|^2 - \frac{\lambda_S}{2}\, |S|^4 - \lambda_{SH_1}\, |S|^2 |H_1|^2 - \lambda_{SH_2}\, |S|^2 |H_2|^2 \\
& - \lambda_{SH_{12}} \left[(H_1^\dagger H_2) S^2 + \text{h.c.} \right],
\end{aligned} \tag{1.51}$$

the H_i in the second line is H_1 for the DFSZ-I model and $H_i = \tilde{H}_2$ for DFSZ-II. In order to ensure the explicit breaking of the $U(1)_{\text{PQ}}$ symmetry, a potential for S needs to be added to the Lagrangian, for instance

$$\mathcal{L}_{\text{DFSZ}} \supset \frac{\kappa^2}{2}\, (S^2 + (S^*)^2)\,. \tag{1.52}$$

For the purpose of finding the effective Lagrangian that contains the ALP and the SM fields only, it is imperative to first write the fields H_1 and H_2 in terms of the SM Higgs and the heavy doublet Φ. This can be done by a rotation $R(\alpha)$ that obeys

$$\begin{pmatrix} H_1 \\ H_2 \end{pmatrix} = R(\alpha) \begin{pmatrix} H \\ \Phi \end{pmatrix} \quad \text{with} \quad R(\alpha)^T \begin{pmatrix} m_{11}^2 & m_{12}^2 \\ m_{12}^2 & m_{22}^2 \end{pmatrix} R(\alpha) = \begin{pmatrix} -\mu^2 & 0 \\ 0 & M_\Phi^2 \end{pmatrix}. \tag{1.53}$$

In the equation above, $m_{ii} = m_i^2 + \lambda_{SH_i} f^2/2$ for $i = 1, 2$ and $m_{12}^2 = \lambda_{SH_{12}} f^2/2$. For the SM Yukawa matrices, this implies

$$\boldsymbol{Y}_u = c_\alpha\, \mathbf{\Gamma}_u\,, \qquad \boldsymbol{Y}_d = s_\alpha\, \mathbf{\Gamma}_d\,, \qquad \boldsymbol{Y}_e = \begin{cases} c_\alpha\, \mathbf{\Gamma}_e & \text{DFSZ-I} \\ s_\alpha\, \mathbf{\Gamma}_e & \text{DFSZ-II} \end{cases}, \tag{1.54}$$

where c_α (s_α) are the cosine (sine) of the rotation angle α. As in the KSVZ model, the next step is to perform field redefinitions such that the ALP is removed from the potential,

$$\begin{aligned}
& H_1 \to e^{\frac{2ia}{f} s_\alpha^2}\, H_1\,, && H_2 \to e^{-\frac{2ia}{f} c_\alpha^2}\, H_2\,, \\
& u_R \to e^{\frac{2ia}{f} s_\alpha^2}\, u_R\,, && d_R \to e^{\frac{2ia}{f} c_\alpha^2}\, d_R\,, && e_R \to e^{-\frac{ia}{f} X_{H_i}}\, e_R\,,
\end{aligned} \tag{1.55}$$

and

$$e_R \to \begin{cases} e^{-\frac{2ia}{f}s_\alpha^2}\, e_R & \text{DFSZ-I} \\ e^{\frac{ia}{f}c_\alpha^2}\, e_R & \text{DFSZ-II} \end{cases} . \tag{1.56}$$

Applying these transformations and integrating out the heavy fields ρ and Φ at tree level with `Matchete` [68] results, up to dimension-six order, in

$$\begin{aligned}
\mathcal{L}_{\text{EFT}} = \mathcal{L}_{\text{SM}} &+ \frac{1}{2}(\partial_\mu a)^2 - \frac{1}{2}m_a^2\, a^2 + 3\,\frac{a}{f}\,\frac{\alpha_s}{4\pi}\, G^A_{\mu\nu}\tilde{G}^{\mu\nu\,A} + c_{BB}\,\frac{a}{f}\,\frac{\alpha_Y}{4\pi}\, B_{\mu\nu}\tilde{B}^{\mu\nu} \\
&+ c_u \frac{\partial_\mu a}{f}\, \bar{u}_R\gamma^\mu u_R + c_d \frac{\partial_\mu a}{f}\, \bar{d}_R\gamma^\mu d_R + c_e \frac{\partial_\mu a}{f}\, \bar{e}_R\gamma^\mu e_R \\
&+ 4\,\frac{m_a^2}{f^2}\,\frac{a^4}{4!} - \left(\frac{\lambda_{SH}}{M_\rho^2} - \frac{s_{2\alpha}^2}{f^2}\right)(\partial_\mu a)^2|H|^2 + \lambda_{SH}\frac{m_a^2}{M_\rho^2}\, a^2\,|H|^2 \\
&- \frac{C_{\psi H}}{M_\Phi^2}\left(t_\alpha\,[\boldsymbol{Y}_u]_{pr}\,[Q_{uH}]_{pr} - t_\alpha^{-1}\,[\boldsymbol{Y}_d]_{pr}\,[Q_{dH}]_{pr} - \eta_\alpha\,[\boldsymbol{Y}_e]_{pr}\,[Q_{eH}]_{pr} + \text{h.c.}\right) \\
&- \frac{[\boldsymbol{Y}_u^*]_{sr}\,[\boldsymbol{Y}_u]_{pt}\,t_\alpha^2}{M_\Phi^2}\left(\frac{1}{6}\,[Q_{qu}^{(1)}]_{prst} + [Q_{qu}^{(8)}]_{prst}\right) \\
&- \frac{[\boldsymbol{Y}_d^*]_{sr}\,[\boldsymbol{Y}_d]_{pt}\,t_\alpha^{-2}}{M_\Phi^2}\left(\frac{1}{6}\,[Q_{qd}^{(1)}]_{prst} + [Q_{qd}^{(8)}]_{prst}\right) \\
&- \frac{[\boldsymbol{Y}_e^*]_{sr}\,[\boldsymbol{Y}_e]_{pt}\,\eta_\alpha^2}{2M_\Phi^2}\,[Q_{le}]_{prst} - \frac{1}{M_\Phi^2}\Big([\boldsymbol{Y}_u]_{pr}\,[\boldsymbol{Y}_d]_{st}\,[Q_{quqd}^{(1)}]_{prst} \\
&- [\boldsymbol{Y}_u]_{st}\,[\boldsymbol{Y}_e]_{pr}\,t_\alpha\eta_\alpha\,[Q_{lequ}^{(1)}]_{prst} - [\boldsymbol{Y}_d^*]_{st}\,[\boldsymbol{Y}_e]_{pr}\,t_\alpha^{-1}\eta_\alpha\,[Q_{ledq}]_{prst} + \text{h.c.}\Big) \\
&+ \frac{C_H}{M_\Phi^2}\,Q_H - \frac{\lambda_{SH}^2 f^2}{2M_\rho^4}\,Q_{H\Box}\,,
\end{aligned} \tag{1.57}$$

where $m_a^2 = 2\kappa^2$ and the dimension-six coefficients in and below the fourth line once more correspond to operators in the Warsaw basis. While the exact relations between the original scalar-potential parameters and the dimension-six ones that appear in (1.57) are not relevant for this work, it is crucial to note that, with $\eta_\alpha = \tan\alpha \equiv t_\alpha$ for DFSZ-I and $\eta_\alpha = t_\alpha^{-1}$ for DFSZ-II, all dimension-five ALP couplings in the two models are now either fixed or depend solely on the angle α. This is shown in detail in Table 1.2.

ALP coupling	KSVZ	DFSZ-I	DFSZ-II
c_u	0	$-2s_\alpha$	$-2s_\alpha$
c_d	0	$-2c_\alpha$	$-2c_\alpha$
c_e	0	$2s_\alpha$	$-2c_\alpha$
c_{GG}	$-\frac{1}{2}$	3	3
c_{WW}	0	0	0
c_{BB}	$-\frac{1}{3}$	2	8

Table 1.2.: ALP couplings in the KSVZ model with $U(1)_{\text{PQ}}$ charges $X_S = 1$, $X_{Q_L} = 1$ and $X_{Q_R} = 0$ and the DFSZ-I and DFSZ-II models at the scale Λ.

1.7. ALP–SMEFT Interference

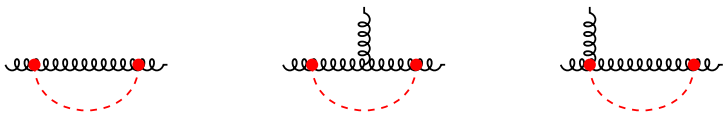

Figure 1.1.: One-loop Feynman diagrams yielding the ALP contribution to the Wilson coefficient of the dimension-six Weinberg operator. The red dashed line indicates the ALP.

While it is straightforward to see that integrating out a heavy particle from a theory generates higher dimensional operators from the matching computation, the situation is far more subtle for light particles. This mechanism, however, is one of the most crucial concepts of this thesis. It relies on the fact that light new states such as the ALP with non-renormalizable interactions with the SM yield a non-trivial RG flow into the SMEFT Wilson coefficients in a process that is independent of the ALP mass. To explain this phenomenon in more detail, consider the one-loop diagrams in Figure 1.1. The amplitude of these Feynman graphs is given by

$$\mathcal{A}(gg(g)) = -\frac{C_{GG}^2}{\epsilon}\,[4g_s\,\langle Q_G\rangle + \dots] + \text{finite}\,, \tag{1.58}$$

where $\langle Q_G\rangle$ denotes the matrix element of the dimension-six Weinberg operator $Q_G = f^{abc}\,G_\mu^{a,\nu}G_\nu^{b,\rho}G_\rho^{c,\mu}$. The dots refer to matrix elements of other operators that are not needed for the illustration of the procedure. In order to remove the $1/\epsilon$ pole multiplying $\langle Q_G\rangle$, the *bare* Wilson coefficient of the Weinberg operator, $C_{G,0}$, needs to have the structure

$$C_{G,0} \ni \frac{4g_s}{(4\pi f)^2}\,C_{GG}^2\left(\frac{1}{\epsilon} + \ln\frac{\mu^2}{M^2} + \dots\right)\,, \tag{1.59}$$

where the dots denote a finite contribution and M is the mass scale of the UV theory. The crucial term, the logarithm of μ^2, arises generically from the loop-integral. When the $1/\epsilon$ pole is removed in order to obtain the renormalized Wilson coefficient from the bare quantity, the μ-dependence remains in the expression, which leads to

$$\frac{d}{d\ln\mu}C_G(\mu) \ni \frac{8}{(4\pi f)^2}\,C_{GG}^2 \equiv \frac{S_G}{(4\pi f)^2}\,. \tag{1.60}$$

In essence, the term in (1.60) parametrizes an inhomogeneous source term in the RG evolution equation of the dimension-six Weinberg operator. In other words: even if the Wilson coefficient C_G is zero above Λ, the presence of the ALP *necessarily* generates a non-zero term, as long as its coupling to gluons, C_{GG}, is non-zero. Via RG flow to lower scales, this effect gets enhanced and by mixing effects with other SMEFT Wilson coefficients it also affects further coefficients. Certainly, C_G is not the only coefficient that gets generated by this mechanism and the whole coupled set of RG equations modified by the inhomogeneous source terms S_i is given by

$$\frac{d}{d\ln\mu}C_i^{\text{SMEFT}} - \gamma_{ji}^{\text{SMEFT}}\,C_j^{\text{SMEFT}} = \frac{S_i}{(4\pi f)^2} \quad (\text{for } \mu < 4\pi f)\,, \tag{1.61}$$

where $\gamma_{ji}^{\text{SMEFT}}$ is the one-loop anomalous dimension matrix of the minimal SMEFT basis and has been found in [69–72]. The full set of inhomogeneous source terms S_i has been obtained as a part of the author's Master's thesis and is published in [35]. An important consequence of this *ALP–SMEFT interference* is that in the presence of the ALP, the correct low-energy effective theory is given by

$$\mathcal{L}_{\text{eff}} = \frac{1}{2}(\partial_\mu a)(\partial^\mu a) - \frac{m_a^2}{2}a^2 + \mathcal{L}_{\text{SM+ALP}} + \mathcal{L}_{\text{SMEFT}}\,, \tag{1.62}$$

with $\mathcal{L}_{\text{SM+ALP}}$ containing all operators parametrizing the SM-ALP interactions.

Chapter 2: A Global SMEFT Analysis of Axion-Like Particle Interactions

In the hunt for a new particle, the most straightforward approach is to search for a direct signal in experimental data. In the case of the ALP, this has been pursued for instance with cosmological [20, 21] and astrophysical [22, 23] observations, as well as collider [24–29] and flavor [19, 30–34] experiments, and these studies have placed stringent constraints on the ALP parameter space. However, the bounds come with conceptual limitations. Many rely on assumptions about ALP properties, such as its lifetime, production mechanism, and decay channels. Additionally, fits to experimental data often assume that only a single ALP–SM coupling is nonzero at the scale Λ. This hypothesis, which would require fine-tuned UV models, does not hold for UV-complete frameworks like the KSVZ and DFSZ models introduced in Section 1.6. This chapter presents an alternative approach to ALP searches via a global, model-independent, indirect analysis based on the *ALP–SMEFT interference*. Specifically, in a scenario where the ALP is the only new-physics particle between Λ and the experimental scale, the ALP-induced dimension-six Wilson coefficients are evolved via RG running down to the experimental scale μ_{exp}. Since these low-scale SMEFT coefficients can be expressed purely in terms of ALP couplings, existing tight constraints on the SMEFT can be translated into bounds on ALP–SM couplings. This procedure is largely ALP-model independent and nearly insensitive to the ALP mass. Nevertheless, this framework yields constraints that are competitive with or even stronger than direct bounds in the GeV to TeV ALP mass range.
This chapter is structured as follows: Section 2.1 describes how the SMEFT RG evolution equations are solved in the presence of the ALP. Section 2.2 outlines the input data sets for the global fit, followed by a presentation of the results in Section 2.3. Finally, Section 2.4 applies the framework to the KSVZ and DFSZ models, before concluding in Section 2.5.

This chapter is based on

[67] **A global analysis of axion-like particle interactions using SMEFT fits**
A. Biekötter, J. Fuentes-Martín, A. M. Galda and M. Neubert
JHEP **09** (2023), 120, [arXiv:2307.10372].

2.1. Solutions of the ALP–SMEFT RG Evolution Equations

Solving the full set of coupled differential equations including the SM, ALP and SMEFT parameters is a very complex, non-trivial task for which no analytical solution exists. Therefore, one is in general forced to simplify the system by employing approximations or imposing assumptions to make the problem tractable. Another option is to choose a numerical framework, which in principle could allow for an exact solution. Given the complexity of the set of equations, this, however, remains computationally

unfeasible. In order to obtain low-energy expressions for the SMEFT coefficients as needed for a global analysis of ALP coefficients, a numerical approach is used where higher orders in the EFT expansion are neglected. To explain the procedure more systematically, it is convenient to write down the coupled differential RG evolution equations in an explicit tensor notation for the dimension-four, dimension-five ALP and dimension-six SMEFT Wilson coefficients as[1]

$$\begin{aligned}
\frac{dC_a^{(4)}(\mu)}{d\ln\mu} &= \gamma_{ba}^{(4)}\big(\boldsymbol{C}^{(4)},\boldsymbol{C}^{(5)},\boldsymbol{C}^{(6)}\big)\, C_b^{(4)}(\mu)\,,\\
\frac{dC_\alpha^{(5)}(\mu)}{d\ln\mu} &= \gamma_{\beta\alpha}^{(5)}\big(\boldsymbol{C}^{(4)}\big)\, C_\beta^{(5)}(\mu)\,,\\
\frac{dC_i^{(6)}(\mu)}{d\ln\mu} &= \gamma_{ji}^{(6)}\big(\boldsymbol{C}^{(4)}\big)\, C_j^{(6)}(\mu) + \gamma_{i\alpha\beta}^{\text{ALP–SMEFT}}\big(\boldsymbol{C}^{(4)}\big)\, C_\alpha^{(5)}(t)\,[C_\beta^{(5)}(\mu)]^*\,.
\end{aligned} \tag{2.1}$$

In the equations above, a factor of $1/(16\pi^2)$ is included in the definitions of the anomalous dimension matrices $\gamma^{(D)}$ of the coefficients of operator dimension D in order to simplify the notation. Greek indices are introduced for the ALP couplings, while dimension-four and dimension-six couplings are dressed with roman letters. The bold face of the coefficients indicates that they are collected into vectors. Since the inhomogeneous ALP–SMEFT source terms S_i defined in (1.61) are always proportional to exactly two ALP couplings, they are parametrized as the tensor $\gamma_{i\alpha\beta}^{\text{ALP–SMEFT}}$ in (2.1). The dimension-four coefficients $C^{(4)}$ are not the SM couplings, as the presence of non-SM operators modifies their scale evolutions. However, since the additional contributions start at $\mathcal{O}(\Lambda^{-2})$, it is a reasonable approximation to use $\boldsymbol{C}^{(4)}(\mu) = \boldsymbol{C}^{\text{SM}}(\mu) + \mathcal{O}(\Lambda^{-2})$, such that the set of equations becomes

$$\begin{aligned}
\frac{dC_\alpha^{(5)}(\mu)}{d\ln\mu} &= \gamma_{\beta\alpha}^{(5)}\big(\boldsymbol{C}^{(\text{SM})}\big)\, C_\beta^{(5)}(\mu)\,,\\
\frac{dC_i^{(6)}(\mu)}{d\ln\mu} &= \gamma_{ji}^{(6)}\big(\boldsymbol{C}^{(\text{SM})}\big)\, C_j^{(6)}(\mu) + \gamma_{i\alpha\beta}^{\text{ALP–SMEFT}}\big(\boldsymbol{C}^{(\text{SM})}\big)\, C_\alpha^{(5)}(\mu)\,[C_\beta^{(5)}(\mu)]^*\,.
\end{aligned} \tag{2.2}$$

The solution to these equations can now be written in a closed form,

$$\begin{aligned}
C_\alpha^{(5)}(\mu_f) &= U_{\alpha\beta}^{(5)}(\mu_f,\mu_0)\, C_\beta^{(5)}(\mu_0)\,,\\
C_i^{(6)}(\mu_f) &= U_{ij}^{(6)}(\mu_f,\mu_0)\, C_j^{(6)}(\mu_0) + U_{i\alpha\beta}^{\text{ALP–SMEFT}}(\mu_f,\mu_0)\, C_\alpha^{(5)}(\mu_0)\,[C_\beta^{(5)}(\mu_0)]^*\,,
\end{aligned} \tag{2.3}$$

where μ_f and μ_0 are the final and initial renormalization scales. The evolution matrices $U^{(5)}$ and $U^{(6)}$ are given by the matrix exponentials

$$\begin{aligned}
U^{(D)}(t_f,t_0) &\equiv \mathcal{T}\exp\left[\int_{t_0}^{t_f} dw\,\big[\gamma^{(D)}\big(\boldsymbol{C}^{\text{SM}}(w)\big)\big]^T\right],\\
&\equiv \mathbb{1} + \sum_{i=1}^{\infty}\bigg(\int_{t_0}^{t_f} dw_1 \int_{t_0}^{w_1} dw_2 \cdots \int_{t_0}^{w_{n-1}} dw_n\\
&\qquad\qquad \times \big[\gamma^{(D)}\big(\boldsymbol{C}^{\text{SM}}(w_1)\big)\big]^T \ldots \big[\gamma^{(D)}\big(\boldsymbol{C}^{\text{SM}}(w_n)\big)\big]^T\bigg)\,,
\end{aligned}$$

[1] In this chapter, the convention employed for the covariant derivative differs by a sign from the one in [35].

$$U^{\text{ALP–SMEFT}}_{i\alpha\beta}(t_f,t_0) \equiv U^{(6)}_{ij}(t_f,t_0)\times \int_{t_0}^{t_f} dw \big[U^{6}_{jk}(t_0,w)\,\gamma^{\text{ALP–SMEFT}}_{k\rho\sigma}\big(\boldsymbol{C}^{\text{SM}}(w)\big) \times U^{(5)}_{\rho\alpha}(w,t_0)\,[U^{(5)}(w,t_0)_{\sigma\beta}]^*\big]\,, \tag{2.4}$$

where $t_i \equiv \ln \mu_i$ and $\mathcal{T}$ denotes the t-ordering of the exponential. While the numerical evaluation of the expressions in (2.4) remains computationally demanding, the crucial advantage is given by the fact that these matrices are initial-condition independent. Thus, it suffices to evaluate the equations once for a set of initial scales, and to interpolate the results. The actual evaluation of concrete low-scale coefficients given a set of coefficients at a high scale Λ is then a straightforward multiplication of the input vector with the previously evaluated evolution matrix $U^{(D)}$ and/or $U^{\text{ALP–SMEFT}}$.

2.2. Input Data Sets and Translation to ALP Coefficients

The input data sets used for the global analysis of ALP coefficients from SMEFT fits can be split into three categories, for which linear parametrizations in terms of SMEFT Wilson coefficients exist. In detail, predictions are taken from

- **Higgs-data**: Expressions in the Higgs sector are taken from [73], as well as references therein. Measurements in this data set constrain the SMEFT coefficients C_{eH}, C_H, C_{HB}, $C_{H\Box}$, C_{Hd}, C_{HD}, C_{He}, C_{HG}, $C^{(1)}_{H\ell}$, $C^{(3)}_{H\ell}$, $C^{(1)}_{Hq}$, $C^{(3)}_{Hq}$, C_{Hu}, C_{HW}, C_{HWB}, $C_{\ell\ell}$, C_{uG}, C_{uH}, C_G and C_W.
- **Top-data**: Expressions from top data are taken from the `fitmaker` database [74], as well as references therein, from which constraints on the coefficients $C^{(3)}_{Hq}$, $C^{(1)}_{qq}$, $C^{(3)}_{qq}$, C_{uW}, C_{HD}, $C^{(3)}_{H\ell}$, C_{HWB}, $C_{\ell\ell}$, C_{uG}, C_{Hd}, C_{He}, $C^{(1)}_{H\ell}$, $C^{(1)}_{Hq}$, C_{Hu}, C_{uB}, C_W, C_G, $C^{(8)}_{qd}$, $C^{(8)}_{qu}$, $C^{(8)}_{ud}$, C_{uu} are obtained.
- **Low-energy data**: The χ^2 function for low-energy experiments provided in [75] and [76] contains tree-level SMEFT predictions for quark pair production in e^+e^- collisions, ν-scattering on electron and nucleon targets, atomic parity violation, as well as pion, neutron, nucleon and τ-decays. These observables are sensitive to the SMEFT coefficients C_{ed}, C_{ee}, C_{eu}, C_{Hd}, C_{HD}, C_{He}, $C^{(1)}_{H\ell}$, $C^{(3)}_{H\ell}$, $C^{(1)}_{Hq}$, $C^{(3)}_{Hq}$, C_{Hu}, C_{Hud}, C_{HWB}, $C_{\ell d}$, $C_{\ell e}$, $C_{\ell edq}$, $C^{(1)}_{\ell equ}$, $C^{(3)}_{\ell equ}$, $C_{\ell\ell}$, $C^{(1)}_{\ell q}$, $C^{(3)}_{\ell q}$, $C_{\ell u}$, C_{qe}.

More details on the observables taken into account can be found in Appendix 2.7.B. The numerical input required for the data sets is G_F, α and M_Z. The Venn diagram relating the constraints for the SMEFT coefficients to the three data sets is shown in Figure 2.1. In order to obtain limits on the ALP coefficients, the total χ^2 function from all three data sets,

$$\chi^2(C_i) = \Big[\vec{d} - \vec{p}(C_i)\Big]^T \boldsymbol{V}^{-1} \Big[\vec{d} - \vec{p}(C_i)\Big]\,, \tag{2.5}$$

with experimental data $\vec{d}$, predictions $\vec{p}$ and covariance matrix $\boldsymbol{V}$, is minimized. While for the low-energy data set the χ^2-function is given in the supplemental material of

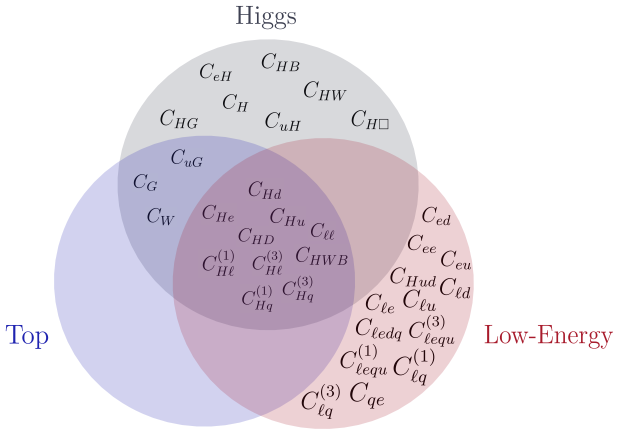

Figure 2.1.: Venn diagram relating the constraints for the SMEFT coefficients to the Higgs, top and low-energy data sets.

[75, 76] and includes all flavor indices, it has to be constructed explicitly for the Higgs- and top-data. To compensate for the fact that some parametrization assume flavor universality, missing flavor indices are replaced by third-generation ones wherever quark-gluon or quark-Higgs SMEFT operators are involved, which concerns $C_{uG} \to [C_{uG}]_{33}$ and $C_{qH} \to [C_{qH}]_{33}$ for $q = u, d$. In all other cases, where first- and second-generations dominate, the the index is set to two, i.e. $C_x \to [C_x]_{22}$.
In the next step, the χ^2-function given purely in terms of SMEFT coefficients needs to be translated to a function of ALP couplings. Remaining model-agnostic, possible matching terms from integrating out the heavy new states are neglected, such that all SMEFT Wilson coefficients that contribute to the data sets at a lower scale $\mu_{\text{exp}} \ll \Lambda$ are only generated via RG evolution from the presence of the inhomogeneous ALP source terms in (1.61). Therefore, solution (2.3) simplifies to

$$C_i^{(6)}(\mu_{\text{exp}}) = U_{i\alpha\beta}^{\text{ALP–SMEFT}}(\mu_{\text{exp}}, \Lambda)\, C_\alpha^{(5)}(\Lambda)\, [C_\beta^{(5)}(\Lambda)]^*\,, \tag{2.6}$$

yielding a direct relation between each low-scale SMEFT Wilson coefficient and the high-scale ALP couplings. This equation implicitly includes the only ALP mass-dependence of the framework: If the experimental scale μ_{exp} in the equation above is lower than the ALP mass, the inhomogeneous new-physics contributions to the RG evolution need to be removed below m_a. This is done via a tree-level matching, after which the pure SMEFT running is employed between m_a and μ_{exp}. If, on the other hand, $m_a < \mu_{\text{exp}}$, the system is evolved down to the scale associated with the observable, e.g. $\mu_{\text{exp}} \sim m_h + 2m_t$ for $t\bar{t}h$ production, without modification.

2.3. Global Fit Results

This section presents the results of the global ALP parameter fit from SMEFT constraints. The individual bounds for the six dimension-five couplings are shown in red in Figure 2.2, together with the results from a one-parameter fit depicted in gray. To obtain these limits, the symmetry breaking scale is taken as $\Lambda = 4\pi\,\text{TeV}$. Certainly, the most prominent feature in the plot is the exclusion of a vanishing ALP-gluon coupling C_{GG} that in principle could be interpreted as a signal of new physics. When

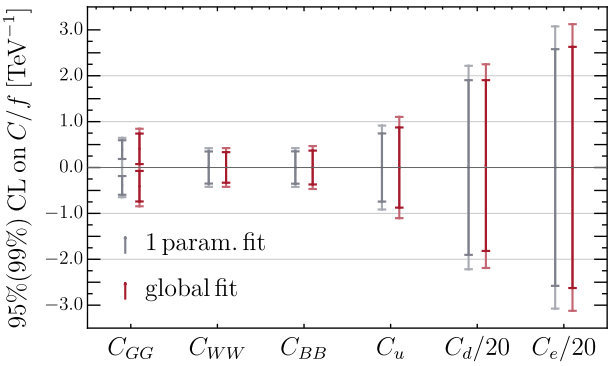

Figure 2.2.: Bounds on ALP couplings at 95% (dark) and 99% (light) confidence limit as obtained from SMEFT constraints, translated via the *ALP–SMEFT interference*. The gray limits are obtained from a one-parameter fit, where only one coupling is constrained at a time, while the red limits correspond to a global fit. The symmetry breaking scale is set to $\Lambda = 4\pi$ TeV.

reconsidering the input data in more detail, it turns out that this effect is caused by an anomaly in the CMS simplified template cross section for $h \to ZZ$ [77], where three correlated bins favor non-zero values for C_{uH} and C_{uG}. This anomaly vanishes at 99% confidence level, as the light lines for C_{GG} in the figure indicate.
Returning to a more general description of the fit results, $\mathcal{O}(1)$ bounds are obtained for the bosonic couplings C_{GG}, C_{WW} and C_{BB} as well as C_u, while the limits on C_d and C_e are weaker by more than an order of magnitude and still allow for values up to $\mathcal{O}(50)$. The global fit results coincide roughly with the one-parameter ones for C_{WW}, C_{BB}, C_e and C_d, but are weaker by $\sim 18\%$ for C_u and by $\sim 25\%$ for C_{GG}.

2.3.1. Leading-Log Approximation

To better understand the quantitative impact of the resummation of logarithms on the bounds, it is instructive to compare the one-parameter results to those obtained using a leading-logarithmic approximation. In this case, the solutions of the SMEFT RG equations simplify to

$$C_i^{\text{SMEFT}}(\mu) \approx \gamma_{i\alpha\beta}^{\text{SMEFT-ALP}}(\Lambda)\, C_\alpha^{(5)}(\Lambda)\, [C_\beta^{(5)}(\Lambda)]^*\, \ln\frac{\mu}{\Lambda}\,, \tag{2.7}$$

and the list of low-energy observables in this leading-logarithmic approximation can be found in Appendix 2.7.A. A schematic comparison of the bounds obtained in the leading-logarithmic (LL) and the fully resummed scenario is depicted in the upper graph of Figure 2.3. While the four coefficients C_{WW}, C_{BB}, C_d and C_e get similar constraints in both methods, this is not the case for C_{GG} and C_u. On general grounds, this can be explained as follows: When truncating the resummation at LL order, essentially only bounds on SMEFT coefficients that are directly sourced by the ALP can contribute to limits on the $C^{(5)}$. Therefore, if a SMEFT coefficient is tightly constrained but has a vanishing ALP source term, then it improves the bounds on the ALP coefficients only starting at next-to-leading logarithmic order. It is thus important to deduce the most relevant SMEFT coefficients that contribute to the bounds on C_u and C_{GG} in more detail:

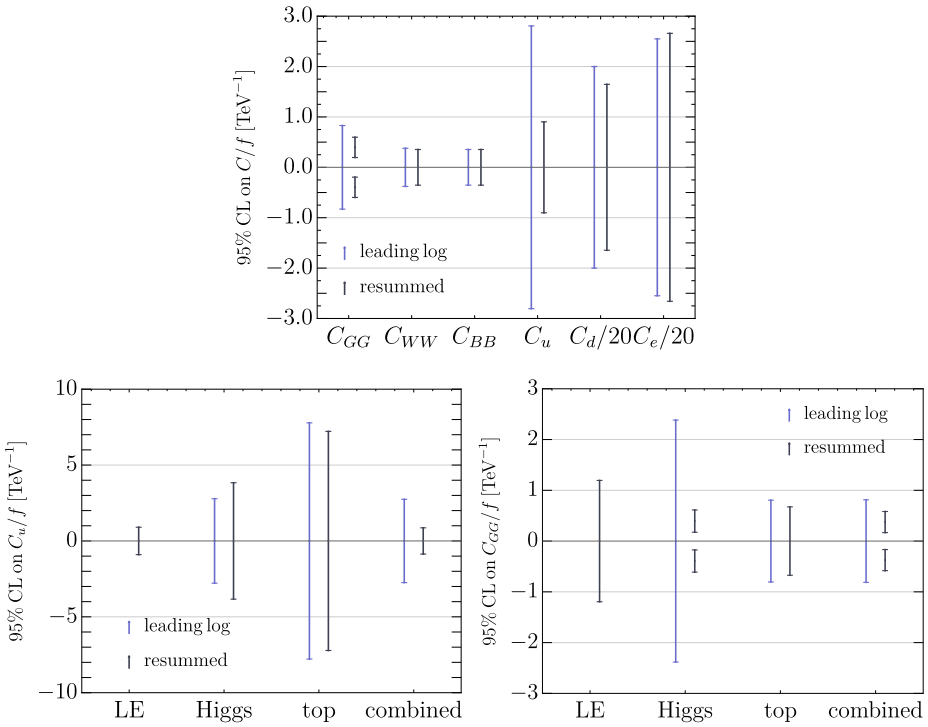

Figure 2.3.: Upper row: Bounds on the ALP-couplings from a one-parameter fit using a leading-logarithmic approximation (blue lines) and the exact, resummed results (black lines). Lower row: Bounds obtained from individual data sets for the coefficients C_u (left) and C_{GG} (right) for the same scenarios.

- The individual bounds obtained from the three different data sets for C_u are shown in the left graph in the second row of Figure 2.3. While Higgs- and top-contributions are rather similar, the leading-logarithmic approximation obtained from low-energy data does not produce a bound on the coupling. Further analyzing this effect reveals that the absence of the strong constraint from C_{HD} is responsible for this discrepancy. Explicitly, the RG equation for C_{HD} reads, in the limit where all contributions proportional to $\alpha_i \neq \alpha_s$ and the Yukawa couplings except for $\alpha_t \equiv y_t^2/(4\pi)$ are neglected [71, 72],

$$\frac{d}{d\ln\mu} C_{HD} = \left(\frac{3\,\alpha_t}{\pi} + \frac{3\,\lambda}{8\pi^2}\right) C_{HD} + \frac{6\,\alpha_t}{\pi}\,[C_{Hq}^{(1)}]_{33} - \frac{6\,\alpha_t}{\pi}\,[C_{Hu}]_{33}\,. \tag{2.8}$$

  Since there is no ALP-induced source term in the equation, these limits do not get translated to ALP-bounds at leading-logarithmic order. The situation changes when non-trivial RG flow of other SMEFT coefficients is taken into account. At lowest order, the relevant terms are [35]

$$\frac{d}{d\ln\mu}\,[C_{Hq}^{(1)}]_{33} = -\pi\,\alpha_t\,C_u^2 + \cdots\,, \qquad \frac{d}{d\ln\mu}\,[C_{Hu}]_{33} = 2\pi\,\alpha_t\,C_u^2 + \cdots\,, \tag{2.9}$$

  which yields the two-loop, lowest-logarithmic solution

$$C_{HD}(\mu) = -9\,\alpha_t^2\,C_u^2\,\ln^2\frac{\mu}{\Lambda}\,, \tag{2.10}$$

that is primarily responsible for the bound shown for the resummed result.

- For the ALP-gluon coupling C_{GG}, the situation is similar to the one of C_u. Again, there is no bound at leading-logarithmic order from the low-energy data set. As these observables only play a minor role in the generation of the bound, the main difference arises from the weaker bound obtained from the Higgs data. In particular, gluon fusion processes put strong bounds on the SMEFT couplings $[C_{uG}]_{33}$ and C_{HG}, whose lowest-logarithmic solutions start at two- and three-loop order, respectively, and are given by

$$[C_{uG}]_{33}(\mu) \supset -\frac{25\, g_s\, y_t\, \alpha_s}{\pi}\, C_{GG}^2\, \ln^2 \frac{\mu}{\Lambda}\,, \quad C_{HG}(\mu) \supset \frac{100\, \alpha_s^2\, \alpha_t}{3}\, C_{GG}^2\, \ln^3 \frac{\mu}{\Lambda}\,, \tag{2.11}$$

when taking into account the running of C_u.

2.3.2. Comparison with Direct Bounds

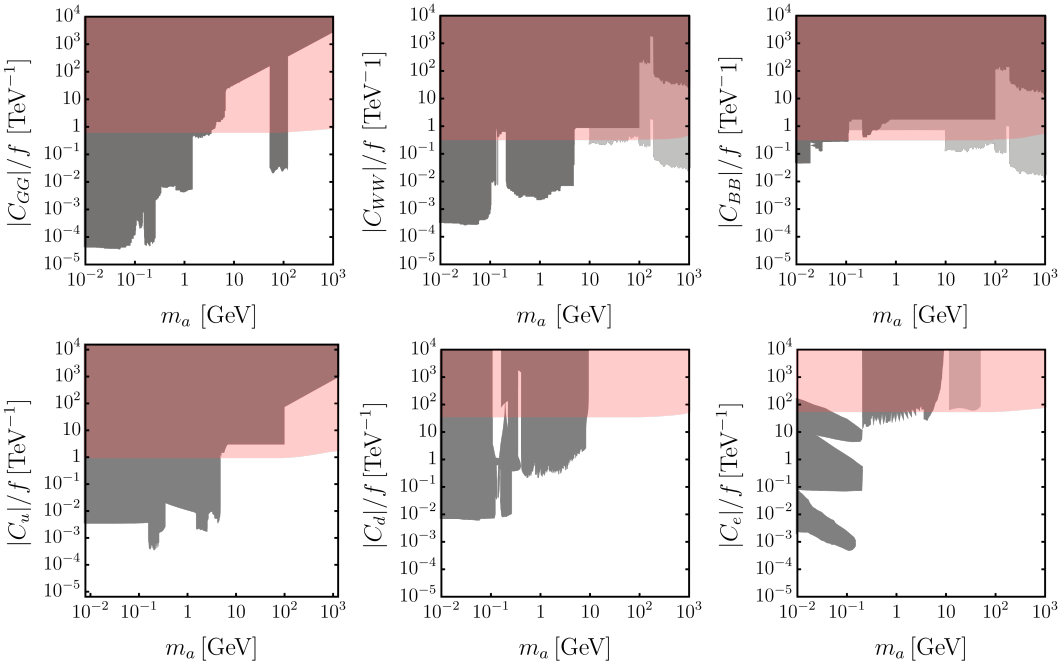

Figure 2.4.: Comparison of the 95% CL indirect bounds as obtained from the global fit based on the *ALP–SMEFT interference* (red) with direct bounds from collider, flavor and beam dump experiments, as well as supernova bounds (dark gray). In the derivation of the direct bounds, only one ALP coupling is assumed to be non-zero at a time. In addition, strongly model-dependent bounds are depicted in light gray as described in the main text. For the ALP-gluon coupling C_{GG}, the lower bound at 95% CL is not shown as it disappears at 99% CL.

To quantify the significance of the indirect, global *ALP–SMEFT interference* bounds presented in Section 2.3, these limits are compared to direct constraints, primarily from flavor [34] and collider [28] experiments, in Figure 2.4 for ALP masses of order

$\mathcal{O}$(GeV). Two important aspects can be inferred from the figure: Firstly, the indirect bounds exhibit a nearly flat behavior as a function of m_a. The slight weakening of the bounds at higher masses arises from integrating out the ALP when the scale m_a is crossed before running down to the experimental scale. Secondly and most importantly, indirect bounds can indeed compete with or even exceed the direct limits in the shown mass range. In a more detailed description, the strongest constraints between $m_a = 10^{-2}\,\text{GeV}$ and $m_a = 10^{3}\,\text{GeV}$ for each coupling are as follows:

- **C_{GG}:** For the ALP coupling to gluons, flavor bounds dominate for $m_a \lesssim \mathcal{O}(1\,\text{GeV})$. Above this scale, the indirect bounds from the *ALP–SMEFT interference* exceed the direct ones except for $m_a \sim 100\,\text{GeV}$, where LHC multijet constraints [78] outperform the indirect limits.

- **C_{BB} and C_{WW}:** Again, flavor bounds pose the strongest constraints on both couplings for low ALP masses. While the indirect ALP–SMEFT limits become important around $\mathcal{O}(0.1\,\text{GeV})$ for C_{BB}, this is only the case around $\mathcal{O}(10\,\text{GeV})$ for C_{WW}. The mass-independent direct bounds that restrict the couplings up to $m_a \sim 100\,\text{GeV}$ stem from non-resonant ALP contributions to vector-boson scattering [79]. Additionally, the light gray regions show collider constraints on the photon coupling $C_{\gamma\gamma} = s_w^2\, C_{WW} + c_w^2\, C_{BB}$, where s_w (c_w) is the sine (cosine) of the weak mixing angle [29]. These bounds originally assume an ALP decay predominantly to photons, which, however, is not likely for $m_a > m_Z$, where further decays become possible, for instance $a \to Z\gamma$ [80]. As a consequence, the same bounds are also shown in dark gray, but with the branching ratio rescaled by a factor of 10^{-3}. It is important to note that strong direct bounds derived from non-resonant gluon-fusion ALP production exist, however, they depend on the product $C_{ZZ}\, C_{GG}$ or $C_{\gamma\gamma}\, C_{GG}$. In particular, the analyses in [81] and [82] yield $|C_{ZZ}\, C_{GG}|/f^2 < 4 \times 10^{-2}$ TeV^{-2} and $|C_{\gamma\gamma}\, C_{GG}|/f^2 < 5 \times 10^{-3}$ TeV^{-2}, respectively. Since the direct bounds shown in the plots are restricted to one non-zero coupling at a time, these results are not included.

- **C_u and C_d:** The direct bounds constraining these two couplings in the mass range shown are obtained from flavor data. In both cases, the indirect *ALP–SMEFT interference* limits become important at around $m_a \sim \mathcal{O}(10\,\text{GeV})$. The additional gray region in the plot for C_u for $m_a \leq 100\,\text{GeV}$ results from LHC $t\bar{t}$ searches [83].

- **C_e:** The direct bounds for C_e up to an ALP mass of $\mathcal{O}(1\,\text{GeV})$ stem from SN1987A supernova observations [84], as well as beam dump experiments at SLAC [85]. For higher masses up to roughly 10 GeV, bounds from flavor and dark photon searches at BaBar are important [86]. The light gray region results from LHC $h \to a\mu\bar{\mu}$ searches [87], which, however, assume that the ALP decays only to muons. When other decays are taken into account as well, for instance to τ leptons, the bound weakens severely. Apart from the region excluded by BaBar, the indirect bounds exclude previously unconstrained parameter space, both for ALPs with masses below 10^{-1} GeV, as well as above 50 GeV.

In short, the indirect bounds for all ALP couplings contribute new constraints to regions in the parameter space that has not been covered by direct bounds before.

While in particular for higher ALP masses above 100 GeV they become relevant for all couplings, also parameters from low-mass ALPs get constrained, most prominently C_e.

2.4. Translation to UV-complete ALP Models

The framework to obtain indirect bounds from the *ALP–SMEFT interference* can also be applied to UV-complete axion models. There are two main differences with respect to the model-independent bounds: First, there are fixed relations among the dimension-five ALP–SM couplings and second, there are non-zero dimension-six SMEFT coefficients from the matching relations at the scale Λ that can modify the limits found above. Concretely, in this section, bounds for the KSVZ and the DFSZ models, as introduced in Section 1.6, are derived.

2.4.1. KSVZ Model

In the KSVZ model, only ALP-gauge boson couplings are non-zero at the scale of global symmetry breaking Λ, but the SMEFT operator $Q_{H\Box}$ arises from the tree-level matching computation independently of the choice of the fermion charges. The operators Q_{dH}, $Q_{Hq}^{(1)}$ and $Q_{Hq}^{(3)}$ appear when the portal coupling y_p in (1.42) is present. Considering the coefficient in front of the operator $Q_{H\Box}$ in (1.47), the constraints on the SMEFT Wilson coefficient $C_{H\Box}$ can directly be translated onto a bound for a combination of the ALP decay constant and parameters of the scalar potential as $|\lambda_S^2 f/\lambda_{SH}| > 2.8$ TeV. While the values of the ALP-gauge boson couplings are fixed for concrete realizations of the KSVZ model as shown in Table 1.2, keeping them general and profiling over the SMEFT coefficients $C_{H\Box}$, C_{dH}, $C_{Hq}^{(1)}$ and $C_{Hq}^{(3)}$ yields results that are in agreement with those presented in Figure 2.2 and remain within a 10% deviation of the one-parameter limits. Finally, the portal coupling y_p gets constrained as $|y_q/M_Q| < 0.1\,\text{TeV}^{-1}$ when assuming a flavor universal scenario.

2.4.2. DFSZ Model

In the DFSZ model, the ALP–SM couplings are all expressed in terms of a single parameter, the angle α. In addition, eleven dimension-six SMEFT operators arise in the effective Lagrangian after the matching at the scale Λ, see (1.57). In order to find limits on the α-f parameter space, two cases are considered: First, a scenario in which the Wilson coefficients of $Q_{\psi H}$, $Q_{H\Box}$ and Q_H are assumed to be suppressed due to small parameters in the scalar potential and second, a scenario in which these Wilson coefficients are profiled over, but including the restriction $|C_{\psi H}|, |C_{H\Box}|\,|C_H| < 1$. Denoting these scenarios by S_1 and S_2, respectively, and given that the fit results are nearly identical for the DFSZ-I and DFSZ-II models, the bounds can be found in Figure 2.5. As can be seen from the plot, the exclusion regions generated by S_1 and S_2 mostly overlap, but the limits from S_1 are slightly stronger for all values of α. The main contributions to the constraints arise from the Wilson coefficients $Q_{qu}^{(1)}$ and $Q_{qu}^{(8)}$, which are generated by the matching computation. In more detail, strong restrictions on these parameters are obtained from RG evolution into C_{HD}, $C_{Hq}^{(1)}$ and $C_{Hq}^{(3)}$, which

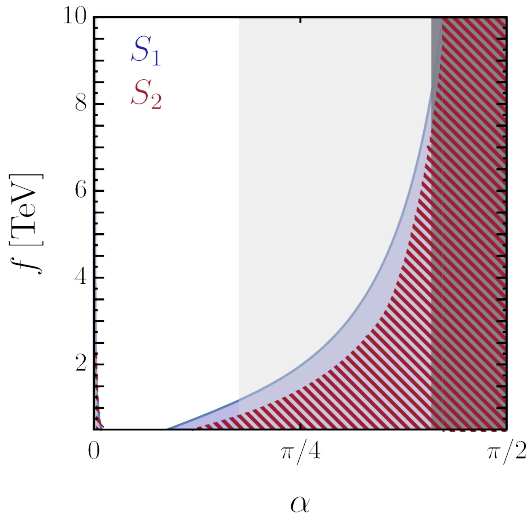

Figure 2.5.: Excluded parameter space derived from the *ALP–SMEFT interference* for the DFSZ model from a scenario in which the scalar potential parameters are suppressed (S_1) and from profiling over the SMEFT Wilson coefficients (S_2). The dark gray region is excluded by the perturbative unitarity bound $\Gamma_u^{33} \lesssim 3$ [88], while the light gray region shows $\Gamma_u^{33} \lesssim 1$.

all have strong bounds at the electroweak scale.
All in all, the indirect bounds are weak for regions in the parameter space where $\Gamma_u^{33} < 1$ and become stronger toward larger values of α. They also overlap nearly completely with the region excluded by perturbative unitarity, $\Gamma_u^{33} \lesssim 3$ [88].

2.5. Summary and Conclusion

In this chapter, a global analysis of ALP interactions from SMEFT fits was presented, based on the phenomenon of the *ALP–SMEFT interference* that describes the appearance of inhomogeneous source terms in the RG evolution equations of the dimension-six SMEFT Wilson coefficients. Employing low-energy, Higgs and top data sets, indirect bounds on dimension-five ALP–SM couplings were deduced that are compatible with or even stronger than direct bounds in the GeV to TeV ALP mass range. In addition to producing strong constraints, it was shown that the indirect procedure offers a two-fold advantage: First, it does not require assumptions about specific ALP properties such as its lifetime, branching ratios or couplings, and second, the results are (mostly) independent of the ALP mass. In order to obtain these results, a semi-analytic solution to the RG equations at dimension six under the assumption of flavor-universal ALP interactions was derived based on evolution tensors. As these tensors are initial-condition independent, they can be pre-computed and therefore largely facilitate future analysis of dimension-six coefficients in the presence of ALPs at any scale. Delving deeper into the constraints on dimension-five couplings obtained in this chapter, the strongest results were found for the bosonic couplings C_{GG}, C_{WW} and C_{BB} that are of $\mathcal{O}(1)$, as is the bound on C_u. The remaining two ALP-fermion couplings C_d and C_e are weaker and still allow for values up to $\mathcal{O}(50)$. Disentangling the effects of RG evolution showed that the leading-logarithmic approx-

imation captures the most important effects for all coefficients except C_{GG} and C_u that get constrained mainly by higher-order terms in the resummation. Following this analysis, the indirect bounds were compared to existing direct limits. It was shown that so far unconstrained parameter space gets excluded by the present analysis for all dimension-five ALP couplings, which underlines the power of the indirect global fit. While this primarily concerns ALP masses above 10 GeV, a significant portion of the parameter space for C_e is also excluded for ALP masses below 1 GeV. Finally, the framework was applied to the UV-complete KSVZ and DFSZ models. In both cases, additional non-zero Wilson coefficients at the scale Λ arise from a tree-level matching computation. In the first case, the KSVZ model, these contributions do not have a significant impact on the coefficients of the theory compared to the vanilla fit without UV completion. In the DFSZ model, by contrast, threshold corrections dominate the constraints on the parameter α, particularly in regions where the UV Yukawa couplings are large. Looking forward, several directions remain to be explored. Certainly, a combined global fit on ALP couplings from both, direct and indirect constraints would be of great value. Concerning the UV-complete models, different assumptions on the mass spectrum might modify the results, as can one-loop matching corrections which remain to be derived.

2.7. Appendix

2.7.A. Contributions to Z-Pole Observables in the LL Approximation

In this section, the leading-logarithmic expressions for the Warsaw basis SMEFT Wilson coefficients that are relevant for the Z-pole observables are given in terms of the ALP coefficients at the scale $\Lambda = 4\pi f$. For simplicity, only the largest entries of the Yukawa matrices are kept, i.e. $[\boldsymbol{Y}_u]_{33} \equiv y_t$, $[\boldsymbol{Y}_d]_{33} \equiv y_b$ and $[\boldsymbol{Y}_e]_{33} \equiv y_\tau$. This yields at the scale $\mu = m_Z$

$$
\begin{aligned}
C_{HWB} &= 4\, g_L\, g_Y\, C_{BB}\, C_{WW}\, \ln\frac{\Lambda}{m_Z}\,, \\
C_{HD} &= -\frac{8}{3}\, g_Y^2\, C_{BB}^2\, \ln\frac{\Lambda}{m_Z}\,, \\
\left[C_{Hq}^{(1)}\right]_{ij} &= \left[-\frac{4}{9}\, g_Y^2\, C_{BB}^2\, \delta_{ij} + \frac{1}{4}\, \left(y_t^2\, C_u^2 - y_b^2\, C_d^2\right) \delta_{i3}\delta_{j3}\right] \ln\frac{\Lambda}{m_Z}\,, \\
\left[C_{Hq}^{(3)}\right]_{ij} &= \left[-\frac{4}{3}\, g_L^2\, C_{WW}^2\, \delta_{ij} - \frac{1}{4}\, \left(y_t^2\, C_u^2 + y_b^2\, C_d^2\right) \delta_{i3}\delta_{j3}\right] \ln\frac{\Lambda}{m_Z}\,, \\
\left[C_{Hu}\right]_{ij} &= \left(-\frac{16}{9}\, g_Y^2\, C_{BB}^2\, \delta_{ij} - \frac{1}{2}\, y_t^2\, C_u^2\, \delta_{i3}\delta_{j3}\right) \ln\frac{\Lambda}{m_Z}\,, \\
\left[C_{Hd}\right]_{ij} &= \left(\frac{8}{9}\, g_Y^2\, C_{BB}^2\, \delta_{ij} + \frac{1}{2}\, y_b^2\, C_d^2\, \delta_{i3}\delta_{j3}\right) \ln\frac{\Lambda}{m_Z}\,, \\
\left[C_{Hud}\right]_{ij} &= y_b\, y_t\, C_d\, C_u\, \delta_{i3}\delta_{j3}\, \ln\frac{\Lambda}{m_Z}\,, \\
\left[C_{Hl}^{(1)}\right]_{ij} &= \left(\frac{4}{3}\, g_Y^2\, C_{BB}^2\, \delta_{ij} - \frac{1}{4}\, y_\tau^2\, C_e^2\, \delta_{i3}\delta_{j3}\right) \ln\frac{\Lambda}{m_Z}\,, \\
\left[C_{Hl}^{(3)}\right]_{ij} &= \left(-\frac{4}{3}\, g_L^2\, C_{WW}^2\, \delta_{ij} - \frac{1}{4}\, y_\tau^2\, C_e^2\, \delta_{i3}\delta_{j3}\right) \ln\frac{\Lambda}{m_Z}\,, \\
\left[C_{He}\right]_{ij} &= \left(\frac{8}{3}\, g_Y^2\, C_{BB}^2\, \delta_{ij} + \frac{1}{2}\, y_\tau^2\, C_e^2\, \delta_{i3}\delta_{j3}\right) \ln\frac{\Lambda}{m_Z}\,, \\
\left[C_{ll}\right]_{1221} &= -\frac{4}{3}\, g_L^2\, C_{WW}^2\, \ln\frac{\Lambda}{m_Z}\,.
\end{aligned}
\tag{A.1}
$$

With this, the modifications of the weak gauge couplings and the W mass, parametrized as in [75], are given by

$$
\begin{aligned}
\delta m_W^2 &= \frac{v^4}{\Lambda^2}\,\frac{g_Y^2\,g_L^2}{g_L^2-g_Y^2}\left(\frac{2}{3}\,C_{BB}^2 - 4\,C_{BB}\,C_{WW} + C_{WW}^2\right)\ln\frac{\Lambda}{m_Z}\,,\\
[\delta g_R^{Wq}]_{ij} &= -\frac{v^2}{\Lambda^2}\,\frac{y_b\,y_t}{2}\,C_d\,C_u\,\delta_{i3}\delta_{j3}\,\ln\frac{\Lambda}{m_Z}\,,\\
[\delta g_L^{Zu}]_{ij} &= \frac{v^2}{\Lambda^2}\left[\frac{\delta_{ij}}{g_L^2-g_Y^2}\left(\frac{1}{9}\,g_Y^2\,(5g_L^2-g_Y^2)\,C_{BB}^2 - \frac{8}{3}\,g_L^2\,g_Y^2\,C_{BB}\,C_{WW}\right.\right.\\
&\qquad\left.\left. - \frac{1}{6}\,g_L^2\,(g_L^2-5g_Y^2)\,C_{WW}^2\right) - \frac{\delta_{i3}\delta_{j3}}{4}\,y_t^2\,C_u^2\right]\ln\frac{\Lambda}{m_Z}\,,\\
[\delta g_L^{Zd}]_{ij} &= \frac{v^2}{\Lambda^2}\left[\frac{\delta_{ij}}{g_L^2-g_Y^2}\left(-\frac{1}{9}\,g_Y^2(g_L^2+g_Y^2)C_{BB}^2 + \frac{4}{3}\,g_L^2\,g_Y^2\,C_{BB}\,C_{WW}\right.\right.\\
&\qquad\left.\left. + \frac{1}{6}\,g_L^2(g_L^2-3g_Y^2)C_{WW}^2\right) + \frac{\delta_{i3}\delta_{j3}}{4}\,y_b^2\,C_d^2\right]\ln\frac{\Lambda}{m_Z}\,,\\
[\delta g_R^{Zu}]_{ij} &= \frac{v^2}{\Lambda^2}\left[\frac{g_Y^2}{g_L^2-g_Y^2}\,\delta_{ij}\left(\frac{4}{9}\,(2g_L^2-g_Y^2)\,C_{BB}^2 - \frac{8}{3}\,g_L^2\,C_{BB}\,C_{WW} + \frac{2}{3}\,g_L^2\,C_{WW}^2\right)\right.\\
&\qquad\left. + \frac{\delta_{i3}\delta_{j3}}{4}\,y_t^2\,C_u^2\right]\ln\frac{\Lambda}{m_Z}\,,\\
[\delta g_R^{Zd}]_{ij} &= \frac{v^2}{\Lambda^2}\left[\frac{g_Y^2}{g_L^2-g_Y^2}\,\delta_{ij}\left(\frac{2}{9}\,(g_Y^2-2g_L^2)\,C_{BB}^2 + \frac{4}{3}\,g_L^2\,C_{BB}\,C_{WW} - \frac{1}{3}\,g_L^2\,C_{WW}^2\right)\right.\\
&\qquad\left. - \frac{\delta_{i3}\delta_{j3}}{4}\,y_b^2\,C_d^2\right]\ln\frac{\Lambda}{m_Z}\,,\\
[\delta g_L^{Wl}]_{ij} &= \frac{v^2}{\Lambda^2}\left[\frac{g_L^2}{g_L^2-g_Y^2}\,\delta_{ij}\left(\frac{2}{3}\,g_Y^2\,C_{BB}^2 - 4\,g_Y^2\,C_{BB}\,C_{WW} - \frac{1}{3}\,(g_L^2-4\,g_Y^2)\,C_{WW}^2\right)\right.\\
&\qquad\left. - \frac{\delta_{i3}\delta_{j3}}{4}\,y_\tau^2\,C_e^2\right]\ln\frac{\Lambda}{m_Z}\,,\\
[\delta g_L^{Ze}]_{ij} &= \frac{v^2}{\Lambda^2}\left[\frac{\delta_{ij}}{g_L^2-g_Y^2}\left(\frac{1}{3}\,g_Y^2(g_Y^2-3g_L^2)\,C_{BB}^2 + 4\,g_L^2\,g_Y^2\,C_{BB}\,C_{WW}\right.\right.\\
&\qquad\left.\left. + \frac{1}{6}g_L^2(g_L^2-7g_Y^2)\,C_{WW}^2\right) + \frac{\delta_{i3}\delta_{j3}}{4}\,y_\tau^2\,C_e^2\right]\ln\frac{\Lambda}{m_Z}\,,\\
[\delta g_R^{Ze}]_{ij} &= \frac{v^2}{\Lambda^2}\left[\frac{g_Y^2}{g_L^2-g_Y^2}\,\delta_{ij}\,\left(\frac{2}{3}(g_Y^2-2g_L^2)\,C_{BB}^2 + 4\,g_L^2\,C_{BB}\,C_{WW} - g_L^2\,C_{WW}^2\right)\right.\\
&\qquad\left. - \frac{\delta_{i3}\delta_{j3}}{4}\,y_\tau^2\,C_e^2\right]\ln\frac{\Lambda}{m_Z}\,,
\end{aligned}
\tag{A.2}
$$

with $\delta g_L^{Z\nu} = \delta g_L^{Ze} + \delta g_L^{Wl}$ and $\delta g_L^{Wq} \approx \delta g_L^{Zu} - \delta g_L^{Zd}$ for $V_{\rm CKM} \approx \mathbb{1}$.

2.7.B. Experimental Higgs and Top Input

In this section, the experimental Higgs and top data used as input for the global fit is summarized.

Experiment/ Facility	Observable	# of Measurements	References
7 and 8 TeV	ATLAS & CMS combination	20	Table 8 of [89]
Run-I data	$h \to \mu\mu$ ATLAS & CMS combination	1	Table 13 of [89]
	$h \to Z\gamma$ (ATLAS)	1	Figure 1 of [90]
ATLAS	$h \to Z\gamma$	1	[91]
13 TeV	$h \to \mu\mu$	1	[92]
Run-II data	$h \to \tau\tau$	4	Figure 14 of [93]
	$h \to bb$ from vector boson fusion	1	[94, 95]
	$h \to bb$ from ttH	1	[94, 95]
	STXS[2] $h \to \gamma\gamma/ZZ/b\bar{b}$	42	Figures 1 and 2 of [96]
	STXS $h \to WW$ in ggF, VBF	11	Figures 12 and 14 of [97]
	$\frac{d\sigma}{d\Delta\phi_{jj}}$ for EW Zjj production	12	Figure 7(d) of [98]
CMS	$h \to WW$ in gluon-gluon fusion	1	[99]
13 TeV	$h \to \mu\mu$	4	Figure 11 of [100]
Run-II data	$h \to \tau\tau/WW$ in $t\bar{t}h$	3	Figure 14 of [101]
	STXS $h \to WW$ in Vh	4	Table 9 of [102]
	STXS $h \to \tau\tau$	11	Figures 11 and 12 of [103]
	STXS $h \to \gamma\gamma$	27	Table 13 and Figure 21 of [104]
	STXS $h \to ZZ$	18	Table 6 and Figure 15 of [77]
	$h \to b\bar{b}$ in Vh	2	Table 4 of [105]

Table 2.1.: Higgs data included in the global fit of the ALP coefficients.

[2]Simplified template cross-sections (STXS) are a model-independent framework to analyze Higgs processes. They provide a tool to reduce the influence of theoretical uncertainties and allow for the combination of different experimental measurements. For more details, see e.g. [106].

Experiment/ Facility	Observable	# of Measurements	References
Tevatron	forward-backward asymmetry $A_{\rm FB}(m_{t\bar{t}})$ for $t\bar{t}$ production	4	[107]
ATLAS & CMS	charge asymmetry $A_C(m_{t\bar{t}})$ for $t\bar{t}$ production in the ℓ+jets channel.	6	[108]
7 and 8 TeV, Run-I	W-boson helicity fractions in top decay	3	[109]
ATLAS	charge asymmetry $A_C(m_{t\bar{t}})$ for $t\bar{t}$ production in the dilepton channel	1	[110]
7 and 8 TeV	$\sigma_{t\bar{t}W}$, $\sigma_{t\bar{t}Z}$	2	[111]
Run-I data	$\frac{d\sigma}{dp_t^T}$, $\frac{d\sigma}{d\lvert y_t\rvert}$ for t-channel single-top production	$4+5$	[112]
	σ_{tW} in the single lepton channel	1	[113]
	σ_{tW} in the dilepton channel	1	[114]
	s-channel single-top cross section	1	[115]
	$\frac{d\sigma}{dm_{t\bar{t}}}$ for $t\bar{t}$ production in the dilepton channel	6	[116]
	$\frac{d\sigma}{dp_t^T}$ for $t\bar{t}$ production in the ℓ+jets channel	8	[117]
CMS	$\sigma_{t\bar{t}\gamma}$ in the ℓ+jets channel	1	[118]
7 and 8 TeV	charge asymmetry $A_C(m_{t\bar{t}})$ for $t\bar{t}$ production in the dilepton channel.	3	[119]
Run-I data	$\sigma_{t\bar{t}W}$, $\sigma_{t\bar{t}Z}$	2	[118]
	$\sigma_{t\bar{t}\gamma}$ in the ℓ+jets channel.	1	[120]
	s-channel single-top cross section	1	[121]
	$\frac{d\sigma}{dp_{t+\bar{t}}^T}$ of t-channel single-top production	6	[122]
	t-channel single-top and anti-top cross sections R_t	1	[123]
	σ_{tW}	1	[124]
	$\frac{d\sigma}{dm_{t\bar{t}}dy_{t\bar{t}}}$ for $t\bar{t}$ production in the dilepton channel	16	[125, 126]
	$\frac{d\sigma}{dp_t^T}$ for $t\bar{t}$ production in the ℓ+jets channel	8	[127, 128]

Table 2.2.: Top physics included in the global fit of the ALP coefficients.

Experiment/ Facility	Observable	# of Measurements	References
ATLAS	σ_{tW}	1	[129]
13 TeV	σ_{tZ}	1	[130]
Run-II data	$\sigma_{t+\bar{t}}$, R_t for t-channel single-top and anti-top cross sections	1+1	[131]
	charge asymmetry $A_C(m_{t\bar{t}})$ for $t\bar{t}$ production	5	[132]
	$\sigma_{t\bar{t}W}$, $\sigma_{t\bar{t}Z}$	2	[133]
	$\frac{d\sigma}{dp_T^T}$ for $t\bar{t}\gamma$ production	11	[134]
CMS	σ_{tW}	1	[135]
13 TeV	σ_{tZ} in the $Z \to \ell^+\ell^-$ channel	1	[136]
Run-II data	$\frac{d\sigma}{dp_{t+\bar{t}}^T}$ and $R_t\left(p_{t+\bar{t}}^T\right)$ for t-channel single-top quark production	$5+5$	[137]
	$\frac{d\sigma}{dm_{t\bar{t}}}$ for $t\bar{t}$ production in the dilepton channel	6	[138]
	$\frac{d\sigma}{dm_{t\bar{t}}}$ for $t\bar{t}$ production in the ℓ+jets channel	15	[139]
	$\sigma_{t\bar{t}W}$	1	[140]
	$\frac{d\sigma}{dp_Z^T}$ for $t\bar{t}Z$ production	4	[141]

Table 2.3.: Top physics included in the global fit of the ALP coefficients.

Chapter 3: ALP–LEFT Interference

So far, phenomenological ALP effects have only been considered above the scale $\mu_w \sim v \approx 246\,\text{GeV}$. When crossing this threshold, several important changes take place: The electroweak symmetry $SU(2)_L \times U(1)_Y$ gets broken down to $U(1)_{\text{EM}}$ via the *Higgs-mechanism*. This process also gives masses to the fermions and the Z and $W^\pm$ gauge bosons. With $m_t \approx 173\,\text{GeV}$, $m_Z \approx 91\,\text{GeV}$, $m_W \approx 80\,\text{GeV}$ and $m_h \approx 125\,\text{GeV}$, the top-quark, the heavy gauge bosons Z and $W^\pm$ and the Higgs boson need to be removed as degrees of freedom below the respective scales. Matching the full SM onto this Low-Energy Effective Field Theory (LEFT) generates non-zero Wilson coefficients of higher-dimensional local operators. For instance, "integrating out" the $W^\pm$ gauge bosons yields dimension-six local four-fermion operators, as the heavy propagator effectively contracts to a point, an effect that is schematically illustrated in Figure 3.1. The operators generated in this procedure are suppressed by powers of $1/v^d$ according to their dimension d.

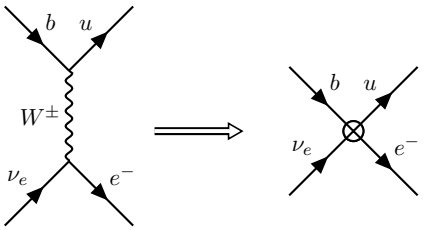

Figure 3.1.: Generation of a local four-fermion interaction by shrinking the $W^\pm$-propagator to a point at scales below m_W.

The presence of axions and ALPs with $m_a \ll \mu_w$ contributes additional terms not only to higher dimensional Wilson coefficients that are present below μ_w from integrating out the heavy SM fields, but also generates additional operators. As in the SMEFT case, this occurs via inhomogeneous source terms added to the RG equations that are obtained from one-loop processes. In order to find the full list of ALP-induced source terms, this chapter starts with a description of the ALP–SM interactions below the electroweak scale. Afterwards, the set of LEFT source terms up to dimension-six order is derived systematically. As an application, these results are then applied to the anomalous magnetic moment of the muon.

This chapter is based on

[142] **ALP–LEFT Interference and the Muon ($g-2$)**
A. M. Galda and M. Neubert
JHEP **11** (2023), 15, [arXiv:2308.01338].

3.1. ALP-Interactions below the Electroweak Scale

Apart from the modifications that occur in the pure SM Lagrangian below the electroweak symmetry breaking, also the ALP-Lagrangian needs to be rewritten in terms of the appropriate effective degrees of freedom for $\mu < \mu_w$, meaning that the heavy states are no longer present and the ALP-photon coupling is incorporated correctly. This yields, up to dimension-six order[1] [60],

$$\begin{aligned}\mathcal{L}_{\text{eff}}^{D\leq 6} = \frac{1}{2}(\partial_\mu a)(\partial^\mu a) - \frac{m_a^2}{2}a^2 + c_{GG}\frac{\alpha_s}{4\pi}\frac{a}{f}G^a_{\mu\nu}\tilde{G}^{\mu\nu,a} + c_{\gamma\gamma}\frac{\alpha}{4\pi}\frac{a}{f}F_{\mu\nu}\tilde{F}^{\mu\nu} \\ + \frac{\partial^\mu a}{f}\Big[\bar{u}_L\boldsymbol{k}_U\gamma_\mu u_L + \bar{u}_R\boldsymbol{k}_u\gamma_\mu u_R + \bar{d}_L\boldsymbol{k}_D\gamma_\mu d_L \\ + \bar{d}_R\boldsymbol{k}_d\gamma_\mu d_R + \bar{e}_L\boldsymbol{k}_E\gamma_\mu e_L + \bar{e}_R\boldsymbol{k}_e\gamma_\mu e_R\Big]\,.\end{aligned} \tag{3.1}$$

The matching conditions that connect Lagrangian (1.34) to this low-energy version have been found in [60]. Remembering that the top-quark has been removed from the theory, the fermion vectors are explicitly given by $u_{L,R} = P_{L,R}\,(u\ c\ 0)^T$ and $d_{L,R} = P_{L,R}\,(d\ s\ b)^T$ with $P_{L,R}$ projecting onto the left/right-handed component of the spinors. The covariant derivative entering the field-strength tensors below μ_w reads $D_\mu = \partial_\mu - ig_sG^a_\mu t^a - ieQA_\mu$. The hermitian matrices $\boldsymbol{k}_i$ are defined in the fermion mass basis and the matrices related to left-handed quarks obey $\boldsymbol{k}_D = \boldsymbol{V}^\dagger\boldsymbol{k}_U\boldsymbol{V}$, where $\boldsymbol{V}$ denotes the CKM matrix.
Integrating by parts and using the equation for the chiral anomaly, the Lagrangian (3.1) can be rewritten in the equivalent form [60, 67]

$$\begin{aligned}\mathcal{L}_{\text{eff}}^{D\leq 6}(\mu<\mu_w) = \frac{1}{2}(\partial_\mu a)(\partial^\mu a) - \frac{m_a^2}{2}a^2 + C_{GG}\frac{a}{f}G^a_{\mu\nu}\tilde{G}^{\mu\nu,a} + C_{\gamma\gamma}\frac{a}{f}F_{\mu\nu}\tilde{F}^{\mu\nu} \\ - \frac{ia}{f}\Big[\bar{u}_L\tilde{\boldsymbol{M}}_u u_R + \bar{d}_L\tilde{\boldsymbol{M}}_d d_R + \bar{e}_L\tilde{\boldsymbol{M}}_e e_R - \text{h.c.}\Big] \\ + \frac{a^2}{2f^2}\Big[\bar{u}_L\boldsymbol{M}'_u u_R + \bar{d}_L\boldsymbol{M}'_d d_R + \bar{e}_L\boldsymbol{M}'_e e_R + \text{h.c.}\Big]\,,\end{aligned} \tag{3.2}$$

which has the advantage that the explicit derivatives acting on the ALP are removed. The matrices $\boldsymbol{k}_F$ $(F = u, d, e, U, D, F)$ now appear in combination with the diagonal mass matrices $\boldsymbol{m}_F$ of the fermions as

$$\tilde{\boldsymbol{M}}_u = \boldsymbol{m}_u\boldsymbol{k}_u - \boldsymbol{k}_U\boldsymbol{m}_u\,,\quad \tilde{\boldsymbol{M}}_d = \boldsymbol{m}_d\boldsymbol{k}_d - \boldsymbol{k}_D\boldsymbol{m}_d\,,\quad \tilde{\boldsymbol{M}}_e = \boldsymbol{m}_e\boldsymbol{k}_e - \boldsymbol{k}_E\boldsymbol{m}_e\,, \tag{3.3}$$

as well as in the matrices parametrizing the dimension-six coupling that appears in (3.2) after the rewriting,

$$\boldsymbol{M}'_u = \boldsymbol{m}_u\boldsymbol{k}_u^2 - 2\boldsymbol{k}_U\boldsymbol{m}_u\boldsymbol{k}_u + \boldsymbol{k}_U^2\boldsymbol{m}_u \quad \text{etc.} \tag{3.4}$$

Effectively, the ALP-fermion coupling is thus related to the mass of the corresponding state, which justifies not writing neutrino terms in the Lagrangian (3.1). Finally, the

[1] Since the Higgs-field has been integrated out, operators of dimension-six are not present in the effective Lagrangian.

relations for the ALP-boson couplings are

$$C_{GG} = \frac{\alpha_s}{4\pi}\left(c_{GG} + \frac{1}{2}\sum_{q\neq t} c_{qq}\right), \quad C_{\gamma\gamma} = \frac{\alpha}{4\pi}\left(c_{\gamma\gamma} + \sum_{f\neq t} N_c^f\, Q_f^2\, c_{ff}\right), \tag{3.5}$$

where the sum extends over all light fermionic degrees of freedom, $N_c^q = 3$ for quarks and $N_c^l = 1$ for leptons.
Following the same concepts as for the *ALP–SMEFT interference* described in Section 1.7, the presence of ALPs below the electroweak scale induced inhomogeneous source terms in the RG evolution equations of Wilson coefficients of higher dimensional operators through Feynman diagrams where the ALP appears as a virtual particle in the loop. Again, the counterterms for these UV-divergences are of dimension six or higher, but now the operators are those of the LEFT and there is one additional, crucial difference: While in the absence of new physics, all Wilson coefficients of the SMEFT are zero, the pure SM matching at μ_w already generates higher-dimensional LEFT operators.
Before moving on to the calculation of the ALP induced inhomogeneous source terms for the LEFT Wilson coefficients, it is instructive to consider this effective theory in a bit more detail. The minimal basis of operators up to mass-dimension six compatible with the remaining $SU(3)_c \times U(1)_{\text{EM}}$ symmetry and the corresponding minimal basis was first found in [143]. Assuming three generations of fermions and including those with non-zero ΔL and ΔB, the SM operators of dimension-four below μ_w are extended by 12 dimension-three, 76 dimension-five, and 5995 dimension-six operators. Certainly, the ALP does not generate all Wilson coefficients of these operators, but this basis captures, in a systematic way, all possible effects of *heavy* new physics that has been integrated out above μ_w, up to mass-dimension six. Since it might correspond to a scale $\Lambda \gg \mu_w$, the LEFT in general is an expansion in two (or more) scales, $1/v$ and $1/\Lambda$, and matching conditions from the SMEFT to the LEFT have been obtained in [143].
Moving now on to the concrete *light* (meaning $m_a < \mu_w$) ALP case, another effect takes place, as already described for the SMEFT: Removing the $1/\epsilon$ poles from the amplitudes of one-loop Feynman diagrams with virtual ALP exchange generates inhomogeneous source terms S_i that enter the RG evolution equations of the LEFT Wilson coefficients via

$$\frac{d}{d\ln\mu} C_i^{\text{LEFT}} - \gamma_{ji}^{\text{LEFT}}\, C_j^{\text{LEFT}} = \frac{S_i}{(4\pi f)^2} \qquad (\text{for } \mu < \mu_w)\,, \tag{3.6}$$

where γ^{LEFT} is the one-loop anomalous dimension matrix for the LEFT Wilson coefficients that has been computed in [144]. The correct effective field theory is thus given by

$$\mathcal{L}_{\text{eff}} = \mathcal{L}_{\text{LEFT}} + \mathcal{L}_{\text{ALP}} + \mathcal{L}_{\text{SM+ALP}}\,. \tag{3.7}$$

3.2. Green's Functions requiring LEFT Counterterms

With these ingredients at hand, it is now possible to move on to the calculation of the ALP-induced inhomogeneous source terms generating the LEFT Wilson coefficients. To this end, it is convenient to work in a Green's basis, i.e. a redundant basis that is complete before applying the equations of motions, since it allows to restrict the analysis to one-particle irreducible diagrams. In principle, there are three different types of such operators at dimension-six, pure gauge boson operators, single and four fermion-current operators, that can each be subdivided into different classes by the number of covariant derivatives, fermion and gauge boson fields as shown in Table 3.1.

Operator Type	Operator Class
pure gauge boson	X^3, X^2D^2, X^2
single fermion-current	ψ^2XD, ψ^2X, ψ^2D^3, ψ^2D^2, ψ^2D, ψ^2
four-fermion	ψ^4

Table 3.1.: LEFT operator classes up to dimension-six that need to be considered for the ALP–LEFT interference. X denotes a normal or dual field strength tensor, ψ is a SM fermion.

In the following sections, all Feynman diagrams with virtual ALP exchange contributing to these classes are computed in the Green's basis and subsequently transformed to the minimal LEFT basis. To this end, the sum of diagrams are written as

$$\sum_i D_i^{\text{ALP}} \equiv \frac{i\mathcal{A}}{(4\pi f)^2} \tag{3.8}$$

throughout and the matrix element of an operator Q is expressed as $\langle Q \rangle$.

3.3. Pure Gauge-Boson Operators

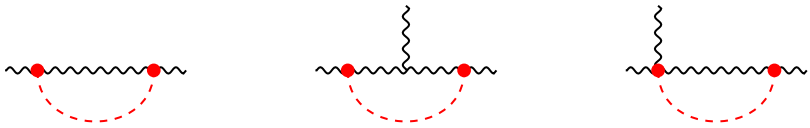

Figure 3.2.: Representative one-loop Feynman diagrams with virtual ALP exchange (red dashed line) requiring pure gauge-boson operators as counterterms. The second and third graph, which involve the three gauge-boson vertices, are both absent for photons.

The Feynman diagrams with one-loop virtual ALP exchange that contribute to the purely bosonic (PB) LEFT counterterms are depicted in Figure 3.2. Defining the auxiliary, redundant operators

$$\begin{aligned} \widehat{Q}_{G,2} &= (D^\rho G_{\rho\mu})^a (D_\omega G^{\omega\mu})^a \,, \\ \widehat{Q}_{\gamma,2} &= (\partial^\rho F_{\rho\mu})(\partial_\omega F^{\omega\mu}) \,, \end{aligned} \tag{3.9}$$

the amplitudes can be written as

$$\begin{aligned}\mathcal{A}(gg(g)) &= -\frac{C_{GG}^2}{\epsilon}\left[4g_s\langle Q_G\rangle + \frac{4}{3}\langle\widehat{Q}_{G,2}\rangle - 2m_a^2\langle G^a_{\mu\nu}G^{\mu\nu,a}\rangle\right] + \text{finite}\,,\\ \mathcal{A}(\gamma\gamma) &= -\frac{C_{\gamma\gamma}^2}{\epsilon}\left[\frac{4}{3}\langle\widehat{Q}_{\gamma,2}\rangle - 2m_a^2\langle F_{\mu\nu}F^{\mu\nu}\rangle\right] + \text{finite}\,,\end{aligned} \tag{3.10}$$

with Q_G as defined below (1.58). From the first term in the amplitude $\mathcal{A}(gg(g))$, the contribution to the inhomogeneous source term of the LEFT Wilson coefficient C_G can directly be read off as $S_G \ni 8g_sC_{GG}^2$. The remaining terms require a more careful examination. Starting with the redundant operators $\hat{Q}_{G,2}$ and $\hat{Q}_{\gamma,2}$, one first needs to apply the equations of motion for the gluon and the photon,

$$(D^\rho G_{\rho\mu})^a = g_s\sum_{q\neq t}\bar{q}\gamma_\mu t^a q\,, \qquad \partial^\rho F_{\rho\mu} = e\sum_{f\neq t}Q_f\,\bar{f}\gamma_\mu f\,, \tag{3.11}$$

where the sum over the quarks q and leptons l include all light fermion mass eigenstates, in order to project them onto the minimal LEFT basis. This yields for the auxiliary gluon operator in the notation of [143]

$$\begin{aligned}\widehat{Q}_{G,2} \cong g_s^2\Bigg[&\frac{1}{2}\left(\left[Q_{uu}^{V,LL}\right]_{pssp} + \left[Q_{uu}^{V,RR}\right]_{pssp} + \left[Q_{dd}^{V,LL}\right]_{pssp} + \left[Q_{dd}^{V,RR}\right]_{pssp}\right)\\ &-\frac{1}{2N_c}\left(\left[Q_{uu}^{V,LL}\right]_{ppss} + \left[Q_{uu}^{V,RR}\right]_{ppss} + \left[Q_{dd}^{V,LL}\right]_{ppss} + \left[Q_{dd}^{V,RR}\right]_{ppss}\right)\\ &+2\left(\left[Q_{uu}^{V8,LR}\right]_{ppss} + \left[Q_{dd}^{V8,LR}\right]_{ppss}\right)\\ &+2\left(\left[Q_{ud}^{V8,LL}\right]_{ppss} + \left[\left[Q_{ud}^{V8,RR}\right]_{ppss} + \left[Q_{ud}^{V8,LR}\right] + \left[Q_{du}^{V8,LR}\right]\right)\right],\end{aligned} \tag{3.12}$$

and for the auxiliary photon operator

$$\begin{aligned}\widehat{Q}_{\gamma,2} \cong e^2\Bigg[&Q_u^2\left(\left[Q_{uu}^{V,LL}\right]_{ppss} + \left[Q_{uu}^{V,RR}\right]_{ppss} + 2\left[Q_{uu}^{V1,LR}\right]_{ppss}\right)\\ &+Q_d^2\left(\left[Q_{dd}^{V,LL}\right]_{ppss} + \left[Q_{dd}^{V,RR}\right]_{ppss} + 2\left[Q_{dd}^{V1,LR}\right]_{ppss}\right)\\ &+Q_e^2\left(\left[Q_{ee}^{V,LL}\right]_{ppss} + \left[Q_{ee}^{V,RR}\right]_{ppss} + 2\left[Q_{ee}^{V,LR}\right]_{ppss}\right)\\ &+2Q_uQ_d\left(\left[Q_{ud}^{V1,LL}\right]_{ppss} + \left[Q_{ud}^{V1,RR}\right]_{ppss} + \left[Q_{ud}^{V1,LR}\right]_{ppss} + \left[Q_{du}^{V1,LR}\right]_{ppss}\right)\\ &+2Q_eQ_u\left(\left[Q_{eu}^{V,LL}\right]_{ppss} + \left[Q_{eu}^{V,RR}\right]_{ppss} + \left[Q_{eu}^{V,LR}\right]_{ppss} + \left[Q_{ue}^{V,LR}\right]_{ppss}\right)\\ &+2Q_eQ_d\left(\left[Q_{ed}^{V,LL}\right]_{ppss} + \left[Q_{ed}^{V,RR}\right]_{ppss} + \left[Q_{ed}^{V,LR}\right]_{ppss} + \left[Q_{de}^{V,LR}\right]_{ppss}\right)\Bigg].\end{aligned} \tag{3.13}$$

In the same way as before, it is now straightforward to read off the contributions to the inhomogeneous source terms of the Wilson coefficients of the respective operators appearing in (3.12) and (3.13). Since other diagrams yield further terms, the full expressions for the S_i are collected at the end of this chapter.
Next, there remain terms multiplied by the ALP mass term in the amplitudes (3.10). Since the m_a^2 multiplies two field strength tensors, these terms yield modifications of the wave-function renormalizations and thus affect the running of the gauge couplings $\alpha_s(\mu)$ and $\alpha(\mu)$. A detailed derivation follows in Section 3.6.

3.4. Single Fermion-Current Operators

Moving on to the single fermion-current operators, only the operator classes $\psi^2 D$, ψ^2 as well as the dipole operators $\psi^2 X$ are generated, while $\psi^2 X D$, $\psi^2 D^3$ and $\psi^2 D^2$ are not sourced by the ALP at one-loop order when working with the second form of the Lagrangian in (3.2). Certainly, the final results are independent of the choice of the Lagrangian.

Dipole Operators

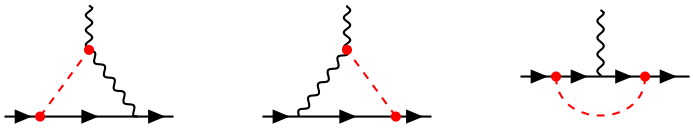

Figure 3.3.: One-loop Feynman diagrams with virtual ALP exchange (red dashed line) requiring dipole operators as counterterms. The fermion line represents a quark or a charged lepton.

The Feynman diagrams describing a chirality changing dipole interaction with a one-loop ALP exchange are depicted in Figure 3.3. While the third diagram is UV-finite, the sum of the first and the second one yields, for the example of $(\bar{L}R)X$ where the fermion line represents a quark, the expression

$$\mathcal{A}(\bar{q}_{L,p}\, q_{R,r}\, g) = -\frac{2g_s}{\epsilon}\left(\tilde{\boldsymbol{M}}_q\right)_{pr} C_{GG}\left[\langle Q_{qG}\rangle\right]_{pr} + \text{finite}\,, \tag{3.14}$$

while for the case where the fermion line is a charged lepton one obtains

$$\mathcal{A}(\bar{f}_{L,p}\, f_{R,r}\, \gamma) = -\frac{2Q_f\, e}{\epsilon}\left(\tilde{\boldsymbol{M}}_f\right)_{pr} C_{\gamma\gamma}\left[\langle Q_{f\gamma}\rangle\right]_{pr} + \text{finite}\,, \quad (f = u, d, e)\,. \tag{3.15}$$

Notably, these amplitudes correspond to those of the dipole operators found in the SMEFT case in [35], however with the external Higgs field replaced by its vacuum expectation value. In both expressions, (3.14) and (3.15), no summation is implied for the indices p and r for a given diagram with external fermion generations p, r.

Fermion Two-Point Functions

Figure 3.4.: One-loop Feynman diagrams with virtual ALP exchange (red dashed line) contributing to the fermion self-energies. The fermion line represents a quark or a charged lepton.

In the SMEFT case, the non-derivative basis ALP–fermion interaction always involves a Higgs field. The absence of this heavy boson below the electroweak symmetry breaking scale leads to the interesting phenomenon that fermion two-point functions are generated, allowing the ALP to influence fermion masses. Systematically, the two self-energy diagrams shown in Figure 3.4 can be decomposed as

$$\boldsymbol{\Sigma}^{(f)}(p) = \boldsymbol{\Sigma}^{(f)}_{LL} + \boldsymbol{\Sigma}^{(f)}_{RR} + \boldsymbol{\Sigma}^{(f)}_{LR} + \boldsymbol{\Sigma}^{(f)}_{RL}\,, \quad (f = u, d, e)\,. \tag{3.16}$$

The different contributions to $\boldsymbol{\Sigma}^{(f)}$ read

$$\begin{aligned}
\boldsymbol{\Sigma}^{(f)}_{LL} &= \frac{1}{(4\pi f)^2}\,\frac{1}{\epsilon}\left(-\frac{\not{p}}{2}\right) P_L\, \tilde{\boldsymbol{M}}_f\, \tilde{\boldsymbol{M}}_f^\dagger + \text{finite}\,,\\
\boldsymbol{\Sigma}^{(f)}_{RR} &= \frac{1}{(4\pi f)^2}\,\frac{1}{\epsilon}\left(-\frac{\not{p}}{2}\right) P_R\, \tilde{\boldsymbol{M}}_f^\dagger\, \tilde{\boldsymbol{M}}_f + \text{finite}\,,\\
\boldsymbol{\Sigma}^{(f)}_{LR} &= \frac{1}{(4\pi f)^2}\,\frac{1}{\epsilon}\, P_R \left(\tilde{\boldsymbol{M}}_f\, \boldsymbol{m}_f\, \tilde{\boldsymbol{M}}_f + \frac{m_a^2}{2}\, \boldsymbol{M}'_f\right) + \text{finite}\,,\\
\boldsymbol{\Sigma}^{(f)}_{RL} &= \frac{1}{(4\pi f)^2}\,\frac{1}{\epsilon}\, P_L \left(\tilde{\boldsymbol{M}}_f^\dagger\, \boldsymbol{m}_f\, \tilde{\boldsymbol{M}}_f^\dagger + \frac{m_a^2}{2}\, \boldsymbol{M}'^\dagger_f\right) + \text{finite}\,.
\end{aligned} \tag{3.17}$$

To obtain the full self-energies, these terms have to be added to the SM expression and brought into canonical, diagonal form through appropriate field redefinitions.

3.5. Four-Fermion Operators

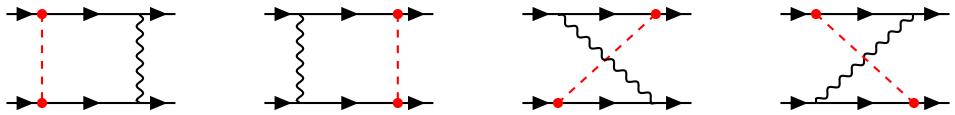

Figure 3.5.: One-loop Feynman diagrams with virtual ALP exchange (red dashed line) contributing to the four-fermion amplitudes. The fermion line represents a quark or a charged lepton. The diagrams are UV-finite.

Finally, the virtual ALP exchange could generate inhomogeneous source terms for four-fermion operators with corresponding diagrams shown in Figure 3.5. When working in the second basis (3.2), it is evident that all diagrams are UV-finite. Clearly, the generation of the source terms must be basis independent. When employing the first basis in (3.1) instead, the ALP-fermion vertices have an additional momentum. In this case, still the sum of the four diagrams is UV-finite.

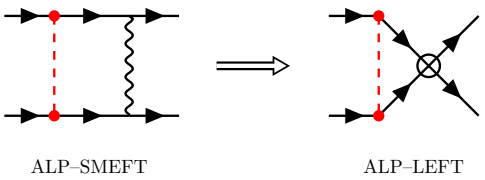

Figure 3.6.: Representative one-loop Feynman diagrams with virtual ALP exchange (red dashed line) requiring four-fermion operators as counterterms in the ALP–SMEFT case (left) and in the ALP–LEFT (right). The fermion line represents a quark or a charged lepton, the black curly line a $W^\pm$ or Z boson and the symbol $\otimes$ denotes an effective dimension-six four-fermion vertex in the LEFT obtained from integrating out the heavy gauge boson. Similar diagrams also exist for virtual Higgs exchange, generating four-fermion vertices of dimension-eight order in the LEFT (not shown).

One could, however, ask the question, why four-fermion operators were generated at dimension-six order in the *ALP–SMEFT interference* case in [35], while this does not happen at low energies. The reason is the following: Considering the derivative basis above μ_w, diagrams of the form as shown on the left-hand side of Figure 3.6 are responsible for these terms. When integrating out the heavy boson, the propagator shrinks to a point and generates the diagram shown on the right-hand side of the figure. The effective four-fermion vertex required in the right-hand side diagram is therefore of order six ($\sim 1/v^2$) or eight ($m_f m_{f'}/v^4$). The counterterms of such diagrams are thus given by dimension-eight operators for a four-fermion vertex generated by integrating out the $W^\pm$ or Z bosons and the Wilson coefficients scale as $1/(\Lambda^2 v^2)$, or by dimension-ten when it was induced by a Higgs with corresponding Wilson coefficient scaling as $1/(\Lambda^2 v^4)$. A concrete example of source terms for dimension-eight operators in the LEFT is shown in Appendix 3.10.A.

3.6. Derivation of the Source Terms

The derivation of the inhomogeneous LEFT source terms from the UV-divergent terms of the one-loop amplitudes follows the exact same logic as explained in Section 1.7. To summarize, if a Green's function contains a term of the form

$$\frac{\xi_i}{(4\pi f)^2}\,\frac{1}{\epsilon}\,\langle Q_i\rangle\,, \tag{3.18}$$

then the source term entering the RG equation of the renormalized Wilson coefficient contains (-2) times the coefficient of the $1/\epsilon$-term multiplying the corresponding matrix element, i.e.

$$\frac{d}{d\ln\mu}\,C_i(\mu) \ni -\frac{2\xi_i}{(4\pi f)^2} \equiv \frac{S_i}{(4\pi f)^2}\,. \tag{3.19}$$

The thus obtained results together with the corresponding operator definitions as given in [143] are shown in Table 3.2.

	Operator Q	Definition	Source Term S
PB	Q_G	$f^{abc}G^{a,\nu}_{\mu}G^{b,\rho}_{\nu}G^{c,\mu}_{\rho}$	$8g_sC^2_{GG}$
Dipole Op.	$[Q_{uG}]_{ij}$	$\bar{u}_{Li}\sigma^{\mu\nu}t^a u_{Rj}G^a_{\mu\nu}$	$4g_sC_{GG}[\tilde{\boldsymbol{M}}_u]_{ij}$
	$[Q_{dG}]_{ij}$	$\bar{d}_{Li}\sigma^{\mu\nu}t^a d_{Rj}G^a_{\mu\nu}$	$4g_sC_{GG}[\tilde{\boldsymbol{M}}_d]_{ij}$
	$[Q_{u\gamma}]_{ij}$	$\bar{u}_{Li}\sigma^{\mu\nu}u_{Rj}F_{\mu\nu}$	$\frac{8}{3}eC_{\gamma\gamma}[\tilde{\boldsymbol{M}}_u]_{ij}$
	$[Q_{d\gamma}]_{ij}$	$\bar{d}_{Li}\sigma^{\mu\nu}d_{Rj}F_{\mu\nu}$	$-\frac{4}{3}eC_{\gamma\gamma}[\tilde{\boldsymbol{M}}_d]_{ij}$
	$[Q_{e\gamma}]_{ij}$	$\bar{e}_{Li}\sigma^{\mu\nu}e_{Rj}F_{\mu\nu}$	$-4eC_{\gamma\gamma}[\tilde{\boldsymbol{M}}_e]_{ij}$
$(\bar{L}L)(\bar{L}L)$ and $(\bar{R}R)(\bar{R}R)$	$[Q^{V,LL}_{ee}]_{ijkl}$	$(\bar{e}_{Li}\gamma^\mu e_{Lj})(\bar{e}_{Lk}\gamma_\mu e_{Ll})$	$\frac{8}{3}e^2C^2_{\gamma\gamma}\delta_{ij}\delta_{kl}$
	$[Q^{V,RR}_{ee}]_{ijkl}$	$(\bar{e}_{Ri}\gamma^\mu e_{Rj})(\bar{e}_{Rk}\gamma_\mu e_{Rl})$	$\frac{8}{3}e^2C^2_{\gamma\gamma}\delta_{ij}\delta_{kl}$
	$[Q^{V,LL}_{eu}]_{ijkl}$	$(\bar{e}_{Li}\gamma^\mu e_{Lj})(\bar{u}_{Lk}\gamma_\mu u_{Ll})$	$-\frac{32}{9}e^2C^2_{\gamma\gamma}\delta_{ij}\delta_{kl}$
	$[Q^{V,RR}_{eu}]_{ijkl}$	$(\bar{e}_{Ri}\gamma^\mu e_{Rj})(\bar{u}_{Rk}\gamma_\mu u_{Rl})$	$-\frac{32}{9}e^2C^2_{\gamma\gamma}\delta_{ij}\delta_{kl}$
	$[Q^{V,LL}_{ed}]_{ijkl}$	$(\bar{e}_{Li}\gamma^\mu e_{Lj})(\bar{d}_{Lk}\gamma_\mu d_{Ll})$	$\frac{16}{9}e^2C^2_{\gamma\gamma}\delta_{ij}\delta_{kl}$
	$[Q^{V,RR}_{ed}]_{ijkl}$	$(\bar{e}_{Ri}\gamma^\mu e_{Rj})(\bar{d}_{Rk}\gamma_\mu d_{Rl})$	$\frac{16}{9}e^2C^2_{\gamma\gamma}\delta_{ij}\delta_{kl}$
	$[Q^{V,LL}_{uu}]_{ijkl}$	$(\bar{u}_{Li}\gamma^\mu u_{Lj})(\bar{u}_{Lk}\gamma_\mu u_{Ll})$	$\frac{32}{27}e^2C^2_{\gamma\gamma}\delta_{ij}\delta_{kl}+\frac{4}{3}g_s^2C^2_{GG}\left(\delta_{il}\delta_{jk}-\frac{1}{N_c}\delta_{ij}\delta_{kl}\right)$
	$[Q^{V,RR}_{uu}]_{ijkl}$	$(\bar{u}_{Ri}\gamma^\mu u_{Rj})(\bar{u}_{Rk}\gamma_\mu u_{Rl})$	$\frac{32}{27}e^2C^2_{\gamma\gamma}\delta_{ij}\delta_{kl}+\frac{4}{3}g_s^2C^2_{GG}\left(\delta_{il}\delta_{jk}-\frac{1}{N_c}\delta_{ij}\delta_{kl}\right)$
	$[Q^{V,LL}_{dd}]_{ijkl}$	$(\bar{d}_{Li}\gamma^\mu d_{Lj})(\bar{d}_{Lk}\gamma_\mu d_{Ll})$	$\frac{8}{27}e^2C^2_{\gamma\gamma}\delta_{ij}\delta_{kl}+\frac{4}{3}g_s^2C^2_{GG}\left(\delta_{il}\delta_{jk}-\frac{1}{N_c}\delta_{ij}\delta_{kl}\right)$
	$[Q^{V,RR}_{dd}]_{ijkl}$	$(\bar{d}_{Ri}\gamma^\mu d_{Rj})(\bar{d}_{Rk}\gamma_\mu d_{Rl})$	$\frac{8}{27}e^2C^2_{\gamma\gamma}\delta_{ij}\delta_{kl}+\frac{4}{3}g_s^2C^2_{GG}\left(\delta_{il}\delta_{jk}-\frac{1}{N_c}\delta_{ij}\delta_{kl}\right)$
	$[Q^{V1,LL}_{ud}]_{ijkl}$	$(\bar{u}_{Li}\gamma^\mu u_{Lj})(\bar{d}_{Lk}\gamma_\mu d_{Ll})$	$-\frac{32}{27}e^2C^2_{\gamma\gamma}\delta_{ij}\delta_{kl}$
	$[Q^{V1,RR}_{ud}]_{ijkl}$	$(\bar{u}_{Ri}\gamma^\mu u_{Rj})(\bar{d}_{Rk}\gamma_\mu d_{Rl})$	$-\frac{32}{27}e^2C^2_{\gamma\gamma}\delta_{ij}\delta_{kl}$
	$[Q^{V8,LL}_{ud}]_{ijkl}$	$(\bar{u}_{Li}\gamma^\mu t^a u_{Lj})(\bar{d}_{Lk}\gamma_\mu t^a d_{Ll})$	$\frac{16}{3}g_s^2C^2_{GG}\delta_{ij}\delta_{kl}$
	$[Q^{V8,RR}_{ud}]_{ijkl}$	$(\bar{u}_{Ri}\gamma^\mu t^a u_{Rj})(\bar{d}_{Rk}\gamma_\mu t^a d_{Rl})$	$\frac{16}{3}g_s^2C^2_{GG}\delta_{ij}\delta_{kl}$
$(\bar{L}L)(\bar{R}R)$	$[Q^{V,LR}_{ee}]_{ijkl}$	$(\bar{e}_{Li}\gamma^\mu e_{Lj})(\bar{e}_{Rk}\gamma_\mu e_{Rl})$	$\frac{16}{3}e^2C^2_{\gamma\gamma}\delta_{ij}\delta_{kl}$
	$[Q^{V,LR}_{eu}]_{ijkl}$	$(\bar{e}_{Li}\gamma^\mu e_{Lj})(\bar{u}_{Rk}\gamma_\mu u_{Rl})$	$-\frac{32}{9}e^2C^2_{\gamma\gamma}\delta_{ij}\delta_{kl}$
	$[Q^{V,LR}_{ed}]_{ijkl}$	$(\bar{e}_{Li}\gamma^\mu e_{Lj})(\bar{d}_{Rk}\gamma_\mu d_{Rl})$	$\frac{16}{9}e^2C^2_{\gamma\gamma}\delta_{ij}\delta_{kl}$
	$[Q^{V,LR}_{ue}]_{ijkl}$	$(\bar{u}_{Li}\gamma^\mu u_{Lj})(\bar{e}_{Rk}\gamma_\mu e_{Rl})$	$-\frac{32}{9}e^2C^2_{\gamma\gamma}\delta_{ij}\delta_{kl}$
	$[Q^{V,LR}_{de}]_{ijkl}$	$(\bar{d}_{Li}\gamma^\mu d_{Lj})(\bar{e}_{Rk}\gamma_\mu e_{Rl})$	$\frac{16}{9}e^2C^2_{\gamma\gamma}\delta_{ij}\delta_{kl}$
	$[Q^{V1,LR}_{uu}]_{ijkl}$	$(\bar{u}_{Li}\gamma^\mu u_{Lj})(\bar{u}_{Rk}\gamma_\mu u_{Rl})$	$\frac{64}{27}e^2C^2_{\gamma\gamma}\delta_{ij}\delta_{kl}$
	$[Q^{V8,LR}_{uu}]_{ijkl}$	$(\bar{u}_{Li}\gamma^\mu t^a u_{Lj})(\bar{u}_{Rk}\gamma_\mu t^a u_{Rl})$	$\frac{16}{3}g_s^2C^2_{GG}\delta_{ij}\delta_{kl}$
	$[Q^{V1,LR}_{ud}]_{ijkl}$	$(\bar{u}_{Li}\gamma^\mu u_{Lj})(\bar{d}_{Rk}\gamma_\mu d_{Rl})$	$-\frac{32}{27}e^2C^2_{\gamma\gamma}\delta_{ij}\delta_{kl}$
	$[Q^{V8,LR}_{ud}]_{ijkl}$	$(\bar{u}_{Li}\gamma^\mu t^a u_{Lj})(\bar{d}_{Rk}\gamma_\mu t^a d_{Rl})$	$\frac{16}{3}g_s^2C^2_{GG}\delta_{ij}\delta_{kl}$
	$[Q^{V1,LR}_{du}]_{ijkl}$	$(\bar{d}_{Li}\gamma^\mu d_{Lj})(\bar{u}_{Rk}\gamma_\mu u_{Rl})$	$-\frac{32}{27}e^2C^2_{\gamma\gamma}\delta_{ij}\delta_{kl}$
	$[Q^{V8,LR}_{du}]_{ijkl}$	$(\bar{d}_{Li}\gamma^\mu t^a d_{Lj})(\bar{u}_{Rk}\gamma_\mu t^a u_{Rl})$	$\frac{16}{3}g_s^2C^2_{GG}\delta_{ij}\delta_{kl}$
	$[Q^{V1,LR}_{dd}]_{ijkl}$	$(\bar{d}_{Li}\gamma^\mu d_{Lj})(\bar{d}_{Rk}\gamma_\mu d_{Rl})$	$\frac{16}{27}e^2C^2_{\gamma\gamma}\delta_{ij}\delta_{kl}$
	$[Q^{V6,LR}_{dd}]_{ijkl}$	$(\bar{d}_{Li}\gamma^\mu t^a d_{Lj})(\bar{d}_{Rk}\gamma_\mu t^a d_{Rl})$	$\frac{16}{3}g_s^2C^2_{GG}\delta_{ij}\delta_{kl}$

Table 3.2.: LEFT operators and their definitions (second and third column) and the one-loop ALP-generated inhomogeneous source terms entering the RG evolution equations of the LEFT Wilson coefficients (last column).

Wave-function, coupling and mass renormalization

Apart from the inhomogeneous source terms that enter the RG evolution equations, ALPs also contribute to amplitudes that require dimension-four SM operators as counterterms. This occurs for the purely gauge-boson amplitudes in (3.10), as well as for the fermion self-energies in (3.17). In the first case, this results in a modification of the wave-function renormalization constants of the gluon- and the photon-field of the form

$$\delta Z_G = \frac{8m_a^2}{(4\pi f)^2}\,\frac{C_{GG}^2}{\epsilon}\,, \qquad \delta Z_\gamma = \frac{8m_a^2}{(4\pi f)^2}\,\frac{C_{\gamma\gamma}^2}{\epsilon}\,. \tag{3.20}$$

From $\alpha_{s,0} = \mu^{2\epsilon}\, Z_{\alpha_s}\, \alpha_s$, where $Z_{\alpha_s} = Z_{\bar{q}qg}^2 Z_q^{-2}\, Z_G^{-1}$, and the fact that $\alpha_{s,0}$ is scale independent follows that

$$\frac{1}{\alpha_s}\frac{d\alpha_s}{d\ln\mu} = -2\epsilon - \frac{1}{Z_{\alpha_s}}\frac{dZ_{\alpha_s}}{d\ln\mu} \quad \text{with } Z_{\alpha_s} = Z_{\alpha_s}^{\text{SM}} - \frac{8m_a^2}{(4\pi f)^2}\frac{C_{GG}^2}{\epsilon}\,, \tag{3.21}$$

such that the β-function of QCD, defined as $d\alpha_s/d\ln\mu \equiv -2\alpha_s\beta_{\text{QCD}}$, gets modified to

$$\beta_{\text{QCD}} = \beta_{\text{QCD}}^{\text{SM}} + \frac{8m_a^2}{(4\pi f)^2}\, C_{GG}^2\,. \tag{3.22}$$

Similarly, for the β-function of Quantum Electrodynamics (QED),

$$\beta_{\text{QED}} = \beta_{\text{QED}}^{\text{SM}} + \frac{8m_a^2}{(4\pi f)^2}\, C_{\gamma\gamma}^2\,. \tag{3.23}$$

Finally, the contributions in (3.17) modify the fermion wave-functions and mass renormalizations. Assuming flavor-diagonal ALP-fermion couplings in the mass basis, the additional terms for a fermion f read

$$\delta Z_f = -\frac{m_f^2}{(4\pi f)^2}\,\frac{c_{ff}^2}{2\epsilon} \quad \text{and} \quad \delta m_f = \frac{m_f}{(4\pi f)^2}\,\frac{c_{ff}^2}{\epsilon}\,\left(m_f^2 + \frac{m_a^2}{2}\right)\,. \tag{3.24}$$

The presence of the $1/\epsilon$ pole in the fermion mass term yields a modification to the RG evolution equation $dm_f/d\ln\mu = \gamma_{m_f}\, m_f$ of the form

$$\gamma_{m_f} = \gamma_{m_f}^{\text{SM}} + \frac{2m_f^2 + m_a^2}{(4\pi f)^2}\, c_{ff}^2\,. \tag{3.25}$$

3.7. ALP–LEFT Contributions to the Muon Anomalous Magnetic Moment

The anomalous magnetic dipole moment (MDM) of the electron and the muon are two important precision observables in particle physics that are highly sensitive to physics beyond the SM. In general terms, the MDM $\vec{\mu}$ quantifies the interaction of the spin of a given fermion f with an external magnetic field and is given by

$$\vec{\mu} = g_f\,\frac{q_f}{2\,m_f}\,\vec{S}\,, \tag{3.26}$$

where q_f and m_f denote the fermion's electric charge and mass and $\vec{S}$ its spin. The Landé-factor g_f can be decomposed as [36]

$$g_f = 2\,[F_1(0) + 2\,F_2(0)] = 2 + 2\,F_2(0)\,. \tag{3.27}$$

Classically, the F_2 term is absent, such that $g_f = 2$. In quantum field theory, however, loop corrections yield a deviation from this result that is typically parametrized as

$$a_f \equiv \frac{(g-2)_f}{2}\,, \tag{3.28}$$

and called the *anomalous magnetic dipole moment*. In the SM, there are three types of diagrams that contribute beyond the leading order: QED, electroweak and hadronic corrections, such that $a_f^{\text{SM}} = a_f^{\text{QED}} + a_f^{\text{EW}} + a_f^{\text{had}}$. Representative lowest-order Feynman graphs for each of these contributions in the SM are shown in Figure 3.7. Certainly, at low energies, graphs containing explicit Z and $W^\pm$ bosons are absent.

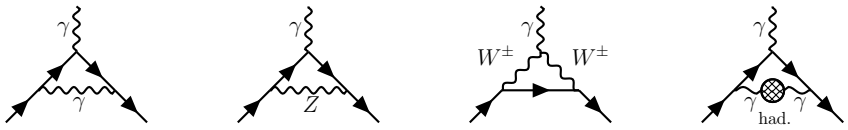

Figure 3.7.: Representative Feynman diagrams contributing to the magnetic dipole moment of the fermions. The first graph from the left shows the one-loop QED correction, which yields the *Schwinger* term $\alpha/(2\pi)$ to $F_2(0)$. The second and third graph are the lowest order weak corrections, while the graph on the right represents hadronic contributions to a_f.

There has been an anomaly in the anomalous magnetic moment of the electron and the muon for a long time, and enormous effort has been made to improve both theory prediction and experimental measurement. In a recent white paper, WP25, of the Muon $g-2$ Theory Initiative [145], the improved lattice QCD average for the hadronic vacuum polarization has led to a substantial upward adjustment of the predicted value of a_μ, which removed the tension between experiment and theory in this quantity. Yet, contributions from ALPs can significantly affect its value and it is therefore still of enormous interest when searching for hints of new physics. In the following section, it will be examined in detail how ALP contributions to a_μ arise from the *ALP–LEFT interference* discussed in the previous section. In the LEFT without ALP, contributions have been discussed in detail in [146]. Including the ALP, the one-loop order result at $\mu_0 \sim m_\mu$ reads[2]

$$\begin{aligned} a_\mu &= \frac{\alpha(\mu_0)}{2\pi} - \frac{4m_\mu}{e}\,\Re e\left[C_{e\gamma}(\mu_0)\right]_{22}\left[1 - \frac{\alpha}{4\pi}\left(5\ln\frac{\mu_0^2}{m_\mu^2} + 2\right)\right] \\ &\quad + a_\mu^{4\ell}(\mu_0) + a_\mu^{2\ell 2q}(\mu_0) + a_\mu^{\text{ALP}}(\mu_0) \\ &\equiv [a_\mu]^{\text{SM}} + [a_\mu]^{\text{ALP}}\,, \end{aligned} \tag{3.29}$$

where $a_\mu^{\text{ALP}}(\mu_0)$ denotes direct ALP contributions, while $[a_\mu]^{\text{ALP}}$ contains all ALP-generated contributions, including indirect ones. The individual terms are represented by the graphs depicted in Figure 3.8. The terms that appear in (3.29) are the following

[2] The SM prediction for a_μ is known to much higher accuracy than the one-loop result included here, see [147].

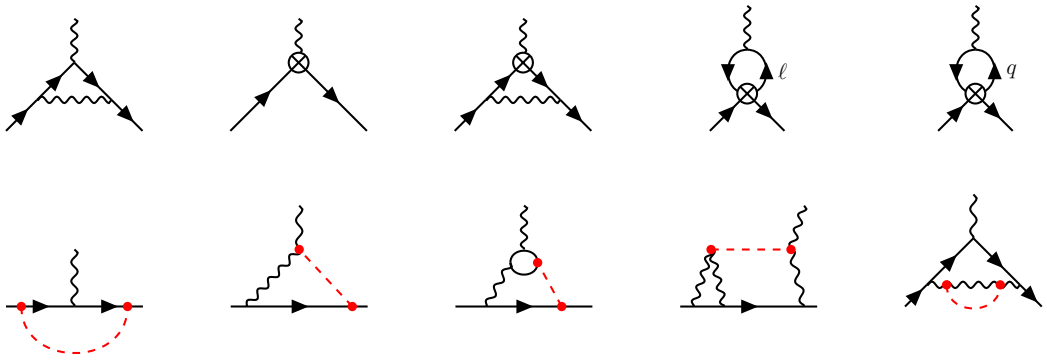

Figure 3.8.: Representative Feynman diagrams contributing to the anomalous magnetic moment of the muon at one- and partial two-loop order when the SM is extended by an ALP. LEFT operators are indicated by the ⊗ symbol, while the red dashed line shown the ALP.

ones:

- The SM *Schwinger* term, $\alpha(\mu_0)/(2\pi)$, results from the one-loop QED correction (first diagram in Figure 3.8).
- The second term in the first line of (3.29) results from the one-loop matrix element of the electromagnetic dipole operator in the LEFT (second and third diagrams in the first row of Figure 3.8). The Wilson coefficient of the LEFT dipole operator contains the pure SM contribution $\left[C_{e\gamma}(\mu_0)\right]_{22}^{\text{SM}} = \frac{G_F\, e m_\mu}{48\sqrt{2}\pi^2}\left(-3 - 8\,s_w^2 + 16\,s_w^4\right)$.
- Penguin diagrams involving four-lepton operators in the LEFT generate the fourth diagram in the first row of Figure 3.8, which arise from the exchange of $W^\pm$ and Z bosons. In detail, the contribution reads

$$a_\mu^{4\ell}(\mu_0) = m_\mu \sum_{\ell=e,\mu,\tau} \frac{m_\ell}{4\pi^2}\left[\ln\frac{\mu_0^2}{m_\ell^2}\,\Re e\left[C_{ee}^{S,RR}(\mu_0)\right]_{2\ell\ell 2} - \Re e\left[C_{ee}^{V,LR}(\mu_0)\right]_{2\ell\ell 2}\right]. \tag{3.30}$$

  Again, besides ALP effects on the coefficient, $C_{ee}^{V,LR}$ already contains the pure SM term $\left[C_{ee}^{V,LR}(\mu_0)\right]_{2\ell\ell 2}^{\text{SM}} = \frac{4G_F}{\sqrt{2}}\left(1 - 2\,s_w^2\right) s_w^2\,\delta_{2\ell}$. $C_{ee}^{S,RR}$ does not get sourced by the ALP and thus does not play a role in the following discussion.
- The term $a_\mu^{2\ell 2q}$ arises from penguin diagrams involving a quark loop (fifth diagram in the first row). It is given in (3.4) and (3.5) of [146] and involves the coefficients $C_{eu}^{T,RR}$ and $C_{ed}^{T,RR}$, which are not sourced by one-loop ALP exchange.
- Finally, there are the direct ALP contributions, shown at one- and partial two-loop order in the second row of Figure 3.8.

The final goal is to obtain an expression for a_μ in terms of the ALP couplings at the UV-scale Λ. This can be done in three steps, and thus the next sections are structured as follows: First, the direct ALP contributions to the muon anomalous magnetic dipole moment are summarized. Subsequently, the relevant coefficients are scale evolved up

to the electroweak scale, where matching corrections need to be taken into account. Finally, the RG evolution above μ_w is applied up to the ALP-scale Λ.

3.7.1. Direct ALP Contributions to a_μ

The direct ALP contributions to a_μ, i.e. those in the second row of Figure 3.8, have been computed in [28, 34] and read

$$\begin{aligned} a_\mu^{\text{ALP}}(\mu_0) = \frac{m_\mu^2}{(4\pi f)^2}\Bigg(& -8\,c_{\mu\mu}(\mu_0)\,C_{\gamma\gamma}(\mu_0)\left[\ln\frac{\mu_0^2}{m_\mu^2}+\delta_2+3-h_2(x_\mu)\right] \\ & -\frac{2\,\alpha(\mu_0)}{\pi}\,c_{\mu\mu}(\mu_0)\sum_{f\neq t}N_c^f\,Q_f^2\,c_{ff}(\mu_0)\int_0^1 dz\,F\big(z(1-z)x_f,x_\mu\big) \\ & +\frac{\alpha(\mu_0)}{\pi}\,C_{\gamma\gamma}^2(\mu_0)\,\Delta_{\text{LbL}}(\mu_0,m_a,m_\mu)-c_{\mu\mu}^2(\mu_0)\,h_1(x_\mu) \\ & +\frac{m_\tau}{m_\mu}\,\Re e\big([k_e]_{23}[k_E]_{23}^*\big)\,h_3(x_\tau) \\ & -\frac{1}{2}\big(|[k_e]_{12}|^2+|[k_E]_{12}|^2\big)\,h_4(x_\mu)\Bigg)\,, \end{aligned} \tag{3.31}$$

where $x_f \equiv m_a^2/m_f^2 + i0$, and the loop functions $h_i(x)$ are given by

$$\begin{aligned} h_1(x) &= 1+2x+x(1-x)\ln x-2x(3-x)\sqrt{\frac{x}{4-x}}\,\arccos\frac{\sqrt{x}}{2}\,, \\ h_2(x) &= 1-\frac{x}{3}+\frac{x^2}{6}\ln x+\frac{2+x}{3}\sqrt{x(4-x)}\,\arccos\frac{\sqrt{x}}{2}\,, \\ h_3(x) &= \frac{1-3x}{(1-x)^2}-\frac{2x^2}{(1-x)^3}\ln x\,, \\ h_4(x) &= 1+2x-2x^2\ln\frac{x}{x-1}\,, \end{aligned} \tag{3.32}$$

and

$$F(y,x) = \frac{1}{1-y}\left[h_2(x)-h_2\left(\frac{x}{y}\right)\right]\,, \tag{3.33}$$

which is a loop function arising at two-loop order from Barr–Zee diagrams [148] (third diagram in the second row of Figure 3.8), calculated in [34, 149]. The constant δ_2 in the first line of (3.31) is a scheme dependent quantity related to the treatment of $\epsilon^{\mu\nu\alpha\beta}$ in dimensional regularization: when treated as four-dimensional, $\delta_2 = 0$, while for a d-dimensional object, $\delta_2 = -3$ [28]. The scale μ_0, where the expression a_μ^{ALP} is evaluated, depends on the mass hierarchy between the ALP and the muon. When one of the two particles is much heavier than the other, one needs to set $\mu_0 \sim \max(m_\mu, m_a)$. In addition, the quantity Δ_{LbL} in (3.31) accounts for the last two diagrams in the second line of Figure 3.8 that show the contributions from light-by-light scattering and ALP vacuum polarization. While this quantity has not yet been fully computed, it was analyzed at leading logarithmic approximation for $\mu \gg m_{\mu,a}$ in [150]. Finally, the flavor off-diagonal contribution to the muon anomalous magnetic dipole moment, the last term in (3.31), stems from the first diagram in the second line of Figure 3.8

when the fermion in the loop is an electron or a tau and the mass ratios m_μ/m_τ and m_e/m_μ are neglected. Since the flavor off-diagonal ALP-fermion couplings are scale independent up to $\mathcal{O}(\alpha^2)$, there is no argument μ_0 in these terms.

3.7.2. Renormalization Group Evolution to the Electroweak Scale

For the goal of expressing the muon anomalous magnetic dipole moment in terms of ALP couplings at the electroweak scale, it is necessary to solve the relevant RG evolution equations, which in the following is performed at lowest non-trivial order in the ALP couplings. In more detail, this requires the solutions to the ALP couplings $c_{\mu\mu}$ and $C_{\gamma\gamma}$, the additional contribution to the scale evolution of α, as well as to the LEFT Wilson coefficients $[C_{e\gamma}]_{22}$ and $[C_{ee}^{V,LR}]_{2\ell\ell 2}$.
For $c_{\mu\mu}$ and $C_{\gamma\gamma}$, the relevant RG evolution equations have been found in [60]. Omitting quadratic and higher order terms of α, as well as its scale dependence, one can deduce the following approximate solutions:

$$\begin{aligned}
\frac{dc_{\mu\mu}}{d\ln\mu} &= \frac{6\alpha}{\pi}\, C_{\gamma\gamma} && \Rightarrow \quad c_{\mu\mu}(\mu_0) \approx c_{\mu\mu}(\mu_w) - \frac{3\alpha}{\pi}\, C_{\gamma\gamma}(\mu_w)\, \ln\frac{\mu_w^2}{\mu_0^2}\,, \\
\frac{dC_{\gamma\gamma}}{d\ln\mu} &= -\beta_0^{\text{QED}}\,\frac{\alpha}{2\pi}\, C_{\gamma\gamma} && \Rightarrow \quad C_{\gamma\gamma}(\mu_0) \approx \left[1 + \beta_0^{\text{QED}}\,\frac{\alpha(\mu_w)}{4\pi}\,\ln\frac{\mu_w^2}{\mu_0^2}\right] C_{\gamma\gamma}(\mu_w)\,.
\end{aligned} \tag{3.34}$$

For the gauge coupling of QED, the ALP induced RG contribution in (3.23) yields, up to linear order in α,

$$\big[\alpha(\mu_0)\big]^{\text{ALP}} \approx \alpha(\mu_w)\left[1 + \frac{8m_a^2}{(4\pi f)^2}\, C_{\gamma\gamma}^2(\mu_w)\,\ln\frac{\mu_w^2}{\mu_0^2}\right]. \tag{3.35}$$

Lastly, the inhomogeneous source terms for the relevant LEFT Wilson coefficients are those summarized in Table 3.2. Since $[C_{ee}^{V,LR}]_{2\ell\ell 2}$ arises only at one-loop order in $a_\mu^{4\ell}$, it suffices to integrate $S_{ee}^{V,LR}$. The situation is only slightly different for the dipole coefficient $[C_{e\gamma}]_{22}$: Even though the coefficient mixes under a scale evolution with itself, with $C_{eu}^{T,RR}$, $C_{ed}^{T,RR}$, $C_{ee}^{S,RR}$ (not ALP sourced), as well as with $C_{e\gamma}$, $C_{u\gamma}$ and $C_{d\gamma}$ times the mass of a light SM fermion [144], these mixing effects do not give rise to contributions at the relevant order. Therefore, when neglecting higher order effects in α, only the scale evolution of $c_{\mu\mu}$ needs to be taken into account when integrating the inhomogeneous source term of $[C_{e\gamma}]_{22}$. In total, this yields

$$\begin{aligned}
\big[C_{e\gamma}(\mu_0)\big]_{22}^{\text{ALP}} &\approx \big[C_{e\gamma}(\mu_w)\big]_{22}^{\text{ALP}} \\
&\quad + \frac{2e\,m_\mu}{(4\pi f)^2}\, C_{\gamma\gamma}(\mu_w)\left[c_{\mu\mu}(\mu_w)\,\ln\frac{\mu_w^2}{\mu_0^2} - \frac{3\alpha}{2\pi}\, C_{\gamma\gamma}(\mu_w)\,\ln^2\frac{\mu_w^2}{\mu_0^2}\right], \\
\big[C_{ee}^{V,LR}(\mu_0)\big]_{2\ell\ell 2}^{\text{ALP}} &\approx \big[C_{ee}^{V,LR}(\mu_w)\big]_{2\ell\ell 2}^{\text{ALP}} - \frac{1}{(4\pi f)^2}\,\frac{32\pi\,\alpha}{3}\, C_{\gamma\gamma}^2(\mu_w)\,\delta_{2\ell}\,\ln\frac{\mu_w^2}{\mu_0^2}\,.
\end{aligned} \tag{3.36}$$

Inserting these results into the direct ALP contributions in (3.31), as well as the Schwinger term in (3.29), and neglecting higher-order loop results of the ALP cou-

plings, the final result in terms of the couplings at μ_w is given by

$$
\begin{aligned}
[a_\mu]^{\text{ALP}} = &-\frac{4m_\mu}{e}\,\Re e\left[C_{e\gamma}(\mu_w)\right]_{22}^{\text{ALP}} - m_\mu \sum_{\ell=e,\mu,\tau} \frac{m_\ell}{4\pi^2}\,\Re e\left[C_{ee}^{V,LR}(\mu_w)\right]_{2\ell\ell 2}^{\text{ALP}} \\
&+ \frac{m_\mu^2}{(4\pi f)^2}\Bigg\{ - c_{\mu\mu}^2(\mu_w)\, h_1(x_\mu) \\
&\quad - 8 c_{\mu\mu}(\mu_w)\, C_{\gamma\gamma}(\mu_w)\left[\ln\frac{\mu_w^2}{m_\mu^2} + \delta_2 + 3 - h_2(x_\mu)\right] \\
&\quad - \frac{2\alpha(\mu_w)}{\pi}\, c_{\mu\mu}(\mu_w) \sum_{f\neq t} N_c^f\, Q_f^2\, c_{ff}(\mu_w) \int_0^1 dz\, F\big(z(1-z)x_f, x_\mu\big) \\
&\quad + \frac{12\alpha(\mu_w)}{\pi}\, C_{\gamma\gamma}^2(\mu_w)\Bigg[\left(2\delta_2 + \frac{56}{9} - 2h_2(x_\mu) + \frac{x_\mu}{3}\right)\ln\frac{\mu_w^2}{\mu_0^2} \\
&\qquad\qquad + \ln^2\frac{\mu_w^2}{m_\mu^2} - \ln^2\frac{\mu_0^2}{m_\mu^2} + \frac{1}{12}\,\Delta_{\text{LbL}}(\mu_0, m_a, m_\mu)\Bigg] \\
&\quad + \frac{m_\tau}{m_\mu}\,\Re e\left([k_e]_{23}\,[k_E]_{23}^*\right) h_3(x_\tau) - \frac{1}{2}\left(|[k_e]_{12}|^2 + |[k_E]_{12}|^2\right) h_4(x_\mu)\Bigg\}\,.
\end{aligned}
\tag{3.37}
$$

From this equation and the necessity of the low-energy scale to cancel out of the expression, one can deduce that the term proportional to $C_{\gamma\gamma}^2$,

$$
\frac{1}{12}\,\Delta_{\text{LbL}}(\mu_0, m_a, m_\mu) - \ln^2\frac{\mu_0^2}{m_\mu^2} - \left(2\delta_2 + \frac{56}{9} - 2h_2(x_\mu) + \frac{x_\mu}{3}\right)\ln\frac{\mu_0^2}{m_\mu^2}\,, \tag{3.38}
$$

must be independent of μ_0.

3.7.3. Electroweak Matching Contributions

As a next step, matching corrections at the electroweak scale need to be taken into account and a rewriting in terms of the appropriate couplings is necessary, since the degrees of freedom change at μ_w. Concretely, this affects the couplings $C_{\gamma\gamma}$, $c_{\mu\mu}$, as well as the LEFT dipole coefficient $[C_{e\gamma}]_{22}^{\text{ALP}}$.
Starting with the ALP coefficients, the matching relations have been obtained in [60]. Defining by μ_w^+ and μ_w^- the scale infinitesimally above or below μ_w, they read

$$
\begin{aligned}
C_{\gamma\gamma}(\mu_w^-) &= C_{\gamma\gamma}(\mu_w^+) - \frac{\alpha(\mu_w)}{4\pi}\, N_c Q_u^2\, c_{tt}(\mu_w^+) \\
&= c_w^2\, C_{BB}(\mu_w^+) + s_w^2\, C_{WW}(\mu_w^+) - \frac{\alpha(\mu_w)}{3\pi}\, c_{tt}(\mu_w^+)\,,
\end{aligned}
\tag{3.39}
$$

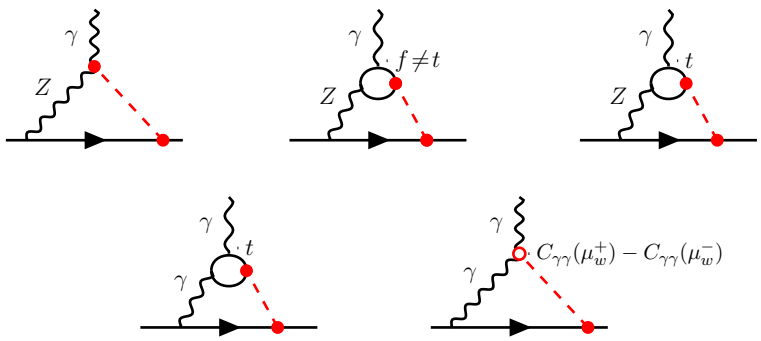

Figure 3.9.: Representative Feynman diagrams contributing to the ALP-induced matching corrections to the LEFT dipole coefficient $C_{e\gamma}$ at the electroweak scale. The open red circle in the last diagram accounts for the matching contribution obtained from the fact that the ALP-photon coupling $C_{\gamma\gamma}$ differs in the effective theories above and below the electroweak scale.

for the case of the photon coupling with short-hand notations $c_w^2 \equiv \cos^2\theta_w = m_W^2/m_Z^2$ and $s_w^2 \equiv \sin^2\theta_w$, and

$$\begin{aligned} c_{\mu\mu}(\mu_w^-) = c_{\mu\mu}(\mu_w^+) &+ \frac{3\alpha_t(\mu_w)}{4\pi}\, c_{tt}(\mu_w^+)\, \ln\frac{\mu_w^2}{m_t^2} \\ &- \frac{\alpha_1(\mu_w)}{4\pi}\, C_{BB}(\mu_w^+)\left[\left(\frac{15}{2} - 12c_w^4\right)\left(\ln\frac{\mu_w^2}{m_Z^2} + \delta_1 + \frac{1}{2}\right) - 6c_w^2\left(1 - 4s_w^2\right)\right] \\ &- \frac{\alpha_2(\mu_w)}{4\pi}\, C_{WW}(\mu_w^+)\left[\left(\frac{9}{2} - 12s_w^4\right)\left(\ln\frac{\mu_w^2}{m_Z^2} + \delta_1 + \frac{1}{2}\right)\right. \\ &\qquad \left. - 3\ln c_w^2 + 6s_w^2\left(1 - 4s_w^2\right)\right], \end{aligned} \tag{3.40}$$

with $m_t \equiv m_t(m_t)$. For the LEFT dipole coefficient relevant Feynman diagrams for the matching include those depicted in Figure 3.9. The three Z-boson graphs in the first row are proportional to $(g_L^e + g_R^e) = (-\frac{1}{2} + 2s_w^2) \approx -0.04$. While the first diagram has been obtained in [28], the last two graphs in the first line of the figure haven not been calculated in the literature before. The second diagram vanishes up to $\mathcal{O}(m_f^2/m_Z^2)$, while the third one gives a contribution proportional to $c_{\mu\mu}\, c_{tt}$, which is independent of the scale μ_w but depends on the ratio m_t^2/m_Z^2. It is a reasonable approximation to neglect this unknown contribution, because it is much smaller than other terms involving the same ALP couplings in the result (3.41) below. Shrinking the heavy-particle propagators to a point and assuming that at least one of the remaining loop momenta is soft leads to the low-energy subgraphs shown in Figure 3.10, where effective vertices in the ALP–LEFT theory are shown as the red $\otimes$ symbols, that scale as $1/(fv^2)$ (first graph) and $1/(f^2v^2)$ (third graph). The operator symbolized by $\otimes$ scales as $1/v^2$. In all three cases, the result is proportional to $\sim m_{\mu,a}^2/v^2$ and can therefore be neglected in the matching.

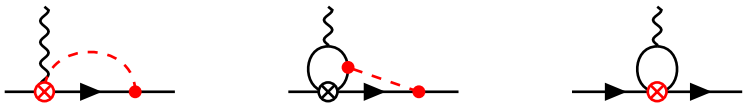

Figure 3.10.: Low-energy subgraphs for the three diagrams in the first row of Figure 3.9. The effective vertex marked by a red ⊗ symbol in the first subgraph from the left corresponds to the dimension-7 operator $(\partial_\mu a)\,\bar{\mu}\gamma_\nu F^{\mu\nu}\mu$, the black ⊗ symbolizes the dimension-six four-lepton LEFT operator and the red ⊗ symbol in the third subgraph is a dimension-8 four-lepton operator. The diagrams are power suppressed and therefore do not contribute to the matching.

The three diagrams shown in the second row of Figure 3.9 correspond to the Barr–Zee contribution of the top quark (first graph) as well as a matching contribution arising from the fact that the ALP-photon coupling $C_{\gamma\gamma}$ in the effective theories just above and below the electroweak scale differs by a contribution involving the top quark. Both diagrams contain a non-zero low-energy contribution sensitive to the masses of the ALP and the muon, but in their sum this contribution cancels out. Combining [28, 34, 143, 149], this yields for the matching of the dipole coefficient at μ_w

$$\begin{aligned}\left[C_{e\gamma}(\mu_w^-)\right]_{22}^{\text{ALP}} = \frac{v}{\sqrt{2}}\left(c_w\left[C_{eB}(\mu_w^+)\right]_{22}^{\text{ALP}} - s_w\left[C_{eW}(\mu_w^+)\right]_{22}^{\text{ALP}}\right)\\ - \frac{e m_\mu}{2(4\pi f)^2}\left(1-4s_w^2\right)c_{\mu\mu}(\mu_w^+)\times\\ \left[C_{BB}(\mu_w^+) - C_{WW}(\mu_w^+)\right]\left(\ln\frac{\mu_w^2}{m_Z^2} + \delta_2 + \frac{3}{2}\right)\\ + \frac{e m_\mu}{(4\pi f)^2}\frac{2\alpha(\mu_w)}{3\pi}c_{\mu\mu}(\mu_w^+)\,c_{tt}(\mu_w^+)\times\\ \left[\left(\ln\frac{\mu_w^2}{m_t^2} + \delta_2 - \frac{1}{2}\right) + (1-4s_w^2)(\dots)\right],\end{aligned} \tag{3.41}$$

where the dots refer to the unknown contribution from the third diagram in Figure 3.9. For the coefficient $C_{ee}^{V,LR}$, one-loop matching corrections arise from diagrams of the form

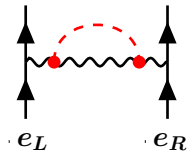

that have not yet been calculated. The relation is therefore written as [143]

$$\left[C_{ee}^{V,LR}(\mu_w^-)\right]_{2\ell\ell 2}^{\text{ALP}} = \left[C_{le}(\mu_w^+)\right]_{2\ell\ell 2}^{\text{ALP}} + \text{loop corrections}\,. \tag{3.42}$$

3.7.4. RG Evolution above the Electroweak Scale

Having obtained an expression for the anomalous magnetic dipole moment of the muon in terms of couplings above the electroweak scale, it is now possible to RG evolve these coefficients up to Λ. To this end it is necessary to collect and derive the

required solutions to the RG equations. Starting once more with the ALP coefficients $c_{\mu\mu}$ and c_{tt}, the leading-order RG-improved result was obtained in [60]. Neglecting the scale dependence of the electroweak gauge couplings α_1 and α_2 as well as of the ALP-boson couplings C_{BB} and C_{WW}, it reads

$$\begin{aligned} c_{\mu\mu}(\mu_w^+) &\approx c_{\mu\mu}(\Lambda) + \hat{I}_t(\mu_w,\Lambda)\, c_{tt}(\Lambda) - \left[\frac{15\alpha_1}{8\pi}\, C_{BB}(\Lambda) + \frac{9\alpha_2}{8\pi}\, C_{WW}(\Lambda)\right] \ln\frac{\Lambda^2}{\mu_w^2}\,, \\ c_{tt}(\mu_w^+) &\approx \left[1 - \frac{3}{2}\,\hat{I}_t(\mu_w,\Lambda)\right] c_{tt}(\Lambda) - \frac{16}{7}\left[\frac{\alpha_s(\mu_w)}{\alpha_s(\Lambda)} - 1\right] C_{GG}(\Lambda) \\ &\quad - \left[\frac{17\alpha_1}{24\pi}\, C_{BB}(\Lambda) + \frac{9\alpha_2}{8\pi}\, C_{WW}(\Lambda)\right] \ln\frac{\Lambda^2}{\mu_w^2}\,, \end{aligned} \tag{3.43}$$

with

$$\hat{I}_t(\mu_w,\Lambda) = \int_{\mu_w}^{\Lambda} \frac{d\mu}{\mu}\, \frac{3\alpha_t(\mu)}{2\pi}\, \frac{c_{tt}(\mu)}{c_{tt}(\Lambda)} = \frac{3\alpha_t(\mu_w)}{\alpha_s(\mu_w)} \left[1 - \left(\frac{\alpha_s(\Lambda)}{\alpha_s(\mu_w)}\right)^{\frac{1}{7}}\right]. \tag{3.44}$$

It is crucial to note that RG evolution effects generate the appearance of the ALP-top quark coupling in the expression for $c_{\mu\mu}(\mu_w^+)$ in (3.43). Even in the absence of a direct coupling to muons at Λ, this term generates a shift in a_μ.
Finally, only the solution to the scale evolution of the SMEFT coefficients C_{eB} and C_{eW} that enter in the expression (3.41) are missing. Taking into account one-loop mixing effects, also the solutions for the ALP-sourced coefficients C_{HB}, C_{HW} and C_{HWB} are needed. Additionally, they also mix with $C_{H\widetilde{B}}$, $C_{H\widetilde{W}}$ and $C_{H\widetilde{W}B}$, which, however, are not generated by the ALP. It is therefore sufficient to obtain the solutions for C_{HB}, C_{HW} and C_{HWB}, which, at leading logarithmic order, are given by

$$\begin{aligned} \big[C_{HB}(\mu)\big]^{\text{ALP}} &\approx \big[C_{HB}(\Lambda)\big]^{\text{ALP}} + \frac{4\pi\,\alpha_1}{(4\pi f)^2}\, C_{BB}^2(\Lambda)\, \ln\frac{\Lambda^2}{\mu^2}\,, \\ \big[C_{HW}(\mu)\big]^{\text{ALP}} &\approx \big[C_{HW}(\Lambda)\big]^{\text{ALP}} + \frac{4\pi\,\alpha_2}{(4\pi f)^2}\, C_{WW}^2(\Lambda)\, \ln\frac{\Lambda^2}{\mu^2}\,, \\ \big[C_{HWB}(\mu)\big]^{\text{ALP}} &\approx \big[C_{HWB}(\Lambda)\big]^{\text{ALP}} + \frac{8\pi\sqrt{\alpha_1\,\alpha_2}}{(4\pi f)^2}\, C_{BB}(\Lambda)\, C_{WW}(\Lambda)\, \ln\frac{\Lambda^2}{\mu^2}\,. \end{aligned} \tag{3.45}$$

Using the above relations, it is straightforward to integrate the RG equations for the dipole coefficients in the leading logarithmic approximation, which results in

$$\begin{aligned} \big[C_{eB}(\mu_w^+)\big]_{22}^{\text{ALP}} &\approx \big[C_{eB}(\Lambda)\big]_{22}^{\text{ALP}} \\ &\quad + \frac{y_\mu}{16\pi^2}\left[\frac{3g_1}{2}\,\big[C_{HB}(\Lambda)\big]^{\text{ALP}} - \frac{3g_2}{4}\,\big[C_{HWB}(\Lambda)\big]^{\text{ALP}}\right] \ln\frac{\Lambda^2}{\mu_w^2} \\ &\quad + \frac{g_1\,y_\mu}{(4\pi f)^2}\, C_{BB}(\Lambda)\left\{\frac{3}{2}\, c_{\mu\mu}(\Lambda)\, \ln\frac{\Lambda^2}{\mu_w^2}\right. \\ &\quad \left. + \left[\frac{9\alpha_t}{16\pi}\, c_{tt}(\Lambda) - \frac{39\alpha_1}{32\pi}\, C_{BB}(\Lambda) - \frac{33\alpha_2}{32\pi}\, C_{WW}(\Lambda)\right] \ln^2\frac{\Lambda^2}{\mu_w^2}\right\}, \end{aligned} \tag{3.46}$$

and

$$\begin{aligned}\left[C_{eW}(\mu_w^+)\right]_{22}^{\text{ALP}} \approx \left[C_{eW}(\Lambda)\right]_{22}^{\text{ALP}} &\\ + \frac{y_\mu}{16\pi^2}\left[\frac{g_2}{2}\left[C_{HW}(\Lambda)\right]^{\text{ALP}} - \frac{3g_1}{4}\left[C_{HWB}(\Lambda)\right]^{\text{ALP}}\right]\ln\frac{\Lambda^2}{\mu_w^2} &\\ + \frac{g_2\, y_\mu}{(4\pi f)^2}\, C_{WW}(\Lambda)\left\{-\frac{1}{2}\, c_{\mu\mu}(\Lambda)\,\ln\frac{\Lambda^2}{\mu_w^2}\right. &\\ \left. + \left[-\frac{3\alpha_t}{16\pi}\, c_{tt}(\Lambda) + \frac{21\alpha_1}{32\pi}\, C_{BB}(\Lambda) + \frac{7\alpha_2}{32\pi}\, C_{WW}(\Lambda)\right]\ln^2\frac{\Lambda^2}{\mu_w^2}\right\}.\end{aligned} \tag{3.47}$$

Finally, for the SMEFT coefficient C_{le} entering in (3.42), only the inhomogeneous ALP source term needs to be integrated, leading to

$$\left[C_{le}(\mu_w^+)\right]_{2\ell\ell 2}^{\text{ALP}} \approx \left[C_{le}(\Lambda)\right]_{2\ell\ell 2}^{\text{ALP}} - \frac{1}{(4\pi f)^2}\,\frac{16\pi\alpha_1}{3}\, C_{BB}^2(\Lambda)\,\delta_{2\ell}\,\ln\frac{\Lambda^2}{\mu_w^2}\,. \tag{3.48}$$

3.7.5. ALP-models with Loop-Suppressed Boson Couplings

Many ALP-models predict loop-suppressed couplings to the SM gauge bosons, which is indicated by the explicit factors of $\alpha_i/(4\pi)$ for $i = 1, 2, s$ in the Lagrangian (3.1). In this case, the ALP-fermion couplings are much larger than C_{BB} and C_{WW} and terms containing these coefficients can be neglected. In particular, in this scenario, also the source term for the Wilson coefficient $C_{ee}^{V,LR}$ vanishes, and the expression for $[a_\mu]^{\text{ALP}}$ gets simplified to

$$\begin{aligned}[a_\mu]^{\text{ALP}} = -\frac{4m_\mu}{e}\,\Re e\left[C_{e\gamma}(\mu_w^-)\right]_{22}^{\text{ALP}} - \frac{m_\mu^2}{(4\pi f)^2}\, c_{\mu\mu}(\mu_w)\times &\\ \left\{c_{\mu\mu}(\mu_w^-)\, h_1(x_\mu) + 8\, C_{\gamma\gamma}(\mu_w^-)\left[\ln\frac{\mu_w^2}{m_\mu^2} + \delta_2 + 3 - h_2(x_\mu)\right]\right. &\\ \left. + \frac{2\alpha(\mu_w)}{\pi}\sum_{f\neq t} N_c^f\, Q_f^2\, c_{ff}(\mu_w^-)\int_0^1 dz\, F\big(z(1-z)x_f, x_\mu\big)\right\}.\end{aligned} \tag{3.49}$$

In this equation, the flavor-changing ALP-fermion couplings have also been omitted, as they are experimentally tightly constrained [34]. In this much simpler expression for the muon anomalous magnetic dipole moment, it is now straightforward to insert the relations for the expressions at the scale Λ obtained in the last sections. This leads

ALP couplings	$f = 100\,\text{GeV}$, $\Lambda = 1.26\,\text{TeV}$			$f = 300\,\text{GeV}$, $\Lambda = 3.77\,\text{TeV}$		
	$m_a = 0$	$0.3\,\text{GeV}$	$1\,\text{GeV}$	$m_a = 0$	$0.3\,\text{GeV}$	$1\,\text{GeV}$
$c_{\mu\mu}^2(\Lambda)$	-668.1	-166.8	-32.5	-74.2	-18.5	-3.6
$c_{\mu\mu}(\Lambda)\, C_{BB}(\Lambda)/\alpha_1(\Lambda)$	-781.63	-653.45	-557.95	-96.76	-82.94	-72.88
$c_{\mu\mu}(\Lambda)\, C_{WW}(\Lambda)/\alpha_2(\Lambda)$	-799.22	-671.04	-575.54	-100.53	-86.71	-75.40
$c_{\mu\mu}(\Lambda)\, c_{tt}(\Lambda)$	31.7	66.9	64.7	-0.66	6.3	7.0
$c_{\mu\mu}(\Lambda)\, c_{dd}(\Lambda)$	15.0	9.0	5.9	1.7	1.0	0.65
$c_{tt}(\Lambda)\, C_{BB}(\Lambda)/\alpha_1(\Lambda)$	-47.75	-40.21	-33.93	-8.67	-7.41	-6.41
$c_{tt}(\Lambda)\, C_{WW}(\Lambda)/\alpha_2(\Lambda)$	-49.01	-41.47	-35.19	-8.92	-7.67	-6.79
$c_{tt}^2(\Lambda)$	4.5	4.7	4.1	0.53	0.71	0.65
$c_{tt}(\Lambda)\, c_{dd}(\Lambda)$	0.92	0.55	0.36	0.15	0.089	0.058

Table 3.3.: Numerical contributions to $[a_\mu]^{\text{ALP}}$ in units of 10^{-11} proportional to different combinations of ALP couplings at $\Lambda = 4\pi f$ assuming flavor-universal ALP-fermion couplings.

to

$$
\begin{aligned}
[a_\mu]^{\text{ALP}} = &-\frac{4m_\mu}{e}\,\frac{v}{\sqrt{2}}\,\Re e\Big(c_w\,\big[C_{eB}(\Lambda)\big]_{22}^{\text{ALP}} - s_w\,\big[C_{eW}(\Lambda)\big]_{22}^{\text{ALP}}\Big) \\
&- \frac{m_\mu^2}{(4\pi f)^2}\left\{\Big[c_{\mu\mu}(\Lambda) + \hat{I}_t(m_t,\Lambda)\,c_{tt}(\Lambda)\Big]^2 h_1(x_\mu)\right. \\
&\qquad + \frac{2\alpha}{\pi}\Big[c_{\mu\mu}(\Lambda) + \hat{I}_t(m_t,\Lambda)\,c_{tt}(\Lambda)\Big] \\
&\qquad \times\left[\left(\frac{3\pi\,C_{BB}(\Lambda)}{\alpha_1\,c_w^2} + \frac{\pi\,C_{WW}(\Lambda)}{\alpha_2\,s_w^2}\right)\left(\ln\frac{\Lambda^2}{m_Z^2} + \delta_2 + \frac{3}{2}\right)\right. \\
&\qquad\quad + \left(\frac{4\pi}{\alpha_1}\,C_{BB}(\Lambda) + \frac{4\pi}{\alpha_2}\,C_{WW}(\Lambda)\right)\left[\ln\frac{m_Z^2}{m_\mu^2} + \frac{3}{2} - h_2(x_\mu)\right] \\
&\qquad\quad \left.\left. + \sum_f N_c^f\,Q_f^2\,c_{ff}(\Lambda)\int_0^1 dz\,F\big(z(1-z)x_f, x_\mu\big)\right]\right\}.
\end{aligned}
\tag{3.50}
$$

Having used that for the top quark

$$
\int_0^1 dz\,F\big(z(1-z)x_t, x_\mu\big) = -\ln\frac{m_t^2}{m_\mu^2} + h_2(x_\mu) - \frac{7}{2}\,, \tag{3.51}
$$

up to power corrections of $\mathcal{O}(m_{\mu,a}^2/m_t^2)$, the sum in the last line now extends over all quark flavors. The coupling α, as well as c_w and s_w, needs to be evaluated at $\mu_w \sim m_Z$.

Certainly, exact values of a_μ in the presence of an ALP can only be given in the context of a UV-model. Omitting the model-dependent terms in the first line of (3.50) that would result from concrete matching computations at Λ, the contributions from the different terms for representative values of m_a and $\Lambda = 4\pi f$ are shown in Table 3.3. The values correspond to the assumption of a flavor-universal ALP, i.e. $c_{ee} = c_{\tau\tau} = c_{\mu\mu}$, $c_{uu} = c_{cc} = c_{tt}$, and $c_{ss} = c_{bb} = c_{dd}$. As an example, choosing $m_a = 300\,\text{MeV}$,

$f = 100\,\text{GeV}$, $c_{\mu\mu}(\Lambda) = 1$ and $C_{BB}(\Lambda) = -7\alpha_1(\Lambda)/(4\pi)$ produces an ALP contribution to a_μ of about 200×10^{-11}, while the ALP parameter set $m_a = 300\,\text{MeV}$, $f = 100\,\text{GeV}$, $c_{\mu\mu}(\Lambda) = 1$, $c_{tt}(\Lambda) = 1$ and $C_{BB}(\Lambda) = -3\alpha_1(\Lambda)/(4\pi)$ produces a positive contribution of about 100×10^{-11}.
Overall, ALPs contribute directly to the theoretical prediction of $(g-2)_\mu$, yielding a shift in its expected value.

3.8. Summary and Conclusions

In this chapter, indirect ALP effects below the scale of electroweak symmetry breaking were examined. Concretely, it was shown that UV-divergences of Green's functions with virtual one-loop ALP exchange and only SM external states require counterterms of operators starting at dimension-three and higher. Similar to the analogous effect in the SMEFT, new operators are thus generated by the presence of the ALP below μ_w. The effective field theory whose minimal basis systematically parametrizes effects of unknown particles below μ_w is called the Low-Energy Effective Field Theory (LEFT). The crucial difference between the SMEFT and the LEFT is that integrating out the top quark, the $W^\pm$ and the Z, as well as the Higgs boson at the electroweak scale already generates a subset of the operators, while the observation of a non-zero SMEFT Wilson coefficient would necessarily imply the existence of new physics. The mechanism by which the ALP generates new terms to the RG evolution equations of the operators, however, remains unchanged with respect to the high-energy regime. The first part of this chapter was dedicated to the derivation of the full set of these inhomogeneous ALP-induced source terms. In the second part, the important phenomenological effects of these indirect ALP imprints on physical observables were investigated. While direct ALP searches often rely strongly on the underlying assumption of the ALP properties, such as its lifetime or branching ratios for decays into Standard Model particles, the source terms derived here are model-independent and hold as long as $m_a < \mu_w$. To highlight the predictive power of this *ALP–LEFT interference* framework, the contributions to the anomalous magnetic moment of the muon were investigated. In this state-of-the-art calculation, all relevant two-loop effects were included. The relevant couplings were scale evolved from the experimental scale up to the electroweak scale, and matching corrections were taken into account. After applying the UV scale evolution up to the scale Λ where the ALP is generated, the expression for the anomalous magnetic dipole moment of the muon was also presented in terms of these high-scale ALP couplings and SMEFT Wilson coefficients. Finally, assuming flavor-universal ALP-fermion couplings, numerical results for the various ALP-induced effects were presented. All in all, this chapter paved the way towards fully model-independent indirect ALP searches for small ALP masses at low energies.

3.10. Appendix

3.10.A. Dimension-8 Source Term Examples

As pointed out in Section 3.5, dimension-six four-fermion operators in the LEFT are not sourced at one-loop order by the ALP, as integrating out the heavy propagators at μ_w already generates effective vertices of higher-dimensional order. The inhomogeneous source terms that are one-loop ALP generated when the Feynman diagram contains such an effective four-fermion LEFT vertex therefore correspond to source terms of dimension-eight or higher. For the case of a LEFT operator with flavor structure $(\bar{u}u)(\bar{e}e)$, obtained when integrating out the Z boson as shown in Figure 3.6, the source terms have the following structure:

$$\begin{aligned}
\left[S_{eu}^{V,LR}\right]_{prst} &= \frac{4}{v^2}\left(16\delta_{st}\, g_R^e g_R^u\, [\tilde{\boldsymbol{M}}_e \tilde{\boldsymbol{M}}_e^\dagger]_{pr} - \delta_{pr}\, g_L^e g_L^u\, [\tilde{\boldsymbol{M}}_u^\dagger \tilde{\boldsymbol{M}}_u]_{st}\right), \\
\left[S_{ue}^{V,LR}\right]_{prst} &= \frac{4}{v^2}\left(16\delta_{st}\, g_L^e g_L^u\, [\tilde{\boldsymbol{M}}_e^\dagger \tilde{\boldsymbol{M}}_e]_{pr} - \delta_{pr}\, g_R^e g_R^u\, [\tilde{\boldsymbol{M}}_u \tilde{\boldsymbol{M}}_u^\dagger]_{st}\right), \\
\left[S_{eu}^{V,LL}\right]_{prst} &= \frac{4}{v^2}\left(16\delta_{st}\, g_R^e g_L^u\, [\tilde{\boldsymbol{M}}_e \tilde{\boldsymbol{M}}_e^\dagger]_{pr} - \delta_{pr}\, g_L^e g_R^u\, [\tilde{\boldsymbol{M}}_u \tilde{\boldsymbol{M}}_u^\dagger]_{st}\right), \\
\left[S_{eu}^{V,RR}\right]_{prst} &= \frac{4}{v^2}\left(16\delta_{st}\, g_L^e g_R^u\, [\tilde{\boldsymbol{M}}_e^\dagger \tilde{\boldsymbol{M}}_e]_{pr} - \delta_{pr}\, g_R^e g_L^u\, [\tilde{\boldsymbol{M}}_u^\dagger \tilde{\boldsymbol{M}}_u]_{st}\right),
\end{aligned} \tag{A.1}$$

and

$$\begin{aligned}
\left[S_{eu}^{S,RL}\right]_{prst} &= \frac{2}{v^2}\, [\tilde{\boldsymbol{M}}_e]_{pr}\, [\tilde{\boldsymbol{M}}_u^\dagger]_{st}\,, \\
\left[S_{eu}^{T,RR}\right]_{prst} &= \frac{2}{v^2}\, (g_R^e + g_L^e)(g_R^u + g_L^u)\, [\tilde{\boldsymbol{M}}_e]_{pr}\, [\tilde{\boldsymbol{M}}_u]_{st}\,, \\
\left[S_{eu}^{S,RR}\right]_{prst} &= \frac{2}{v^2}\, [\tilde{\boldsymbol{M}}_e]_{pr}\, [\tilde{\boldsymbol{M}}_u]_{st}\,,
\end{aligned} \tag{A.2}$$

where $g_L^e = (-\frac{1}{2} + s_w^2)$, $g_R^e = s_w^2$ and $g_L^u = (\frac{1}{2} - \frac{2}{3}s_w^2)$, $g_R^u = -\frac{2}{3}s_w^2$ denote the relevant Z-boson couplings. For the hermitian conjugate operators of those in (A.2) one needs to exchange $\tilde{\boldsymbol{M}}_f \leftrightarrow \tilde{\boldsymbol{M}}_f^\dagger$.

Chapter 4: $K^{\pm} \to \pi^{\pm} a$ at Next-to-Leading Order in Chiral Perturbation Theory

The Flavor-Changing Neutral Current (FCNC) decays $K^{\pm} \to \pi^{\pm}\nu\bar{\nu}$ are predicted by the SM to be exceedingly rare processes, making them are extremely sensitive to contributions from physics beyond the SM. With a value of $\mathcal{B}(K^{+} \to \pi^{+}\nu\bar{\nu}) = (13.0^{+3.3}_{-3.0}) \times 10^{-11}$, this branching ratio is currently the smallest that has ever been measured at a 5σ significance level, but agrees with the SM prediction only within $1.7\,\sigma$ [151]. Since the two neutrinos are only detected through missing energy and momentum, the decay of the charged kaon to a pion and an ALP, $K^{\pm} \to \pi^{\pm} a$, could potentially significantly enhance the measured branching ratios. This is especially true for large ALP couplings and hence the decay poses an important probe of ALP–SM interactions.
Considering the kaon decay in its rest frame, a crucial modification of the fundamental degrees of freedom with respect to the previous chapters needs to be taken into account for the accurate description of this low-energy process. Given that $N_c = 3$ and n_q the number of active quark flavors, the β-function of QCD describing the scale evolution of the strong coupling α_s, at leading order given by [152, 153]

$$\frac{d\,\alpha_s(\mu)}{d\ln\mu} = -\frac{\alpha_s^2}{2\pi}\left(\frac{11}{3}\,N_c - \frac{2}{3}\,n_q\right), \tag{4.1}$$

is always negative. Thus, when approaching lower and lower energy scales, α_s becomes larger, until a perturbative expansion in this coupling is no longer possible. Instead, the appropriate fundamental degrees of freedom below $\mu_\chi \approx 1.6\,\text{GeV}$ are the pseudoscalar mesons which are color-neutral bound states of quark-antiquark pairs. To analyze ALP interactions with mesons, this particle thus first needs to be incorporated consistently into the appropriate effective field theory for parametrizing interactions below μ_χ, the so-called Chiral Perturbation Theory (χPT). Before delving into the embedding of ALPs into this framework, a brief introduction to χPT is given based on [154]. Afterwards, this effective theory is extended to allow for the presence of ALPs, followed by a detailed analysis of the process $K^{\pm} \to \pi^{\pm} a$ at next-to-leading order (NLO).

This chapter is based on

[155] **$K^{\pm} \to \pi^{\pm} a$ at Next-to-Leading Order in Chiral Perturbation Theory and Updated Bounds on ALP Couplings**
C. Cornella, A. M. Galda, M. Neubert and D. Wyler
JHEP **06** (2024), 29, [arXiv:2308.16903].

4.1. Chiral Perturbation Theory

In the limit of zero quark masses, the global, *chiral* symmetry group of QCD is

$$\mathcal{G}_\chi \times U(1)_A \coloneqq SU(n_q)_L \times SU(n_q)_R \times U(1)_V \times U(1)_A \,, \tag{4.2}$$

with $n_q = 3$ below μ_χ. While the $U(1)_V$ vector symmetry ensures baryon number conservation, the $U(1)_A$ axial symmetry is explicitly broken at the quantum level, giving rise to the heavy η' meson. For the description of the low-energy interactions, the relevant generators are therefore those of $SU(3)_L \times SU(3)_R$, which can be rearranged to form the axial and vectorial combinations $Q_V^a = Q_R^a + Q_L^a$ and $Q_V^a = Q_R^a - Q_L^a$. While it can be shown that the low-energy spectrum is still invariant under the subgroup $SU(3)_V$ [156], Coleman's theorem [157] requires that degenerate states of opposite parity would need to exist for the Q_A^a to annihilate the ground state. Since this contradicts experimental observations, it follows that below μ_χ, the chiral symmetry is broken down to

$$SU(3)_L \times SU(3)_R \times U(1)_V \times U(1)_A \to SU(3)_V \times U(1)_V =: \mathcal{H}_\chi \times U(1)_V \,. \tag{4.3}$$

Physically, the reason for this spontaneous chiral symmetry breaking is that the large value of α_s leads to a non-vanishing chiral quark condensate, that is

$$\langle 0|\bar{q}q|0\rangle \neq 0 \,. \tag{4.4}$$

From Goldstone's theorem [158, 159] it is known that for each generator of a broken global symmetry, there exists a massless Nambu-Goldstone boson. Taking into account that quantum effects break the $U(1)_A$ symmetry already above μ_χ which generates the η', one expects to find $\dim(\mathcal{G}_\chi) - \dim(\mathcal{H}_\chi) = 8$ *pseudo* Nambu-Goldstone bosons[1]. Indeed, the neutral and charged pions and kaons and the octet component of the η-field, that is π^0, $\pi^\pm$, K^0, $\bar{K}^0$, $K^\pm$, η_8, are parity odd pseudoscalar mesons that form the octet as expected.

4.2. Construction of the Effective Lagrangian

Although the exact Lagrangian of QCD at high energies is known, the low-energy effective theory in terms of the pseudoscalar mesons cannot be derived straightforwardly by a matching computation due to the non-perturbatvity of the strong coupling below μ_χ. Thus, χPT needs to be constructed in a bottom-up procedure, relying solely on symmetry arguments. For the construction of the effective Lagrangian it is therefore necessary to first determine the transformation properties of the pseudoscalar meson octet under $\mathcal{G}_\chi$. To this end, one defines a vector space V spanned by the eight-component vectors built out of the pseudo Nambu–Goldstone fields that are described by continuous scalar functions ϕ^a from the four-dimensional Minkowski space to $\mathbb{R}$. It can then be shown [154] that V is connected to the left coset or quotient group $\mathcal{G}_\chi/\mathcal{H}_\chi \coloneqq \{g\,\mathcal{H}_\chi | g \in \mathcal{G}_\chi\}$ by an isomorphic mapping $\varphi : \mathcal{G}_\chi \times V \to V$ that transforms any vector according to the group action, $\vec{\phi} \to \vec{\phi}' = \varphi(g, \vec{\phi})$. In order to obtain a

[1] Since the chiral symmetry is only approximate due to the finite quark masses, the resulting bosons are also not exactly massless.

transformed state $\vec{\phi}'$ from $\vec{\phi} = \varphi(gh, \vec{0})$, it needs to be mapped with the appropriate g',

$$\vec{\phi}' = \varphi(g, \vec{\phi}) = \varphi(g'gh, \vec{0})\,. \tag{4.5}$$

Concretely for the chiral symmetry of $\mathcal{G}_\chi$, $g = (g_L, g_R)$, where $g_L \in SU(3)_L$ and equivalently for g_R. The left coset, $g\mathcal{H}_\chi = \{(g_L V, g_R V) | V \in \mathcal{H}_\chi\}$, can be rearranged to $g\mathcal{H}_\chi = (\mathbb{1}, g_R g_L^\dagger)\,\mathcal{H}_\chi$ and thus transforms according to $g'g\mathcal{H}_\chi = (\mathbb{1}, g_R\,(g_R g_L^\dagger)\,g_L^\dagger)\,\mathcal{H}_\chi$. Hence, if one defines an $SU(3)$ matrix[2] $\Sigma_0^\dagger \coloneqq g_R g_L^\dagger \cong \vec{\phi}$, it transforms under $\mathcal{G}_\chi$ as

$$\Sigma_0^\dagger \to (\Sigma_0^\dagger)' = g_R\,\Sigma_0^\dagger\,g_L^\dagger\,, \tag{4.6}$$

and equivalently,

$$\Sigma_0 \to \Sigma_0' = g_L\,\Sigma_0\,g_R^\dagger\,. \tag{4.7}$$

In the *canonical form*, Σ_0 is written as

$$\Sigma_0(x) = \exp\left[\frac{i\sqrt{2}}{F}\,\Phi(x)\right]\,, \tag{4.8}$$

where F is the meson decay constant, which can experimentally be extracted from the charged pion decay $\pi^+ \to \mu^+\nu$ ($F \approx F_\pi$ with $\langle 0|\bar{q}\gamma^\mu\gamma_5 q|\pi^+(p)\rangle = i\sqrt{2}F_\pi p^\mu$), yielding $F \approx 130.2\,\text{MeV}$ [160]. Finally, the eight pseudo Nambu–Goldstone fields are collected in the matrix $\Phi(x)$ as

$$\Phi(x) = \lambda^a\,\pi^a(x) = \begin{pmatrix} \frac{1}{\sqrt{2}}\,\pi^0 + \frac{1}{\sqrt{6}}\,\eta_8 & \pi^+ & K^+ \\ \pi^- & -\frac{1}{\sqrt{2}}\,\pi^0 + \frac{1}{\sqrt{6}}\,\eta_8 & K^0 \\ K^- & \bar{K}^0 & -\frac{2}{\sqrt{6}}\,\eta_8 \end{pmatrix}\,, \tag{4.9}$$

where the λ^a are the Gell-Mann matrices, i.e. the generators of the broken $SU(3)_A$.

4.3. Power Counting in χPT

The non-perturbative nature of QCD within the validity range of χPT is manifest due to the infinite number of possible interaction terms for the pseudoscalar mesons. This raises questions about the predictability of the theory. Although a counting scheme in terms of α_s is not possible, one can however still define an alternative power expansion that offers a systematic framework for perturbative predictions of the interactions. Given that the momenta and masses of the mesons are small at the given energy scale, a meaningful ansatz is to define the scaling [154]

$$\partial^\mu \sim p^\mu \to t\,p^\mu \quad \text{and} \quad M^2 \to t^2\,M^2\,, \tag{4.10}$$

[2] This definition is different from the convention in [154], where $U = \Sigma_0^\dagger$ is chosen. The meson octet then transforms as $U \to U' = g_R\,U\,g_L^\dagger$, while in this work, $\Sigma_0 \to \Sigma_0' = g_L\,\Sigma_0\,g_R^\dagger$. The index "0" is chosen to distinguish this quantity from the analogous one in the presence of the ALP that is introduced later.

where M denotes a pseudoscalar meson mass and p^{μ} the four-momentum. The full effective Lagrangian of χPT can then be decomposed as

$$\mathcal{L}_{\chi\mathrm{PT}}(\Sigma_0) = \sum_{n=1}^{\infty} \mathcal{L}_{\chi\mathrm{PT}}^{(p^{2n})}(\Sigma_0)\,, \tag{4.11}$$

where the index $(2n)$ denotes the *chiral dimension* D of the operators at the given order. For instance, the terms in $\mathcal{L}_{\chi\mathrm{PT}}^{(p^2)}$ may contain operators with two derivatives or one mass term. Since the operators need to respect Lorentz-invariance, only an even number of derivatives is allowed, hence the factor of two[3]. Even before constructing the concrete operator basis at this order, it is now possible to assign a scaling dimension to an amplitude obtained from a given diagram in χPT by [154]

$$\mathcal{M}(t\,p_i\,, t^2\,m_q) = t^D\,\mathcal{M}(p_i\,, m_q)\,, \tag{4.12}$$

where m_q denotes a quark mass and p_i the external momenta. The chiral dimension D can be obtained from the number of loops in the diagram, N_L, and the number of vertices from $\mathcal{L}_{\chi\mathrm{PT}}^{(2n)}$, N_{2n}, via

$$D = 2 + \sum_{n=1}^{\infty} 2\,(n-1)\,N_{2n} + 2N_L\,. \tag{4.13}$$

This becomes clear when taking into account that each loop comes with an integral of the form

$$\int \frac{d^4k}{(2\pi)^4} \to t^4 \int \frac{d^4k}{(2\pi)^4}\,, \tag{4.14}$$

and each propagator contributes a factor

$$\frac{i}{k^2 - M^2 + i\epsilon} \to \frac{i}{t^2\,k^2 - t^2\,M^2 + i\epsilon} = t^{-2}\,\frac{i}{k^2 - M^2 + i\epsilon'}\,. \tag{4.15}$$

Denoting by ■ a vertex stemming from an arbitrary operator in $\mathcal{L}_{\chi\mathrm{PT}}^{(p^2)}$, the two diagrams

thus both have $D = 4$ in the chiral power counting scheme[4]. From this also immediately follows that the term that renormalizes the divergence resulting from the loop

[3] While this limits the number of possible operators at each dimension, the fact that the meson octet appears as the exponent in Σ_0 still gives rise to an infinite tower of interaction vertices at each order.

[4] Two-point vertices indeed appear in χPT and are discussed in more detail in Section 4.8.1.

integral in these graphs must necessarily come from the operators in the $\mathcal{L}^{(p^4)}_{\chi\mathrm{PT}}$-basis. Denoting the corresponding vertex by $\square$, the Feynman graph is of the form

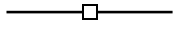

4.4. Spurion Analysis and Lowest Order Strong Chiral Lagrangian

While in the symmetry considerations above, the lightest quark flavors, u, d, and s, were assumed to be massless, taking into account their mass terms leads to a different breaking pattern. In detail, assuming $m_u = m_d \neq m_s$, the low-energy symmetry is $SU(2)_V \times U(1)_S \times U(1)_V$, where $SU(2)_V$ is called *isospin symmetry* and $U(1)_S$ accounts for the conservation of strangeness in the process. If instead no equal masses are assumed, i.e. $m_u \neq m_d \neq m_s$, then the resulting low-energy symmetry is $U(1)_V \times U(1)_Q \times U(1)_S$, which includes electromagnetic charge conservation via $U(1)_Q$.
The systematic procedure to incorporate effects of small breaking terms of a given symmetry such as the finite quark masses is called *spurion analysis*. Here, symmetry breaking terms are treated as external sources and assigned transformation properties under $SU(3)_L \times SU(3)_R$ such that the symmetry is preserved. In detail, the full QCD Lagrangian is then written as a massless term $\mathcal{L}^{(0)}_{\mathrm{QCD}}$ and general source terms,

$$\mathcal{L}_{\mathrm{QCD}} = \mathcal{L}^{(0)}_{\mathrm{QCD}} + \bar{q}\,\gamma^{\mu}\,(v^{\mathrm{SM}}_{\mu} + \gamma_5\, a^{\mathrm{SM}}_{\mu})\,q - \bar{q}\,(s - i\gamma_5\, p)\,q\,. \tag{4.16}$$

At low energies, where the dynamical degrees of freedom are the mesons, photons and gluons, the terms in (4.16) are, by comparison with the full QCD Lagrangian, given by

$$\begin{aligned} s = \mathrm{diag}(m_u,\, m_d,\, m_s)\,, \quad p = 0\,, \\ v^{\mathrm{SM}}_{\mu} = e\,Q\,A_{\mu}\,, \quad a^{\mathrm{SM}}_{\mu} = 0\,, \end{aligned} \tag{4.17}$$

with $Q = \frac{1}{3}\,\mathrm{diag}(2, -1, -1)$. The necessary spurious transformation properties of these terms are thus

$$\begin{aligned} \chi \equiv 2B_0(s + ip) &\to g_L\,\chi\,g_R^{\dagger}\,, \\ l^{\mathrm{SM}}_{\mu} \equiv v^{\mathrm{SM}}_{\mu} - a^{\mathrm{SM}}_{\mu} &\to g_L\,l^{\mathrm{SM}}_{\mu}\,g_L^{\dagger} + i\,g_L \partial_{\mu} g_L^{\dagger}\,, \\ r^{\mathrm{SM}}_{\mu} \equiv v^{\mathrm{SM}}_{\mu} + a^{\mathrm{SM}}_{\mu} &\to g_R\,r^{\mathrm{SM}}_{\mu}\,g_R^{\dagger} + i\,g_R \partial_{\mu} g_R^{\dagger}\,, \end{aligned} \tag{4.18}$$

where the terms containing the partial derivative in the second and third line of (4.18) ensure local invariance. The constant B_0 appearing in the equation for χ is an a priori undetermined parameters of mass dimension one.
In order to retain invariant Lagrangian terms, this automatically implies that the covariant derivative acting on the object Σ_0 defined in (4.8) must read [161]

$$\begin{aligned} D_{\mu}\Sigma_0 &= \partial_{\mu}\Sigma_0 - i\,l^{\mathrm{SM}}_{\mu}\Sigma_0 + i\,\Sigma_0\,r^{\mathrm{SM}}_{\mu} = \partial_{\mu}\Sigma_0 - i\,eA_{\mu}[Q, \Sigma_0]\,, \\ D_{\mu}\Sigma_0^{\dagger} &= \partial_{\mu}\Sigma_0^{\dagger} - i\,r^{\mathrm{SM}}_{\mu}\Sigma_0^{\dagger} + i\,\Sigma_0^{\dagger}\,l^{\mathrm{SM}}_{\mu} = \partial_{\mu}\Sigma_0^{\dagger} - i\,eA_{\mu}[Q, \Sigma_0^{\dagger}]\,. \end{aligned} \tag{4.19}$$

The leading order strong chiral Lagrangian that includes the meson mass terms can then be written in terms of these ingredients. Since $\Sigma_0^\dagger \Sigma_0 = \mathbb{1}$, it necessarily needs to contain at least two covariant derivatives or one insertion of χ in combination with Σ_0 and is thus of order p^2 in the chiral power counting. Denoting the trace in flavor space by $\langle \dots \rangle$, it reads [161]

$$\begin{aligned}\mathcal{L}^{(p^2)}_{\chi\text{QCD}} &= \frac{F^2}{8} \langle (D_\mu \Sigma_0^\dagger)(D^\mu \Sigma_0) + \chi \Sigma_0^\dagger + \Sigma_0 \chi^\dagger \rangle \\ &= \frac{F^2}{8} \langle L_{0\mu} L_0^\mu + S_0 \rangle \,, \end{aligned} \tag{4.20}$$

where in the second line the chiral representation of the left-handed current, $L_0^\mu = i\, \Sigma_0 D^\mu \Sigma_0^\dagger$, is used together with the identity

$$D_\mu(\Sigma_0 \Sigma_0^\dagger) = 0 \quad \Leftrightarrow \quad \Sigma_0\, D_\mu \Sigma_0^\dagger = -(D_\mu \Sigma_0)\, \Sigma_0^\dagger \,, \tag{4.21}$$

and $S_0 = \chi \Sigma_0^\dagger + \Sigma_0 \chi^\dagger$.

4.5. Lowest Order Non-Leptonic Weak Chiral Lagrangian

For $|\Delta S| = 1$ strangeness changing processes below μ_χ, the strong chiral Lagrangian derived above is not sufficient. Instead, the effective weak interactions as obtained after integrating out the $W^\pm$-bosons as well as the top-, bottom- and charm-quarks also need to be represented in terms of the pseudoscalar mesons. Neglecting the electroweak penguin operators, the relevant transformation properties under $SU(3)_L \times SU(3)_R$ of the operators in the effective weak Hamiltonian at the partonic level are $(8_L,\, 1_R)$ and $(27_L,\, 1_R)$ [162]. Thus, the effective weak chiral Lagrangian at order $\mathcal{O}(p^2)$ can be constructed by collecting all possible operators obeying these transformation rules. To describe the $s \to d$ transitions, it is convenient to define

$$\lambda_+ = \frac{1}{2}\,(\lambda_6 + i\,\lambda_7) \,, \tag{4.22}$$

where λ_6 and λ_7 are Gell-Mann matrices. An insertion of this matrix then ensures the selection of $|\Delta S| = 1$ processes. With this, one finds that $\mathcal{L}^{(p^2)}_{\chi\text{weak}}$ can be written as [163, 164]

$$\mathcal{L}^{(p^2)}_{\chi\text{weak}} = \frac{F^4}{4} \Big[G_8 \mathcal{O}_8 + G_{27}^{1/2} \mathcal{O}_{27}^{1/2} + G_{27}^{3/2} \mathcal{O}_{27}^{3/2} + \text{h.c.} \Big] \,, \tag{4.23}$$

where

$$\begin{aligned} \mathcal{O}_8 &= \langle \lambda_+ L_{0\mu} L_0^\mu \rangle \,, \\ \mathcal{O}_{27}^{1/2} &= [L_{0\mu}]_{32} [L_0^\mu]_{11} + [L_{0\mu}]_{31} [L_0^\mu]_{12} + 2\,[L_{0\mu}]_{32} [L_0^\mu]_{22} - 3\,[L_{0\mu}]_{32} [L_0^\mu]_{33} \,, \\ \mathcal{O}_{27}^{3/2} &= [L_{0\mu}]_{32} [L_0^\mu]_{11} + [L_{0\mu}]_{31} [L_0^\mu]_{12} - [L_{0\mu}]_{32} [L_0^\mu]_{22} \,, \end{aligned} \tag{4.24}$$

and L_0^μ as defined below (4.20). The 27-plet operators $\mathcal{O}_{27}^{1/2}$ and $\mathcal{O}_{27}^{3/2}$ describe isospin changing interactions with $\Delta I = \frac{1}{2}$ and $\Delta I = \frac{3}{2}$, respectively. The coefficients G_i can

be decomposed as

$$G_i = -\frac{G_F}{\sqrt{2}} V_{ud}^* V_{us} \left(g_i - \frac{V_{td}^* V_{ts}}{V_{ud}^* V_{us}} g_i^t \right) . \tag{4.25}$$

Since the ratio of the CKM matrix elements is small, $\frac{V_{td}^* V_{ts}}{V_{ud}^* V_{us}} \sim \mathcal{O}(10^{-3})$, the second term in the bracket above is neglected in the following and with it the imaginary contributions to the G_i, that hence become real quantities. The numerical values of the g_i including isospin-breaking corrections are [165, 166]

$$g_8 = 3.61 \pm 0.28 \,, \quad g_{27} \equiv 9\, g_{27}^{1/2} = 0.297 \pm 0.028 \,, \quad g_{27}^{3/2} = 5\, g_{27}^{1/2} \,, \tag{4.26}$$

which yields[5]

$$g_{27}^{1/2} \approx 0.033 \pm 0.003 \,, \quad g_{27}^{3/2} \approx 0.165 \pm 0.016 \,. \tag{4.27}$$

In the equation above, the values for the g_{27}^i are deduced assuming an exact $SU(3)$ symmetry, implying

$$G_{27}^{1/2}\, \mathcal{O}_{27}^{1/2} + G_{27}^{3/2}\, \mathcal{O}_{27}^{3/2} = 9\, G_{27}^{1/2} \left([L_{0\mu}]_{32} [L_0^\mu]_{11} + \frac{2}{3} [L_{0\mu}]_{31} [L_0^\mu]_{12} - \frac{1}{3} [L_{0\mu}]_{32} \langle L_0^\mu \rangle \right). \tag{4.28}$$

In the SM, $\langle L_0^\mu \rangle = 0$. This is no longer true when adding the ALP as is discussed in Section 4.8.2. In principle, it is possible to add another octet operator to (4.23), the so-called *weak mass term* $G_8' \langle \lambda_+ S \rangle$. It is, however, redundant in the SM and can therefore be dropped from the Lagrangian. This does no longer hold true when adding the ALP to the theory and it is therefore imperative to fully understand the reasoning, that has first been described in [167]. The weak mass term itself contributes non-zero tadpole vertices, which are a sign of an expansion around the wrong vacuum. Indeed, $\Sigma_0 = \mathbb{1}$ is not the correct ground state in this case. Crewther found that a chiral transformation of the form

$$\Sigma_0 \to g_L\, \Sigma_0\, g_R^\dagger = e^{i\,\alpha_L}\, \Sigma_0\, e^{-i\,\alpha_R} \,, \tag{4.29}$$

with

$$\begin{aligned} \alpha_L &= G_8' F^2 \left(\frac{m_s + m_d}{m_s - m_d} + \frac{m_s - m_d}{m_s + m_d} \right) \lambda_7 \,, \\ \alpha_R &= G_8' F^2 \left(\frac{m_s + m_d}{m_s - m_d} - \frac{m_s - m_d}{m_s + m_d} \right) \lambda_7 \,, \end{aligned} \tag{4.30}$$

removes the weak mass term explicitly. This is the case as under the redefinition, $\Sigma_0 \to \Sigma_0 + \delta\Sigma_0$, where

$$\delta\Sigma_0 = i\alpha_L\, \Sigma_0 - i\Sigma_0\, \alpha_R + \mathcal{O}(G_F^2) \,, \tag{4.31}$$

the kinetic term remains invariant, while

$$\chi^D \equiv \left(1 + 2F^2 G_8'\, \lambda_6\right) \chi \to \chi + \mathcal{O}(G_F^2) \,. \tag{4.32}$$

[5]The hierarchy between the g_{27} and g_8 is also referred to as the $\Delta I = \frac{1}{2}$ selection rule.

The fact that the weak mass term is redundant reflects itself in the fact that when summing up all amplitudes to a given SM process, the contributions from this term cancel. For instance, the tree-level terms for the process $K_S \to \pi^0\pi^0$ corresponding to the Feynman graphs

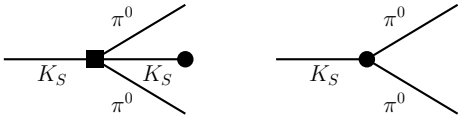

where the black dot ● denotes an insertion of the weak mass term operator and the black square ■ an insertion of a term from the strong chiral Lagrangian of order $\mathcal{O}(p^2)$, is zero.

4.6. The Strong Chiral Lagrangian at $\mathcal{O}(p^4)$

SM Object	Definition
S_0	$\chi\Sigma_0^\dagger + \Sigma_0\chi^\dagger$
P_0	$i(\chi\Sigma_0^\dagger - \Sigma_0\chi^\dagger)$
L_0^μ	$\Sigma_0\, i(D^\mu\Sigma_0)^\dagger$
$W_0^{\mu\nu}$	$2\,(D^\mu L_0^\nu + D^\nu L_0^\mu)$
$A_{\mu\nu}$	$\Sigma_0\, F_{\mu\nu}^R\, \Sigma_0^\dagger - F_{\mu\nu}^L$
$V_{\mu\nu}$	$\Sigma_0\, F_{\mu\nu}^R\, \Sigma_0^\dagger + F_{\mu\nu}^L$

Table 4.1.: Building blocks as needed for the construction of the $\mathcal{O}(p^4)$ chiral effective Lagrangian.

In addition to the objects S_0 and L_0^μ defined above, several additional building blocks are needed for the construction of the $\mathcal{O}(p^4)$ strong chiral effective Lagrangian. They are summarized in Table 4.1. The left- and right-handed field strength tensors are defined in terms of the external sources,

$$F_{\mu\nu}^{R,\,L} = \partial_\mu F_\nu^{R,\,L} - \partial_\nu F_\mu^{R,\,L} - i\,[F_\mu^{R,\,L},\, F_\nu^{R,\,L}]\,, \tag{4.33}$$

where

$$F_\mu^R = v_\mu^{\rm SM} + a_\mu^{\rm SM}\,, \quad F_\mu^L = v_\mu^{\rm SM} - a_\mu^{\rm SM}\,. \tag{4.34}$$

With this, the basis of the 12 non-redundant operators for SM processes at $\mathcal{O}(p^4)$ has first been derived in [161]. It is conventionally written as

$$\mathcal{L}_{\chi\rm QCD}^{(p^4)} = \sum_{i=1}^{10} L_i\, O_i + \sum_{i=11}^{12} H_i\, O_i\,, \tag{4.35}$$

with the concrete operators as given in Table 4.3. A coefficient L_i or H_i is called a low-energy constant (LEC), and the bare quantity is related to the scale dependent one via

$$L_i = L_{i,r}^{(\theta)}(\mu) + \lambda\, \Gamma_i\,. \tag{4.36}$$

The values of the anomalous dimensions Γ_i have been obtained in [161] and are shown in the third and last column of Table 4.3. Finally,

$$\lambda = \frac{\mu^{d-4}}{32\pi^2}\left(\frac{2}{d-4} - \ln 4\pi + \gamma_E - 1\right), \tag{4.37}$$

with d the number of spacetime dimensions. The scale evolutions of the LECs are governed by the evolution equations

$$\frac{d}{d\ln\mu}\, L_{i,r}(\mu) = -\frac{\Gamma_i}{16\pi^2}\,. \tag{4.38}$$

For the numerical values of these coefficients, there exist phenomenological estimates that also assign an uncertainty at the scale $\mu = m_\rho \approx 775$ MeV. In this work, two different data sets are used: On one hand, the values obtained from a p^4 fit given in [168], and on the other hand the results from a lattice computation of the HPQCD collaboration [169]. While the last one does not provide a value for L_7, it is in good agreement with the large-N_c results in [170], such that the missing fit for this coefficient is taken from these results, together with a conservative estimate of the uncertainty[6], i.e. $L_7 = (-0.175 \pm 0.2) \times 10^{-3}$. The values of the LECs that are relevant for this work are summarized in Table 4.2 and the corresponding scale dependence is depicted in Figure 4.1.

$10^3\, L_{i,r}$	Ref. [168]	Ref. [169]
$10^3\, L_{4,r}(\mu)$	0.0 ± 0.3	0.09 ± 0.34
$10^3\, L_{5,r}(\mu)$	1.2 ± 0.1	1.19 ± 0.25
$10^3\, L_7$	-0.3 ± 0.2	–
$10^3\, L_{8,r}(\mu)$	0.5 ± 0.2	0.55 ± 0.15

Table 4.2.: Phenomenological values of the relevant renormalized QCD low-energy constants, evaluated at the scale $\mu = m_\rho$. L_7 is scale independent.

The Chiral Power Expansion

Before moving on the the weak analogous of (4.35), it is instructive to consider again the chiral expansion: Writing down the full strong Lagrangian, one obtains a sum of

[6] While this justifies the replacement of L_7, there are two problems with the results obtained in the large-N_c limit. First, there is no scale associated to the LECs and second, the value of g_8 obtained in this limit is off by more than a factor of two [166]. Therefore, only the data sets in [168, 169] are used in this analysis.

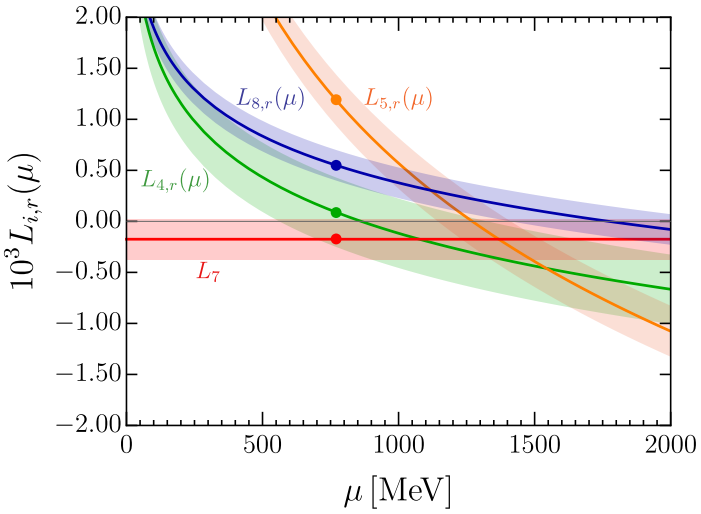

Figure 4.1.: Scale dependence of the relevant QCD LECs $L_{i,r}(\mu)$. The colored bands show the corresponding uncertainties and the dots show to the values as obtained in [169].

i	O_i	Γ_i	i	O_i	Γ_i
1	$\langle L_0^2 \rangle^2$	$\frac{3}{32}$	7	$-\langle P_0 \rangle^2$	0
2	$\langle L^\mu L^\nu \rangle \langle L_{0\mu} L_{0\nu} \rangle$	$\frac{3}{16}$	8	$\frac{1}{2}\langle S_0^2 - P_0^2 \rangle$	$\frac{5}{48}$
3	$\langle L_0^4 \rangle$	0	9	$\frac{i}{2}\langle V_{\mu\nu}\,[L_0^\mu,\, L_0^\nu] \rangle$	$\frac{1}{4}$
4	$\langle L_0^2 \rangle \langle S_0 \rangle$	$\frac{1}{8}$	10	$\frac{1}{2}\left(V_{\mu\nu}V^{\mu\nu} - A_{\mu\nu}A^{\mu\nu}\right)$	$-\frac{1}{4}$
5	$\langle L_0^2 S_0 \rangle$	$\frac{3}{8}$	11	$\frac{1}{2}\left(V_{\mu\nu}V^{\mu\nu} + A_{\mu\nu}A^{\mu\nu}\right)$	$-\frac{1}{8}$
6	$\langle S_0 \rangle^2$	$\frac{11}{144}$	12	$\frac{1}{4}\langle S_0^2 + P_0^2 \rangle$	$\frac{5}{24}$

Table 4.3.: Operators in the $\mathcal{O}(p^4)$ strong chiral effective Lagrangian (4.35). In the expressions in the table, $L_0^2 \equiv L_{0\mu} L_0^\mu$. The coefficients Γ_i are taken from [161].

the form

$$\mathcal{L}_{\chi\text{QCD}} = \frac{F^2}{8} \sum_i O_i^{(p^2)} + \sum_i L_i^{(p^4)}\, O_i^{(p^4)} + \frac{1}{F^2} \sum_i L_i^{(p^6)}\, O_i^{(p^6)} + \dots \,. \tag{4.39}$$

In a "classical" EFT, the Wilson coefficients are of $\mathcal{O}(1)$. Taking into account that a chiral effective operator of p^{2n} scales as m_K^{2n} or m_π^{2n}, one would naively expect that the series shown above does not converge, as it produces matrix elements of the form

$$\mathcal{M} \propto F^2\, m_{K,\pi}^2 + L_i^{(p^4)} m_{K,\pi}^4 + \frac{1}{F^2}\, L_i^{(p^6)} m_{K,\pi}^6 + \dots \,. \tag{4.40}$$

Considering the values in Table 4.2 or the plot in Figure 4.1, it is clear that the phenomenological values of the LECs are, in fact, strongly suppressed. Rescaling these coefficients according to

$$L_i^{(p^{2n})} \equiv \frac{\hat{L}_i^{(p^{2n})}}{8\,(4\pi)^{2n-2}}\,, \tag{4.41}$$

does lead to an explicit convergence. The Lagrangian now reads

$$\mathcal{L}_{\chi\text{QCD}} = \frac{F^2}{8}\left[O^{(p^2)} + \frac{1}{(4\pi F)^2}\sum_i \hat{L}_i^{(p^4)}\, O_i^{(p^4)} + \frac{1}{(4\pi F)^4}\sum_i \hat{L}_i^{(p^6)}\, O_i^{(p^6)} + \dots\right], \tag{4.42}$$

where the effective scale of the chiral expansion, $\mu_\chi \approx 4\pi F$, is now explicit in the sum. Even though the rescaling factor is large, e.g. $8\,(4\pi)^2 \approx 1263$ for the case of the p^4 LECs, the new coefficients are now indeed of $\mathcal{O}(1)$ as shown in Table 4.4.

$\hat{L}_{i,r}$	Ref. [168]	Ref. [169]
$\hat{L}_{4,r}(\mu)$	0.0 ± 0.38	0.11 ± 0.43
$\hat{L}_{5,r}(\mu)$	1.52 ± 0.13	1.50 ± 0.32
$\hat{L}_7$	-0.38 ± 0.25	–
$\hat{L}_{8,r}(\mu)$	0.63 ± 0.25	0.69 ± 0.19

Table 4.4.: Rescaled low-energy constants $\hat{L}_i^{(p^4)}$ of the strong chiral effective Lagrangian at $\mu = m_\rho$.

4.7. The Weak Chiral Lagrangian at $\mathcal{O}(p^4)$

When computing one-loop processes involving the weak effective chiral Lagrangian at $\mathcal{O}(p^2)$, clearly also the Lagrangian $\mathcal{L}^{(p^4)}_{\chi\text{weak}}$ is needed to remove the arising divergences from the expressions. As the contributions from the octet operators are strongly enhanced in comparison to the 27-plet operators, a fact commonly referred to as the $\Delta I = 1/2$ selection rule, the NLO computation of the kaon decays $K^\pm \to \pi^\pm a$ and $K_{S,L} \to \pi^0 a$ is limited to the octet operators, besides the contributions from the strong chiral ones. It is therefore sufficient to restrict the following discussion on p^4 weak chiral operators to those transforming as $(8_L, 1_R)$. The complete, non-redundant basis was first derived in [171]. It consists of 37 operators but, as in the previous cases, is only valid in the pure SM framework and is therefore extended in Section 4.8. The Lagrangian is normalized as

$$\mathcal{L}^{(p^4)}_{\chi\text{weak}} = \frac{G_8 F^2}{2}\sum_{i=1}^{37} N_i\, W_i^8 = \frac{G_8\, F^4}{4}\,\frac{1}{(4\pi F)^2}\sum_{i=1}^{37}\hat{N}_i\, W_i^8\,, \tag{4.43}$$

where in the second step the N_i are, similarly to (4.41), rescaled as

$$N_i \equiv \frac{\hat{N}_i}{2\,(4\pi)^2}\,, \tag{4.44}$$

in order to make the convergence of the chiral expansion manifest. Out of these 37 operators, the ones that are relevant for the kaon decays to an ALP and a pion are shown in Table 4.5. In particular, all operators containing four times the object L_0^μ cannot contribute, since the presence of four covariant derivatives acting on a Σ_0 selects processes with at least four particles. Equivalently to (4.36), the renormalized

i	W_i^8	Z_i	Z_i'	i	W_i^8	Z_i	Z_i'
6	$\langle\lambda_6 L_{0\mu}\rangle\,\langle S L_0^\mu\rangle$	$-\frac{1}{4}$	0	12	$-\langle\lambda_6 P_0^2\rangle$	$-\frac{5}{12}$	$\frac{5}{12}$
7	$\langle\lambda_6 S_0\rangle\,\langle L_0^2\rangle$	$-\frac{9}{8}$	$\frac{1}{2}$	13	$-\langle\lambda_6 P_0\rangle\,\langle P_0\rangle$	0	0
8	$\langle\lambda_6 L_0^2\rangle\,\langle S_0\rangle$	$-\frac{1}{2}$	0	20	$\frac{i}{2}\,\langle\lambda_6\,[l_\mu, \{L_{0\nu}, W_0^{\mu\nu}\}]\rangle$	$\frac{3}{4}$	0
9	$i\,\langle\lambda_6[P_0,\, L_0^2]\rangle$	$\frac{3}{4}$	$-\frac{3}{4}$	21	$-\langle\lambda_6\,[l_\mu, [S_0\,, L_0^\mu]]\rangle$	$\frac{5}{6}$	0
10	$\langle\lambda_6 S_0^2\rangle$	$\frac{2}{3}$	$\frac{5}{12}$	23	$-i\,\langle\lambda_6\,[l_\mu, \{P_0\,, L_0^\mu\}]\rangle$	$\frac{5}{12}$	0
11	$\langle\lambda_6 S_0\rangle\,\langle S_0\rangle$	$-\frac{13}{18}$	$\frac{11}{18}$	24	$-i\,\langle\lambda_6\,[l_\mu, L_0^\mu]\rangle\,\langle P_0\rangle$	0	0

Table 4.5.: Operators of the $\mathcal{L}^{(p^4)}_{\chi\text{weak}}$ weak effective chiral Lagrangian as found in [171] that are important for the processes $K^\pm \to \pi^\pm\, a$. The Z_i denote the corresponding anomalous dimensions. The anomalous dimension coefficients Z_i' become important when adding the ALP.

weak LECs are defined as

$$N_i = N_{i,r}(\mu) + \lambda\, Z_i\,, \tag{4.45}$$

with evolution equation

$$\frac{d}{d\ln\mu}\, N_{i,r}(\mu) = -\frac{1}{16\pi^2}\, Z_i\,. \tag{4.46}$$

In contrast to the strong LECs, these coefficients have not been consistently estimated in the literature so far[7]. For the phenomenological analysis, these values therefore need to be estimated, which is explained in detail in Section 4.10.

[7] From the $K \to 3\pi$ data, three combinations of the coefficients have been constrained in [172–174]. They are, however, not relevant for the decay $K^\pm \to \pi^\pm a$, as most operators associated with the coefficients in this combination do not contribute to the charged kaon decay to a pion and an ALP. In addition, the uncertainties are of order $\mathcal{O}(1)$ to $\mathcal{O}(10)$, and hence these findings are not included in the following.

4.8. ALP Chiral Perturbation Theory

For the extension of χPT to ALP Chiral Perturbation Theory (χ_aPT), the ALP–SM interaction terms need to be mapped onto operators containing the pseudo-Goldstone boson fields. Since the heavy gauge fields and the top-, bottom- and charm-quarks are not present at and below μ_χ and omitting ALP-lepton terms, the effective Lagrangian has the form

$$\begin{aligned}\mathcal{L}_{\text{SM+ALP}} = & c_{GG}\,\frac{\alpha_s}{4\pi}\,\frac{a}{f}\,G^a_{\mu\nu}\tilde{G}^{a,\mu\nu} + c_{\gamma\gamma}\,\frac{\alpha}{4\pi}\,\frac{a}{f}\,F_{\mu\nu}\tilde{F}^{\mu\nu} \\ & + \frac{\partial_\mu a}{f}\,(\bar{q}_L k_Q \gamma^\mu q_L + \bar{q}_R k_q \gamma^\mu q_R)\,, \end{aligned} \tag{4.47}$$

with $q = (u\ d\ s)^T$. The matrices k_Q and k_q thus contain only five possible non-zero entries,

$$k_Q = \begin{pmatrix} [k_U]_{11} & 0 & 0 \\ 0 & [k_D]_{11} & [k_D]_{12} \\ 0 & [k_D]_{21} & [k_D]_{22} \end{pmatrix}, \qquad k_q = \begin{pmatrix} [k_u]_{11} & 0 & 0 \\ 0 & [k_d]_{11} & [k_d]_{12} \\ 0 & [k_d]_{21} & [k_d]_{22} \end{pmatrix}. \tag{4.48}$$

The ALP-gluon coupling in (4.47), however, poses a problem: the explicit appearance of α_s parametrizes a non-perturbative interaction and prohibits meaningful predictions for physical processes at energy scales where α_s is large. Therefore, it is crucial to remove this term by a suitable field redefinition. In detail, this can be achieved by means of a chiral rotation on the quark fields,

$$q(x) \to \exp\left[-i\,(\delta_q + \kappa_q\,\gamma_5)\,c_{GG}\,\frac{a(x)}{f}\right]\,q(x) \equiv U(x)\,q(x)\,, \tag{4.49}$$

with δ_q and κ_q being arbitrary hermitian 3×3 matrices in flavor space. Following [175], the reason why (4.49) eliminates the ALP coupling to gluons is as follows: Since $\bar{U}U \neq \mathbb{1}$, the quark measures transform non-trivially,

$$\int \mathcal{D}q\mathcal{D}\bar{q} \to \int \mathcal{D}q\mathcal{D}\bar{q}\,(\det(\bar{\mathcal{U}}\mathcal{U}))^{-1}\,, \tag{4.50}$$

where $\langle x|\mathcal{U}|y\rangle = \delta^{(4)}(x-y)\,U(x)$. Inserting $\mathbb{1} = \int d^4x\,|x\rangle\langle x|$ and using that $\exp(\langle\log(U)\rangle)) = \det(U)$ with $\det(\bar{U}U))^{-1} = \det(\exp(-2i\,\kappa_q\,\gamma_5\,c_{GG}\,\frac{a}{f}))^{-1}$, one finds

$$(\det(\bar{\mathcal{U}}\mathcal{U}))^{-1} = \exp\left[2i\int d^4x\,\delta^{(4)}(0)\,\langle\kappa_q\,\gamma_5\rangle\,c_{GG}\,\frac{a}{f}\right]. \tag{4.51}$$

To regulate the divergence, a function $f\big(\left(i\not{D}/M\right)^2\big)$ with a cut-off M is inserted. Based on the technical derivation in [175], that essentially Taylor expands this function for small momenta and writes explicitly the gauge field strength tensors, one finally arrives at

$$\begin{aligned}(\det(\bar{\mathcal{U}}\mathcal{U}))^{-1} = \exp\Bigg[- i\int d^4x\,c_{GG}\,\frac{a}{f}\Bigg(&\langle\kappa_q\rangle\,\frac{\alpha_s}{4\pi}\,G^a_{\mu\nu}\,\tilde{G}^{\mu\nu,\,a} \\ & + \frac{\alpha}{4\pi}(2N_c)\,\langle\kappa_q Q^2\rangle\,F_{\mu\nu}\,\tilde{F}^{\mu\nu}\Bigg)\Bigg]. \end{aligned} \tag{4.52}$$

The additional term in (4.52) obtained by the chiral rotation cancels the ALP-gluon term in (4.47) when imposing the condition

$$\langle \kappa_q \rangle = \kappa_u + \kappa_d + \kappa_s = 1\,. \tag{4.53}$$

In addition, the ALP-photon coupling gets shifted to

$$\hat{c}_{\gamma\gamma} = c_{\gamma\gamma} + 2N_c\,\langle \kappa_q\, Q^2 \rangle\, c_{GG}\,. \tag{4.54}$$

It is essential to note that the parameters of the chiral rotation in (4.49) are unphysical, which means that in any physical quantity they must necessarily cancel.

4.8.1. Strong Chiral Lagrangian at $\mathcal{O}(p^2)$ including the ALP

With the ALP-gluon term removed from the Lagrangian (4.47), it is now possible to find its equivalent form in terms of the pseudoscalar mesons instead of the explicit quark fields. To accomplish this, three steps must be completed: Firstly, the ALP needs to be included in the external sources, similar to (4.16). Secondly, the chiral rotation in (4.49) has to be consistently translated onto the chiral building blocks. Finally, the presence of the ALP necessitates the introduction of new operators that extend the basis and must be identified.
Starting with the first point and following the literature convention for the naming of external sources [161], the ALP is parametrized in a $\theta(x)$ source as

$$\mathcal{L}_{\text{QCD}} \supset \bar{q}\,\gamma^\mu\,(v_\mu + \gamma_5\, a_\mu)\,q - \bar{q}\,(s - i\gamma_5\, p)\,q - \frac{\alpha_s}{8\pi}\,\theta(x)\,G^a_{\mu\nu}(x)\,\tilde{G}^{\mu\nu,\,a}\,, \tag{4.55}$$

such that

$$\theta(x) = -2\,c_{GG}\,\frac{a(x)}{f}\,. \tag{4.56}$$

The external sources $v_\mu(x)$ and $a_\mu(x)$, defined equivalently to (4.18), can then be identified as

$$v_\mu(x) = v_\mu^{\text{SM}}(x) + c^v\,\frac{\partial_\mu\, a(x)}{2f}\,, \quad a_\mu(x) = a_\mu^{\text{SM}}(x) + c^a\,\frac{\partial_\mu\, a(x)}{2f}\,, \tag{4.57}$$

with vector and axial couplings $c^v = k_q + k_Q$ and $c^a = k_q - k_Q$, respectively, while s and p remain unchanged with respect to the pure SM case. Neglecting electroweak interactions, which is a reasonable approximation for processes like $K^\pm \to \pi^\pm\, a$, the SM contributions to $v_\mu(x)$ and $a_\mu(x)$ are absent and only the ALP terms in (4.57) remain. Next, the chiral rotation performed on the quark fields needs to be translated to χ_aPT. This can be achieved by promoting

$$\Sigma(x) = e^{-\frac{i}{2}\theta(x)\,\kappa_q}\,\Sigma_0(x)\,e^{-\frac{i}{2}\theta(x)\,\kappa_q}\,. \tag{4.58}$$

The determinant of this object is no longer zero. Instead,

$$\det \Sigma(x) = \exp(-i\,\theta(x))\,, \tag{4.59}$$

which reflects the fact that the symmetry group in the presence of a non-zero θ is changed to $\mathcal{G}_{\chi,\,a} = U(3)_L \times U(3)_R$. Under this symmetry, the ALP transforms as

$$\theta(x) \to \theta(x) + i \log(\det(g_L g_R^{\dagger}))\,, \tag{4.60}$$

and the covariant derivative can be defined as

$$D_\mu \theta = \partial_\mu \theta - 2\,\langle a_\mu \rangle = -2\,\tilde{c}_{GG}(\mu_\chi)\,\frac{\partial_\mu a}{f}\,, \tag{4.61}$$

where $\tilde{c}_{GG}$ denotes the effective coupling at the chiral scale μ_χ,

$$\tilde{c}_{GG} = c_{GG} + \frac{c^a_{uu} + c^a_{dd} + c^a_{ss}}{2}\,. \tag{4.62}$$

The strong chiral Lagrangian at order $\mathcal{O}(p^2)$ with external ALP fields is the equivalent to the Lagrangian given in (4.20), but with the corresponding building blocks substituted by those accounting for the external source and one additional operator, i.e.

$$\begin{aligned}\mathcal{L}^{(p^2)}_{\chi\mathrm{QCD}} &= \frac{F^2}{8}\,\langle (D_\mu \Sigma^\dagger)(D^\mu \Sigma) + \chi \Sigma^\dagger + \Sigma \chi^\dagger \rangle + \frac{F^2}{8}\,H_0\,(D_\mu \theta)(D^\mu \theta) \\ &= \frac{F^2}{8}\,\langle L_\mu L^\mu + S \rangle + \frac{F^2}{8}\,H_0\,(D_\mu \theta)((D^\mu \theta)\,,\end{aligned} \tag{4.63}$$

where H_0 is an undetermined constant. Since it multiplies a term containing two ALP fields, it is not relevant to the subsequent analysis of the decay of kaons to a pion and an ALP at order $\mathcal{O}(1/f)$, but it is included here for completeness. Omitting again electroweak interaction terms, the covariant derivative is given by

$$\begin{aligned} D_\mu \Sigma &= \partial_\mu \Sigma - i\, l_\mu \Sigma + i\, \Sigma\, r_\mu = \partial_\mu \Sigma - i\,\frac{\partial_\mu a}{f}\,(k_Q\,\Sigma - \Sigma\, k_q)\,, \\ D_\mu \Sigma^\dagger &= \partial_\mu \Sigma^\dagger - i\, r_\mu \Sigma^\dagger + i\, \Sigma^\dagger\, l_\mu = \partial_\mu \Sigma^\dagger - i\,\frac{\partial_\mu a}{f}\,(k_q\,\Sigma^\dagger - \Sigma^\dagger\, k_Q)\,. \end{aligned} \tag{4.64}$$

Diagonalization of the strong chiral Lagrangian

Since the chiral effective theory including the ALP comprises three electrically neutral states, that is the ALP, π^0 and η_8, the general Lagrangian contains terms that describe kinetic and mass mixing of these fields. It is therefore convenient to diagonalize $\mathcal{L}$ in order to remove the two-particle vertices from the theory. The diagonalization has already been performed in [60] at order $\mathcal{O}(p^2)$ for the π^0-a mixing, while in the following also the η_8 is included. Collecting these particles as $\varphi^T = (\pi^0,\, \eta_8,\, a)$, the kinetic and mass terms can be written as

$$\mathcal{L}^{\mathrm{ALP}}_{\chi} \supset \frac{1}{2}(\partial_\mu \varphi)^T Z\,(\partial_\mu \varphi) - \frac{1}{2}\,\varphi^T M^2\,\varphi\,. \tag{4.65}$$

By comparison, the matrices Z and M read

$$Z = \begin{pmatrix} 1 & 0 & \frac{F}{f}\,\frac{\hat{c}^a_{uu}-\hat{c}^a_{dd}}{2\sqrt{2}} \\ 0 & 1 & \frac{F}{f}\,\frac{\hat{c}^a_{uu}+\hat{c}^a_{dd}-2\hat{c}^a_{ss}}{2\sqrt{6}} \\ \frac{F}{f}\,\frac{\hat{c}^a_{uu}-\hat{c}^a_{dd}}{2\sqrt{2}} & \frac{F}{f}\,\frac{\hat{c}^a_{uu}+\hat{c}^a_{dd}-2\hat{c}^a_{ss}}{2\sqrt{6}} & 1+\frac{F^2}{4f^2}\left(\langle \hat{c}^a \hat{c}^a\rangle + H_0\left(\langle c^a\rangle + 2c_{GG}\right)^2\right) \end{pmatrix}, \tag{4.66}$$

and

$$M^2 = \begin{pmatrix} B_0(m_u+m_d) & \frac{B_0(m_u-m_d)}{\sqrt{3}} & \frac{\sqrt{2}B_0 c_{GG} F\, g_\kappa(m_u,-m_d,0)}{f} \\ \frac{B_0(m_u-m_d)}{\sqrt{3}} & \frac{B_0(4m_s+m_u+m_d)}{3} & \frac{\sqrt{2}c_{GG}B_0 F\, g_\kappa(m_u,m_d,-2m_s)}{\sqrt{3}f} \\ \frac{\sqrt{2}c_{GG}B_0 F\, g_\kappa(m_u,-m_d,0)}{f} & \frac{\sqrt{2}c_{GG}B_0 F\, g_\kappa(m_u,m_d,-2m_s)}{\sqrt{3}f} & m^2_{a,0}+\frac{2c^2_{GG}B_0F^2}{f^2}\langle m_q\kappa^2_q\rangle \end{pmatrix},$$

and the short-hand notation

$$\begin{aligned} \hat{c}^a &= c^a + 2c_{GG}\,\kappa_q\,, \\ g_\kappa(a,b,c) &= a\,\kappa_u + b\,\kappa_d + c\,\kappa_s\,, \end{aligned} \tag{4.67}$$

was introduced. In order to remove the mixing, three redefinitions of φ need to be performed:

- First, the redefinition $\varphi \to U_Z\,\varphi$, with an orthogonal matrix U_Z, diagonalizes the kinetic term such that $U_Z^T\,Z\,U_Z = Z_{\text{diag}}$.
- Then, to normalize this term, another rescaling of the form $\varphi \to Z_{\text{diag}}^{-1/2}\,\varphi$ needs to be performed.
- Finally, to diagonalize the mass term as well, a rotation matrix is needed that yields $U_M^T\,Z_{\text{diag}}^{-1/2}\,U_Z^T\,M^2\,U_Z\,Z_{\text{diag}}^{-1/2}\,U_M = M^2_{\text{diag}}$, which means that the neutral states are once more rescaled, $\varphi \to U_M\,\varphi$.

In total, the Lagrangian states are connected to the physical fields via a total rotation R as

$$\varphi = R\,\varphi_{\text{phys}}\,, \quad \text{with} \quad R = U_Z\,Z_{\text{diag}}^{-1/2}\,U_M\,, \tag{4.68}$$

that can be written as

$$R = \begin{pmatrix} 1 & 0 & \theta_{\pi^0 a} \\ 0 & 1 & \theta_{\eta_8 a} \\ \theta_{a\pi^0} & \theta_{a\eta_8} & 1 \end{pmatrix} + \mathcal{O}\left(\frac{F^2}{f^2}\right). \tag{4.69}$$

As stated above, the rewriting in terms of these physical fields removes the two-point interactions from the strong chiral Lagrangian in the presence of the ALP. Since the analysis is performed at $\mathcal{O}(p^2)$, two-point vertices, however, reappear in any higher order as well as in the lowest order weak chiral effective Lagrangian as shown later.

In the *isospin limit*, where $m_u = m_d$, the explicit expressions for the *mixing angles* θ in (4.69) between the neutral states are, up to order $\mathcal{O}(F/f)$,

$$\begin{aligned}
\theta_{\pi^0 a} &= \frac{F}{f}\,\frac{(\hat{c}^a_{uu} - \hat{c}^a_{dd})\, m^2_{a,0} - 2c_{GG}\,(\kappa_u - \kappa_d)\,\tilde{m}^2_{\pi^0}}{2\sqrt{2}\,(\tilde{m}^2_{\pi^0} - m^2_{a,0})}\,,\\
\theta_{\eta_8 a} &= \frac{F}{f}\,\frac{(\hat{c}^a_{uu} + \hat{c}^d_{dd} - 2\hat{c}^a_{ss})\, m^2_{a,0} - 2c_{GG}\,\tilde{m}^2_{\pi^0} + 6c_{GG}\,\kappa_s\,\tilde{m}^2_{\eta_8}}{2\sqrt{6}\,(\tilde{m}^2_{\eta_8} - m^2_{a,0})}\,,\\
\theta_{a\pi^0} &= -\frac{F}{f}\,\frac{(c^a_{uu} - c^a_{dd})\,\tilde{m}^2_{\pi^0}}{2\sqrt{2}\,(\tilde{m}^2_{\pi^0} - m^2_{a,0})}\,,\\
\theta_{a\eta_8} &= -\frac{F}{f}\,\frac{(\hat{c}^a_{uu} + \hat{c}^a_{dd} - \hat{c}^a_{ss} + 6c_{GG}\,\kappa_s)\,\tilde{m}^2_{\eta_8} - 2c_{GG}\,\tilde{m}^2_{\pi^0}}{2\sqrt{6}\,(\tilde{m}^2_{\eta_8} - m^2_{a,0})}\,.
\end{aligned} \tag{4.70}$$

The tilde on the meson masses and the index on $m_{a,0}$ in the relations above indicates bare Lagrangian parameters that receive corrections that are discussed at the end of this section. There is no mixing between the neutral mesons for $m_u = m_d$ as can be seen in (4.66), since the corresponding entries in M^2 vanish in this limit. Before moving on to the physical masses, there are two features in the mixing angles that need to be discussed in more detail: First, there are divergences that arise when the ALP mass is exactly equal to the mass of one of the neutral mesons. On one hand, this is an artefact of the linearization in F/f and the expressions are only valid in a regime where $|\tilde{m}^2_i - m^2_{a,0}| \gg \tilde{m}^2_i \times F/f$ for $i \in \{\pi^0, \eta_8\}$. On the other hand, the exact degeneracy scenarios are even experimentally excluded, as they would alter the behavior of the neutral mesons, for instance in the decay $\pi^0 \to \gamma\gamma$. The second detail that requires some discussion is the explicit appearance of the chiral rotation parameters κ_q. As such, they are unphysical and need to cancel in physical expressions. This implies that the mixing angles themselves are not physical quantities, and the κ_q parameters need to vanish when writing down the full decay amplitudes.
Finally, from the considerations above, the physical masses of the neutral states are obtained by computing the eigenvalues of the mass matrix $\hat{M}^2$ after the transformations, which is given by

$$\hat{M}^2 = Z^{-1/2}_{\text{diag}}\, U^T_Z\, M^2\, U_Z\, Z^{-1/2}_{\text{diag}}\,. \tag{4.71}$$

This leads to

$$\begin{aligned}
m^2_{\pi^0} &= \tilde{m}^2_{\pi^0}\left[1 + \frac{F^2}{8f^2}\,\frac{\tilde{m}^2_{\pi^0}}{\tilde{m}^2_{\pi^0} - m^2_{a,0}}\,(c^a_{uu} - c^a_{dd})^2\right],\\
m^2_{\eta_8} &= \tilde{m}^2_{\eta_8}\left[1 + \frac{F^2}{24f^2}\frac{\tilde{m}^2_{\eta_8}}{\tilde{m}^2_{\eta_8} - m^2_{a,0}}\left(4c_{GG}\,\frac{m_s - \hat{m}}{2m_s + \hat{m}} + c^a_{uu} + c^a_{dd} - 2c^a_{ss}\right)^2\right],\\
m^2_a &= m^2_{a,0}\left\{1 - \frac{F^2}{4f^2}\left[\Delta + H_0\,(\langle c^a\rangle + 2c_{GG})^2 + \frac{m^2_a}{2\,(\tilde{m}^2_{\pi^0} - m^2_{a,0})}\,(c^a_{uu} - c^a_{dd})^2\right]\right\}\\
&\quad + c^2_{GG}\,\frac{F^2\,\tilde{m}^2_{\pi^0}}{2f^2} - \frac{F^2}{24f^2}\,\frac{\left((c^a_{uu} + c^a_{dd} - 2c^a_{ss})\, m^2_{a,0} + 2c_{GG}\,(m^2_{a,0} - \tilde{m}^2_{\pi^0})\right)^2}{\tilde{m}^2_{\eta_8} - m^2_{a,0}}\,,
\end{aligned} \tag{4.72}$$

with

$$\Delta = 2c_{GG}\left(c_{GG} + c^a_{uu} + c^a_{dd}\right) + \langle c^a c^a \rangle \,. \tag{4.73}$$

The masses of the kaons do not receive corrections in F/f,

$$\begin{aligned} m^2_{K^-} &= B_0\left(m_u + m_s\right), \\ m^2_{\bar{K}^0} &= B_0\left(m_d + m_s\right). \end{aligned} \tag{4.74}$$

Using that $\langle \kappa_q \rangle = 1$, the relations between the zeroth order physical mass parameters in F^2/f^2 in (4.72) and the quark masses are given by

$$\tilde{m}^2_{\pi^0} = \tilde{m}^2_{\pi^-} = B_0\left(m_u + m_d\right), \tag{4.75}$$

$$\tilde{m}^2_{\eta_8} = \frac{B_0}{3}\left(m_u + m_d + 4m_s\right). \tag{4.76}$$

Finally, in the isospin limit where $m^2_{K^-} = m^2_{\bar{K}^0}$, the mass of the η_8 reads

$$\tilde{m}^2_{\eta_8} = \frac{4m^2_{K^-} - m^2_{\pi^-}}{3}\,. \tag{4.77}$$

4.8.2. Weak Chiral Lagrangian at $\mathcal{O}(p^2)$ including the ALP

Similar to the strong chiral effective Lagrangian, the transition from the pure SM case to the ALP scenario primarily has the effect of dropping the index "0" from the building blocks of the Lagrangian. However, as pointed out in Section 4.5, the transformation that removes the weak mass term in the pure SM case does no longer eliminate this operator, and the full Lagrangian becomes

$$\begin{aligned} \mathcal{L}^{(p^2)}_{\chi\text{weak}} = \frac{F^4}{4}\Big[& G_8\mathcal{O}_8 + G_8'\left\langle \lambda_+ S\right\rangle + G_8^\theta\left(D_\mu\theta\right)\left\langle \lambda_+ L^\mu\right\rangle \\ & + G_{27}^{1/2}\,\mathcal{O}_{27}^{1/2} + G_{27}^{3/2}\,\mathcal{O}_{27}^{3/2} + \text{h.c.}\Big], \end{aligned} \tag{4.78}$$

where $\mathcal{O}_8$, $\mathcal{O}_{27}^{1/2}$ and $\mathcal{O}_{27}^{3/2}$ as defined in (4.24), but with the replacement $L_0^\mu \to L^\mu$. The presence of the ALP also implies that

$$\langle L^\mu \rangle = -D^\mu\theta\,. \tag{4.79}$$

The reason why the weak mass term $\langle \lambda_+ S\rangle$ is now necessarily present in (4.78) is the following: Consider again the chiral transformation in (4.29), but this time applied to the matrix Σ instead of Σ_0. In contrast to the SM situation, the kinetic term is no longer invariant, as the covariant derivative becomes

$$D_\mu\Sigma \to D_\mu\Sigma + i\left(\alpha_L D_\mu\Sigma - D_\mu\Sigma\,\alpha_R\right) - \left[\alpha_L, l_\mu\right]\Sigma + \Sigma\left[\alpha_R, r_\mu\right]. \tag{4.80}$$

The main difference is the appearance of the commutator terms, that are zero as long as the sources l_μ and r_μ contain only the photon field, since $[Q,\,\lambda_7] = 0$. For general ALP couplings, the commutators evaluate to

$$\begin{aligned} \left[i\lambda_7, l_\mu\right] &= \frac{\partial_\mu a}{f}\left[\left([k_Q]_{33} - [k_Q]_{22}\right)\lambda_6 + \text{Re}\,[k_Q]_{23}\left(\sqrt{3}\,\lambda_8 - \lambda_3\right)\right], \\ \left[i\lambda_7, r_\mu\right] &= \frac{\partial_\mu a}{f}\left[\left([k_q]_{33} - [k_q]_{22}\right)\lambda_6 + \text{Re}\,[k_q]_{23}\left(\sqrt{3}\,\lambda_8 - \lambda_3\right)\right]. \end{aligned} \tag{4.81}$$

All in all, this demonstrates that the weak mass term is not a redundant operator when the ALP with general, non flavor-universal couplings is present. Instead of employing the original form of this operator as given in (4.78), in what follows, the rotated version after the transformation is used. In total, this amounts to using a weak chiral Lagrangian of the form

$$\begin{aligned}\mathcal{L}'^{(p^2)}_{\chi\text{weak}} = \frac{F^4}{4}\Big[G_8\mathcal{O}_8 + G_8^{\theta}\,(D_\mu\theta)\,\langle\lambda_+ L^\mu\rangle + G_{27}^{1/2}\,\mathcal{O}_{27}^{1/2} + G_{27}^{3/2}\,\mathcal{O}_{27}^{3/2} + \text{h.c.}\Big] \\ + \frac{F^2}{4}\,\langle[i\alpha_L, l_\mu]L^\mu + [i\alpha_R, r_\mu]R^\mu\rangle\ ,\end{aligned} \tag{4.82}$$

where the right-handed object R_μ is defined as

$$R_\mu = -\Sigma^\dagger\, L_\mu\, \Sigma = \Sigma^\dagger\, iD_\mu\Sigma\,. \tag{4.83}$$

Certainly, this still removes the tadpole diagrams at order $\mathcal{O}(p^2)$, however, they reappear at higher orders. In addition to the modifications at order p^2, the transformation (4.29) needs to be applied in higher order operators as well, generating additional terms. Since the transformations already contain one factor of the Fermi constant and the following analysis is performed at first order in G_F, it is sufficient to additionally apply (4.29) only in the strong chiral effective Lagrangian at $\mathcal{O}(p^4)$. This amounts to shifting the building blocks of the corresponding operators by some additional term as discussed in the following section.

4.8.3. Strong Chiral Lagrangian at $\mathcal{O}(p^4)$ including the ALP

As in the previous sections, the construction of $\mathcal{L}^{(p^4)}_{\chi\text{QCD}}$ including the ALP first requires to drop the index "0" from all the building blocks in the p^4 operators in Table 4.3. In the case where electroweak interactions are neglected, the external sources only contain the ALP term, such that the field strength tensors defined in (4.33) vanish, since

$$F^{R,L}_{\mu\nu} = k_{q,Q}\left(\partial_\mu\,\partial_\nu\,\frac{a}{f}\right) - k_{q,Q}\left(\partial_\nu\,\partial_\mu\,\frac{a}{f}\right) - k_{q,Q}\left[\frac{\partial_\mu\, a}{f},\,\frac{\partial_\nu\, a}{f}\right] = 0\,. \tag{4.84}$$

Thus, $O_{9,10,11} = 0$. In addition, operator O_{12} does not have any field dependence and therefore does not contribute to amplitudes. On the other hand, the basis needs to be extended by operators linear in the ALP field, i.e. one insertion of the object $D_\mu\theta$. A basis with corresponding external sources was derived in [176]. Here, working to first order in $1/f$, it suffices to include the three operators shown in Table 4.6.

	O_i^θ	Γ_i^θ
1	$-(\partial^\mu D_\mu\theta)\,\langle P\rangle$	0
2	$-(D_\mu\theta)\,\langle L^\mu S\rangle$	$-\frac{1}{4}$
3	$(D_\mu\theta)\,\langle L^\mu L^2\rangle$	0

Table 4.6.: Operators extending the basis of $\mathcal{L}^{(p^4)}_{\chi\text{QCD}}$ in the presence of the ALP. The coefficients Γ_i^θ were derived in [176].

4.8.3.1. Additional Operators from the Weak Mass Term

If the tadpoles stemming from the weak mass term had not been rotated away by the transformation in (4.29), the list of QCD p^4 operators above would be exhaustive for the decay of a kaon to a pion and an ALP. Instead, in this case, additional operators are generated due to effective shifts of the building blocks,

$$\begin{aligned} L_\mu &\to g_L\, L_\mu\, g_L^\dagger + \delta L_\mu\,, \\ S &\to g_L\, S\, g_L^\dagger + \delta S\,, \\ P &\to g_L\, P\, g_L^\dagger + \delta P\,. \end{aligned} \tag{4.85}$$

The expressions for δS and δP have already been derived in [177],

$$\begin{aligned} \delta S &= -G_8' F^2 \big(\{\lambda_6, S\} - i\,[\lambda_6, P]\big)\,, \\ \delta P &= -G_8' F^2 \big(\{\lambda_6, P\} + i\,[\lambda_6, S]\big)\,. \end{aligned} \tag{4.86}$$

Additionally,

$$\delta L_\mu = [i\alpha_L, l_\mu] - \Sigma\,[i\alpha_R, r_\mu]\,\Sigma^\dagger\,. \tag{4.87}$$

Effectively, this can be translated to a shift of the operators

$$O_i^{(\theta)} \to O_i^{(\theta)} + \delta O_i^{(\theta)}\,. \tag{4.88}$$

Inserting (4.86) and (4.87) into the definition of the O_i, one obtains the explicit expressions of the additional δO_i terms,

$$\begin{aligned} \delta O_1 &= 4\,\langle [i\alpha_L, l_\mu] L^\mu + [i\alpha_R, r_\mu] R^\mu \rangle\, \langle L^2 \rangle\,, \\ \delta O_2 &= 4\,\langle [i\alpha_L, l_\mu] L_\nu + [i\alpha_R, r_\mu] R_\nu \rangle\, \langle L^\mu L^\nu \rangle\,, \\ \delta O_3 &= 2\,\langle [i\alpha_L, l_\mu] \{L^\mu, L^2\} + [i\alpha_R, r_\mu] \{R^\mu, R^2\} \rangle\,, \\ \delta O_4 &= -2 G_8' F^2\, \langle \lambda_6 S \rangle\, \langle L^2 \rangle \\ &\quad + 2\,\langle [i\alpha_L, l_\mu] L^\mu + [i\alpha_R, r_\mu] R^\mu \rangle\, \langle S \rangle\,, \\ \delta O_5 &= -G_8' F^2\, \langle \lambda_6 \left(\{S, L^2\} - i\,[P, L^2]\right) \rangle \\ &\quad + \langle [i\alpha_L, l_\mu] \{L^\mu, S\} + [i\alpha_R, r_\mu] \{R^\mu, S_R\} \rangle\,, \\ \delta O_6 &= -4 G_8' F^2\, \langle \lambda_6 S \rangle\, \langle S \rangle\,, \\ \delta O_7 &= \quad 4 G_8' F^2\, \langle \lambda_6 P \rangle\, \langle P \rangle\,, \\ \delta O_8 &= -2 G_8' F^2\, \langle \lambda_6 (S^2 - P^2) \rangle\,, \end{aligned} \tag{4.89}$$

and

$$\begin{aligned} \delta O_1^\theta &= 2 G_8' F^2\, (\partial^\mu D_\mu \theta)\, \langle \lambda_6 P \rangle\,, \\ \delta O_2^\theta &= G_8' F^2\, (D_\mu \theta)\, \langle \lambda_6\, (\{L^\mu, S\} + i\,[L^\mu, P]) \rangle \\ &\quad - (D_\mu \theta)\, \langle [i\alpha_L, l_\mu] S + [i\alpha_R, r_\mu] S_R \rangle\,, \\ \delta O_3^\theta &= (D_\mu \theta)\, \langle [i\alpha_L, l_\mu] L^2 + [i\alpha_R, r_\mu] R^2 \rangle \\ &\quad + (D_\mu \theta)\, \langle [i\alpha_L, l_\nu] \{L^\mu, L^\nu\} + [i\alpha_R, r_\nu] \{R^\mu, R^\nu\} \rangle\,, \end{aligned} \tag{4.90}$$

where S_R, P_R and R^μ are right-handed objects transforming as $S_R \to g_R\, S_R\, g_R^\dagger$ and equivalently for P_R and R^μ. These additional objects, that are not relevant when working purely in a SM context, are defined in Table 4.7. Here, also their transformation properties, along with those of the left-handed counterparts defined earlier, are presented.

SM Object	Definition	P	C	CP
S	$\chi\Sigma^\dagger + \Sigma\chi^\dagger$	$S \to S_R$	$S \to (S_R)^T$	$S \to S^T$
P	$i(\chi\Sigma^\dagger - \Sigma\chi^\dagger)$	$P \to P_R$	$P \to -(P_R)^T$	$P \to -P^T$
L_μ	$\Sigma\, i(D_\mu\Sigma)^\dagger$	$L_\mu \to R^\mu$	$L_\mu \to -(R_\mu)^T$	$L_\mu \to -(L^\mu)^T$
$W_{\mu\nu}$	$2\,(D_\mu L_\nu + D_\nu L_\mu)$	$W_{\mu\nu} \to W^{R\,\mu\nu}$	$W_{\mu\nu} \to -(W^R_{\mu\nu})^T$	$W_{\mu\nu} \to -(W^{\mu\nu})^T$
ALP Object	**Definition**	P	C	CP
$D_\mu\theta$	$\partial_\mu\theta - 2\,\langle a_\mu\rangle$	$D_\mu\theta \to -D^\mu\theta$	$D_\mu\theta \to D_\mu\theta$	$D_\mu\theta \to -D^\mu\theta$
S_R	$\chi^\dagger\Sigma + \Sigma^\dagger\chi$	$S_R \to S$	$S_R \to S^T$	$S_R \to (S_R)^T$
P_R	$i(\chi^\dagger\Sigma - \Sigma^\dagger\chi)$	$P_R \to P$	$P_R \to -P^T$	$P_R \to -(P_R)^T$
R_μ	$\Sigma^\dagger i D_\mu\Sigma$	$R_\mu \to L^\mu$	$R_\mu \to -(L_\mu)^T$	$R_\mu \to -(R^\mu)^T$
$W^R_{\mu\nu}$	$2\,(D_\mu R_\nu + D_\nu R_\mu)$	$W^R_{\mu\nu} \to W^{\mu\nu}$	$W^R_{\mu\nu} \to -(W_{\mu\nu})^T$	$W^R_{\mu\nu} \to -(W^{R\,\mu\nu})^T$

Table 4.7.: Building blocks and corresponding transformation properties under parity P, charge conjugation C and CP of the chiral effective Lagrangians. While all building blocks implicitly contain an ALP field after the substitution $\Sigma_0 \to \Sigma$, the first block shows objects that are needed to describe kaon decays in the pure SM case and were defined in [161, 177]. The "ALP Object" part of the table refers to objects needed when adding a pseudoscalar singlet such as axions or axion-like particles as external sources.

In (4.89), all terms that do not contain an insertion of l_μ or r_μ are of a structure of the building blocks that already appeared in the SM construction of the weak NLO chiral Lagrangian, see Table 4.5. Effectively, the weak mass term transformation therefore modifies the weak LECs according to

$$N_i \to N_i'\,, \tag{4.91}$$

with

$$\begin{aligned}
N_5' &= N_5 - 2\,\frac{G_8'}{G_8}\,L_5\,, & N_{11}' &= N_{11} - 8\,\frac{G_8'}{G_8}\,L_6\,,\\
N_7' &= N_7 - 4\,\frac{G_8'}{G_8}\,L_4\,, & N_{12}' &= N_{12} - 4\,\frac{G_8'}{G_8}\,L_8\,,\\
N_9' &= N_9 + 2\,\frac{G_8'}{G_8}\,L_5\,, & N_{13}' &= N_{13} - 8\,\frac{G_8'}{G_8}\,L_7\,,\\
N_{10}' &= N_{10} - 4\,\frac{G_8'}{G_8}\,L_8\,,
\end{aligned} \tag{4.92}$$

and the remaining N_i are unchanged. Since in the SM the weak mass term does not contribute to UV divergences from one-loop diagrams, the additional poles provided by the bare L_i must cancel in the N_i'. This uniquely fixes the values of the Z_i' in Table 4.5. For instance,

$$\lambda\,\frac{G_8'}{G_8}\,\left(Z_{11}' - 8\,\Gamma_6\right) \stackrel{!}{=} 0 \quad \Rightarrow \quad Z_{11}' = \frac{11}{18}\,. \tag{4.93}$$

While expressions containing a combination of $D_\mu\theta$ and r_μ or l_μ are of order $\mathcal{O}(1/f^2)$ and are henceforth neglected, terms in (4.90) that do contain one explicit insertion of the ALP field via $D_\mu\theta$ instead parametrize operators that have not been discussed so far. Similarly to the weak SM LECs, also the Wilson coefficients of these operators then need to be shifted. In detail,

$$\begin{aligned} N_1^{\theta\prime} &= N_1^\theta + 2\,\frac{G_8'}{G_8}\,L_2^\theta\,, \\ N_2^{\theta\prime} &= N_2^\theta + 2\,\frac{G_8'}{G_8}\,L_2^\theta\,, \\ N_5^{\theta\prime} &= N_5^\theta + 4\,\frac{G_8'}{G_8}\,L_1^\theta\,, \end{aligned} \tag{4.94}$$

Finally, there remain terms in (4.89) that have exactly one insertion of r_μ or l_μ, but no $D_\mu\theta$. While they cannot be cast into a structure containing only the building blocks of Table 4.7, it is nonetheless necessary to take them into account. In particular, they are crucial for the cancellation of the poles arising from one-loop diagrams.

4.8.4. Weak Chiral Lagrangian at $\mathcal{O}(p^4)$ including the ALP

As before, the first step to extend the weak chiral basis at $\mathcal{O}(p^4)$ to account for the ALP is to perform the substitution $B_0 \to B$ for all building blocks $B_0 \in \{S_0,\, L_0^\mu,\, P_0\}$ in Table 4.5. Since an exhaustive list of operators containing the ALP does not exist in the literature at this order, the next step is to write down all allowed combinations of $D_\mu\theta$ with the building blocks that generate a p^4 operator. This results in the following 12 combinations:

$$\begin{aligned} &1) \quad (\partial^\mu D_\mu\theta)\,\langle\lambda_6 P\rangle\,, && 7) \quad (\Box D_\mu\theta)\,\langle\lambda_6 L^\mu\rangle\,, \\ &2) \quad (\partial_\nu D_\mu\theta)\,\langle\lambda_6 W^{\mu\nu}\rangle\,, && 8) \quad (D_\mu\theta)\,\langle\lambda_6\{L^\mu, L^2\}\rangle\,, \\ &3) \quad (D_\mu\theta)\,\langle\lambda_6\{L^\mu, S\}\rangle\,, && 9) \quad (D_\mu\theta)\,\langle\lambda_6 L_\nu L^\mu L^\nu\rangle\,, \\ &4) \quad i(D_\mu\theta)\,\langle\lambda_6[L^\mu, P]\rangle\,, && 10) \quad (D_\mu\theta)\,\langle\lambda_6 L^\mu\rangle\,\langle L^2\rangle\,, \\ &5) \quad i(D_\mu\theta)\,\langle\lambda_6[L_\nu, W^{\mu\nu}]\rangle\,, && 11) \quad (D_\mu\theta)\,\langle\lambda_6 L_\nu\rangle\,\langle L^\mu L^\nu\rangle\,, \\ &6) \quad (D_\mu\theta)\,\langle\lambda_6 L^\mu\rangle\,\langle S\rangle\,, && 12) \quad i\epsilon_{\mu\nu\rho\sigma}(D^\mu\theta)\,\langle\lambda_6 L^\nu L^\rho L^\sigma\rangle\,. \end{aligned} \tag{4.95}$$

Two relationships significantly limit the number of terms in (4.95): First, any covariant derivative that acts on a $B \in \{S,\, P,\, W_{\mu\nu}\}$ can be moved to the θ-term via integration by parts, so that these terms do not need to be written down. Second, contracted indices on W_μ^μ do not appear, since the equation [161]

$$W_\mu^\mu + 2P - \frac{2}{3}\,\langle P\rangle\,\mathbb{1} + \frac{4}{3}\,\partial^\mu D_\mu\theta\,\mathbb{1} = \mathcal{O}(G_F) \tag{4.96}$$

implies that these terms can be eliminated. Still, the list above contains redundant operators that need to be reduced. Integrating by parts and recalling the definition $W_\mu^\nu = 2\,(D_\mu L_\nu + D_\nu L_\mu)$, operator seven in (4.95) can be rewritten as

$$(\Box D_\mu\theta)\,\langle\lambda_6 L^\mu\rangle = \frac{1}{2}\,(\partial^\mu D_\mu\theta)\,\langle\lambda_6 P\rangle + \mathcal{O}\left(\frac{a^2}{f^2}\right). \tag{4.97}$$

This also automatically implies that in the second operator, the covariant derivative inside the $W^{\mu\nu}$ can be moved to the θ part, such that

$$(\partial_\nu D_\mu\theta)\,\langle\lambda_6 W^{\mu\nu}\rangle = -4\,(\Box D_\mu\theta)\,\langle\lambda_6 L^\mu\rangle = -2\,(\partial^\mu D_\mu\theta)\,\langle\lambda_6 P\rangle\ . \tag{4.98}$$

This already reduces the list from 12 to 10 additional operators. An additional one, operator nine, can be removed by the Cayley-Hamilton theorem, that implies [177]

$$\begin{aligned}(D_\mu\theta)\,\langle\lambda_6 L_\nu L^\mu L^\nu\rangle = &-(D_\mu\theta)\,\langle\lambda_6\{L^\mu, L^2\}\rangle + (D_\mu\theta)\,\langle\lambda_6 L_\nu\rangle\,\langle L^\mu L^\nu\rangle \\ &+\frac{1}{2}(D_\mu\theta)\,\langle\lambda_6 L^\mu\rangle\,\langle L^2\rangle + \mathcal{O}\left(\frac{a^2}{f^2}\right).\end{aligned} \tag{4.99}$$

While this yields the final, non-redundant list of nine operators containing $D_\mu\theta$, in principle a "weak mass term"-like operator including an insertion of $m_{a,0}^2$ is possible. Since this term certainly needs to vanish in the SM limit, it must contain $(D_\mu\theta)$, such that the only possible form is $m_{a,0}^2\,(D_\mu\theta)(\lambda_6 L^\mu)$. However, rewriting the mass in terms of derivatives yields

$$m_{a,0}^2\,(D_\mu\theta)\,\langle\lambda_6 L^\mu\rangle = -(\Box D_\mu\theta)\,\langle\lambda_6 L^\mu\rangle = -\frac{1}{2}\,(\partial^\mu D_\mu\theta)\,\langle\lambda_6 P\rangle\ , \tag{4.100}$$

such that it clearly is redundant.
After these considerations, the full weak chiral Lagrangian at $\mathcal{O}(p^4)$ can be written as

$$\begin{aligned}\mathcal{L}_{\chi\text{weak}}^{(p^4)} =&\frac{G_8 F^2}{2}\left(\sum_{i=1}^{37} N_i\,W_i^8 + \sum_{i=1}^{9} N_i^\theta\,W_i^{\theta\,8}\right)\ , \\ =&\frac{G_8 F^4}{4}\frac{1}{(4\pi F)^2}\left(\sum_{i=1}^{37}\hat{N}_i\,W_i^8 + \sum_{i=1}^{9}\hat{N}_i^\theta\,W_i^{\theta\,8}\right)\ ,\end{aligned} \tag{4.101}$$

and in the second line again the rescaling of the weak LECs as defined in (4.44) is performed. The bare weak LECs are now related to the scale dependent ones via

$$\begin{aligned}N_i &= N_{i,r}(\mu) + \lambda\left(Z_i + \frac{G_8'}{G_8}\,Z_i'\right)\ , \\ N_i^\theta &= N_{i,r}^\theta(\mu) + \lambda\left(Z_i^\theta + \frac{G_8'}{G_8}\,Z_i'^\theta + \frac{G_8^\theta}{G_8}\,Z_i^{\theta\theta}\right)\ .\end{aligned} \tag{4.102}$$

The full list of additional weak chiral ALP operators is shown in Table 4.8 together with the corresponding anomalous dimensions. The values of the Z_i' and $Z_i'^\theta$ were determined from the considerations described in Section 4.8.3.1. Requiring the cancellation of the pole terms from the one-loop integrals yields relations between the remaining coefficients, but does not fix all free parameters. In particular, for the Z_i^θ it yields

$$Z_1^\theta = \frac{1}{2} + \frac{1}{2}\,Z_5^\theta\,, \qquad Z_2^\theta = -\frac{1}{2} + 2Z_3^\theta + \frac{1}{2}\,Z_5^\theta\,, \tag{4.103}$$

and for the $Z_i^{\theta\theta}$

$$Z_1^{\theta\theta} = \frac{3}{4} + \frac{1}{2}\,Z_5^{\theta\theta}\,, \qquad Z_2^{\theta\theta} = 2Z_3^{\theta\theta} + \frac{1}{2}\,Z_5^{\theta\theta}\,. \tag{4.104}$$

In the relations above, G_8' and G_8^θ are defined in analogy to (4.25), but with so far undetermined values for g_8' and g_8^θ.

i	$W_i^{\theta\,8}$	Z_i^{θ}	$Z_i^{\prime\theta}$	$Z_i^{\theta\theta}$	i	$W_i^{\theta\,8}$	Z_i^{θ}	$Z_i^{\prime\theta}$	$Z_i^{\theta\theta}$
1	$(D_\mu\theta)\,\langle\lambda_6\{L^\mu, S\}\rangle$	(4.103)	$\frac{1}{2}$	(4.104)	6	$(D_\mu\theta)\,\langle\lambda_6\{L^\mu, L^2\}\rangle$	–	0	–
2	$i(D_\mu\theta)\,\langle\lambda_6[L^\mu, P]\rangle$	(4.103)	$\frac{1}{2}$	(4.104)	7	$(D_\mu\theta)\,\langle\lambda_6 L^\mu\rangle\,\langle L^2\rangle$	–	0	–
3	$i(D_\mu\theta)\,\langle\lambda_6[L_\nu, W^{\mu\nu}]\rangle$	Z_3^{θ}	0	$Z_3^{\theta\theta}$	8	$(D_\mu\theta)\,\langle\lambda_6 L_\nu\rangle\,\langle L^\mu L^\nu\rangle$	–	0	–
4	$(D_\mu\theta)\,\langle\lambda_6 L^\mu\rangle\,\langle S\rangle$	$-\frac{3}{4}$	0	$\frac{1}{2}$	9	$i\epsilon_{\mu\nu\rho\sigma}(D^\mu\theta)\,\langle\lambda_6 L^\nu L^\rho L^\sigma\rangle$	–	0	–
5	$(\partial^\mu D_\mu\theta)\,\langle\lambda_6 P\rangle$	Z_5^{θ}	0	$Z_5^{\theta\theta}$					

Table 4.8.: Additional operators extending the $\mathcal{O}(p^4)$ weak octet chiral Lagrangian when the SM is extended by an ALP. The values of the anomalous dimensions Z_i^{θ}, $Z_i^{\prime\theta}$ and $Z_i^{\theta\theta}$ are derived by requiring that the poles in the amplitudes $K^{\pm} \to \pi^{\pm} a$ cancel. If no value is given, the coefficient does not get constrained by this computation.

4.9. Calculation of the Decays $K^{\pm} \to \pi^{\pm}\, a$ at NLO

Contribution	G_8	G_8'	G_8^{θ}	$G_{27}^{1/2}$	$G_{27}^{3/2}$	$\epsilon^{(2)}$
LO	✓	✓	✓	✓	✓	✓
NLO	✓	✓	✓	✗	✗	✗

Table 4.9.: Contributions to the LO and NLO amplitude as computed for the decay $K^- \to \pi^- a$.

With all the necessary building blocks in place to compute the decays $K^{\pm} \to \pi^{\pm}\, a$ in χ_aPT, it is now possible to move on to determining the amplitude up to next-to-leading order. More concretely, this section presents detailed expressions for $K^- \to \pi^-\, a$ at first order in $1/f$ and G_F. The corresponding decay of a positively charged kaon can be obtained by taking the complex conjugate of the results. In the following discussion, products of flavor-changing ALP couplings and G_F are consistently neglected. On the other hand, isospin-breaking corrections at first order in $(m_u - m_d)$ are included at leading order (LO). In addition, due to the fact that g_8 is much larger than $g_{27}^{1/2}$ and $g_{27}^{3/2}$, contributions from the 27-plet operators are only considered at LO in what follows. A full summary of the computed contributions to the LO and the NLO is shown in Table 4.9.

The structure of the amplitude can be decomposed into a piece in which the flavor-violating $s \to d$ transition is mediated by a flavor off-diagonal ALP coupling $[k_D]_{12}$ or $[k_d]_{12}$, in the following denoted by $\mathcal{A}^{\mathrm{FV}}$, and a piece where the flavor change stems from the SM flavor violation in the weak sector, which is referred to as $\mathcal{A}^{\mathrm{FC}}$. Therefore, the full amplitude can schematically be written as

$$\mathcal{A} = \mathcal{A}^{\mathrm{FV}} + \mathcal{A}^{\mathrm{FC}}\,, \tag{4.105}$$

where the explicit ALP couplings in these partial amplitudes are

$$\begin{aligned} \mathcal{A}^{\mathrm{FV}} &= -(m_{K^-}^2 - m_{\pi^-}^2)\,\frac{[k_d + k_D]_{12}}{2f}\,A^{\mathrm{FV}}\,, \\ \mathcal{A}^{\mathrm{FC}} &= \sum_{c_{\mathrm{ALP}},\,G} \frac{G\,F_{\pi^-}^2\,m_{K^-}^2\,c_{\mathrm{ALP}}}{2f}\,A^{G,\,c_{\mathrm{ALP}}}\,, \end{aligned} \tag{4.106}$$

with[8]

$$\begin{aligned} G &\in \left\{G_8, G_8^{\theta}, G_8', G_{27}^{1/2}, G_{27}^{3/2}\right\}, \\ c_{\text{ALP}} &\in \left\{\tilde{c}_{GG}, c_{uu}^a, (c_{dd}^a + c_{ss}^a), (c_{dd}^a - c_{ss}^a), (c_{dd}^v - c_{ss}^v)\right\}. \end{aligned} \tag{4.107}$$

As the flavor-change in $\mathcal{A}^{\text{FC}}$ is solely mediated by the weak interactions, the amplitude is also referred to as *weak amplitude*, while $\mathcal{A}^{\text{FV}}$ is called *QCD* or *strong amplitude*. Certainly both, A^{FC} and A^{FV}, have leading order, i.e. $\mathcal{O}(p^2)$, and NLO, i.e. $\mathcal{O}(p^4)$, contributions, that are discussed in detail the following section.

4.9.1. Leading Order Amplitude

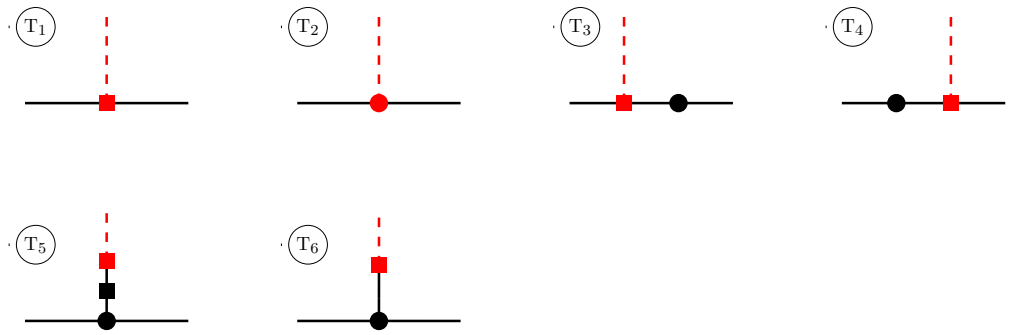

Figure 4.2.: Tree level graphs contributing to the decay $K^- \to \pi^- a$ at leading order in the chiral expansion. The ALP is shown as a dashed line. Insertions from the strong chiral Lagrangian at $\mathcal{O}(p^2)$ are indicated as the square ■, while vertices from the weak $\mathcal{O}(p^2)$ chiral Lagrangian are shown as a dot ●. The fact that the diagonalization of the strong chiral Lagrangian is performed in the isospin conserving limit reflects itself in the reappearance of the two-particle vertices $\pi^0 - \eta_8$, $\pi^0 - a$ and $\eta_8 - a$ in diagrams T_5 and T_6, where isospin breaking terms are taken into account.

At leading order in the chiral expansion, the Feynman diagrams that contribute to the decay amplitude of the process $K^- \to \pi^- a$ are tree level graphs with an arbitrary number of vertices from the QCD effective chiral Lagrangian, zero or one insertion of the weak effective chiral Lagrangian and exactly one ALP interaction that is either flavor violating (if the graph has an insertion of a term from $\mathcal{L}_{\chi\text{weak}}^{(p^2)}$), or flavor conserving (no insertion of $\mathcal{L}_{\chi\text{weak}}^{(p^2)}$). This yields the six distinct topologies that are shown in Figure 4.2.

[8] As the vector currents $\bar{f}\gamma^{\mu} f$ are conserved, only the difference of the ALP–SM couplings $(c_{dd}^v - c_{ss}^v)$ is observable, while the sum $(c_{dd}^v + c_{ss}^v)$ remains unobservable when considering flavor-changing neutral-current processes.

Leading Order QCD Amplitude

At leading order, there is only the tree level diagram T_1 that contributes to the pure QCD piece of the amplitude. Factoring out $[k_D]_{12}$ and $[k_d]_{12}$ according to (4.106), it is simply given by

$$iA_{\text{LO}}^{\text{FV}} = 1\,. \tag{4.108}$$

Leading Order Weak Amplitude

In diagrams T_2 to T_6, the flavor change is mediated by an insertion of a CKM matrix element stemming from $\mathcal{L}_{\chi\text{weak}}^{(p^2)}$. At this order, also isospin breaking terms are taken into account that are suppressed by

$$\varepsilon^{(2)} = \frac{m_d - m_u}{m_s - \hat{m}} \approx 0.028\,, \qquad \hat{m} = \frac{m_u + m_d}{2}\,. \tag{4.109}$$

These terms lead to the diagrams in the second row of Figure 4.2, where the two-point vertices are present because the strong chiral effective Lagrangian is only diagonalized in the isospin conserving limit in Section 4.8.1. Defining the mass ratios of the ALP and pion to the kaon mass as

$$x = \frac{m_a^2}{m_K^2}\,, \qquad y = \frac{m_\pi^2}{m_K^2}\,, \tag{4.110}$$

the full, weak leading order contribution to the decay can be expressed as

$$\begin{aligned}
iA_{\text{LO}}^{G_8,\,\tilde{c}_{GG}} &= \frac{8\,(1-x)(1-y)}{4-y-3\,x}\left[1-\varepsilon^{(2)}\,\frac{2(1-y)}{4-y-3\,x}\right],\\
iA_{\text{LO}}^{G_8,\,c_{uu}^a} &= -\frac{y(1-y)}{4-y-3x}\left[1-\varepsilon^{(2)}\,\frac{(1-y)\left(8\,y-x\,(4+7\,y)+3\,x^2\right)}{y\,(y-x)(4-y-3\,x)}\right],\\
iA_{\text{LO}}^{G_8,\,(c_{dd}^a+c_{ss}^a)} &= -\frac{(1-y)(4+y-6\,x)}{2\,(4-y-3\,x)}\\
&\quad\times\left[1-\varepsilon^{(2)}\,\frac{(1-y)\left(16\,y-x\,(20+17\,y)+21\,x^2\right)}{(y-x)(4+y-6\,x)(4-y-3\,x)}\right],\\
iA_{\text{LO}}^{G_8,\,(c_{dd}^a-c_{ss}^a)} &= \frac{x\,(1+2\,y-3\,x)}{2\,(4-y-3\,x)}\\
&\quad\times\left[1-\varepsilon^{(2)}\,\frac{(1-y)\left(4+13\,y+y^2-3\,x\,(7+5\,y)+18\,x^2\right)}{(y-x)(1+2\,y-3\,x)(4-y-3\,x)}\right],\\
iA_{\text{LO}}^{G_8,\,(c_{dd}^v-c_{ss}^v)} &= \frac{1-x+y}{2}\,,
\end{aligned} \tag{4.111}$$

as well as

$$iA_{\text{LO}}^{G_8^\theta,\,\tilde{c}_{GG}} = -2\,(1-y)\,. \tag{4.112}$$

Furthermore,

$$\begin{aligned} iA_{\mathrm{LO}}^{G_8',(c_{dd}^a - c_{ss}^a)} &= (1-y)^2 \left[1 - \varepsilon^{(2)}\,(1-y)\right], \\ iA_{\mathrm{LO}}^{G_8',(c_{dd}^v - c_{ss}^v)} &= -\left[1 + \varepsilon^{(2)}\,(1-y)\right], \end{aligned} \tag{4.113}$$

and all G_8' contributions from the remaining coefficients vanish. The two 27-plet tree-level contributions read

$$\begin{aligned} iA_{\mathrm{LO}}^{G_{27}^{1/2},\tilde{c}_{GG}} &= \frac{4\,(1-y)(4-3\,y-x)}{4-y-3\,x}\left[1 - \varepsilon^{(2)}\,\frac{(1-y)(4-5\,y+x)}{(4-y-3\,x)(4-3\,y-x)}\right], \\ iA_{\mathrm{LO}}^{G_{27}^{1/2},c_{uu}^a} &= \frac{4\,y\,(1-y)}{4-y-3\,x}\left[1 + \varepsilon^{(2)}\,\frac{(1-y)\left(y\,(4-5\,y)+x\,(8-y)-6x^2\right)}{2\,y\,(y-x)(4-y-3\,x)}\right], \\ iA_{\mathrm{LO}}^{G_{27}^{1/2},(c_{dd}^a + c_{ss}^a)} &= -\frac{(1-y)(12-7\,y-3\,x)}{4-y-3\,x} \\ &\quad \times \left[1 - \varepsilon^{(2)}\,\frac{(1-y)\left(2\,y\,(4-5\,y)-x\,(20-19\,y)+3\,x^2\right)}{(y-x)(4-y-3\,x)(12-7\,y-3\,x)}\right], \\ iA_{\mathrm{LO}}^{G_{27}^{1/2},(c_{dd}^a - c_{ss}^a)} &= \frac{1}{2\,(4-y-3\,x)}\left[20 - 25\,y + 5\,y^2 + x + 2\,x\,y - 3\,x^2\right. \\ &\quad \left. - \varepsilon^{(2)}\,\frac{6\,x(1-y)\left(4+3\,y-4\,y^2-x\,(11-5\,y)+3\,x^2\right)}{(y-x)(4-y-3x)}\right], \\ i\,A_{\mathrm{LO}}^{G_{27}^{1/2},(c_{dd}^v - c_{ss}^v)} &= \frac{1}{2}\,(1-x+y)\,, \end{aligned} \tag{4.114}$$

and

$$\begin{aligned} iA_{\mathrm{LO}}^{G_{27}^{3/2},\tilde{c}_{GG}} &= \frac{4\,(1-x)(1-y)}{4-y-3\,x} \\ &\quad \times \left[1 + \varepsilon^{(2)}\,\frac{(1-y)\left(12-13\,y+9\,x\,y-1\,x+x^2+2\,y^2\right)}{(1-x)(y-x)(4-y-3\,x)}\right], \\ iA_{\mathrm{LO}}^{G_{27}^{3/2},c_{uu}^a} &= \frac{2\,y\,(1-y)(3-y-2\,x)}{(y-x)(4-y-3x)} \\ &\quad \times \left[1 - \varepsilon^{(2)}\,\frac{(1-y)}{y\,(3-y-2\,x)}\left(5-2\,y-4\,x-\frac{2(4-7\,x+3\,x^2)}{4-y-3\,x}\right)\right], \\ iA_{\mathrm{LO}}^{G_{27}^{3/2},(c_{dd}^a + c_{ss}^a)} &= -\frac{(1-y)}{(y-x)(4-y-3\,x)}\left[y\,(6-y)-x\,(3+5\,y)+3\,x^2\right. \\ &\quad \left. + \varepsilon^{(2)}\,\frac{1-y}{4-y-3\,x}\left(24-26\,y+4\,y^2-x\,(16-17\,y)-3\,x^2\right)\right], \end{aligned}$$

$$
\begin{aligned}
i A_{\text{LO}}^{G_{27}^{3/2},\,(c_{dd}^a - c_{ss}^a)} &= -\frac{1}{2(y-x)(4-y-3x)} \\
&\quad \times \left[y\left(4 - 5\,y + y^2\right) + x\left(2 - 8\,y + 3\,y^2\right) + x^2\left(1 + 5\,y\right) - 3\,x^3 \right. \\
&\quad \left. - \varepsilon^{(2)}\, \frac{6\,x\,(1-y)\left(2 - 6\,y + y^2 + x\,(2+4\,y) - 3\,x^2\right)}{4 - y - 3\,x} \right], \\
i\,A_{\text{LO}}^{G_{27}^{3/2},\,(c_{dd}^v - c_{ss}^v)} &= \frac{1}{2}\,(1 - x + y)\,.
\end{aligned}
\tag{4.115}
$$

The isospin limits of the G_8 and G_{27} terms have already been computed in [56] and [34], respectively. Several features of these amplitudes need to be highlighted:

- The κ_q parameters cancel in the amplitudes. This is an important cross-check of the results, as the rotation (4.49) is unphysical.
- While the isospin breaking effects are suppressed by $(m_d - m_u)/m_s$ for terms proportional to G_8 and $G_{27}^{1/2}$ (as also found in [56]), this suppression does not apply to the $G_{27}^{3/2}$ terms, which are proportional to $(m_d - m_u)/\hat{m}$.
- Some amplitudes in (4.111), (4.113) and (4.115) diverge in the limit $m_a \to \tilde{m}_{\pi^0}$ (or $x \to y$). Although maximal π^0–ALP mixing is experimentally excluded, it is insightful to better understand this diagonalization remnant up to first order in F/f of the leading order strong chiral Lagrangian. For terms proportional to G_8 and $G_{27}^{1/2}$, it happens only in the isospin breaking corrections proportional to $\epsilon^{(2)}$, while in some terms proportional to $G_{27}^{3/2}$ this already appears in the isospin conserving limit. It is illuminating to examine it in the unrotated basis, where the neutral mesons again mix via explicit two-particle vertices. Here, the following diagrams are responsible for the divergences:

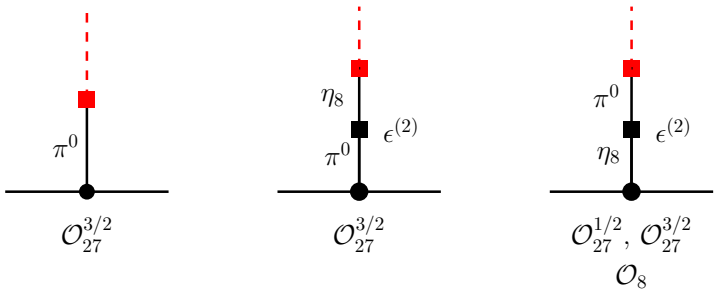

Focusing on the first diagram from the left, the pole that creates the divergence in the unrotated basis stems from the pion propagator and is of the form $1/(\tilde{m}_{\pi^0}^2 - m_a^2)$ (or the corresponding factor in the mixing angle $\theta_{\pi^0 a}$ in the rotated basis). This requires the transition $K^- \to \pi^-\,\pi^0$, which cannot be mediated on-shell by the operators $\mathcal{O}_8$ and $\mathcal{O}_{27}^{1/2}$, as they only describe isospin changes of $\Delta I = 1/2$. These two operator types instead generate vertices proportional to $(\tilde{m}_{\pi^0}^2 - p_{\pi^0}^2)$ that cancel the pole. The operator $\mathcal{O}_{27}^{3/2}$, in contrast, does provide the

necessary isospin transition for this process. Hence, there is no cancellation of the divergence, even in the isospin conserving limit. The middle diagram shows the same situation, but with an additional isospin violating vertex that mixes the neutral pion and the η_8-meson. The last diagram above requires the transition $K^- \to \pi^- \eta_8$ that is allowed for all operator types $\mathcal{O}_8$, $\mathcal{O}_{27}^{1/2}$ and $\mathcal{O}_{27}^{3/2}$. To generate a divergence, the η_8 needs to mix into the neutral pion, which, again, is of $\mathcal{O}(\epsilon^{(2)})$. Thus, this behavior only appears in the isospin violating limit for $\mathcal{O}_8$ and $\mathcal{O}_{27}^{1/2}$.
Due to kinematic constraints, there is no corresponding pole for $m_a \to \tilde{m}_{\eta_8}$, as only $m_a < m_K - m_\pi$ is allowed.

4.9.2. Next-to-Leading Order Amplitude

At NLO in the chiral expansion, one must compute one-loop diagrams generated by $\mathcal{O}(p^2)$ operators, as well as tree-level diagrams with insertions of $\mathcal{O}(p^4)$ operators. Furthermore, the meson masses and the pion decay constant get a correction, and external leg corrections yield wave-function renormalizations that multiply the leading order. The sum of the LO and NLO amplitudes can thus schematically be written as

$$(\mathcal{A}_{\text{LO}} + \mathcal{A}_{\text{NLO}})|_{\text{NLO}} = \sqrt{Z_\pi Z_K}\, \mathcal{A}'_{\text{LO}} + \mathcal{A}^{(p^4)}_{\Delta m_i^2,\, \Delta F_\pi} + \mathcal{A}^{(p^4)}_{\text{1-loop}} + \mathcal{A}^{(p^4)}_{\text{tree}}\,, \tag{4.116}$$

where the Z_π and Z_K denote the wave-function renormalizations of the pion and the kaon, respectively. In the expression above,

$$\mathcal{A}_{\text{LO}}(m_i^2, F) = \mathcal{A}_{\text{LO}}(m_{i,\text{NLO}}^2, F_\pi) + \mathcal{A}^{(p^4)}_{\Delta m_i^2,\, \Delta F_\pi} \equiv \mathcal{A}'_{\text{LO}} + \mathcal{A}^{(p^4)}_{\Delta m_i^2,\, \Delta F_\pi}\,. \tag{4.117}$$

Both amplitudes on the right-hand side of (4.117) are computed from the tree-level diagrams in Figure 4.2, but in the second term, $\mathcal{A}^{(p^4)}_{\Delta m_i^2,\, \Delta F_\pi}$, NLO corrections for the meson masses and the decay constant F are inserted. Therefore, only $\mathcal{A}'_{\text{LO}}$ is formally of order $\mathcal{O}(p^2)$ (and thus gets multiplied by the wave-function renormalization factors Z_i such that the product is a NLO term), while $\mathcal{A}^{(p^4)}_{\Delta m_i^2,\, \Delta F_\pi}$ is already of order $\mathcal{O}(p^4)$. The term $\mathcal{A}^{(p^4)}_{\text{1-loop}}$ represents all one-particle irreducible one-loop diagrams with $\mathcal{O}(p^2)$ vertices, while the last term in (4.116) denotes tree-level graphs built out of $\mathcal{O}(p^4)$ vertices. Details on the calculation of all NLO contributions are given in the next sections.
Given that $g_{27}^{1/2}/g_8 \approx 0.01$ and $g_{27}^{3/2}/g_8 \approx 0.05$, the 27-plet contributions are neglected in the NLO amplitude. In addition, also isospin corrections are not taken into account at this order. In contrast, since no estimates of g_8' and g_8^θ exist, they are included for completeness. As the analytic expression for the NLO amplitude is rather elaborate, the following text focusses on the conceptual aspects, while the full result is presented in the appendix of this chapter.

4.9.2.1. Wave-Function Renormalization and Mass Correction

Figure 4.3.: Feynman graphs contributing to the mesons self-energy at NLO in the chiral expansion. The black square ■ denotes the insertion of a vertex from the $\mathcal{O}(p^2)$ QCD Lagrangian in (4.63), while the empty square □ refers to a vertex from the $\mathcal{O}(p^4)$ QCD Lagrangian in (4.35).

Both the external leg and mass correction are derived from the self-energy[9] Σ, that is computed from the Feynman diagrams shown in Figure 4.3. It is important to note again that neither the ALP mass nor its external legs receive corrections, since every ALP interaction is already suppressed by its decay constant and additional corrections should not be taken into account when working consistently at $\mathcal{O}(1/f)$. External leg and mass corrections hence only need to be computed for the pion and the kaon. The expressions for the wave-function renormalization factors Z_i are obtained from the self-energies Σ_i via

$$Z_i^{-1} = 1 - \left.\frac{d\Sigma_i(p^2)}{dp^2}\right|_{p^2=m_i^2} . \tag{4.118}$$

Concretely, this yields

$$\begin{aligned} Z_K = 1 - \frac{1}{(4\pi F)^2}\Bigg[&\left(4m_K^{d-2} + \frac{1}{2}\, m_\pi^{d-2} - \frac{1}{2}\, m_{\eta_8}^{d-2}\right)\left(\frac{2}{d-4} - \ln 4\pi + \gamma_E - 1\right) \\ &+ 5m_K^2 \ln\frac{\mu^2}{m_K^2} + m_\pi^2 \ln\frac{\mu^2}{m_\pi^2} \\ &+ 2m_K^2\left(2\hat{L}_{4,r}(\mu) + \hat{L}_{5,r}(\mu)\right) + 2m_\pi^2\, \hat{L}_{4,r}(\mu)\Bigg] , \end{aligned} \tag{4.119}$$

$$\begin{aligned} Z_\pi = 1 - \frac{1}{(4\pi F)^2}\Bigg[&\left(\frac{4}{3}\, m_K^{d-2} + \frac{8}{3}\, m_\pi^{d-2}\right)\left(\frac{2}{d-4} - \ln 4\pi + \gamma_E - 1\right) \\ &+ 2m_K^2 \ln\frac{\mu^2}{m_K^2} + 4m_\pi^2 \ln\frac{\mu^2}{m_\pi^2} \\ &+ 4m_K^2\, \hat{L}_{4,r}(\mu) + 2m_\pi^2\left(\hat{L}_{4,r}(\mu) + \hat{L}_{5,r}(\mu)\right)\Bigg] . \end{aligned}$$

The *Lagrangian masses* get shifted via $\Delta m_i^2 = \Sigma_i(m_i^2)$ to the NLO masses as

$$m_{i,\mathrm{NLO}}^2 = m_i^2 + \Delta m_i^2 , \tag{4.120}$$

[9] Although the matrix containing the exponential of the meson fields is also denoted by Σ, the standard convention for the self-energy is maintained here, as the context makes it clear which quantity is being referred to.

where, in agreement with [161],

$$\begin{aligned}\Delta m^2_{\pi^-} &= \frac{m_\pi^2}{(4\pi F)^2}\left[- m_\pi^2 \ln\frac{\mu^2}{m_\pi^2} + \frac{m_{\eta_8}^2}{3}\ln\frac{\mu^2}{m_{\eta_8}^2}\right.\\ &\qquad \left. + (4m_K^2 + 2m_\pi^2)\left(2\hat{L}_{6,r}(\mu) - \hat{L}_{4,r}(\mu)\right) + 2m_\pi^2\left(2\hat{L}_{8,r}(\mu) - \hat{L}_{5,r}(\mu)\right)\right],\\ \Delta m^2_{K^-} &= \frac{m_K^2}{(4\pi F)^2}\left[- \frac{2}{3} m_{\eta_8}^2 \ln\frac{\mu^2}{m_{\eta_8}^2}\right.\\ &\qquad \left. + (4m_K^2 + 2m_\pi^2)\left(2\hat{L}_{6,r}(\mu) - \hat{L}_{4,r}(\mu)\right) + 2m_K^2\left(2\hat{L}_{8,r}(\mu) - \hat{L}_{5,r}(\mu)\right)\right].\end{aligned} \tag{4.121}$$

The expression for the NLO pion decay constant was derived in [161]. Taking into account the different normalization and rewriting the LECs according to (4.41), the correction reads

$$F_\pi = F + \Delta F_\pi\,, \tag{4.122}$$

with

$$\begin{aligned}\Delta F_\pi = \frac{F_\pi}{(4\pi F)^2}\Big[&m_K^2 \ln\frac{\mu^2}{m_K^2} + 2m_\pi^2 \ln\frac{\mu^2}{m_\pi^2} + 2m_K^2\,\hat{L}_{4,r}(\mu)\\ &+ m_\pi^2\left(\hat{L}_{4,r}(\mu) + \hat{L}_{5,r}(\mu)\right)\Big].\end{aligned} \tag{4.123}$$

4.9.2.2. One-Loop Amplitude

In the next step, all one-particle irreducible one-loop Feynman diagrams are added to the NLO amplitude as parametrized by the term $\mathcal{A}^{(p^4)}_{\text{1-loop}}$ in (4.116). As in the tree-level graphs, the flavor-changing interaction needed for the decay $K^- \to \pi^- a$ can be provided by a flavor off-diagonal ALP coupling or by the insertion of a corresponding weak interaction, and both contributions are considered separately in what follows.

One-Loop QCD Amplitude

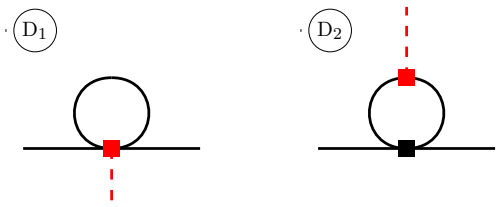

Figure 4.4.: Feynman graphs with a flavor-violating ALP coupling, contributing to the $K^- \to \pi^- a$ decay amplitude at NLO in the chiral expansion. The black and red squares denote the insertion of a vertex from the $\mathcal{O}(p^2)$ QCD Lagrangian in (4.63).

There are only two one-loop topologies for $K^- \to \pi^- a$ that do not require an insertion of a weak $\mathcal{O}(p^2)$ operator, which are shown in Figure 4.4. In topology D_1, five different

internal states in the loop ($K^{\pm}$, $\pi^{\pm}$, η_8, π^0, $K^0/\bar{K}^0$) contribute to the amplitude, while in D_2, the combinations K^0-η_8, K^0-π^0 and $K^{\pm}$-$\pi^{\pm}$ are possible.

One-Loop Weak Amplitude

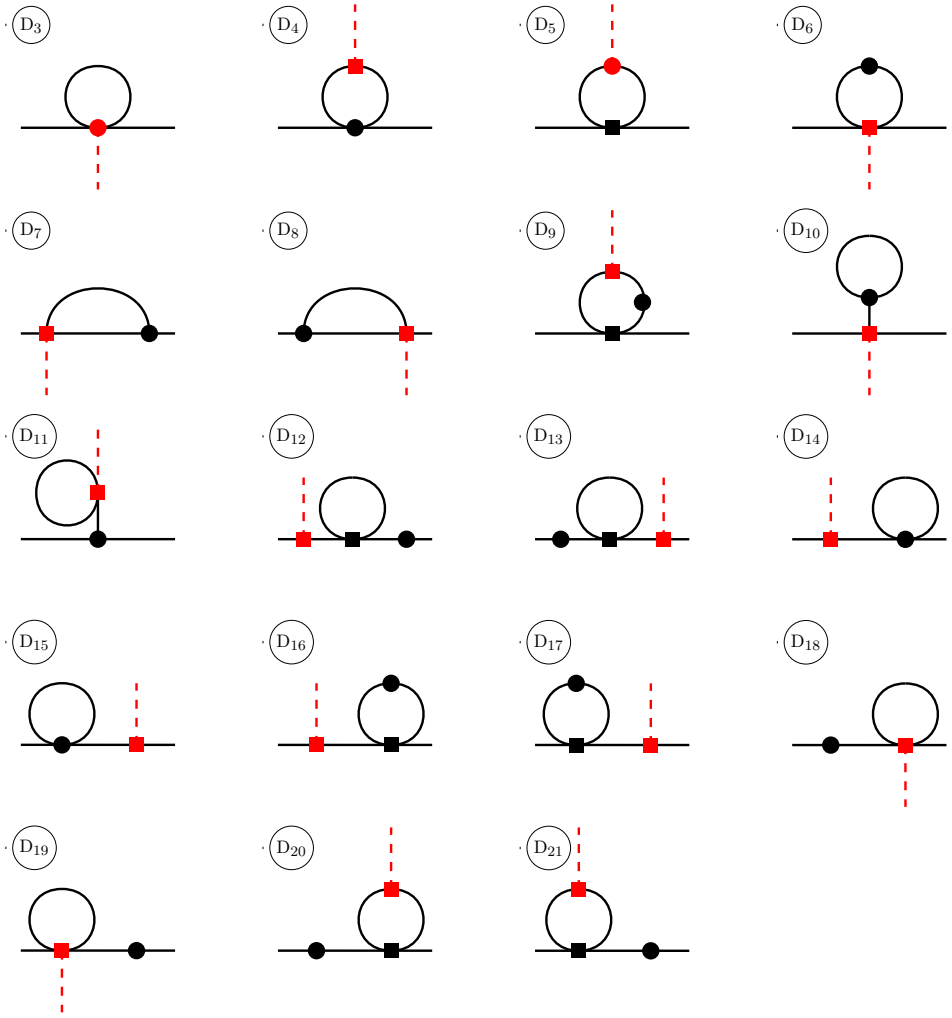

Figure 4.5.: One-loop Feynman graphs with ALP flavor-conserving ALP interactions contributing to the $K^- \to \pi^- a$ decay amplitude at NLO in the chiral expansion. The flavor change results from an insertion of a vertex from the $\mathcal{O}(p^2)$ weak chiral Lagrangian in (4.78) (black and red dots ●). The black and red squares refer to a vertex from the $\mathcal{O}(p^2)$ QCD chiral Lagrangian in (4.63).

All one-loop topologies with exactly one insertion of a weak $\mathcal{O}(p^2)$ vertex are depicted in Figure 4.5. Since the diagonalization of the Lagrangian is only performed in the LO strong chiral Lagrangian in (4.63), the mixing is still present in the weak $\mathcal{O}(p^2)$ Lagrangian and in particular also reappears at NLO, which can be seen in D_{11}. In the sum of the diagrams, the unphysical rotation parameters κ_q cancel as they

should. While in principle one would expect absorptive parts from diagrams where the internal state pions can go on-shell (i.e. in D_4, D_8, D_9, D_{20}, D_{21}), this feature is entirely absent in the amplitude. The reason is that the necessary isospin transitions (e.g. $K^- \to \pi^-\pi^0$ for the case of D_8) are not allowed by $\mathcal{O}_8$. If isospin-violating corrections were considered at NLO as well, imaginary contributions would indeed appear in the amplitude.

4.9.2.3. NLO Tree-Level Amplitude

At NLO in the chiral expansion, also $\mathcal{O}(p^4)$ tree-level graphs contribute to the process, which are discussed below.

NLO QCD Tree-Level Amplitude

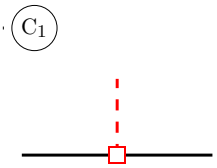

Figure 4.6.: The Feynman tree-level graph that contributes to the $K^- \to \pi^- a$ decay amplitude at NLO in the chiral expansion involving only flavor-violating ALP interactions and one insertion of the $\mathcal{O}(p^4)$ QCD Lagrangian in (4.35) (empty square $\square$).

The single $\mathcal{O}(p^4)$ QCD tree-level Feynman diagram describing the decay $K^- \to \pi^- a$ is shown in Figure 4.6, contributing ALP flavor-changing couplings to the amplitude. This diagram possesses a finite and a UV-divergent piece, and the latter needs to cancel the divergence stemming from the one-loop diagrams discussed above. Indeed, when adding up D_1, D_2 and C_1, this divergence vanishes.

NLO Weak Tree-Level Amplitude

The $\mathcal{O}(p^4)$ weak tree-level Feynman diagrams that describe the decay $K^- \to \pi^- a$ are shown in Figures 4.7, contributing ALP flavor conserving couplings to the amplitude. As for the flavor-violating part, the divergence from the one-loop weak Feynman diagrams needs to be canceled by the NLO weak tree level contributions. The situation, however, is more subtle than in the pure QCD case: In the limit where $\theta = 0$ and $\langle a_\mu \rangle = 0$, the anomalous dimension coefficients Z_i, Γ_i and Γ_i^θ, shown in Tables 4.3, 4.5 and 4.6, ensure the necessary cancellation. With non-zero ALP source, the additional anomalous coefficients, Z_i', $Z_i'^\theta$, Z_i^θ and $Z_i^{\theta\theta}$, as introduced in (4.102), need to be fixed such that the full UV-pole cancels. While the values of the Z_i' have already been obtained in Section 4.8.3 (for the explicit results, see Table 4.5), this requirement can be used to deduce values for the coefficients $Z_4^\theta = -3/4$ and $Z_4^{\theta(\theta)} = 1/2$. The remaining $Z_i^{\theta(\theta)}$ are only constrained up to the consistency relations (4.103) and (4.104), or not fixed at all by the charged kaon decay to a pion and an ALP.

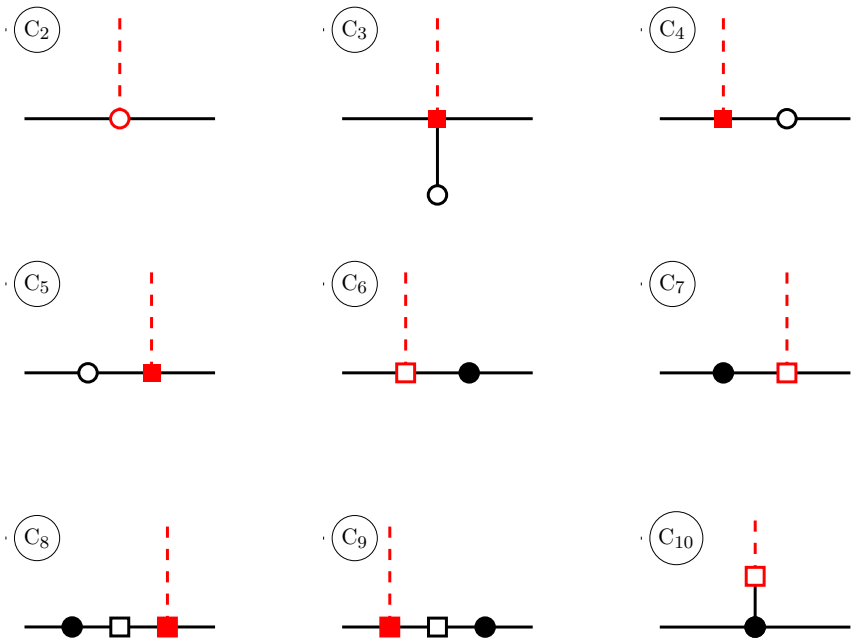

Figure 4.7.: Feynman graphs contributing to the $K^- \to \pi^- a$ decay amplitude at NLO in the chiral expansion involving only flavor-conserving ALP interactions and one insertion of the $\mathcal{O}(p^4)$ QCD Lagrangian in (4.35) (empty square $\square$) or $\mathcal{O}(p^4)$ weak Lagrangian in (4.35) (empty dot $\circ$). The black and red squares $\blacksquare$ (circle $\bullet$) refer to an insertion from the $\mathcal{O}(p^2)$ QCD (weak) chiral Lagrangian.

In the thus obtained finite NLO expression for the decay amplitude, also the μ-dependence from the loops is removed by the scale dependence of the low-energy constants. The final result then still contains the unknown LECs $N_{i,r}^{(\theta)}$. Since a phenomenological analysis of the decay process requires assigning reasonable values to these parameters, an estimate and the corresponding reasoning is presented in the next section.

4.10. Phenomenological Implications

Quantity	Value	Reference
m_{K^-}	493.7 MeV	[40]
m_{π^-}	139.6 MeV	[40]
Γ_{K^-}	5.31×10^{-14} MeV	[40]
F_{π^-}	(130.2 ± 0.8) MeV	[160]

Table 4.10.: Numerical input values for the meson masses, the kaon decay width and the pion decay constant.

This section examines the phenomenological consequences of the NLO $K^- \to \pi^- a$ decay amplitude. Concretely, the numerical sizes of the LO and NLO contributions from the various couplings are analyzed as a function of the ALP mass. The numerical results are then translated to bounds on the effective scales $\Lambda_{c_i}^{\text{eff}} \equiv f/|c_i|$. Finally, implications for bounds to neutrons and protons are deduced.
The numerical input values of m_{K^-}, m_{π^-}, Γ_{K^-} and F_{π^-} as required for the phenomenological analysis of the NLO contributions are collected in Table 4.10. The relevant renormalized strong low-energy constants $L_{i,r}$ from fits to low-energy data and lattice QCD are presented in Table 4.2 along with the corresponding uncertainties. However, no numerical analysis exists for the remaining weak LECs $N_{i,r}^{(\theta)\prime}$, nor for the $L_{i,r}^{\theta}$. In order to estimate these coefficients, it is instructive to reconsider the scale evolution of the strong LECs in Figure 4.1. While the numerical values have been obtained at $\mu = m_\rho$, it is evident that around $\mu = 1.4\,\text{GeV}$, all coefficients are roughly compatible with zero. The reason behind this behavior is that around the scale of chiral symmetry breaking, these effective Wilson coefficients are naturally free of large logarithms. It is thus reasonable to assume that the unknown coefficients exhibit similar patterns, and setting all $N_{i,r}^{(\prime\theta)}(\mu_0 = 1.4\,\text{GeV}) = 0$ appears to be a sensible choice. To assign an uncertainty to this consideration, a variation of this default scale μ_0 by a factor of $\sqrt{2}$ is taken into account and added in quadrature to the remaining LEC uncertainties in the following analysis.

4.10.1. ALP Flavor-Violating Contributions to the Amplitude

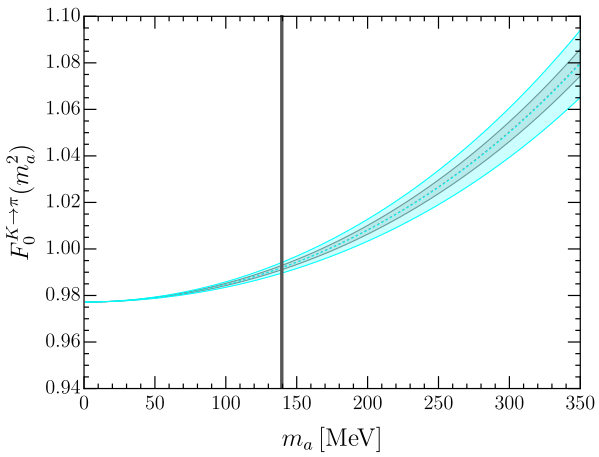

Figure 4.8.: LO + NLO contribution of the ALP flavor-violating couplings to the decay amplitude of the process $K^- \to \pi^- a$. The dashed lines show the results for the central value of the QCD low-energy constant $L_{5,r}$ from the first (second) column of Table 4.2 in gray (blue), the colored bands correspond to the 1σ uncertainties presented in the same table. The gray vertical line at $m_a \approx m_{\pi^0}$ indicates that this region is experimentally excluded.

Starting with the flavor-violating ALP couplings and employing again the parametrization in (4.106), the dimensionless decay amplitude equals the $K^- \to \pi^-$ form factor $F_0^{K\to\pi}$ at $q^2 = m_a^2$ [34]. At LO, this quantity is momentum-independent and equals 1. The sum of the LO and NLO is shown in Figure 4.8 as a function of the ALP mass m_a. There is only one strong LEC that enters the amplitude, $L_{5,r}$, and clearly no weak LEC. Taking into account the uncertainty of $L_{5,r}$, the NLO amounts to a correction of less than 10% over the entire kinematically allowed ALP mass range. It decreases the amplitude for $m_a \lesssim 170\,\text{MeV}$ and increases it for larger ALP masses. In particular, for the case of a vanishing ALP mass, the flavor-violating contribution reads

$$i\mathcal{A}^{\text{FV}}_{\text{LO+NLO}} = -(m_K^2 - m_\pi^2)\,\frac{[k_d + k_D]_{12}}{2f}\,(1_{\,\text{LO}} - 0.023_{\,\text{NLO}})\,. \tag{4.124}$$

Since in the limit $m_a = 0$ the analytical expression is independent of $L_{5,r}$, the uncertainty on the values in (4.124) is negligible.

4.10.2. ALP Flavor-Conserving Contributions to the Amplitude

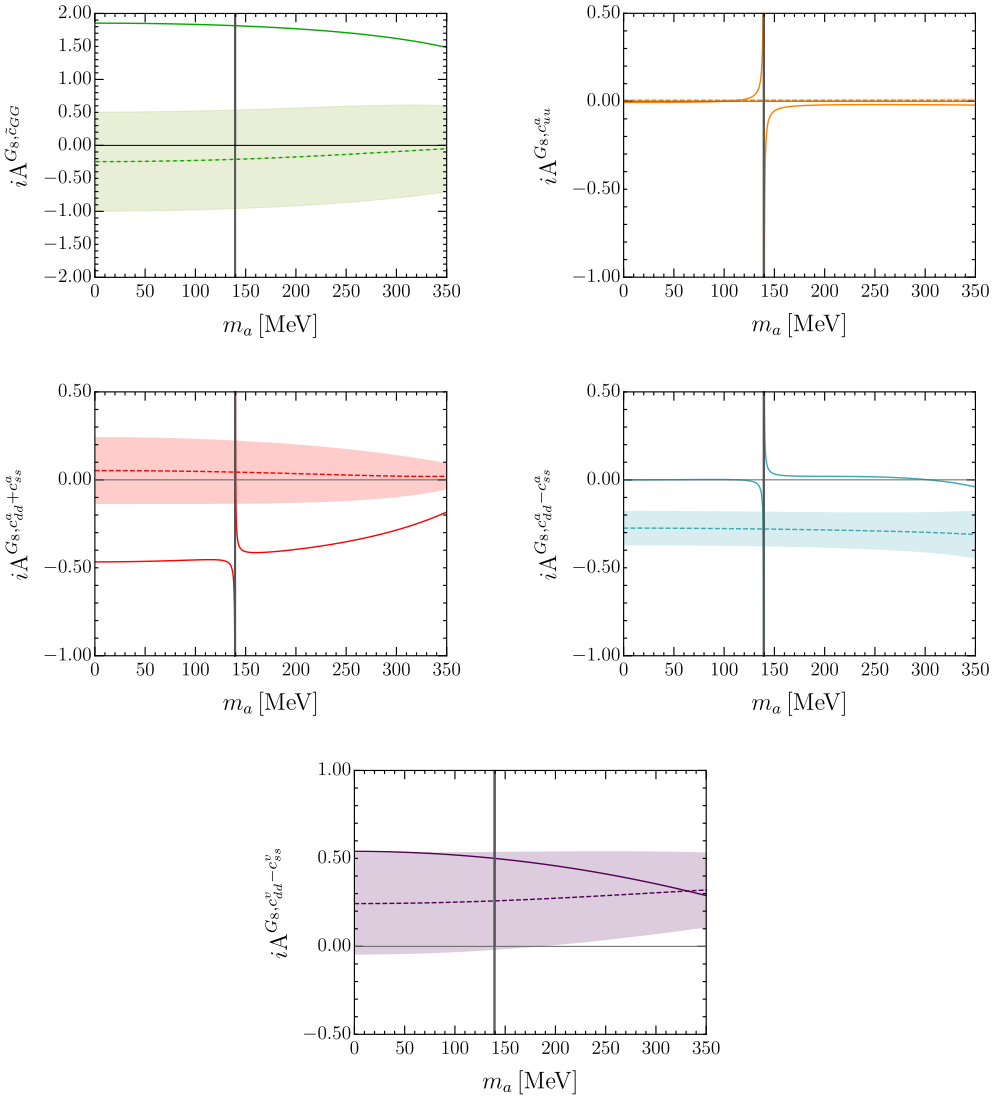

Figure 4.9.: LO (solid line) and NLO (dashed line) contributions of the G_8 ALP flavor-conserving couplings to the decay amplitude of the process $K^- \to \pi^- a$. The colored bands comprise the uncertainties from the QCD LECs, as well as from the variation of the scale μ_0, where all unknown weak LECs are set to zero.

The contributions from flavor-conserving ALP couplings proportional to G_8 are depicted in Figure 4.9, individually for the LO (solid line) and NLO (dashed line). Here, the uncertainties from the QCD low-energy constants and the scale variation around the default choice of $\mu_0 = 1.4\,\text{GeV}$ (the scale where the 18 weak LECs entering the analytical expressions are set to zero) are combined in quadrature to generate the colored uncertainty bands around the central dashed lines in the plots. In total, this results in corrections ranging from a few percent up to approximately 60% for most couplings. An exception is given by $iA^{G_8,\, c^a_{dd}-c^a_{ss}}$, since it is mostly zero at LO over

the allowed ALP mass range. The corresponding expressions for $m_a = 0$ are given by

$$\begin{aligned} i\mathcal{A}^{G_8}_{\mathrm{LO}} &= \frac{G_8 F_\pi^2 m_K^2}{2f}\Big[\left(1.88 - 0.88\,\varepsilon^{(2)}\right)\tilde{c}_{GG} - \left(0.02 - 0.44\,\varepsilon^{(2)}\right)c^a_{uu} \\ &\qquad - \left(0.48 - 0.44\,\varepsilon^{(2)}\right)(c^a_{dd} + c^a_{ss}) + 0.54\,(c^v_{dd} - c^v_{ss})\Big]\,, \\ i\mathcal{A}^{G_8}_{\mathrm{NLO}} &= \frac{G_8 F_\pi^2 m_K^2}{2f}\Big[(-0.25 \pm 0.43 \pm 0.61)\,\tilde{c}_{GG} \\ &\qquad + (5.21 \pm 1.03 \pm 6.52) \times 10^{-3}\, c^a_{uu} \\ &\qquad + (0.06 \pm 0.11 \pm 0.16)\,(c^a_{dd} + c^a_{ss}) \\ &\qquad - (0.27 \pm 0.10 \pm 0)\,(c^a_{dd} - c^a_{ss}) \\ &\qquad + (0.24 \pm 0.23 \pm 0.18)\,(c^v_{dd} - c^v_{ss})\Big]\,, \end{aligned} \tag{4.125}$$

where the first uncertainty represents the variation of μ_0 and the second one stems from the QCD LECs as given in Table 4.2. Again, the combination $c^v_{dd}+c^v_{ss}$ is absent in the expressions, as only the difference, $c^v_{dd}-c^v_{ss}$, becomes observable when considering flavor-changing neutral currents. As mentioned before, the divergence that can be seen at LO for some couplings in Figure 4.9 is an artifact of the linearization in F/f that would vanish in an all-order diagonalization. Nonetheless, the different limits for $m_a \to m^+_{\pi^0}$ and $m_a \to m^-_{\pi^0}$ are physical: in the scenario of maximal mixing, the neutral pion and the ALP become indistinguishable. Thus, it is necessary to also include the amplitude of the orthogonal state in order to obtain the physical result. Only the sum of the two expressions is continuous over the entire ALP mass range. As experiments exclude this scenario, this computation is not presented here.
Finally, the new octet operators proportional to G'_8 and G^θ_8 yield the amplitudes depicted in Figure 4.10, and the numerical evaluation for vanishing ALP mass reads

$$\begin{aligned} i\mathcal{A}^{G'_8}_{\mathrm{LO}} &= \frac{G'_8 F_\pi^2 m_K^2}{2f}\left[\left(0.85 - 0.78\,\varepsilon^{(2)}\right)(c^a_{dd} - c^a_{ss}) - \left(1 + 0.92\,\varepsilon^{(2)}\right)(c^v_{dd} - c^v_{ss})\right]\,, \\ i\mathcal{A}^{G'_8}_{\mathrm{NLO}} &= \frac{G'_8 F_\pi^2 m_K^2}{2f}\left[(-0.29 \pm 0.14)\,(c^a_{dd} - c^a_{ss}) + (0.35 \pm 0.16)\,(c^v_{dd} - c^v_{ss})\right]\,. \end{aligned} \tag{4.126}$$

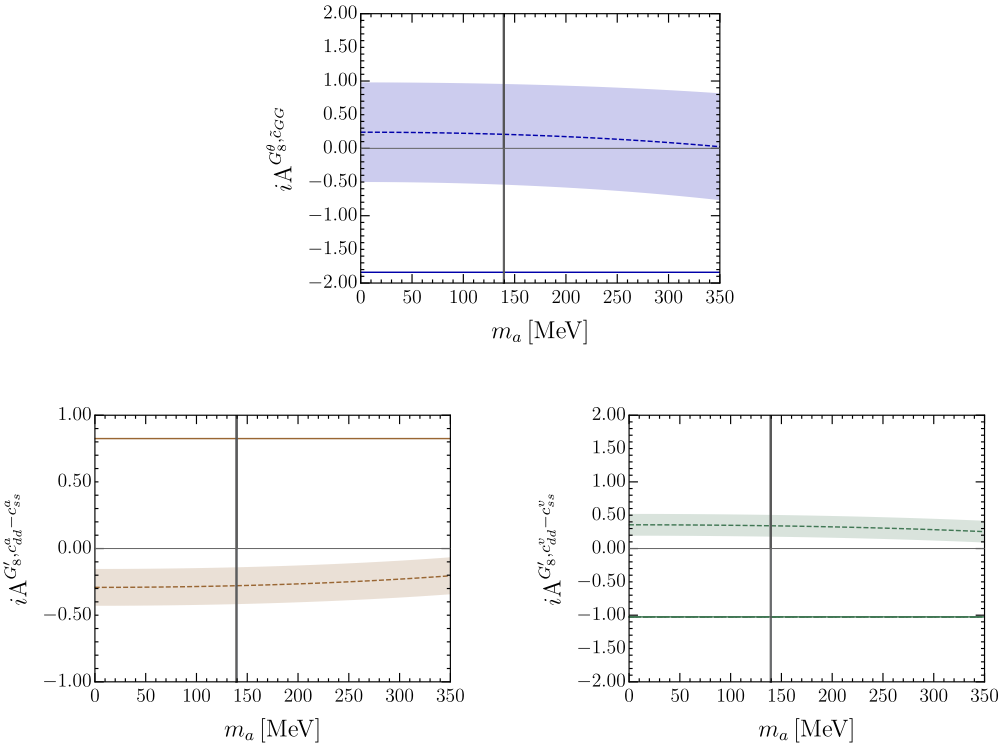

Figure 4.10.: LO (solid line) and NLO (dashed line) contributions of the G_8' and G_8^θ ALP flavor-conserving couplings to the decay amplitude of the process $K^- \to \pi^- a$. The colored bands comprise the uncertainties from the QCD LECs, as well as from the variation of the scale μ_0, where all unknown weak LECs are set to zero.

For completeness, the LO contributions from the 27-plets for $m_a = 0$ are

$$\begin{aligned} i\mathcal{A}_{\text{LO}}^{G_{27}^{1/2}} &= \frac{G_{27}^{1/2} F_\pi^2\, m_K^2}{2f} \Big[\left(3.53 - 0.79\,\varepsilon^{(2)}\right) \tilde{c}_{GG} + \left(0.08 + 0.40\,\varepsilon^{(2)}\right) c_{uu}^a \\ &\quad - \left(2.7 - 0.4\,\varepsilon^{(2)}\right) (c_{dd}^a + c_{ss}^a) + 2.31\,(c_{dd}^a - c_{ss}^a) \\ &\quad + 0.54\,(c_{dd}^v - c_{ss}^v) \Big]\,, \\ i\mathcal{A}_{\text{LO}}^{G_{27}^{3/2}} &= \frac{G_{27}^{3/2} F_\pi^2\, m_K^2}{2f} \Big[\left(0.9 + 30.2\,\varepsilon^{(2)}\right) \tilde{c}_{GG} + \left(1.4 - 15.1\,\varepsilon^{(2)}\right) c_{uu}^a \\ &\quad - \left(1.4 + 15.1\,\varepsilon^{(2)}\right) (c_{dd}^a + c_{ss}^a) - 0.46\,(c_{dd}^a - c_{ss}^a) \\ &\quad + 0.54\,(c_{dd}^v - c_{ss}^v) \Big]\,. \end{aligned} \tag{4.127}$$

4.10.3. Bounds on ALP couplings from $K^- \to \pi^- a$

The most stringent bounds on rare kaon decays such as $K^{\pm} \to \pi^{\pm} X$ are currently provided by the NA62 experiment at CERN. In the SM, such a process is given by the FCNC decay with $X = \bar{\nu}\nu$, while the process $K^{\pm} \to \pi^{\pm} a$ represents a beyond

$c_i(\mu_\chi)$	$\Lambda_{c_i}^{\text{eff}}$ [TeV]	
	$m_a = 0$	$m_a = 200\,\text{MeV}$
$[k_D + k_d]_{12}$	2.9×10^8	6.5×10^8
$\tilde{c}_{GG}{}^{(*)}$	43	84
c^a_{uu}	1.5	4.3
$c^a_{dd} + c^a_{ss}$	15	19
$c^a_{dd} - c^a_{ss}{}^{(**)}$	8	8
$c^v_{dd} - c^v_{ss}{}^{(**)}$	23	47

Table 4.11.: Lower bounds on the effective scales $\Lambda_{c_i}^{\text{eff}} \equiv f/|c_i|$ at μ_χ with 90% CL for one non-zero ALP coupling at a time as obtained from the upper limit on the branching ratio as given by NA62 in [178]. In these results, $g_8^\theta = g_8' = 0$ was used. The $^{(*)}$ highlights that the result for the coupling depends on the value of g_8^θ, while $^{(**)}$ refers to a dependence on g_8'.

the Standard Model (BSM) example. In order to access information on the branching ratios, a proton beam from the Super Proton Synchrotron (SPS) is used that hits a fixed beryllium target. Among the cascade of secondary particles, approximately 6% are positively charged kaons. They get extracted by a series of dipole magnets and collimation systems, and their subsequent decay is studied. For X being a light pseudoscalar particle, this yields the bounds[10] $\mathcal{B}(K^+ \to \pi^+ X) < (3\text{–}6) \times 10^{-11}$ at 90% CL for $m_X \in [0, 110]\,\text{MeV}$, and $\mathcal{B}(K^+ \to \pi^+ X) < 1 \times 10^{-11}$ (90% CL) for $m_X \in [160, 260]$ [178].
Using the decay width of the kaon in Table 4.10, along with these upper bounds on the branching ratios, lower limits on the effective scales $\Lambda_{c_i}^{\text{eff}} \equiv f/|c_i|$ can be obtained for one non-zero ALP coupling at a time. When working with the amplitudes obtained in Section 4.9, where implicitly $c_i \equiv c_i(\mu_\chi)$, the thus obtained results refer to the couplings at this scale μ_χ. Setting the unknown coefficients g_8' and g_8^θ to zero, the corresponding results for $m_a = 0$ and $m_a = 200\,\text{GeV}$ are listed in Table 4.11. Clearly, $g_8' = g_8^\theta = 0$ is a choice that impacts the concrete values of the bounds. For instance, $\Lambda^{\text{eff}}_{\tilde{c}_{GG}} \gtrsim 10$ TeV for $g_8^\theta = 1$ and $m_a = 0$.

4.10.4. Decay amplitudes in terms of UV couplings

In addition to constraints on the couplings at μ_χ, RG evolution equations obtained in [60, 61] can be used to express the amplitudes in terms of the couplings at the scale Λ of global $U(1)_{\text{PQ}}$ symmetry breaking. As flavor-violating couplings are strongly constrained by experiment (see e.g. [34]), it is a reasonable choice to consider an ALP that has only flavor-conserving, universal couplings at Λ. Working in the basis in which the shift-symmetry is manifest via the derivative interactions to fermions, i.e. the Lagrangian in 1.34, this assumption then translates to

$$\tilde{\boldsymbol{c}}_F(\Lambda) = \tilde{c}_F(\Lambda)\,\mathbb{1} \quad \text{for} \quad F = u,\, d,\, Q,\, e,\, L\,. \tag{4.128}$$

[10] These limits correspond to the most recent bounds at the time when this analysis was performed, while the measured branching ratio in [151] and the analysis in [179] were published afterwards.

$c_i(\Lambda)$	$\Lambda_{c_i}^{\text{eff}}$ [TeV] $m_a = 0$	$m_a = 200\,\text{MeV}$
$\tilde{c}_{GG}(\Lambda)$	49	97
$\tilde{c}_{WW}(\Lambda)$	2.6	6
$\tilde{c}_{BB}(\Lambda)$	0.02	0.04
$\tilde{c}_u(\Lambda)$	1.9×10^3	4.2×10^3
$\tilde{c}_d(\Lambda)$	51	78

Table 4.12.: 90% CL lower bounds on the effective scales $\Lambda_{c_i}^{\text{eff}} \equiv f/|c_i|$ of the ALP couplings c_i at the high scale Λ in the flavor-universal ALP model for the cases $m_a = 0$ and $m_a = 200\,\text{MeV}$. The bounds are derived by setting $\Lambda = 4\pi f$ with $f = 1\,\text{TeV}$, and using the 90% CL upper bound on the $K^+ \to \pi^+ X$ branching ratio provided by NA62 [178]. The bounds shown here are obtained by setting $g_8^\theta = 0$.

Although this ensures flavor symmetry at Λ, flavor off-diagonal entries are nonetheless generated via RG flow, but they remain CKM suppressed, in detail, for the $s \to d$ transition, via an insertion of $V_{td}^\star V_{ts} \approx -(3.0 + 1.3\,i) \times 10^{-4}$ [40]. In particular, for the choice $f = 1\,\text{TeV}$, this yields at the top-quark scale [34]

$$\begin{aligned}[k_D(m_t)]_{ij}^{\text{univ}} \simeq\; & 10^{-5}\, V_{ti}^* V_{tj} \big[-6.1\, \tilde{c}_{GG}(\Lambda) - 2.8 \tilde{c}_{WW}(\Lambda) \\ & - 0.02\, \tilde{c}_{BB}(\Lambda) + 1.9 \times 10^3\, \tilde{c}_u(\Lambda) \big]\,, \\ [k_d(m_t)]_{ij}^{\text{univ}} = & \,0\,. \end{aligned} \tag{4.129}$$

Furthermore, since k_D is approximately scale invariant below m_t, $[k_D(m_t)]_{ij} = [k_D(\mu_\chi)]_{ij}$. The remaining relations, that have also been obtained in [34], are given by

$$\begin{aligned}[c_{uu}^a(\mu_\chi)]^{\text{univ}} \simeq & \, 0.90\, \tilde{c}_u(\Lambda) + 0.008\, \tilde{c}_d(\Lambda) - 0.042\, \tilde{c}_{GG}(\Lambda) \\ & - 10^{-4} \big[2.1\, \tilde{c}_{WW}(\Lambda) + 0.34\, \tilde{c}_{BB}(\Lambda) \big]\,, \\ [c_{dd,ss}^a(\mu_\chi)]^{\text{univ}} \simeq & \, 0.13\, \tilde{c}_u(\Lambda) + 1.00\, \tilde{c}_d(\Lambda) - 0.042\, \tilde{c}_{GG}(\Lambda) \\ & - 10^{-4} \big[2.3\, \tilde{c}_{WW}(\Lambda) + 0.10\, \tilde{c}_{BB}(\Lambda) \big]\,. \\ [c_{dd}^v(\mu_\chi)]^{\text{univ}} = & \, [c_{ss}^v(\mu_\chi)]^{\text{univ}}\,. \end{aligned} \tag{4.130}$$

The last relation above removes the vector couplings from the amplitude, since they appear only in the combination $(c_{dd}^v - c_{ss}^v)$, which in particular also removes the dependences on g_8'. The full, numerical expression of the NLO amplitude for $f = 1\,\text{TeV}$ in the limit where $g_8^\theta = 0$ then becomes

$$\begin{aligned} i\mathcal{A}^{\text{univ}} = -10^{-11}\,\text{GeV} \left[\frac{1\,\text{TeV}}{f}\right] \Big[& (2.4 \pm 1.0 + 0.1\,i)\, \tilde{c}_{GG}(\Lambda) \\ & + (9.37 \pm 0.02 + 3.97\,i) \times 10^{-2}\, \tilde{c}_{WW}(\Lambda) \\ & + (0.57 \pm 0.02 + 0.26\,i) \times 10^{-3}\, \tilde{c}_{BB}(\Lambda) \\ & - (68 \pm 1 + 28\,i)\, \tilde{c}_u(\Lambda) - (2.5 \pm 1.0)\, \tilde{c}_d(\Lambda) \Big]\,. \end{aligned} \tag{4.131}$$

The errors in the expression again combine the uncertainties from the scale variation of μ_0 and the uncertainties on the strong LECs. As before, this amplitude in terms of the UV scale coefficients can now be used to obtain lower bounds on the effective scales $\Lambda_{c_i}^{\text{eff}} \equiv f/|c_i|$ of the ALP couplings. The results for turning on one such coupling at a time are shown in Table 4.12 for $f = 1\,\text{TeV}$. The flavor-universal and flavor-conserving partial amplitudes thereby contribute as follows:

- The bounds on the effective scales of the couplings $\tilde{c}_u(\Lambda)$, $\tilde{c}_{WW}(\Lambda)$ and $\tilde{c}_{BB}(\Lambda)$ are dominated by their contributions to the flavor-violating coupling $k_D(\mu_\chi)$ via RG evolution (see (4.129)). The fact that $\tilde{c}_u(\Lambda)$ appears with an additional factor of 10^3 reflects itself in a bound that is of three orders of magnitude stronger than the one on the effective scale of $\tilde{c}_{WW}(\Lambda)$ and five orders of magnitude stronger than the one on the effective scale of $\tilde{c}_{BB}(\Lambda)$, which only appears at a two-loop order in (4.129).

- The bounds on the effective scales of the couplings $\tilde{c}_{GG}(\Lambda)$ and $\tilde{c}_d(\Lambda)$ are instead dominated by the flavor-conserving part of the decay amplitude. Due to the large uncertainties provided by the strong and weak LECs, the bounds obtained from the NLO amplitude are weaker than the ones obtained at LO. For instance, the LO amplitude, where no weak LECs enter, would, for $m_a = 0$, result in $\Lambda_{\tilde{c}_{GG}}^{\text{eff,LO}} \gtrsim 73\,\text{TeV}$ and $\Lambda_{\tilde{c}_d}^{\text{eff,LO}} \gtrsim 76\,\text{TeV}$ instead of $\Lambda_{\tilde{c}_{GG}}^{\text{eff,NLO}} \gtrsim 49\,\text{TeV}$ and $\Lambda_{\tilde{c}_d}^{\text{eff,NLO}} \gtrsim 51\,\text{TeV}$.

Clearly, the concrete choice of the ALP decay constant influences the bounds. For f between 1 TeV and 1 PeV, these dependences are shown in Figure 4.11 for $m_a = 0$ and $m_a = 200\,\text{MeV}$. While most bounds on the effective scales only vary weakly when increasing the scale of global $U(1)_{\text{PQ}}$ symmetry breaking, they generally become stronger for larger values of f. This is a result of the longer scale evolution down to μ_χ, which yields large logarithms and therefore strengthens the bounds on the $\Lambda_{c_i}^{\text{eff}}$.

All in all, the bounds obtained from $K^\pm \to \pi^\pm a$ pose the strongest constraints on the ALP–SM couplings for m_a smaller or approximately equal to 350 MeV. In particular, the effective scale of flavor off-diagonal couplings mediating a $s \to d$ quark transition needs to exceed $10^9\,\text{GeV}$, yielding a lower value for the decay constant of $f \gtrsim 10^{11}\,\text{GeV}$, which contradicts (model-dependent) cosmological bounds [180].

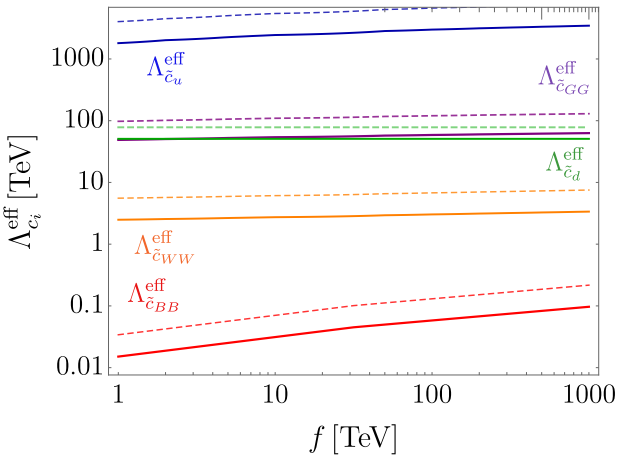

Figure 4.11.: Lower bounds on the effective scales $\Lambda^{\rm eff}_{c_i} \equiv f/|c_i|$ as a function of the ALP decay constant f for $g_8^\theta = 0$ in a flavor-universal scenario. The solid (dashed) line corresponds to $m_a = 0$ ($m_a = 200\,\text{MeV}$).

4.10.5. Bounds on ALP-Nucleon Couplings

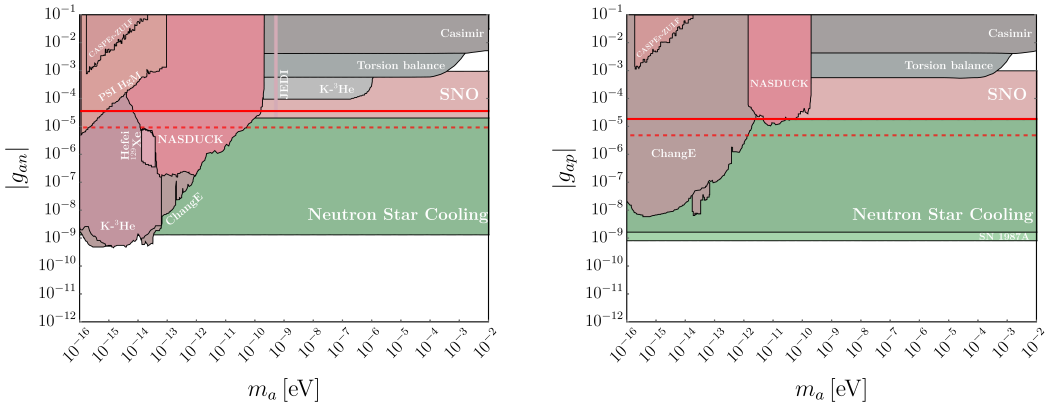

Figure 4.12.: Excluded regions of the ALP-neutron (left) and ALP-proton (right) couplings from various experiments (adapted from [181]). The red solid lines correspond to the bounds obtained from the analysis of the decay $K^{\pm} \to \pi^{\pm} a$.
The red dashed lines indicate a potential exclusion limit, assuming that both the theoretical uncertainty and the experimental bound can be improved by a factor of 3.

By comparison with the effective Lagrangian describing the interaction of ALPs with protons and neutrons, the bounds obtained in the previous section can also be translated to bounds on the ALP-nucleon couplings. Denoting the neutron and the proton by ψ_n and ψ_p with masses m_n and m_p, respectively, the Lagrangian can be written as [181]

$$\mathcal{L}_{aN} = \frac{g_{an}}{2m_n} \left(\partial_\mu a\right) \bar{\psi}_n \gamma^\mu \gamma_5 \psi_n + \frac{g_{ap}}{2m_p} \left(\partial_\mu a\right) \bar{\psi}_p \gamma^\mu \gamma_5 \psi_p \,. \tag{4.132}$$

It is possible to decompose the ALP-nucleon couplings in terms of the ALP-fermion and ALP-gluon couplings as [34]

$$g_{an} = \frac{m_n}{2}\left(g_0\, c^+ - g_A\, \frac{m_\pi^2}{m_\pi^2 - m_a^2}\, c^-\right), \quad g_{ap} \quad = \frac{m_p}{2}\left(g_0\, c^+ + g_A\, \frac{m_\pi^2}{m_\pi^2 - m_a^2}\, c^-\right), \tag{4.133}$$

where

$$c^+ = \left[\frac{c_{uu}^a}{f} + \frac{c_{dd}^a}{f} + 2\,\frac{c_{GG}}{f}\right] \quad \text{and} \quad c^- = \left[\frac{c_{uu}^a}{f} - \frac{c_{dd}^a}{f} + 2\frac{c_{GG}}{f}\,\frac{m_u - m_d}{m_u + m_d}\right], \tag{4.134}$$

with dimensionless constants $g_0 = 0.440(44)$ and $g_A = 1.2754(13)$ [182]. When employing the limits on the couplings c_{GG} (instead of $\tilde{c}_{GG}$) and c_{qq}^a obtained from the analysis of the charged kaon decay[11] and avoiding assumptions on the underlying structure of the couplings at μ_χ, however, no competitive limits on g_{an} and g_{ap} can be found. The situation changes when assuming the scenario of flavor-universal couplings at $\Lambda = 4\pi\,\text{TeV}$, although the bound on $\Lambda_{\tilde{c}_d}^{\text{eff}}$ is relaxed from 51 TeV to 22 TeV when working with c_{GG} instead of $\tilde{c}_{GG}$, while $\Lambda_{\tilde{c}_u}^{\text{eff}}$ does not change significantly. The NLO bounds on the ALP-nucleon couplings are then approximately

$$g_{an} < \frac{m_n}{2\Lambda_{\tilde{c}_d}^{\text{eff}}}\,|g_0 + g_A| \approx 3.7 \times 10^{-5}\,, \quad g_{ap} < \frac{m_p}{2\Lambda_{\tilde{c}_d}^{\text{eff}}}\,|g_0 - g_A| \approx 1.8 \times 10^{-5}\,. \tag{4.135}$$

Figure 4.12 compares these limits with the exclusion regions from various experiments for illustration. Additionally, hypothetical results are shown for the scenario where both the theoretical uncertainty and the experimental bound are improved by a factor of 3. Importantly, the bounds obtained from the charged kaon decay represent the sole particle-physics probes of the ALP-nucleon couplings in the mass range shown in the figure. While for ALP masses smaller than $10^{-10}\,\text{eV}$, a variety of experiments pose stronger bounds on g_{an} and g_{ap}, the results from the analysis of $K^\pm \to \pi^\pm a$ can compete with most bounds above this scale. SN 1987A supernova and neutron star cooling bounds are several orders of magnitude stronger than the limits in (4.135), but they have the disadvantage of being highly model dependent. More specifically, several assumptions, including those regarding the core composition, are incorporated into the derivations, but have yet to be validated.

[11] As $\tilde{c}_{GG}$ and c_{qq}^a are not independent parameters, these bounds do not correspond to those presented in Table 4.11.

4.11. Summary and Conclusions

In this chapter, ALP effects at and below $\mu_\chi \sim 1.6$ GeV were investigated. At this scale, quarks are confined to color-neutral bound states, such that the fundamental degrees of freedom are the pseudoscalar mesons. To analyze ALP interactions in this regime, a consistent incorporation of the ALP into chiral perturbation theory was presented, up to order $\mathcal{O}(p^4)$ in the chiral expansion. This extended effective field theory framework allowed for the study of the rare kaon decays $K^{\pm} \to \pi^{\pm} a$ at next-to-leading order. These flavor-changing processes are especially powerful for constraining ALP–SM couplings due to the extremely suppressed branching ratio $\mathcal{B}(K^{\pm} \to \pi^{\pm} X)$. As a result, the analysis of these decays provide the strongest particle-physics bounds on ALP couplings for ALP masses $m_a \lesssim 350$ MeV.
More specifically, the analysis presented here expanded on the existing leading-order calculation in several key aspects:

- Operator basis extension at $\mathcal{O}(p^2)$: The presence of the ALP necessitated an enlargement of the chiral operator basis already at leading order. Notably, the so-called *weak mass term*, which is redundant in the pure SM case, had to be accounted for, which is an observation that had not been made in the literature before. Additionally, an operator explicitly involving an ALP source emerged in the $\mathcal{O}(p^2)$ weak chiral basis.

- Operator basis extension at $\mathcal{O}(p^4)$: At $\mathcal{O}(p^4)$, the situation became even more intricate: the strong chiral Lagrangian at NLO had to be extended by three operators, while nine new operators needed to be added to the weak chiral Lagrangian when the ALP is present. This yielded a complete basis as required for the computation of the full NLO amplitude for $K^- \to \pi^- a$.

- Tree-level and loop contributions: The full NLO amplitude for the decay $K^- \to \pi^- a$ was presented in this chapter. At $\mathcal{O}(p^2)$, the literature result was extended by isospin breaking corrections of first order in $(m_d - m_u)$, while at NLO, the analysis included the 89 possible one-loop Feynman diagrams and the 11 NLO tree-level graphs.

- Numerical results and uncertainties: It was shown that the NLO correction proportional to ALP flavor-violating couplings ranges between roughly -3% and $+8\%$, depending on the value of m_a, and the only source of uncertainty is the low-energy constant $L_{5,r}$. The contributions from the part of the NLO amplitude in which the flavor change results from the SM weak interaction involved the two unknown couplings g_8' and g_8^θ, as well as 15 independent combinations of weak low-energy constants, which provide a significant source of uncertainty. In order to estimate the size of the weak NLO corrections, the unknown LECs were set to zero at the scale $\mu_0 \sim \mu_\chi$ and an uncertainty to these values was assigned by varying μ_0 and employing the corresponding RG equations. With this setup, it was shown that the contributions of the amplitude proportional to g_8 and the two unknown couplings g_8' and g_8^θ ranges between a few percent up to $\pm 60\%$, with an exception given by $i\mathrm{A}^{G_8,\,(c^a_{dd}-c^a_{ss})}$ for which the LO is almost zero for the entire allowed ALP mass range.

- Bounds on effective scales and ALP-nucleon interactions: The derived results were used to deduce bounds on the effective scales of the ALP–SM couplings, $\Lambda_{c_i}^{\text{eff}} \equiv f/|c_i|$, for $m_a = 0$ and $m_a = 200$ MeV, both at the scale μ_χ, and, by applying the ALP RG equations, also at the symmetry breaking scale Λ. While it was shown that the concrete choice of Λ has little impact on the bounds, the fact that the two coefficients g_8' and g_8^θ are unknown significantly limits the conclusiveness of the results. While the NLO results slightly weaken the bounds compared to the LO one, they nevertheless remain the strongest limits on ALP couplings in the kinematically allowed mass range. Finally, by comparison with the effective Lagrangian parametrizing the ALP-nucleon interactions, bounds on the respective couplings were obtained. Remarkably, these results represent not only the sole particle-physics probes of these parameters, but are even competitive with non-accelerator and astrophysical limits.

To conclude, this chapter presented the first rigorous chiral effective field theory framework for studying ALP-meson interactions, which was applied to the flavor-violating decays $K^{\pm} \to \pi^{\pm} a$. While this allowed for constraining ALP-meson interactions with a yet unprecedented precision, it remains to be stressed that a better determination of the QCD low-energy constants, as well as of the many completely unknown additional low-energy constants is of great importance for obtaining robust results.

4.13. Appendix

4.13.A. $\mathcal{A}^{\mathrm{FC}}$ at NLO

In the following, the contributions $A^{G,c_{\mathrm{ALP}}}$ entering the $\mathcal{A}^{\mathrm{FC}}$ term in (4.106) at NLO are collected. The low-energy constants $\hat{L}_{i,r}$, $\hat{L}^{\theta}_{i,r}$, $\hat{N}'_{i,r}$, and $\hat{N}^{\theta\prime}_{i,r}$ appearing in this appendix are understood to be evaluated at the scale μ.

4.13.A.1. G_8 contribution

For the G_8 contribution proportional to $\tilde{c}_{GG}$, one finds

$$
\begin{aligned}
iA^{G_8,\tilde{c}_{GG}}_{\mathrm{NLO}} = \frac{m^2_{K^-}}{8\pi^2 F_\pi^2}\Bigg\{ & \ln\frac{\mu}{m_K} g^{G_8,\tilde{c}_{GG}}(x,y) + f_0^{G_8,\tilde{c}_{GG}}(x,y) + \sum_{i=1}^{7} s_i(x,y) f_i^{G_8,\tilde{c}_{GG}}(x,y) \\
& - \frac{4(1-y)(1-x)}{(4-y-3x)^2}\Bigg[\hat{L}_{5,r}\left(4+9y-4y^2-x-5xy-3x^2\right) \\
& + 4\hat{L}_{4,r}(2+y)(4-y-3x) - \hat{L}_{7,r}\frac{6y(4-y^2)-4x(2+11y-4y^2)+6x^2(2+y)}{1-x} \\
& - 2\hat{L}_{8,r}\frac{1-y}{1-x}\left(y(2+y)-2x(1+2y)+3x^2\right)\Bigg] \\
& + \frac{2(1-y)}{(4-y-3x)}\Bigg[x(2+y-3x)(\hat{L}^{\theta}_{1,r}-\hat{L}^{\theta}_{2,r}) \\
& + 4\left(\hat{N}'_{5,r}+2\hat{N}'_{8,r}+\hat{N}'_{9,r}-\hat{N}^{\theta\prime}_{1,r}+\hat{N}^{\theta\prime}_{2,r}-2\hat{N}^{\theta\prime}_{3,r}-2\hat{N}^{\theta\prime}_{4,r}\right) \\
& + y\Big(6\hat{N}'_{5,r}+6\hat{N}'_{6,r}+4\hat{N}'_{8,r}-8\hat{N}'_{10,r}-12\hat{N}'_{12,r}-12\hat{N}'_{13,r}-3\hat{N}^{\theta\prime}_{1,r}+3N^{\theta\prime}_{2,r} \\
& \qquad -6\hat{N}^{\theta\prime}_{3,r}-2\hat{N}^{\theta\prime}_{4,r}\Big) \\
& - y^2\left(2\hat{N}'_{5,r}+3\hat{N}'_{6,r}-4\hat{N}'_{10,r}-4\,\hat{N}'_{12,r}-6\hat{N}'_{13,r}-\hat{N}^{\theta\prime}_{1,r}+N^{\theta\prime}_{2,r}-2N^{\theta\prime}_{3,r}-\hat{N}^{\theta\prime}_{4,r}\right) \\
& - x\Big(2\hat{N}'_{5,r}+2\hat{N}'_{6,r}+8\hat{N}'_{8,r}+4\hat{N}'_{9,r}-4\hat{N}'_{12,r}-4\hat{N}'_{13,r}+\hat{N}^{\theta\prime}_{1,r}+7N^{\theta\prime}_{2,r}-14\hat{N}^{\theta\prime}_{3,r} \\
& \qquad -6\hat{N}^{\theta\prime}_{4,r}-4\hat{N}^{\theta\prime}_{5,r}\Big) \\
& - xy\Big(4\hat{N}'_{5,r}+\hat{N}'_{6,r}+4\hat{N}'_{8,r}-4N'_{10,r}-4\hat{N}'_{12,r}-2\hat{N}'_{13,r}-4\hat{N}^{\theta\prime}_{1,r}+2\hat{N}^{\theta\prime}_{2,r} \\
& \qquad -4\hat{N}^{\theta\prime}_{3,r}-3\hat{N}^{\theta\prime}_{4,r}+\hat{N}^{\theta\prime}_{5,r}\Big) \\
& \qquad - x^2\left(2\,\hat{N}'_{5,r}-3\hat{N}^{\theta\prime}_{1,r}-3\hat{N}^{\theta\prime}_{2,r}+6\hat{N}^{\theta\prime}_{3,r}+3\hat{N}^{\theta\prime}_{5,r}\right)\Bigg]\Bigg\},
\end{aligned}
\tag{A.1}
$$

where the functions $g^{G_8,\tilde{c}_{GG}}(x,y)$ and $f^{G_8,\tilde{c}_{GG}}_{0,1,\ldots,7}(x,y)$ are given by

$$
\begin{aligned}
g^{G_8,\tilde{c}_{GG}}(x,y) &= -\frac{4\,(1-y)}{3(4-y-3x)^2}\left[2(24+36y-10y^2+y^3)\right.\\
&\quad \left.-x(108+139y-16y^2)+3x^2(29+23y)-27x^3\right]\,,\\
f_0^{G_8,\tilde{c}_{GG}}(x,y) &= -\frac{2(1-y)}{3xy(4-y-3x)}\left[5y(1-y)^2+x\left(2-7y+16y^2-5y^3\right)\right.\\
&\quad \left.-x^2\left(2+5y+8y^2\right)+9x^3y\right]\,,\\
f_1^{G_8,\tilde{c}_{GG}}(x,y) &= -\frac{(1-y)(1-x)}{3x\,(4-y-3x)}\left(2(1+y)-3x+\frac{(1-y)^2}{x}\right)\,,\\
f_2^{G_8,\tilde{c}_{GG}}(x,y) &= -\frac{4\,y(1-y)(2-x-y)}{3\,(4-y-3x)}\,,\\
f_3^{G_8,\tilde{c}_{GG}}(x,y) &= -\frac{1}{18x^2y^2(4-y-3x)^2}\left[-y^2(4-y)(1-y)^4\right.\\
&\quad +xy^2(1-y)^2\left(83-54y+14y^2-y^3\right)\\
&\quad -x^2\left(4-93y+255y^2-432y^3-169y^4+333y^5-130y^6+16y^7\right)\\
&\quad +x^3\left(7-190y+403y^2-747y^3-107y^4+266y^5-64y^6\right)\\
&\quad \left.-3x^4\left(1-30\,y+25y^2-44y^3-40y^4+16y^5\right)+27x^5y^2(1-y)\right]\,,\\
f_4^{G_8,\tilde{c}_{GG}}(x,y) &= \frac{1}{18x^2y^2(4-y-3x)^2}\left[-27y^2(4-y)(1-y)^4\right.\\
&\quad +9xy^2(1-y)^2\left(25-42y+26\,y^2-3y^3\right)\\
&\quad -x^2\left(36-261\,y+423\,y^2-1534y^3+1283y^4-153\,y^5-26y^6+16y^7\right)\\
&\quad +x^3\left(63-414y+135y^2-1625y^3+1323y^4+150y^5-64y^6\right)\\
&\quad \left.-3x^4\left(9-54y-87y^2-128y^3+172y^4+16y^5\right)-135x^5y^2(1-y)\right]\,,\\
f_5^{G_8,\tilde{c}_{GG}}(x,y) &= -\frac{1-y}{3y^2(4-y-3\,x)}\left(1-7y^2+4y^3-x(1-7y+4y^2)\right)\,,\\
f_6^{G_8,\tilde{c}_{GG}}(x,y) &= -\frac{1-y}{y(4-y-3x)}\left(\frac{1}{y}-4+y+x\left(3-\frac{1}{y}\right)\right)\,,\\
f_7^{G_8,\tilde{c}_{GG}}(x,y) &= -\frac{(1-x)(1-y)}{x\,(4-y-3x)}\left(\frac{3(1-y)^2}{x}+2(1+y)-5x\right)\,.
\end{aligned}
\tag{A.2}
$$

The contribution proportional to c_{uu}^a are

$$
\begin{aligned}
iA_{\text{NLO}}^{G_8,c_{uu}^a} = \frac{m_{K^-}^2}{8\pi^2 F_\pi^2}\Bigg\{ & \ln\frac{\mu}{m_K} g^{G_8,c_{uu}^a}(x,y) + f_0^{G_8,c_{uu}^a}(x,y) + \sum_{i=1}^{7} s_i(x,y) f_i^{G_8,c_{uu}^a}(x,y) \\
& + \frac{y(1-y)}{2(4-y-3x)^2}\Bigg[4\hat{L}_{4,r}(2+y)(4-y-3x) \\
& - \hat{L}_{5,r}\left(4-7y+3y^2-x(17-5y)+12x^2\right) - 24\hat{L}_{7,r}\left(4-y^2-2x(4-y)+3x^2\right) \\
& \qquad - 8\hat{L}_{8,r}\left(2-y-y^2-3x(1-y)\right)\Bigg] \\
& + \frac{y(1-y)}{4-y-3x}\Bigg[-3\hat{N}'_{5,r} - 2\hat{N}'_{6,r} - 2\hat{N}'_{8,r} + 3\hat{N}'_{9,r} + 8\hat{N}'_{10,r} + 12\hat{N}'_{12,r} + 12\hat{N}'_{13,r} \\
& \qquad + y\left(\hat{N}'_{5,r} + 2\hat{N}'_{6,r} - \hat{N}'_{8,r} - \hat{N}'_{9,r} - 4\hat{N}'_{10,r} - 4\hat{N}'_{12,r} - 6\hat{N}'_{13,r}\right) \\
& \qquad + x\left(\hat{N}'_{5,r} - 3\hat{N}'_{9,r} - 6\hat{N}'_{10,r} - 6\hat{N}'_{12,r} - 6\hat{N}'_{13,r}\right)\Bigg]\Bigg\},
\end{aligned}
\tag{A.3}
$$

with

$$
\begin{aligned}
g^{G_8,c_{uu}^a}(x,y) &= \frac{y\,(1-y)}{6(4-3x-y)^2}\left[4y(25-4y)+3x(16-35y)-27x^2\right], \\
f_0^{G_8,c_{uu}^a}(x,y) &= \frac{(1-y)\left((1-y)^2(8+3y)-2\,x\left(10-27y+5\,y^2\right)+x^2(12-45\,y)\right)}{12\,x(4-3\,x-y)}, \\
f_1^{G_8,c_{uu}^a}(x,y) &= -\frac{y\,(1-y)(1-x)}{6\,x^2(x-y)(4-3\,x-y)}\left((1-y)^2+2\,x(1+y)-3\,x^2\right), \\
f_2^{G_8,c_{uu}^a}(x,y) &= \frac{y(1-y)(4-3\,x-2\,y)}{3(4-3\,x-y)}, \\
f_3^{G_8,c_{uu}^a}(x,y) &= -\frac{1}{72x^2\,y(4-y-3x)^2}\left[8y-34\,y^2+56y^3-44\,y^4+16y^5-2\,y^6\right. \\
&\quad + x\left(8-200y+496y^2-454\,y^3+182\,y^4-34\,y^5+2\,y^6\right) \\
&\quad - x^2\left(26-589y+1256y^2+147y^3-635y^4+259y^5-32\,y^6\right) \\
&\quad + x^3\left(27-633y+1464\,y^2+393y^3-639y^4+144\,y^5\right) \\
&\quad \left.-x^4\left(9-225y+360y^2+324\,y^3-144\,y^4\right)\right], \\
f_4^{G_8,c_{uu}^a}(x,y) &= \frac{1}{72x^2\,y(4-y-3x)^2}\left[72\,y-270y^2+351y^3-144\,y^4-54\,y^5+54\,y^6\right. \\
&\quad - 9y^7 + x\left(72-360y+873y^2-1125y^3+711y^4-171y^5\right) \\
&\quad - x^2\left(234-837y+1259y^2+449y^3-864\,y^4+223y^5-32\,y^6\right) \\
&\quad + x^3\left(243-783y+777y^2+1902y^3-1203y^4+144\,y^5\right) \\
&\quad \left.-x^4\left(81-243y+153y^2+801y^3-144y^4\right)\right],
\end{aligned}
$$

$$
\begin{aligned}
f_5^{G_8,c^a_{uu}}(x,y) &= \frac{(1-y)\left(2+3y+5y^2-6y^3-x\left(5+8y-12y^2\right)+x^2(3-6y)\right)}{12y\,(4-3x-y)(x-y)}\,,\\
f_6^{G_8,c^a_{uu}}(x,y) &= \frac{(1-y)\left(2+3y-y^2-x(5+2y)+3x^2\right)}{4y\,(4-3x-y)(x-y)}\,,\\
f_7^{G_8,c^a_{uu}}(x,y) &= -\frac{y(1-y)\left(2-3y+y^3+x\left(1+10y-3y^2\right)-5x^2(2+y)+7x^3\right)}{4\,x^2(x-y)(4-3x-y)}\,.
\end{aligned}
\tag{A.4}
$$

The contribution proportional to $(c^a_{dd}+c^a_{ss})$ is given by

$$
\begin{aligned}
iA_{\rm NLO}^{G_8,c^a_{dd}+c^a_{ss}} = \frac{m_{K^-}^2}{8\pi^2F_\pi^2}\Bigg\{ & \ln\frac{\mu}{m_K}g^{G_8,c^a_{dd}+c^a_{ss}}(x,y)+f_0^{G_8,c^a_{dd}+c^a_{ss}}(x,y)\\
&+\sum_{i=1}^{7}s_i(x,y)f_i^{G_8,c^a_{dd}+c^a_{ss}}(x,y)\\
&+\frac{(1-y)}{4(4-3\,x-y)^2}\Big[4\,\hat L_{4,r}(2+y)\left(16-3\,x(12-y)+18x^2-y^2\right)\\
&+\hat L_{5,r}\left(16+y\,(32-9y-3y^2)-x(44+61y-21y^2)+6x^2(5+3\,y)\right)\\
&-48\hat L_{7,r}\left(3\,x^2-x\left(2+7y-3y^2\right)+y\left(4-y^2\right)\right)\\
&+8\hat L_{8,r}(1-y)\left(3\,x(2+3y)-9x^2-2\,y(2+y)\right)\Big]\\
&-\frac{1}{2\,(4-y-3x)}\Big[4\left(\hat N'_{5,r}-2\hat N'_{6,r}+2\hat N'_{8,r}+\hat N'_{9,r}\right)\\
&+y\left(5\hat N'_{5,r}+22\hat N'_{6,r}-2\hat N'_{8,r}-7\hat N'_{9,r}-16\hat N'_{10,r}-24\hat N'_{12,r}-24\hat N'_{13,r}\right)\\
&-y^2\left(12\hat N'_{5,r}+20\hat N'_{6,r}+5\hat N'_{8,r}-4\hat N'_{9,r}-24\hat N'_{10,r}-32\hat N'_{12,r}-36\hat N'_{13,r}\right)\\
&+y^3\left(3\hat N'_{5,r}+6\hat N'_{6,r}-\hat N'_{8,r}-\hat N'_{9,r}-8(\hat N'_{10,r}+\hat N'_{12,r})-12\,\hat N'_{13,r}\right)\\
&-2\,x\left(4\hat N'_{5,r}+6\hat N'_{8,r}-\hat N'_{9,r}-6\hat N'_{12,r}-6\hat N'_{13,r}\right)\\
&+xy\left(5\hat N'_{5,r}+6\hat N'_{8,r}-\hat N'_{9,r}+6\hat N'_{10,r}-6\hat N'_{12,r}-12\hat N'_{13,r}\right)\\
&+xy^2\left(3\hat N'_{5,r}+6\hat N'_{8,r}-\hat N'_{9,r}-6\hat N'_{10,r}-6\hat N'_{12,r}\right)-6\,x^2\hat N'_{9,r}(1-y)\Big]\Bigg\}\,,
\end{aligned}
\tag{A.5}
$$

with

$$
\begin{aligned}
g^{G_8,c^a_{dd}+c^a_{ss}}(x,y) &= \frac{1-y}{12(4-y-3x)^2}\left[192+4y(72+5y-2y^2)\right.\\
&\quad \left.-3x(144+284y-9y^2-3x(44+59y)+54x^2)\right]\,,\\
f_0^{G_8,c^a_{dd}+c^a_{ss}}(x,y) &= \frac{1-y}{24xy(4-y-3x)}\left[y(1-y)^2(12+7y)\right.\\
&\quad \left.+6x\left(4-2y^3+9y^2-11y\right)-3x^2\left(8-8y+15y^2\right)+54x^3y\right]\,,\\
f_1^{G_8,c^a_{dd}+c^a_{ss}}(x,y) &= -\frac{1-y}{24x^2(x-y)(4-y-3x)}\left[y^2(1-y)^2+2x\left(2y^2+y-1\right)\right.\\
&\quad \left.-x^2\left(4y^2+14y+1\right)+12x^3(1+y)-9x^4\right]\,,\\
f_2^{G_8,c^a_{dd}+c^a_{ss}}(x,y) &= \frac{y(1-y)(8-4y-3x)}{6(4-y-3x)}\,,\\
f_3^{G_8,c^a_{dd}+c^a_{ss}}(x,y) &= \frac{1}{144x^2y^2(4-y-3x)^2}\left[-y^3(4-y)(1-y)^4\right.\\
&\quad + xy(1-y)^2\left(8-14y+82y^2-41y^3+7y^4\right)\\
&\quad - x^2\big(24-532y+1196y^2-34y^3-2118y^4+1747y^5\\
&\qquad -563y^6+64y^7\big)\\
&\quad + 3x^3\left(14-371y+850y^2-655y^3-281y^4+343y^5-80y^6\right)\\
&\quad \left.-9x^4\left(16y^5-53y^4+12y^3+46y^2-59y+2\right)+81x^5y^2(1-y)\right],\\
f_4^{G_8,c^a_{dd}+c^a_{ss}}(x,y) &= \frac{1}{144x^2y^2(4-y-3x)^2}\left[18y^2(1-y)^4\left(8+2y-y^2\right)\right.\\
&\quad - 9xy(1-y)^2\left(8+38y-57y^2+36y^3-y^4\right)\\
&\quad + x^2\big(216-1332y+2250y^2-3463y^3+1442y^4+954y^5\\
&\qquad -347y^6+64y^7\big)\\
&\quad - 3x^3(126-747y+726y^2-1578y^3+1174y^4\\
&\qquad +307y^5-80y^6)\\
&\quad + 9x^4\big(18-99y-18y^2-155y^3+238y^4+16y^5\big)\\
&\quad \left.+405x^5y^2(1-y)\right]\,,
\end{aligned}
$$

$$
\begin{aligned}
f_5^{G_8,c_{dd}^a+c_{ss}^a}(x,y) &= \frac{1-y}{24y^2(x-y)(4-y-3x)}\left[-y\left(8+3y-37y^2+18y^3\right)\right.\\
&\qquad \left.+x\left(6+11y-76y^2+36y^3\right)-3x^2\left(2-13y+6y^2\right)\right]\,,\\
f_6^{G_8,c_{dd}^a+c_{ss}^a}(x,y) &= -\frac{(1-y)}{8y^2(x-y)(4-y-3x)}\left[y\left(8-21y+5y^2\right)\right.\\
&\qquad \left.-x\left(6-13y-10y^2\right)+x^2(6-15y)\right]\,,\\
f_7^{G_8,c_{dd}^a+c_{ss}^a}(x,y) &= \frac{1-y}{8x^2(x-y)(3x+y-4)}\left[2y\left(2-3y+y^3\right)+x^3(16+19y)\right.\\
&\qquad \left.-x\left(6-3y-14y^2+7y^3\right)+x^2\left(5-30y+y^2\right)-15x^4\right]\,. \qquad \text{(A.6)}
\end{aligned}
$$

The contribution proportional to $(c_{dd}^a - c_{ss}^a)$ reads

$$
\begin{aligned}
iA_{\text{NLO}}^{G_8,c_{dd}^a-c_{ss}^a} &= \frac{m_{K^-}^2}{8\pi^2F_\pi^2}\left\{\ln\frac{\mu}{m_K}g^{G_8,c_{dd}^a-c_{ss}^a}(x,y)+f_0^{G_8,c_{dd}^a-c_{ss}^a}(x,y)\right.\\
&\quad+\sum_{i=1}^{7}s_i(x,y)f_i^{G_8,c_{dd}^a-c_{ss}^a}(x,y)\\
&\quad-\frac{x}{4(4-3x-y)^2}\left[4\hat{L}_{4,r}(2+y)\left(4+7y-2y^2-3x(y+5)+9x^2\right)\right.\\
&\quad-\hat{L}_{5,r}\left(4-y(31+19y-10y^2)+3x(1+24y-y^2-3x-9xy)\right)\\
&\qquad\left.+24(2\hat{L}_{7,r}+\hat{L}_{8,r})(1-y)^2(2+y-3x)\right]\\
&\quad-\frac{1}{2(4-y-3x)}\left[4\left(\hat{N}'_{5,r}+2\hat{N}'_{6,r}-\hat{N}'_{9,r}-4\hat{N}'_{10,r}-4\hat{N}'_{11,r}+\hat{N}'_{21,r}+\hat{N}'_{23,r}\right)\right.\\
&\quad-y\left(9\hat{N}'_{5,r}+18\hat{N}'_{6,r}-9\hat{N}'_{9,r}-36\hat{N}'_{10,r}-28\hat{N}'_{11,r}+9\hat{N}'_{21,r}+9\hat{N}'_{23,r}\right)\\
&\quad+6y^2\left(\hat{N}'_{5,r}+2\hat{N}'_{6,r}-\hat{N}'_{9,r}-4\hat{N}'_{10,r}-\hat{N}'_{11,r}+\hat{N}'_{21,r}+\hat{N}'_{23,r}\right)\\
&\quad-y^3\left(\hat{N}'_{5,r}+2\hat{N}'_{6,r}-\hat{N}'_{9,r}-4\hat{N}'_{10,r}+8\hat{N}'_{11,r}+\hat{N}'_{21,r}+\hat{N}'_{23,r}\right)+2y^4\hat{N}'_{11,r}\\
&\quad-x\left(6\hat{N}'_{5,r}+2\hat{N}'_{8,r}+2\hat{N}'_{9,r}-12\hat{N}'_{10,r}-12\hat{N}'_{11,r}+12\hat{N}'_{12,r}+12\hat{N}'_{13,r}\right.\\
&\qquad\left.-4\hat{N}'_{20,r}-\hat{N}'_{21,r}+7\hat{N}'_{23,r}\right)\\
&\quad+xy\left(\hat{N}'_{5,r}-5\hat{N}'_{8,r}-7\hat{N}'_{9,r}-18\hat{N}'_{10,r}-18\hat{N}'_{11,r}\right.\\
&\qquad\left.+18\hat{N}'_{12,r}+24\hat{N}'_{13,r}+3\hat{N}'_{20,r}+\hat{N}'_{21,r}+3\hat{N}'_{23,r}\right)\\
&\quad-xy^2\left(\hat{N}'_{5,r}+2\hat{N}'_{8,r}-3\hat{N}'_{9,r}-6\hat{N}'_{10,r}+6\hat{N}'_{12,r}+12\hat{N}'_{13,r}+\hat{N}'_{20,r}\right.\\
&\qquad\left.+2\hat{N}'_{21,r}+2\hat{N}'_{23,r}\right)\\
&\quad+6xy^3\hat{N}'_{11,r}+x^2\left(6\hat{N}'_{5,r}+6\hat{N}'_{8,r}+6\hat{N}'_{9,r}-7\hat{N}'_{20,r}-3\hat{N}'_{21,r}+3\hat{N}'_{23,r}\right)\\
&\quad\left.+x^2y\left(3\hat{N}'_{8,r}-2\hat{N}'_{20,r}+3\hat{N}'_{21,r}+3\hat{N}'_{23,r}\right)+3x^3\hat{N}'_{20,r}\right]\Bigg\}\,, \qquad \text{(A.7)}
\end{aligned}
$$

where

$$
\begin{aligned}
g^{G_8,c^a_{dd}-c^a_{ss}}(x,y) = \frac{1}{36(4-3x-y)^2}\Big[&-2(31+26y)\left(4-5y+y^2\right)^2 \\
&+12x\left(68-138y-146y^2+143y^3-26y^4\right) \\
&+9x^2\left(74+143y+126y^2-52y^3\right) \\
&-27x^3(29+33y)+243x^4\Big]\,, \\
f_0^{G_8,c^a_{dd}-c^a_{ss}}(x,y) = -\frac{1}{72xy(4-y-3x)}\Big[&4y(4-y)(1-y)^3 \\
&+x\left(72-271y+460y^2-347y^3+86y^4\right) \\
&-3x^2\left(24-109y+112y^2-51y^3\right)-9x^3y(9+8y)+81x^4y\Big]\,, \\
f_1^{G_8,c^a_{dd}-c^a_{ss}}(x,y) = -\frac{1}{144x^2(x-y)(4-y-3x)}\Big[&y(4-y)(1-y)^3 \\
&-x\left(16-54y+53y^2-20y^3+5y^4\right) \\
&-x^2\left(17+43y-38y^2+14y^3\right) \\
&+3x^3\left(23+4y+6y^2\right)-9x^4(7+3y)+27x^5\Big]\,, \\
f_2^{G_8,c^a_{dd}-c^a_{ss}}(x,y) = -\frac{xy(1-y)}{2(4-y-3x)}\,, \\
f_3^{G_8,c^a_{dd}-c^a_{ss}}(x,y) = -\frac{1}{864x^2y^2(4-y-3x)^2}\Big[&(4-y)^2(1-y)^4y^2 \\
&-2xy(1-y)^2\left(24+110y-89y^2+19y^3-y^4\right) \\
&-3x^2\left(48-1120y+4715y^2-6236y^3+3792y^4\right. \\
&\qquad\left.-1136y^5+161y^6-8y^7\right) \\
&+18x^3(14-375y+1438y^2-1788y^3+923y^4 \\
&\qquad-236y^5+24y^6) \\
&-27x^4\left(4-118y+258y^2-254y^3+141y^4-40y^5\right) \\
&\qquad+162x^5y^2(3-2y)+243x^6y^2\Big]\,,
\end{aligned}
$$

$$
\begin{aligned}
f_4^{G_8, c_{dd}^a - c_{ss}^a}(x,y) = &-\frac{1}{96x^2y^2(4-y-3x)^2}\left[3y^2(4-y)^2(1-y)^4\right.\\
&+6xy(1-y)^2\left(8-18y+52y^2-40y^3+7y^4\right)\\
&+3x^2\big(48-352y+801y^2-906y^3+836y^4-722y^5\\
&\qquad+247y^6-24y^7\big)\\
&-2x^3\big(126-783y+1572y^2-1261y^3+1944y^4\\
&\qquad-1290y^5+232y^6\big)\\
&+3x^4\left(36-198y+458y^2+228y^3+561y^4-248y^5\right)\\
&\left.-18x^5y^2(52y+23)+135x^6y^2\right]\,,\\
f_5^{G_8, c_{dd}^a - c_{ss}^a}(x,y) = &\frac{1-y}{24y^2(x-y)(4-y-3x)}\left[y\left(4+3y-9y^2+2y^3\right)\right.\\
&\left.-x\left(6+7y-48y^2+20y^3\right)+3x^2\left(2-13y+6y^2\right)\right]\,,\\
f_6^{G_8, c_{dd}^a - c_{ss}^a}(x,y) = &\frac{1-y}{8y^2(x-y)(4-y-3x)}\left[y\left(4-21y+21y^2-4\,y^3\right)\right.\\
&\left.-x\left(6-17y+6y^2+8y^3\right)+3x^2\left(2-5y+4y^2\right)\right]\,,\\
f_7^{G_8, c_{dd}^a - c_{ss}^a}(x,y) = &\frac{1}{16x^2(x-y)(4-y-3x)}\left[y(4-y)(1-y)^3\right.\\
&+xy\left(8+7y-26y^2+11y^3\right)-x^2\left(3+25y-48y^2+8y^3\right)\\
&\left.+x^3\left(7-26y-20y^2\right)+x^4(11+31y)-15x^5\right]\,. \qquad \text{(A.8)}
\end{aligned}
$$

Finally, the contribution proportional to $(c_{dd}^v - c_{ss}^v)$ is given by

$$
\begin{aligned}
iA_{\text{NLO}}^{G_8,c_{dd}^v-c_{ss}^v} = \frac{m_{K^-}^2}{8\pi^2 F_\pi^2}\Bigg\{ & \ln\frac{\mu}{m_K} g^{G_8,c_{dd}^v-c_{ss}^v}(x,y) + f_0^{G_8,c_{dd}^v-c_{ss}^v}(x,y) \\
& + \sum_{i=1}^{7} s_i(x,y) f_i^{G_8,c_{dd}^v-c_{ss}^v}(x,y) - (1-x+y)\left[\hat{L}_{4,r}(2+y) + \hat{L}_{5,r}\frac{1+3y}{4}\right] \\
& + \frac{1}{2(4-y-3x)}\Big[4\left(2\hat{N}'_{5,r} + 2\hat{N}'_{8,r} - 4\hat{N}'_{10,r} - 4\hat{N}'_{11,r} + \hat{N}'_{21,r} + \hat{N}'_{23,r}\right) \\
& + y\left(6\hat{N}'_{5,r} + 10\hat{N}'_{8,r} + 4\hat{N}'_{10,r} - 4\hat{N}'_{11,r} - 16\hat{N}'_{12,r} - 9\hat{N}'_{21,r} - 9\hat{N}'_{23,r}\right) \\
& - y^2\left(2\hat{N}'_{5,r} - \hat{N}'_{8,r} - 2\hat{N}'_{11,r} - 4\hat{N}'_{12,r} - 6\hat{N}'_{21,r} - 6\hat{N}'_{23,r}\right) \\
& - y^3\left(\hat{N}'_{8,r} + \hat{N}'_{21,r} + \hat{N}'_{23,r}\right) \\
& - x\left(14\hat{N}'_{5,r} + 14\hat{N}'_{8,r} - 12\hat{N}'_{10,r} - 12\hat{N}'_{11,r} - 4\hat{N}'_{20,r} - \hat{N}'_{21,r} + 7\hat{N}'_{23,r}\right) \\
& - xy\left(4\hat{N}'_{5,r} + 11\hat{N}'_{8,r} - 6\hat{N}'_{11,r} - 12\hat{N}'_{12,r} - 3\hat{N}'_{20,r} - \hat{N}'_{21,r} - 3\hat{N}'_{23,r}\right) \\
& - xy^2\left(2\hat{N}'_{8,r} + \hat{N}'_{20,r} + 2\hat{N}'_{21,r} + 2\hat{N}'_{23,r}\right) \\
& + x^2\left(6\hat{N}'_{5,r} + 6\hat{N}'_{8,r} - 7\hat{N}'_{20,r} - 3\hat{N}'_{21,r} + 3\hat{N}'_{23,r}\right) \\
& + x^2 y\left(3\hat{N}'_{8,r} - 2\hat{N}'_{20,r} + 3\hat{N}'_{21,r} + 3\hat{N}'_{23,r}\right) + 3x^3\hat{N}'_{20,r}\Big]\Bigg\}, \qquad \text{(A.9)}
\end{aligned}
$$

with

$$
\begin{aligned}
g^{G_8,c_{dd}^v-c_{ss}^v}(x,y) &= \frac{13}{18} - \frac{35}{9}y - \frac{5}{2}y^2 + \frac{23}{12}x + \frac{13}{4}xy - \frac{3}{4}x^2\,, \\
f_0^{G_8,c_{dd}^v-c_{ss}^v}(x,y) &= -\frac{1}{72}\Bigg(\frac{(1-y)^2(17+13y)}{x} + 1 + 54y - 7y^2 \\
&\qquad - x(45+33y-27x)\Bigg)\,, \\
f_1^{G_8,c_{dd}^v-c_{ss}^v}(x,y) &= -\frac{(7-y)(1-y)^2 + x\left(11+18y-5y^2\right) - 3x^2(y+9) + 9x^3}{144x^2}\,, \\
f_{2,5,6}^{G_8,c_{dd}^v-c_{ss}^v}(x,y) &= 0\,, \\
f_3^{G_8,c_{dd}^v-c_{ss}^v}(x,y) &= \frac{1}{864x^2}\left((7-y)(1-y)^3 - 4x\left(34-49y+17y^2-2y^3\right)\right. \\
&\qquad \left. -6x^2\left(59-3y^2-8y\right) + x^3(72-54y) + 27x^4\right)\,, \\
f_4^{G_8,c_{dd}^v-c_{ss}^v}(x,y) &= -\frac{1-x+y}{32x^2}\left(3(1-y)^3 - x(1-y^2) - x^2(7+33y) + 5x^3\right)\,, \\
f_7^{G_8,c_{dd}^v-c_{ss}^v}(x,y) &= -\frac{3}{16x^2}(1-y)^2(1+y) + \frac{1}{16x}\left(1-10y+y^2\right)\,, \\
&\quad + \frac{7}{16}(1+y) - \frac{5}{16}x\,. \qquad \text{(A.10)}
\end{aligned}
$$

4.13.A.2. G_8^θ contribution

By construction, the G_8^θ contribution is proportional to the single ALP coupling $\tilde{c}_{GG}$. It is given by

$$\begin{aligned}
iA_{\text{NLO}}^{G_8^\theta,\tilde{c}_{GG}} = \frac{m_{K^-}^2}{8\pi^2 F_\pi^2}\Bigg\{&(1-y)(4+8y-3x)\ln\frac{\mu}{m_K}\\
&+\frac{1}{6x}(1-y)(4x(1+y)-9x^2+5(1-y)^2)\\
&+\frac{s_1(x,y)}{12}\frac{1-y}{x}\left(\frac{(y-1)^2}{x}+2(1+y)-3x\right)\\
&-\frac{s_3(y)}{72}\left(\frac{(1-y)^4}{x^2}-(19-5y)\frac{(1-y)^2}{x}-9x(1-y)-3\left(15+10y-y^2\right)\right)\\
&+\frac{s_4(y)}{8}\left(\frac{3(1-y)^4}{x^2}-\frac{(1+y)(1-y)^2}{x}-7-26y+25y^2+5x(1-y)\right)\\
&+\frac{s_7(x,y)}{4}\frac{1-y}{x}\left(3\frac{(1-y)^2}{x}+2(1+y)-5x\right)\\
&+(1-y)\big(2(4+2y)\hat{L}_{4,r}+(1+3y)\hat{L}_{5,r}\big)\Bigg\}. \qquad \text{(A.11)}
\end{aligned}$$

4.13.A.3. G_8' contribution

The contribution proportional to G_8' is non-zero only for two combinations of ALP couplings, $(c_{dd}^a - c_{ss}^a)$ and $(c_{dd}^v - c_{ss}^v)$. The corresponding NLO contributions to $\mathcal{A}^{\text{FC}}$ are given by

$$\begin{aligned}
iA_{\text{NLO}}^{G_8',c_{dd}^a-c_{ss}^a} = \frac{m_{K^-}^2}{8\pi^2 F_\pi^2}\frac{(1-y)^2}{2}\Bigg\{&-\left(4+\frac{16}{3}y-3x\right)\ln\frac{\mu}{m_K}\\
&-\frac{5(1-y)^2}{6x}-\frac{2}{3}(1+y)+\frac{3}{2}x-\frac{s_1(x,y)}{12}\left(\frac{(1-y)^2}{x^2}+2\frac{1+y}{x}-3\right)\\
&+\frac{s_3(y)}{72}\Bigg(\frac{(1-y)(1-2y+y^2)}{x^2}-\frac{(1-y)(19-5y)}{x}\\
&\qquad -9\frac{\left(5+14y-3y^2\right)}{1-y}-9x\Bigg)\\
&+\frac{s_4(y)}{8}\left(-3\frac{(1-y)^3}{x^2}+\frac{1-y^2}{x}+\frac{7+26y-17y^2}{1-y}-5x\right)\\
&-\frac{s_7(x,y)}{4}\left(-5+2\frac{1+y}{x}+3\frac{(1-y)^2}{x^2}\right)\\
&-2(2+y)\hat{L}_{4,r}+x\hat{L}_{5,r}-4y\hat{L}_{8,r}\Bigg\},
\end{aligned}$$

$$
\begin{aligned}
iA_{\rm NLO}^{G_8',c_{dd}^v-c_{ss}^v} = \frac{m_{K^-}^2}{8\pi^2 F_\pi^2}\Bigg\{ & \left(2+\frac{16}{3}y-\frac{3}{2}x\right)\ln\frac{\mu}{m_K} \\
& -\frac{3}{4}x+\frac{5}{12x}(1-y)^2+\frac{1+y}{3}+\frac{s_1(x,y)}{24}\left(\frac{(1-y)^2}{x^2}+2\frac{1+y}{x}-3\right) \\
& +\frac{s_3(y)}{144}\left(-\frac{(1-y)^3}{x^2}+\frac{19-24y+5y^2}{x}+3(15-7y)+9x\right) \\
& +\frac{s_4(y)}{16}\left(3\frac{(1-y)^3}{x^2}-\frac{1-y^2}{x}-7-33y+5x\right) \\
& +\frac{s_7(x,y)}{8}\left(3\frac{(1-y)^2}{x^2}+2\frac{1+y}{x}-5\right) \\
& +(2+y)\hat{L}_{4,r}+\frac{4y-x}{2}\hat{L}_{5,r}-2y\hat{L}_{8,r}\Bigg\}\,.
\end{aligned}
\tag{A.12}
$$

4.13.B. $\mathcal{A}^{\rm FV}$ at NLO

Finally, the contribution proportional to flavor-violating ALP couplings between strange and down quarks is

$$
\begin{aligned}
iA_{\rm NLO}^{\rm FV} = \frac{m_{K^-}^2}{8\pi^2 F_\pi^2}\Bigg\{ & \frac{3}{2}x\ln\frac{\mu}{m_K}-\frac{5}{12}\frac{(1-y)^2}{x}-\frac{1+y}{3}+\frac{3}{4}x \\
& -\frac{s_1(x,y)}{24}\left(\frac{(1-y)^2}{x^2}+2\frac{(1+y)}{x}-3\right) \\
& +\frac{s_3(y)}{144}\left(\frac{(1-y)^3}{x^2}-\frac{19-5y}{x}(1-y)-3\frac{15+10y-y^2}{1-y}-9x\right) \\
& -\frac{s_4(y)}{16}\left(3\frac{(1-y)^3}{x^2}-\frac{1-y^2}{x}-\frac{7-6y+7y^2}{1-y}+5x\right) \\
& -\frac{s_7(x,y)}{8}\left(3\frac{(1-y)^2}{x^2}+2\frac{1+y}{x}-5\right)+\frac{1}{2}x\hat{L}_{5,r}\Bigg\}\,.
\end{aligned}
\tag{A.13}
$$

Chapter 5: Saving or Destroying the Universe with Axion-Like Particles

The experimental confirmation of the Higgs boson at the LHC by the ATLAS and CMS collaborations in 2012 [1, 2] was a landmark achievement that validated the mechanism of electroweak symmetry breaking, which endows elementary particles with mass. This discovery not only marked a major milestone in particle physics but also showcased the remarkable synergy between theoretical predictions and experimental verification. Yet, while the completion of the SM was a triumph, a closer analysis of the results has led to new, unexpected questions, revealing that our understanding of fundamental nature is far from complete. As already indicated in Section 1.4, one of the most intriguing questions emerging from this discovery is the so-called Higgs instability: Precise measurements of the Higgs mass of 125.25 ± 0.17 GeV [40] suggest that the electroweak vacuum does not correspond to the absolute minimum of the Higgs potential. Instead, it resides in a long-lived yet ultimately temporary state, which, in principle, could undergo a global phase transition at any given time. For humanity, this would be a rather unpleasant event, as it would mean the destruction of the Universe as we know it! Fortunately, since the SM is unlikely to be the ultimate theory of fundamental physics, there may be a mechanism beyond it that prevents us from this terrifying scenario. In particular, the question arises of how the presence of the ALP would change this situation.
In order to reveal whether ALPs drive the Universe's fate rather towards a stable or unstable future, in this chapter, the ALP-SMEFT contributions to the β-function of the Higgs quartic coupling is examined. Depending on the magnitude of the additional dimension-five couplings, the ALP could either exacerbate or alleviate the stability problem of the Universe. By requiring that the Universe remains at least in a metastable state, these effects can be used to derive constraints on the ALP–SM couplings.
Finally, at the end of this chapter, it is also shown that through modifications of the β-function of the three gauge couplings, ALPs can lead to a unification around the Planck scale, even in non-supersymmetric models.

This chapter is based on

[183] **Saving or Destroying the Universe with Axion-Like Particles**
A. M. Galda and M. Neubert
[arXiv:2506.06426].

5.1. Instability of the Electroweak Vacuum in the Standard Model and Beyond

In the SM, the Higgs potential is given by

$$V = \frac{\lambda}{2}\,(H^\dagger H)^2 - m_H^2\, H^\dagger H\,, \tag{5.1}$$

where the physical mass m_h of the Higgs particle is related to the mass parameter of the quadratic term via $m_h = \sqrt{2} m_H = 125.25\,\text{GeV}$. For large values of the Higgs field where its mass can be neglected and the field value is approximated by the RG scale μ, the quartic term dominates and it therefore suffices to analyze the behavior of this quantity when determining the stability of the electroweak vacuum: In a scenario where the quartic coupling λ is larger than zero for all RG scales, the electroweak vacuum would be absolutely stable. On the other hand, when λ becomes negative at an instability scale Λ_I, the electroweak vacuum does not correspond to the true ground state and a non-zero tunneling probability from this *false vacuum* to the true ground state arises. Without additional new physics, solving the one-loop order β-function of the quartic coupling yields an instability scale around 10^{11} GeV, as shown in Figure 5.1. The exact value of the instability scale is highly sensitive to the input

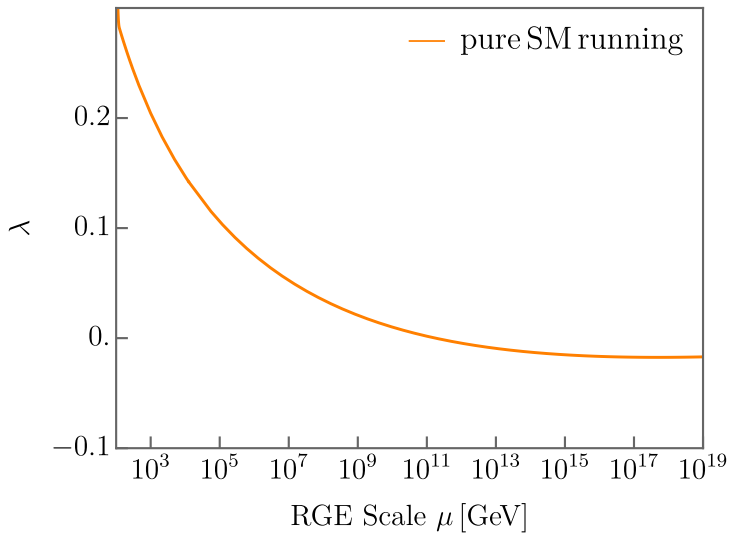

Figure 5.1.: Scale dependence of the Higgs quartic coupling λ in the SM. Around 10^{11} GeV, λ becomes negative.

parameters. A smaller Higgs mass would lower the instability scale, whereas a larger value of m_H could stabilize the Universe (see e.g. [7–11] for more detailed studies). In other words, any kind of physics beyond the SM that has a direct or indirect influence on the RG evolution of λ can potentially relax or worsen the instability of the electroweak vacuum.
The presence of the ALP modifies the RG evolution equations of the quartic coupling

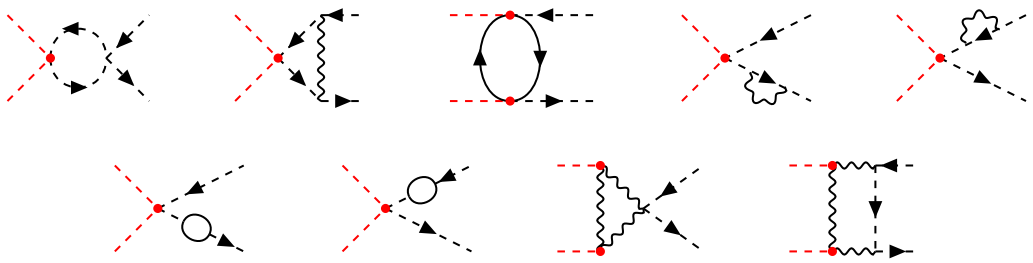

Figure 5.2.: Feynman diagrams contributing to the RG evolution of the coefficient C_{HH} multiplying the dimension-6 operator that contains two ALP and two Higgs fields as defined in (1.34). A red dotted line represents the ALP, while the Higgs fields are shown as black dashed lines with the arrow pointing in the direction of the $SU(2)_Y$ charge flow.

by two-fold: First, a direct contribution proportional to the dimension-five coupling C_{WW} enters the equation for λ as [35]

$$\frac{d\lambda}{d\ln\mu} \supset \frac{16 g_s^2}{3} \frac{m_H^2}{(4\pi f)^2} C_{WW}^2 \,, \tag{5.2}$$

where also the Higgs mass receives a contribution from the dimension-6 operator in (1.34) that reads [67]

$$\frac{dm_H^2}{d\ln\mu} \supset \frac{2 m_a^4}{(4\pi f)^2} C_{HH} \,. \tag{5.3}$$

To fully solve the set of coupled differential equations, in principle the RG evolution equation of C_{HH} is also required. The Feynman diagrams that contribute are those depicted in Figure 5.2, yielding, for $N_c = 3$, the β-function

$$\begin{aligned}\frac{d\,C_{HH}}{d\ln\mu} = \frac{1}{(4\pi)^2}\Big(&36\, g_L^2\, C_{WW}^2 + 12\, g_Y^2\, C_{BB}^2 - 6\,\mathrm{Tr}[\tilde{\boldsymbol{Y}}_d \tilde{\boldsymbol{Y}}_d^\dagger + \tilde{\boldsymbol{Y}}_u \tilde{\boldsymbol{Y}}_u^\dagger + \frac{1}{3}\tilde{\boldsymbol{Y}}_e \tilde{\boldsymbol{Y}}_e^\dagger] \\ &- \frac{3}{2} C_{HH}\left(3\, g_L^2 + g_Y^2 - 4\,\lambda - 4\,\mathrm{Tr}[\boldsymbol{Y}_d \boldsymbol{Y}_d^\dagger + \boldsymbol{Y}_u \boldsymbol{Y}_u^\dagger + \frac{1}{3}\boldsymbol{Y}_e \boldsymbol{Y}_e^\dagger]\right)\Big) \,.\end{aligned} \tag{5.4}$$

In the RG equation of λ, the explicit Higgs mass m_H enters only via dimension-six SMEFT coefficients [71], or via the term in (5.2). Thus, effects of C_{HH} are at least two-loop power suppressed and do not have a significant effect on the scale evolution of the Higgs quartic coupling. In the following discussion, it will therefore be dropped.
The second mechanism by which the ALP modifies λ is the generation of SMEFT coefficients of dimension-six order, via the *ALP–SMEFT interference*, that enter the RG equation. Thus, it does not suffice to consider the pure SM running only, but the full SMEFT running, which has been obtained in [70–72], needs to be taken into account when evaluating ALP effects on the stability of the electroweak vacuum.
In detail, these ALP effects can be obtained in the following way: For a given scale of global symmetry breaking $\Lambda = 4\pi f$, ALP mass m_a and ALP–SM couplings at Λ, the SMEFT and ALP couplings at M_Z need to be obtained by solving the full set

of SMEFT RG evolution equations. Depending on the ALP mass, this either means running the full dimension-six system including the ALP coefficients down to the scale where λ is measured (for $m_a \leq M_Z$), or integrating out the ALP in an intermediate step (which is preformed at tree level) and continue with the pure SMEFT running without ALP modifications. The thus obtained initial conditions of the dimension-five ALP and dimension-six SMEFT parameters are then used as inputs at the appropriate scale (i.e. ALP couplings only contribute for $\mu \geq m_a$).
The concrete effect of the ALP generated SMEFT contributions is non-trivial and depends on the configuration of ALP–SM couplings at the scale of global symmetry breaking Λ. This is the case, as the RG flow generates different sets of SMEFT and ALP couplings at low scales, and modifications to the SM couplings can thus be generated even without the direct contribution of C_{WW} in (5.2). While one would maybe expect that this direct ALP contribution dominates the evolution of λ in the presence of the ALP and that one-loop suppressed ALP contributions play a minor role in the evolution of λ, terms that are proportional to m_a^2 can get strongly enhanced for large ALP masses as will be shown later.
This setup therefore allows to constrain the ALP–SM couplings, which are assumed to be flavor-universal in the UV, from the requirement that the electroweak vacuum is supposed to remain (at least) in a meta-stable state also in the presence of the ALP, i.e. the resulting lifetime is larger than the age of the Universe.

5.2. Effects of the ALP on the Quartic Higgs Coupling

In the pure SM scenario without additional new physics, the instability scale of the electroweak vacuum is approximately given by $\Lambda_I = 10^{11}\,\text{GeV}$. The objective is to analyze how different ALP couplings influence this scale. To this end, the two benchmark cases $m_a = 0$ and $m_a = 100\,\text{GeV}$ are considered, with one non-zero dimension-five coupling at a time at the scale of global $U(1)_{\text{PQ}}$ symmetry breaking Λ. Employing the RG evolution equations for the ALP coefficients [60] and SMEFT Wilson coefficients [71, 72] within a modified version of the `DsixTools` framework, and using the input values provided in [184, 185], the numerical values of all relevant coefficients governing the scale evolution of λ at the electroweak scale are obtained, keeping $\lambda(M_Z) \approx 0.28$ fixed. The magnitude of the ALP-induced SMEFT Wilson coefficients at the electroweak scale depends on their evolution from Λ down to μ. Specifically, when symmetry breaking occurs at a very high scale, the ratio Λ/μ generates large logarithms that enhance the effects of the SMEFT and ALP coefficients.
For illustration, the parameter f is set to 1 TeV, and the resulting modifications to the instability scale for various ALP couplings are shown in Figure 5.3. As expected, the direct contribution of C_{WW} to the RG evolution of λ in (5.2) shifts the instability scale Λ_I towards higher values, thereby making the electroweak vacuum more stable. While this effect is relatively straightforward to understand, disentangling the influence of other parameters is more nuanced:

- $\boldsymbol{C_{GG}}$: Any nonzero value of C_{GG} generally shifts the instability scale to higher values. Although this coupling does not directly enter the RG equation of λ, it induces nonzero SMEFT Wilson coefficients and modifies the β-function of the

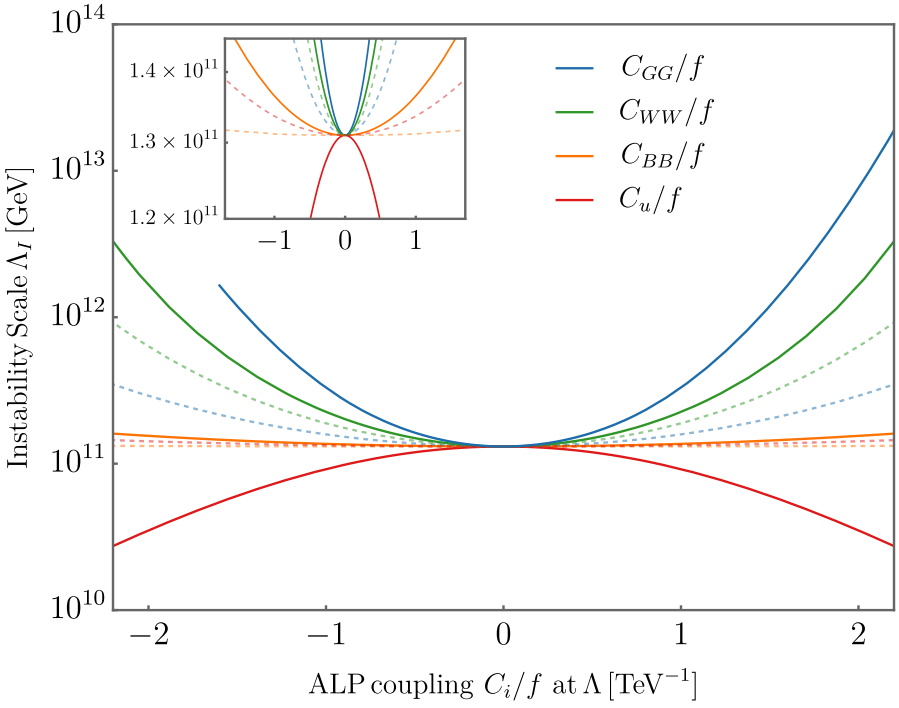

Figure 5.3.: Instability scale of the electroweak vacuum in the presence of nonzero ALP-SM couplings. The solid lines show the result for $m_a = 100$ GeV, while the dashed lines assume a vanishing ALP mass.

strong coupling through an ALP-mass-dependent term:

$$\frac{d\alpha_s}{d\ln\mu} \supset -16\,\alpha_s \frac{m_a^2}{\Lambda^2}\, C_{GG}^2\,. \tag{5.5}$$

Since the dominant contribution of the strong coupling to the RG evolution of λ is given by $d\lambda/d\ln\mu \supset -\alpha_s\,[\boldsymbol{Y}_u]_{3,3}$, the signs cancel, resulting in a positive contribution to the evolution of λ and shifting the instability scale upward. When $m_a = 0$, the generation of SMEFT Wilson coefficients, particularly $C_{Hq}^{(3)}$, still raises Λ_I, but the effect is much smaller than for $m_a = 100$ GeV, as can be seen in Figure 5.3.

- $\boldsymbol{C_{WW}}$: Similar to the ALP-gluon coupling, nonzero ALP couplings to W-bosons have a stabilizing effect on the electroweak vacuum. This occurs because the square of this Wilson coefficient directly contributes to the RG evolution of λ with a positive sign, as shown in Eq. (5.2).

- $\boldsymbol{C_u}$: The coupling of ALPs to up-type quarks, parameterized by $\tilde{\boldsymbol{Y}}_u = i\,C_u\,\boldsymbol{Y}_u$ and $\boldsymbol{Y}_u' = C_u^2\,\boldsymbol{Y}_u$ in the flavor-universal scenario, has the strongest destabilizing effect among all ALP coefficients for $m_a = 100$ GeV. However, it has almost no impact when $m_a = 0$, as illustrated in Figure 5.3. This behavior arises because

C_u enters the RG equation of y_t via the term

$$\frac{d\,y_t}{d\ln\mu} \supset -\frac{m_a^2}{2\Lambda^2}\,C_u^2\,y_t, \tag{5.6}$$

leading to a destabilizing effect in the flavor-universal scenario.

- $\boldsymbol{C_{BB}}$: Similarly to the ALP-gluon case, the coupling C_{BB} enters the scale evolution of λ mainly via the SM gauge coupling α_1 with

$$\frac{d\alpha_1}{d\ln\mu} \supset -16\,\alpha_1\frac{m_a^2}{\Lambda^2}\,C_{BB}^2\,. \tag{5.7}$$

  The effect is, however, small in comparison to C_{GG}.

- $\boldsymbol{C_e}$, $\boldsymbol{C_d}$,: These ALP couplings have no significant impact on the scale evolution of λ.

5.3. Bounds on the ALP Couplings from the Higgs Instability

After analyzing the effects of individual nonzero dimension-five ALP–SM couplings on the instability scale Λ_I, this section presents two-dimensional results for the stability of the electroweak vacuum, both for varying ALP mass and one non-zero ALP-SM coupling, as well as two nonzero ALP-SM couplings and fixed ALP mass.

5.3.1. Estimating the Lifetime of the Electroweak Vacuum

To estimate the lifetime of the electroweak vacuum, τ_{EW}, the approach outlined in [11] is followed. Below, their key findings are summarized.
Approximating the Universe as a sphere with radius $c\,T_U$, where the age of the Universe T_U and the Hubble constant H_0 are related by $T_U \approx 0.96\,H_0$, the probability of vacuum decay to the true ground state is given by

$$p_0 = 0.15\,\frac{\Lambda_B^4}{H_0^4}\,e^{-S(\Lambda_B)}\,, \tag{5.8}$$

where the action S is related to the quartic Higgs coupling by

$$S(\Lambda_B) = \frac{16\pi^2}{3|\lambda(\Lambda_B)|}\,. \tag{5.9}$$

In this expression, Λ_B corresponds to the scale at which $\lambda(\Lambda_B)$ reaches its minimum. In a vacuum-energy-dominated Universe, the electroweak vacuum lifetime is given by

$$\tau_{\mathrm{EW}} = \frac{3H^3 e^{S(\Lambda_B)}}{4\pi\Lambda_B^4} \approx \frac{0.02\,T_U}{p_0}\,. \tag{5.10}$$

Thus, the tunneling probability to the true electroweak vacuum depends on both the scale at which λ is minimized and the magnitude of λ at this point.

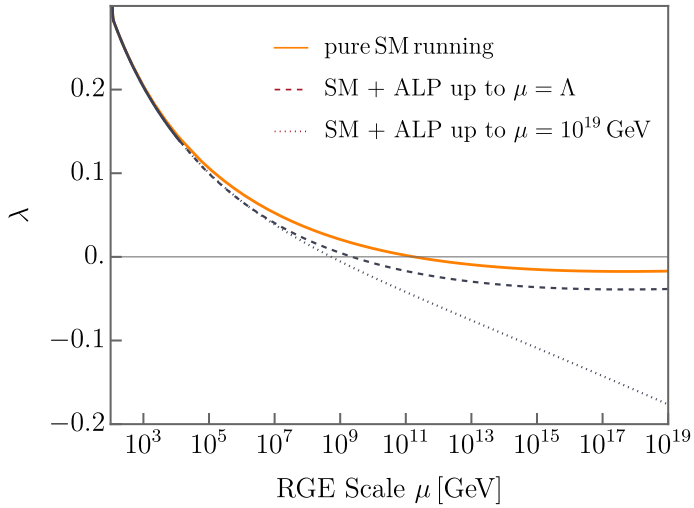

Figure 5.4.: Scale evolution of λ for the case $C_{WW}/f = 5\,\text{TeV}^{-1}$, $m_a = 90\,\text{GeV}$. The gray solid line shows the ALP + SM running until $\Lambda = 4\pi\,\text{TeV}$. Above this scale, the dashed gray line is obtained by taking only SM effects into account, while the dotted line employs ALP effects on the running up to the Planck scale. The orange line shows the pure SM case (no ALP) for comparison.

5.3.2. Scanning ALP–SM Couplings and Electroweak Vacuum Stability

The following section presents a scan of the ALP–SM couplings C_i/f in the range $0 - 12\,\text{TeV}^{-1}$ for $\Lambda = 4\pi$ TeV, identifying those couplings that lower the lifetime of the false electroweak vacuum to values below the age of the Universe. In general, effects from additional model-dependent degrees of freedom arising from heavy new physics can further modify the behavior of λ above Λ, meaning that precise conclusions can only be drawn up to this scale. To consider the most conservative scenario, the ALP–SM RG evolution is applied up to the scale of $U(1)_{\text{PQ}}$ symmetry breaking, with ALP effects neglected above Λ. A direct comparison of this scenario with the case where ALP effects are included up to the Planck scale is depicted in Figure 5.4. As shown in the plot, the extended ALP running imposes even tighter constraints on the couplings, as the instability becomes more severe.
In Figure 5.5, results are shown for one nonzero coupling at the UV scale Λ and an ALP mass m_a varied between 0 and 200 GeV. Each plot also includes the quartic Higgs coupling λ as a function of the RG scale μ, comparing a parameter point in the meta-stable and (un)stable regions with the pure SM running as a reference. While the coupling C_u exhibit a destabilizing effect on the Higgs quartic coupling, as previously observed in Section 5.2, large values of C_{WW} and C_{GG} at Λ can result in a stable Universe. In Figure 5.6, the ALP mass is fixed to either 0 or 100 GeV, and the regions of stability, meta-stability, and instability are shown for two nonzero coefficients at $\Lambda = 4\pi$ TeV. Certainly, larger values of ALP couplings have stronger stabilizing or destabilizing effects on the electroweak vacuum. Consequently, the strongest effects are tightly constrained by experimental bounds. While for low ALP masses, direct

collider, flavor, and astrophysical constraints provide the most stringent limits, the indirect bounds obtained in [67] dominate for $m_a \sim \mathcal{O}(\text{GeV})$. As a result, the coefficients required for the (de)stabilizing effects are experimentally excluded by several orders of magnitude for $m_a = 0$. However, for $m_a = 100\,\text{GeV}$, bounds on C_{GG}/f, C_{WW}/f, and C_u/f in TeV^{-1} are of $\mathcal{O}(1)$. While the precise non-metastable regions identified in this study lie within excluded parameter spaces, it is important to stress that already small modifications from a UV completion of the ALP model can be sufficient to evade these bounds.

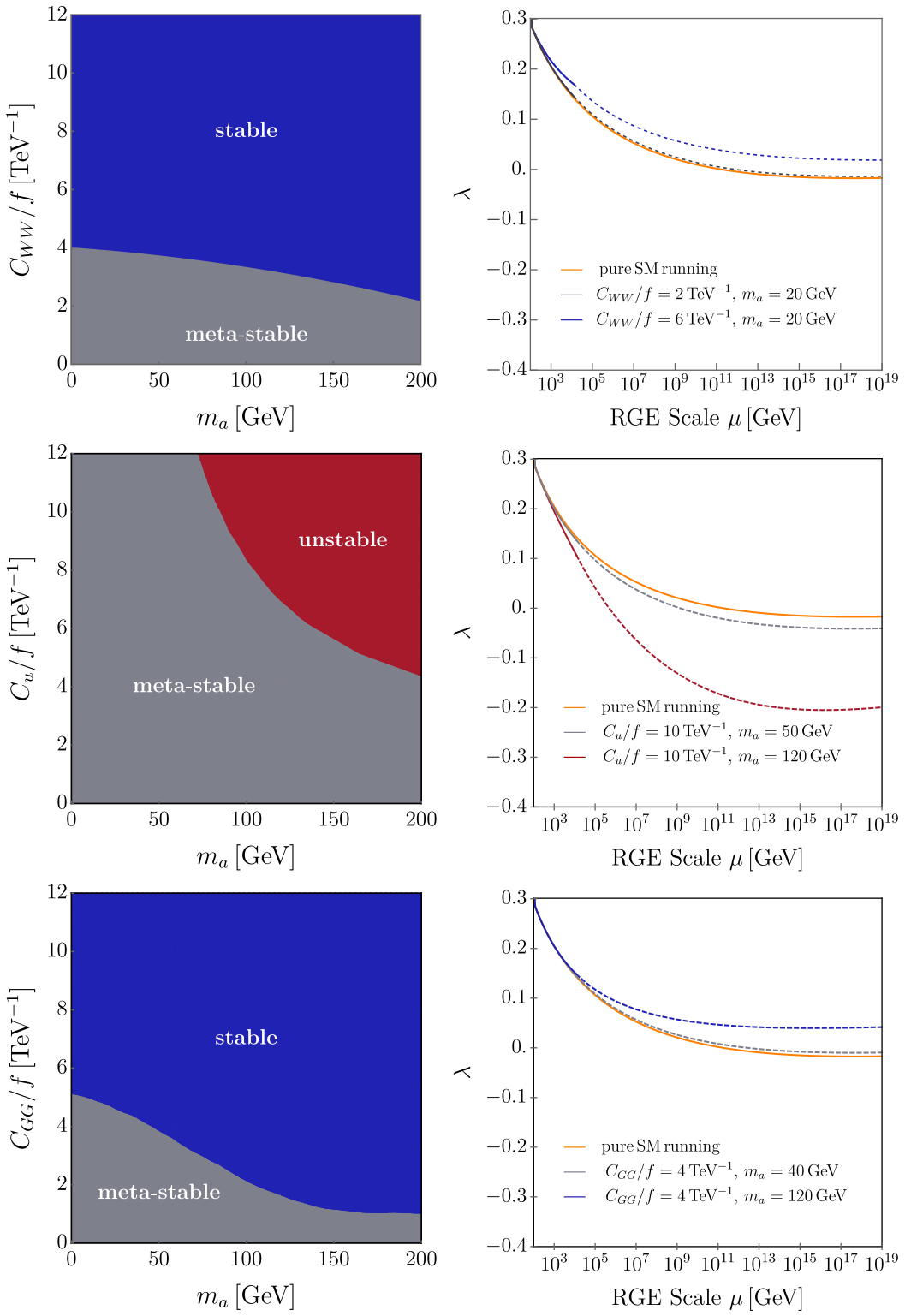

Figure 5.5.: Left: Unstable (red), stable (blue), and meta-stable (gray) regions for various ALP masses between 0 GeV and 200 GeV with one coupling turned on at the UV-scale at $\Lambda = 4\pi$ TeV. Right: Exemplary RG evolution of λ. The kink at 4π TeV arises from the generation of the ALP at this scale, which modifies the set of beta functions. The solid line represents the evolution below 4π TeV, where ALP effects influence the running.

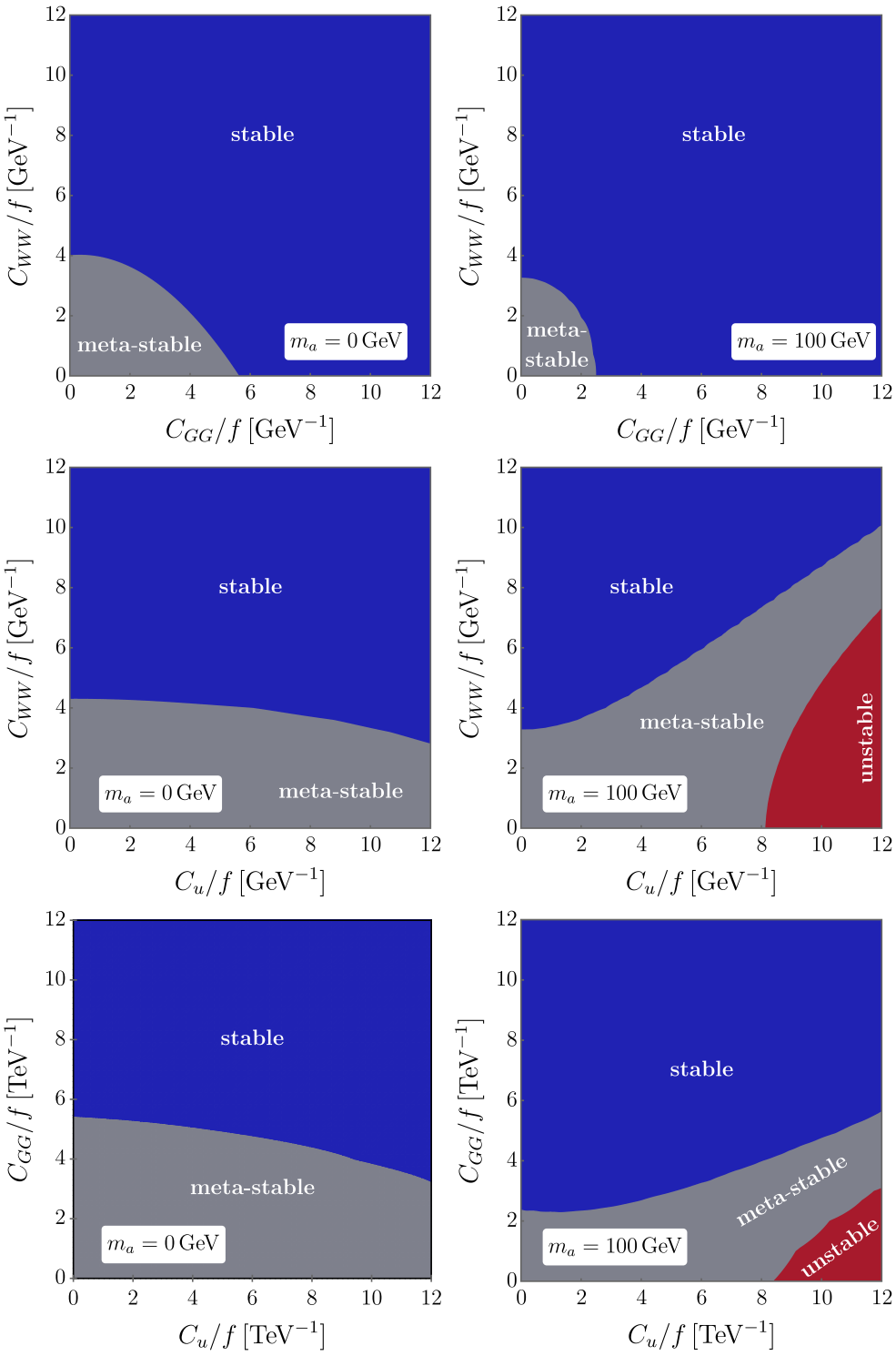

Figure 5.6.: Unstable (red), meta-stable (gray), and stable (blue) regions for various pairs of ALP couplings turned on at the scale $\Lambda = 4\pi$ TeV for a massless ALP and $m_a = 100$ GeV.

5.4. ALP unifying Gauge Forces?

In addition to the Higgs quartic coupling λ, ALP–SM interactions also modify the β-functions of the three gauge couplings. Defining $d\alpha_s/d\ln\mu \equiv -2\alpha_s\,\beta^{(3)}(\{\alpha_i\})$ and equivalently for α_1 and α_2, ALP interactions modify the SM contributions directly via [35]

$$\begin{aligned}
\beta^{(1)}(\{\alpha_i\}) &= \beta^{(1)}_{\text{SM}}(\{\alpha_i\}) + \frac{40}{3}\frac{m_a^2}{\Lambda^2}\,C_{BB}^2\,,\\
\beta^{(2)}(\{\alpha_i\}) &= \beta^{(2)}_{\text{SM}}(\{\alpha_i\}) + \frac{8m_a^2}{\Lambda^2}\,C_{WW}^2\,,\\
\beta^{(3)}(\{\alpha_i\}) &= \beta^{(3)}_{\text{SM}}(\{\alpha_i\}) + \frac{8m_a^2}{\Lambda^2}\,C_{GG}^2\,,
\end{aligned} \tag{5.11}$$

where in the first line the $SU(5)$ GUT normalization, $g_1 = \sqrt{5/3}\,g_Y$, was used [11]. Any ALP with nonzero mass will thus necessarily have an impact on the RG evolution of the gauge couplings. An example for a specific ALP–SM configuration at the scale of global symmetry breaking $\Lambda = 4\pi$ TeV that results in a unification of α_1, α_2 and α_s at around 10^{15} GeV is shown in Figure 5.7. Here, $m_a = 120$ GeV, as well as the ALP-boson couplings at Λ as $C_{GG} = 5.2\,\text{TeV}^{-1}$, $C_{WW} = 5.0\,\text{TeV}^{-1}$, $C_{BB} = 1.0\,\text{TeV}^{-1}$ are chosen.

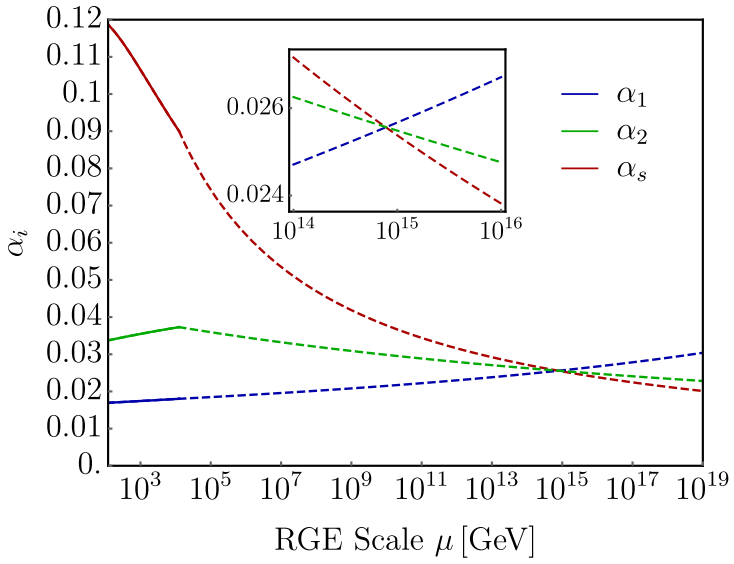

Figure 5.7.: RG evolution of α_1, α_2 and α_s in the presence of an ALP with $m_a = 120$ GeV, $\Lambda = 4\pi$ TeV and $C_{GG} = 5.2\,\text{TeV}^{-1}$, $C_{WW} = 5.0\,\text{TeV}^{-1}$, $C_{BB} = 1.0\,\text{TeV}^{-1}$. The solid line shows the evolution below 4π TeV, where ALP effects modify the running, while the dashed lines above Λ would in principle be subject to additional new physics in concrete ALP models.

5.5. Summary and Conclusion

In this chapter, ALP effects on the electroweak instability were investigated. While a direct contribution to the β-function of the Higgs quartic coupling proportional to the ALP-W-boson coupling C_{WW} generated by the *ALP-SMEFT interference* relaxes the Higgs instability problem and can, depending on its magnitude and the ALP mass, even stabilize the Universe, also indirect, higher-loop contributions impact the electroweak vacuum. In particular, also the ALP-gluon coupling C_{GG} relaxes the instability scenario, while the coupling C_u, on the other hand, tends to drive the Higgs quartic coupling to values lower than in the SM. The coefficients C_{BB}, C_e and C_d have only minor effects on the scale evolution. Assuming flavor-universal ALP-fermion couplings in the UV, this setup therefore enabled a systematic analysis to exclude couplings that would drive the Universe from a metastable to an unstable state. After briefly reviewing the estimate of the Universe's lifetime based on the tunneling probability to the true ground state, this analysis was performed for various combinations of ALP masses and couplings, identifying regions of total stability, meta- and instability. Although the concrete values found to generate the (un)stable regions are already excluded by experiment, it needs to be stressed that the analysis was performed in a minimal, model-independent framework. While applying the setup to concrete ALP models would require the derivation of the respective β-functions of the UV-couplings, these contributions could, together with possible threshold corrections, modify the scenario and tighten of relaxing the scenario.
In addition to the effects on the electroweak vacuum, this chapter also investigated the ALP contributions to the SM gauge couplings. Specifically, it examined whether these modifications could enable a unification at a high scale, which was found to occur near $\mu \approx 10^{15}$ GeV. As before, UV-complete models would modify the conservative approach presented here.
In summary, this chapter showed that ALPs may contribute to resolving two further key challenges of the SM: the electroweak vacuum meta-stability and the non-unification of gauge couplings. Through their impact on the Higgs potential and the SM gauge couplings, via modifications to the RG evolution equations, ALPs once again prove to be well-motivated extensions, with meaningful implications for high-energy physics, including the UV regime.

Epilogue: The ALPine Path Traversed and Journeys Ahead

In this thesis, we explored the theoretical and phenomenological landscape of ALPs, unveiling new trails in the ongoing pursuit of physics beyond the Standard Model. Traversing a wide range of energy scales, we advanced the search for these elusive particles by constructing consistent effective field theories, mapping their phenomenological imprints, and translating these insights into stringent bounds on the ALP–SM couplings.

We started our journey at the scale of global $U(1)_{\mathrm{PQ}}$ symmetry breaking Λ, where the ALP is generated. At this scale, we encountered a well-known phenomenon, the so-called *ALP–SMEFT interference*, which describes the generation of dimension-six operators of the SMEFT from virtual ALPs in one-loop diagrams. Building on this framework, we found that the non-trivial renormalization group flow of ALP couplings into SMEFT Wilson coefficients at lower energies enables a new, systematic global analysis that has not been performed so far: Running the ALP-induced SMEFT Wilson coefficients down until the experimental scale yields expressions that relate these coefficients to the dimension-five ALP couplings at the high scale Λ, enhanced by the corresponding logarithmic scale ratio obtained from the scale evolution. By employing existing SMEFT bounds derived from Higgs, top, and low-energy data, this procedure enabled us to constrain the ALP couplings in a model-independent and indirect approach. Notably, for ALPs with masses in the GeV to TeV range, these indirect bounds turned out to be competitive with, or even stronger than, many direct constraints, which often rely on specific model assumptions such as the ALP lifetime or branching ratios.

Subsequently, our path took us to even lower energies: As we crossed the scale of electroweak symmetry breaking, the heavy fields of the SM were removed from the theory, and also the effective SM–ALP Lagrangian was modified accordingly. To extend the model-independent predictive power of the *ALP–SMEFT interference* also to this energy regime, the source terms induced by virtual ALP exchange were deduced for the appropriate effective field theory, the LEFT. Following a systematic derivation of these inhomogeneous terms, we highlighted the phenomenological impact of this formalism by applying it to an important observable: Including all relevant two-loop effects, we derived the expression of the anomalous magnetic dipole moment of the muon in terms of ALP couplings and SMEFT Wilson coefficients, both at the scale Λ and the electroweak scale, and found numerical contributions for the case of a flavor-universal ALP.

We then continued our journey below the scale of chiral symmetry breaking, where the effective degrees of freedom changed once more. Here, our goal was to investigate the processes $K^{\pm} \to \pi^{\pm} a$ at next-to-leading order. Due to the tiny branching fraction of these decays, they impose the strongest constraints on ALP-gluon and ALP-fermion couplings for $m_a < 300$ MeV and are therefore of extreme phenomenological importance. These processes were recently revisited in [56] at LO, where it was found that the decay rates are approximately 37 times larger than those obtained using the effec-

tive chiral Lagrangian derived in [59], due to an omission in the representation of the weak-interaction quark currents in the effective theory. Yet, we found that already at this order, two additional operators must be included, which had not been considered before. First, the so-called "weak-mass term" becomes non-redundant in the presence of the ALP and second, the operator involving the explicit ALP source term θ with coupling G_8^θ had also been omitted in the literature so far. At NLO, we encountered an even more intricate situation, as further non-trivial extensions of the QCD and weak Lagrangian operator bases were required. After deriving the consistent bases also at NLO, we turned towards the computation of the one-loop amplitudes for $K^\pm \to \pi^\pm a$. One of the main purposes of deriving these NLO expressions is to assign a theoretical uncertainty to the amplitudes and branching ratios. While we found that the part of the amplitude proportional to the low-energy flavor-violating ALP couplings depends only on one QCD low-energy constant with minor uncertainty, the part of the amplitudes proportional to the flavor-conserving ALP couplings involves not only known QCD low-energy constants but also 17 additional, independent, and currently unknown parameters, resulting in a significant theoretical uncertainty. Estimating these coefficients by setting them to zero at the scale $\mu_0 \sim \mu_\chi$, we found corrections to the LO amplitudes between a few and ± 60 percent. Another core result of this chapter was the translation of the amplitude to the NLO lower bounds on the effective scales of the ALP coupling $\Lambda_{c_i}^{\text{eff}} = f/|c_i|$ for two ALP mass values, $m_a = 0$ and $m_a = 200$ GeV. This was done both at the scale μ_χ, and, employing the solutions of the RG evolution equations for the ALP couplings, also at the high scale Λ. Once more, the result depends on the choice of the new, so far unconstrained parameters, g_8^θ and g_8'. This showcases the extreme importance to determine the values of these constants in order to make meaningful statements about the bounds. Lastly, we translated our results onto bounds on the ALP couplings to nucleons. This result is particularly significant as it provides the first particle-physics probe of the effective ALP-nucleon interaction in this mass range.

In the last section of this thesis, we climbed the energy scales back up and even further, until the Planck scale at $\mathcal{O}(10^{19}\,\text{GeV})$. From this highest summit, we reviewed the metastability of the electroweak vacuum, which, while having a lifetime larger than the age of the Universe, resides in a long-lived yet temporary state, such that in principle, a global phase transition is possible at any given time. We found that the ALP plays a significant role in this setup, as its couplings to the SM particles modify the β-function of the quartic Higgs coupling λ in two distinct ways: First, a direct contribution from the ALP-W-boson coupling C_{WW} and second, higher loop contributions, mostly from modifications of the β-functions of the top-quark Yukawa coupling and the SM gauge couplings. All in all, we found that the couplings C_{GG} and C_{WW} have a stabilizing effect on the electroweak vacuum by shifting the instability scale towards higher energies, while C_u has a (mostly) destabilizing effect. C_{BB}, C_e and C_d do not have a significant effect on the scale evolution of λ. We then proceeded by scanning over various combinations of ALP–SM couplings and ALP masses in order to deduce stable or unstable regions. We also saw that the modifications of the SM β-functions by the presence of the ALP in principle allow for a unification around 10^{15} GeV. In the approach chosen in this thesis, a focus was given on model agnostic ALPs. Therefore, in concrete models, threshold corrections and additional modifications to the scale evolution of λ can arise, which would yield additional mod-

ifications of the scale evolution of λ. However, even in this conservative scenario, we saw that significant changes in the Higgs vacuum stability and the gauge couplings can be obtained.

To conclude, this thesis advanced the search for ALPs in several direction by combining complementary approaches and effective field theories across different energy scales. We have seen that these elusive particles could play a key role in resolving several of the most pressing and unresolved questions in the SM. To push the search forward, this work laid the foundation for several important further steps, such as a combined, global fit from both direct and indirect bounds for improved constraints in the ALP–SM couplings or the application of the framework established for the ALP in the chiral perturbation context to scenarios such as $K_L \to \pi^0 a$ or $\pi^- \to e^- \bar{\nu}_e a$. In this context, determining the currently unknown LECs is of critical importance for achieving reliable and predictive theoretical results. Moreover, rigorously assessing the electroweak vacuum instability in the context of specific ALP models could yield valuable insights and presents a promising avenue for future investigation.
All in all, while this thesis has taken us along several remarkable and previously unexplored ALP trails, much remains to be discovered along the ALPine path that lies ahead.

Acronyms

χ_a**PT** ALP Chiral Perturbation Theory

ALP axion-like particle

BSM beyond the Standard Model

CMB cosmic microwave background

χ**PT** Chiral Perturbation Theory

CKM Cabibbo–Kobayashi–Maskawa

CMS Compact Muon Solenoid

DFSZ Dine-Fischler-Srednicki-Zhitnitsky

EDM electric dipole moment

EFT effective field theory

FCNC Flavor-Changing Neutral Current

GUT Grand Unified Theory

KSVZ Kim-Shifman-Vainshtein-Zakharov

LEFT Low-Energy Effective Field Theory

LEC low-energy constant

LHC Large Hadron Collider

LL leading-logarithmic

LO leading order

MDM magnetic dipole moment

NLO next-to-leading order

PB purely bosonic

PMNS Pontecorvo–Maki–Nakagawa–Sakata

QCD Quantum Chromodynamics

QED Quantum Electrodynamics

RG renormalization group

SM Standard Model of Particle Physics

SMEFT Standard Model Effective Field Theory

SPS Super Proton Synchrotron

UV ultra-violet

vev vacuum expectation value

List of Figures

List of Tables

Bibliography

[1] ATLAS collaboration, G. Aad et al., *Observation of a new particle in the search for the Standard Model Higgs boson with the ATLAS detector at the LHC*, *Phys. Lett. B* **716** (2012) 1–29, [1207.7214].

[2] CMS collaboration, S. Chatrchyan et al., *Observation of a New Boson at a Mass of 125 GeV with the CMS Experiment at the LHC*, *Phys. Lett. B* **716** (2012) 30–61, [1207.7235].

[3] D. Hanneke, S. Fogwell and G. Gabrielse, *New Measurement of the Electron Magnetic Moment and the Fine Structure Constant*, *Phys. Rev. Lett.* **100** (2008) 120801, [0801.1134].

[4] D. Hanneke, S. F. Hoogerheide and G. Gabrielse, *Cavity Control of a Single-Electron Quantum Cyclotron: Measuring the Electron Magnetic Moment*, *Phys. Rev. A* **83** (2011) 052122, [1009.4831].

[5] Planck collaboration, N. Aghanim et al., *Planck 2018 results. VI. Cosmological parameters*, *Astron. Astrophys.* **641** (2020) A6, [1807.06209].

[6] T. Kajita, *Nobel Lecture: Discovery of atmospheric neutrino oscillations*, *Rev. Mod. Phys.* **88** (2016) 030501.

[7] P. Q. Hung, *Vacuum instability and new constraints on fermion masses*, *Phys. Rev. Lett.* **42** (Apr, 1979) 873–876.

[8] N. Cabibbo, L. Maiani, G. Parisi and R. Petronzio, *Bounds on the Fermions and Higgs Boson Masses in Grand Unified Theories*, *Nucl. Phys. B* **158** (1979) 295–305.

[9] M. Lindner, *Implications of Triviality for the Standard Model*, *Z. Phys. C* **31** (1986) 295.

[10] G. Degrassi, S. Di Vita, J. Elias-Miro, J. R. Espinosa, G. F. Giudice, G. Isidori et al., *Higgs mass and vacuum stability in the Standard Model at NNLO*, *JHEP* **08** (2012) 098, [1205.6497].

[11] D. Buttazzo, G. Degrassi, P. P. Giardino, G. F. Giudice, F. Sala, A. Salvio et al., *Investigating the near-criticality of the Higgs boson*, *JHEP* **12** (2013) 089, [1307.3536].

[12] F. Wilczek, *Time's (Almost) Reversible Arrow*, *Quanta Magazine* (2016) .

[13] B. Gripaios, A. Pomarol, F. Riva and J. Serra, *Beyond the Minimal Composite Higgs Model*, *JHEP* **04** (2009) 070, [0902.1483].

[14] G. Ferretti and D. Karateev, *Fermionic UV completions of Composite Higgs models*, *JHEP* **03** (2014) 077, [1312.5330].

[15] A. E. Nelson and N. Seiberg, *R symmetry breaking versus supersymmetry breaking*, *Nucl. Phys. B* **416** (1994) 46–62, [hep-ph/9309299].

[16] J. Bagger, E. Poppitz and L. Randall, *The R axion from dynamical supersymmetry breaking*, *Nucl. Phys. B* **426** (1994) 3–18, [hep-ph/9405345].

[17] B. Bellazzini, A. Mariotti, D. Redigolo, F. Sala and J. Serra, *R-axion at colliders*, *Phys. Rev. Lett.* **119** (2017) 141804, [1702.02152].

[18] F. Chadha-Day, J. Ellis and D. J. E. Marsh, *Axion dark matter: What is it and why now?*, *Sci. Adv.* **8** (2022) abj3618, [2105.01406].

[19] M. Bauer, M. Neubert, S. Renner, M. Schnubel and A. Thamm, *Axionlike Particles, Lepton-Flavor Violation, and a New Explanation of a_μ and a_e*, *Phys. Rev. Lett.* **124** (2020) 211803, [1908.00008].

[20] D. Cadamuro and J. Redondo, *Cosmological bounds on pseudo Nambu-Goldstone bosons*, *JCAP* **02** (2012) 032, [1110.2895].

[21] M. Millea, L. Knox and B. Fields, *New Bounds for Axions and Axion-Like Particles with keV-GeV Masses*, *Phys. Rev. D* **92** (2015) 023010, [1501.04097].

[22] A. Payez, C. Evoli, T. Fischer, M. Giannotti, A. Mirizzi and A. Ringwald, *Revisiting the SN1987A gamma-ray limit on ultralight axion-like particles*, *JCAP* **02** (2015) 006, [1410.3747].

[23] J. Jaeckel, P. C. Malta and J. Redondo, *Decay photons from the axionlike particles burst of type II supernovae*, *Phys. Rev. D* **98** (2018) 055032, [1702.02964].

[24] K. Mimasu and V. Sanz, *ALPs at Colliders*, *JHEP* **06** (2015) 173, [1409.4792].

[25] J. Jaeckel and M. Spannowsky, *Probing MeV to 90 GeV axion-like particles with LEP and LHC*, *Phys. Lett. B* **753** (2016) 482–487, [1509.00476].

[26] S. Knapen, T. Lin, H. K. Lou and T. Melia, *Searching for Axionlike Particles with Ultraperipheral Heavy-Ion Collisions*, *Phys. Rev. Lett.* **118** (2017) 171801, [1607.06083].

[27] I. Brivio, M. B. Gavela, L. Merlo, K. Mimasu, J. M. No, R. del Rey et al., *ALPs Effective Field Theory and Collider Signatures*, *Eur. Phys. J. C* **77** (2017) 572, [1701.05379].

[28] M. Bauer, M. Neubert and A. Thamm, *Collider Probes of Axion-Like Particles*, *JHEP* **12** (2017) 044, [1708.00443].

[29] M. Bauer, M. Heiles, M. Neubert and A. Thamm, *Axion-Like Particles at Future Colliders*, *Eur. Phys. J. C* **79** (2019) 74, [1808.10323].

[30] B. Batell, M. Pospelov and A. Ritz, *Multi-lepton Signatures of a Hidden Sector in Rare B Decays*, *Phys. Rev. D* **83** (2011) 054005, [0911.4938].

[31] M. Freytsis, Z. Ligeti and J. Thaler, *Constraining the Axion Portal with $B \to K l^+ l^-$*, *Phys. Rev. D* **81** (2010) 034001, [0911.5355].

[32] M. J. Dolan, F. Kahlhoefer, C. McCabe and K. Schmidt-Hoberg, *A taste of dark matter: Flavour constraints on pseudoscalar mediators*, *JHEP* **03** (2015) 171, [1412.5174].

[33] J. Martin Camalich, M. Pospelov, P. N. H. Vuong, R. Ziegler and J. Zupan, *Quark Flavor Phenomenology of the QCD Axion*, *Phys. Rev. D* **102** (2020) 015023, [2002.04623].

[34] M. Bauer, M. Neubert, S. Renner, M. Schnubel and A. Thamm, *Flavor probes of axion-like particles*, *JHEP* **09** (2022) 056, [2110.10698].

[35] A. M. Galda, M. Neubert and S. Renner, *ALP — SMEFT interference*, *JHEP* **06** (2021) 135, [2105.01078].

[36] M. E. Peskin and D. V. Schroeder, *An Introduction to quantum field theory*. Addison-Wesley, Reading, USA, 1995, 10.1201/9780429503559.

[37] M. D. Schwartz, *Quantum Field Theory and the Standard Model*. Cambridge University Press, 3, 2014.

[38] M. Gell-Mann, *The interpretation of the new particles as displaced charge multiplets*, *Nuovo Cim.* **4** (1956) 848–866.

[39] T. Nakano and K. Nishijima, *Charge Independence for V-particles*, *Prog. Theor. Phys.* **10** (1953) 581–582.

[40] Particle Data Group collaboration, R. L. Workman et al., *Review of Particle Physics*, *PTEP* **2022** (2022) 083C01.

[41] R. Penco, *An Introduction to Effective Field Theories*, 2006.16285.

[42] M. Neubert, *Effective field theory and heavy quark physics*, in *Theoretical Advanced Study Institute in Elementary Particle Physics: Physics in $D \geqq 4$*, pp. 149–194, 12, 2005, hep-ph/0512222, DOI.

[43] S. Weinberg, *Baryon and Lepton Nonconserving Processes*, *Phys. Rev. Lett.* **43** (1979) 1566–1570.

[44] B. Henning, X. Lu, T. Melia and H. Murayama, *2, 84, 30, 993, 560, 15456, 11962, 261485, ...: Higher dimension operators in the SM EFT*, *JHEP* **08** (2017) 016, [1512.03433].

[45] C. B. Marinissen, R. Rahn and W. J. Waalewijn, *..., 83106786, 114382724, 1509048322, 2343463290, 27410087742, ... efficient Hilbert series for effective theories*, *Phys. Lett. B* **808** (2020) 135632, [2004.09521].

[46] B. Grzadkowski, M. Iskrzynski, M. Misiak and J. Rosiek, *Dimension-Six Terms in the Standard Model Lagrangian*, *JHEP* **10** (2010) 085, [1008.4884].

[47] G. Gabadadze and M. Shifman, *QCD vacuum and axions: What's happening?*, *Int. J. Mod. Phys. A* **17** (2002) 3689–3728, [hep-ph/0206123].

[48] C. Abel et al., *Measurement of the Permanent Electric Dipole Moment of the Neutron*, *Phys. Rev. Lett.* **124** (2020) 081803, [2001.11966].

[49] H. Georgi and S. L. Glashow, *Unity of All Elementary Particle Forces*, *Phys. Rev. Lett.* **32** (1974) 438–441.

[50] P. Fileviez Perez, *Renormalizable adjoint SU(5)*, *Phys. Lett. B* **654** (2007) 189–193, [hep-ph/0702287].

[51] F. Zwicky, *Die Rotverschiebung von extragalaktischen Nebeln*, *Helvetica Physica Acta* **6** (Jan., 1933) 110–127.

[52] V. C. Rubin and W. K. Ford, Jr., *Rotation of the Andromeda Nebula from a Spectroscopic Survey of Emission Regions*, *Astrophys. J.* **159** (1970) 379–403.

[53] R. D. Peccei and H. R. Quinn, *CP Conservation in the Presence of Instantons*, *Phys. Rev. Lett.* **38** (1977) 1440–1443.

[54] A. Hook, *TASI Lectures on the Strong CP Problem and Axions*, *PoS* **TASI2018** (2019) 004, [1812.02669].

[55] G. Grilli di Cortona, E. Hardy, J. Pardo Vega and G. Villadoro, *The QCD axion, precisely*, *JHEP* **01** (2016) 034, [1511.02867].

[56] M. Bauer, M. Neubert, S. Renner, M. Schnubel and A. Thamm, *Consistent Treatment of Axions in the Weak Chiral Lagrangian*, *Phys. Rev. Lett.* **127** (2021) 081803, [2102.13112].

[57] M. A. Shifman, A. I. Vainshtein and V. I. Zakharov, *Can Confinement Ensure Natural CP Invariance of Strong Interactions?*, *Nucl. Phys. B* **166** (1980) 493–506.

[58] P. Di Vecchia and G. Veneziano, *Chiral dynamics in the large n limit*, *Nuclear Physics B* **171** (1980) 253–272.

[59] H. Georgi, D. B. Kaplan and L. Randall, *Manifesting the Invisible Axion at Low-energies*, *Phys. Lett. B* **169** (1986) 73–78.

[60] M. Bauer, M. Neubert, S. Renner, M. Schnubel and A. Thamm, *The Low-Energy Effective Theory of Axions and ALPs*, *JHEP* **04** (2021) 063, [2012.12272].

[61] M. Chala, G. Guedes, M. Ramos and J. Santiago, *Running in the ALPs*, *Eur. Phys. J. C* **81** (2021) 181, [2012.09017].

[62] J. E. Kim, *Weak Interaction Singlet and Strong CP Invariance*, *Phys. Rev. Lett.* **43** (1979) 103.

[63] M. Shifman, A. Vainshtein and V. Zakharov, *Can confinement ensure natural cp invariance of strong interactions?*, *Nuclear Physics B* **166** (1980) 493–506.

[64] M. Dine, W. Fischler and M. Srednicki, *A Simple Solution to the Strong CP Problem with a Harmless Axion*, *Phys. Lett. B* **104** (1981) 199–202.

[65] A. R. Zhitnitsky, *On Possible Suppression of the Axion Hadron Interactions. (In Russian)*, *Sov. J. Nucl. Phys.* **31** (1980) 260.

[66] F. Arias-Aragón, J. Quevillon and C. Smith, *Axion-like ALPs*, *JHEP* **03** (2023) 134, [2211.04489].

[67] A. Biekötter, J. Fuentes-Martín, A. M. Galda and M. Neubert, *A global analysis of axion-like particle interactions using SMEFT fits*, *JHEP* **09** (2023) 120, [2307.10372].

[68] J. Fuentes-Martín, M. König, J. Pagès, A. E. Thomsen and F. Wilsch, *A Proof of Concept for Matchete: An Automated Tool for Matching Effective Theories*, 2212.04510.

[69] J. Elias-Miro, J. R. Espinosa, E. Masso and A. Pomarol, *Higgs windows to new physics through d=6 operators: constraints and one-loop anomalous dimensions*, *JHEP* **11** (2013) 066, [1308.1879].

[70] E. E. Jenkins, A. V. Manohar and M. Trott, *Renormalization Group Evolution of the Standard Model Dimension Six Operators I: Formalism and lambda Dependence*, *JHEP* **10** (2013) 087, [1308.2627].

[71] E. E. Jenkins, A. V. Manohar and M. Trott, *Renormalization Group Evolution of the Standard Model Dimension Six Operators II: Yukawa Dependence*, *JHEP* **01** (2014) 035, [1310.4838].

[72] R. Alonso, E. E. Jenkins, A. V. Manohar and M. Trott, *Renormalization Group Evolution of the Standard Model Dimension Six Operators III: Gauge Coupling Dependence and Phenomenology*, *JHEP* **04** (2014) 159, [1312.2014].

[73] Anisha, S. Das Bakshi, S. Banerjee, A. Biekötter, J. Chakrabortty, S. Kumar Patra et al., *Effective limits on single scalar extensions in the light of recent LHC data*, *Phys. Rev. D* **107** (2023) 055028, [2111.05876].

[74] J. Ellis, M. Madigan, K. Mimasu, V. Sanz and T. You, *Top, Higgs, Diboson and Electroweak Fit to the Standard Model Effective Field Theory*, *JHEP* **04** (2021) 279, [2012.02779].

[75] A. Falkowski, M. González-Alonso and K. Mimouni, *Compilation of low-energy constraints on 4-fermion operators in the SMEFT*, *JHEP* **08** (2017) 123, [1706.03783].

[76] A. Efrati, A. Falkowski and Y. Soreq, *Electroweak constraints on flavorful effective theories*, *JHEP* **07** (2015) 018, [1503.07872].

[77] CMS collaboration, A. M. Sirunyan et al., *Measurements of production cross sections of the Higgs boson in the four-lepton final state in proton–proton collisions at* $\sqrt{s} = 13$ *TeV*, *Eur. Phys. J. C* **81** (2021) 488, [2103.04956].

[78] A. Mariotti, D. Redigolo, F. Sala and K. Tobioka, *New LHC bound on low-mass diphoton resonances*, *Phys. Lett. B* **783** (2018) 13–18, [1710.01743].

[79] J. Bonilla, I. Brivio, J. Machado-Rodríguez and J. F. de Trocóniz, *Nonresonant searches for axion-like particles in vector boson scattering processes at the LHC*, *JHEP* **06** (2022) 113, [2202.03450].

[80] G. Alonso-Álvarez, M. B. Gavela and P. Quilez, *Axion couplings to electroweak gauge bosons*, *Eur. Phys. J. C* **79** (2019) 223, [1811.05466].

[81] CMS collaboration, A. Tumasyan et al., *Search for heavy resonances decaying to ZZ or ZW and axion-like particles mediating nonresonant ZZ or ZH production at* $\sqrt{s}$ *= 13 TeV*, *JHEP* **04** (2022) 087, [2111.13669].

[82] M. B. Gavela, J. M. No, V. Sanz and J. F. de Trocóniz, *Nonresonant Searches for Axionlike Particles at the LHC*, *Phys. Rev. Lett.* **124** (2020) 051802, [1905.12953].

[83] F. Esser, M. Madigan, V. Sanz and M. Ubiali, *On the coupling of axion-like particles to the top quark*, *JHEP* **09** (2023) 063, [2303.17634].

[84] G. Lucente and P. Carenza, *Supernova bound on axionlike particles coupled with electrons*, *Phys. Rev. D* **104** (2021) 103007, [2107.12393].

[85] R. Essig, R. Harnik, J. Kaplan and N. Toro, *Discovering New Light States at Neutrino Experiments*, *Phys. Rev. D* **82** (2010) 113008, [1008.0636].

[86] BaBar collaboration, J. P. Lees et al., *Search for a Dark Photon in* e^+e^- *Collisions at BaBar*, *Phys. Rev. Lett.* **113** (2014) 201801, [1406.2980].

[87] A. Biekötter, M. Chala and M. Spannowsky, *New Higgs decays to axion-like particles*, *Phys. Lett. B* **834** (2022) 137465, [2203.14984].

[88] L. Allwicher, P. Arnan, D. Barducci and M. Nardecchia, *Perturbative unitarity constraints on generic Yukawa interactions*, *JHEP* **10** (2021) 129, [2108.00013].

[89] ATLAS, CMS collaboration, G. Aad et al., *Measurements of the Higgs boson production and decay rates and constraints on its couplings from a combined ATLAS and CMS analysis of the LHC pp collision data at* $\sqrt{s} = 7$ *and 8 TeV*, *JHEP* **08** (2016) 045, [1606.02266].

[90] ATLAS collaboration, G. Aad et al., *Measurements of the Higgs boson production and decay rates and coupling strengths using pp collision data at* $\sqrt{s} = 7$ *and 8 TeV in the ATLAS experiment*, *Eur. Phys. J.* **C76** (2016) 6, [1507.04548].

[91] ATLAS collaboration, G. Aad et al., *A search for the* $Z\gamma$ *decay mode of the Higgs boson in pp collisions at* $\sqrt{s}$ *= 13 TeV with the ATLAS detector*, 2005.05382.

[92] ATLAS collaboration, G. Aad et al., *A search for the dimuon decay of the Standard Model Higgs boson with the ATLAS detector*, *Phys. Lett. B* **812** (2021) 135980, [2007.07830].

[93] ATLAS Collaboration collaboration, *Measurements of Higgs boson production cross-sections in the $H \to \tau^+\tau^-$ decay channel in pp collisions at $\sqrt{s} = 13$ TeV with the ATLAS detector*, tech. rep., CERN, Geneva, Aug, 2021.

[94] ATLAS collaboration, G. Aad et al., *Measurements of Higgs bosons decaying to bottom quarks from vector boson fusion production with the ATLAS experiment at $\sqrt{s} = 13$ TeV*, *Eur. Phys. J. C* **81** (2021) 537, [2011.08280].

[95] ATLAS collaboration, *Measurement of the Higgs boson decaying to b-quarks produced in association with a top-quark pair in pp collisions at $\sqrt{s} = 13$ TeV with the ATLAS detector*, *ATLAS-CONF-2020-058* (11, 2020) .

[96] ATLAS collaboration, *Interpretations of the combined measurement of Higgs boson production and decay*, *ATLAS-CONF-2020-053* (10, 2020) .

[97] ATLAS collaboration, *Measurements of gluon fusion and vector-boson-fusion production of the Higgs boson in $H \to WW^* \to e\nu\mu\nu$ decays using pp collisions at $\sqrt{s} = 13$ TeV with the ATLAS detector*, *ATLAS-CONF-2021-014* (3, 2021) .

[98] ATLAS collaboration, G. Aad et al., *Differential cross-section measurements for the electroweak production of dijets in association with a Z boson in proton–proton collisions at ATLAS*, *Eur. Phys. J. C* **81** (2021) 163, [2006.15458].

[99] CMS collaboration, A. M. Sirunyan et al., *Measurement of the inclusive and differential Higgs boson production cross sections in the leptonic WW decay mode at $\sqrt{s} = 13$ TeV*, *JHEP* **03** (2021) 003, [2007.01984].

[100] CMS collaboration, A. M. Sirunyan et al., *Evidence for Higgs boson decay to a pair of muons*, *JHEP* **01** (2021) 148, [2009.04363].

[101] CMS collaboration, A. M. Sirunyan et al., *Measurement of the Higgs boson production rate in association with top quarks in final states with electrons, muons, and hadronically decaying tau leptons at $\sqrt{s} = 13$ TeV*, *Eur. Phys. J. C* **81** (2021) 378, [2011.03652].

[102] CMS collaboration, *Measurement of Higgs boson production in association with a W or Z boson in the $H \to$ WW decay channel*, *CMS-PAS-HIG-19-017* (2021) .

[103] CMS collaboration, *Measurement of Higgs boson production in the decay channel with a pair of τ leptons*, *CMS-PAS-HIG-19-010* (2020) .

[104] CMS collaboration, A. M. Sirunyan et al., *Measurements of Higgs boson production cross sections and couplings in the diphoton decay channel at $\sqrt{s} = 13$ TeV*, *JHEP* **07** (2021) 027, [2103.06956].

[105] CMS collaboration, *Combined Higgs boson production and decay measurements with up to 137 fb-1 of proton-proton collision data at sqrts = 13 TeV*, *CMS-PAS-HIG-19-005* (2020) .

[106] N. Berger et al., *Simplified Template Cross Sections - Stage 1.1*, 1906.02754.

[107] CDF, D0 collaboration, T. A. Aaltonen et al., *Combined Forward-Backward Asymmetry Measurements in Top-Antitop Quark Production at the Tevatron*, *Phys. Rev. Lett.* **120** (2018) 042001, [1709.04894].

[108] ATLAS, CMS collaboration, M. Aaboud et al., *Combination of inclusive and differential* $\mathrm{t\bar{t}}$ *charge asymmetry measurements using ATLAS and CMS data at* $\sqrt{s} = 7$ *and 8 TeV*, *JHEP* **04** (2018) 033, [1709.05327].

[109] CMS, ATLAS collaboration, G. Aad et al., *Combination of the W boson polarization measurements in top quark decays using ATLAS and CMS data at* $\sqrt{s} = 8$ *TeV*, *JHEP* **08** (2020) 051, [2005.03799].

[110] ATLAS collaboration, G. Aad et al., *Measurements of the charge asymmetry in top-quark pair production in the dilepton final state at* $\sqrt{s} = 8$ *TeV with the ATLAS detector*, *Phys. Rev. D* **94** (2016) 032006, [1604.05538].

[111] ATLAS collaboration, G. Aad et al., *Measurement of the* $t\bar{t}W$ *and* $t\bar{t}Z$ *production cross sections in pp collisions at* $\sqrt{s} = 8$ *TeV with the ATLAS detector*, *JHEP* **11** (2015) 172, [1509.05276].

[112] ATLAS collaboration, M. Aaboud et al., *Fiducial, total and differential cross-section measurements of t-channel single top-quark production in pp collisions at 8 TeV using data collected by the ATLAS detector*, *Eur. Phys. J. C* **77** (2017) 531, [1702.02859].

[113] ATLAS collaboration, G. Aad et al., *Measurement of single top-quark production in association with a W boson in the single-lepton channel at* $\sqrt{s} = 8$ *TeV with the ATLAS detector*, *Eur. Phys. J. C* **81** (2021) 720, [2007.01554].

[114] ATLAS collaboration, G. Aad et al., *Measurement of the production cross-section of a single top quark in association with a W boson at 8 TeV with the ATLAS experiment*, *JHEP* **01** (2016) 064, [1510.03752].

[115] ATLAS collaboration, G. Aad et al., *Evidence for single top-quark production in the s-channel in proton-proton collisions at* $\sqrt{s}$ *=8 TeV with the ATLAS detector using the Matrix Element Method*, *Phys. Lett. B* **756** (2016) 228–246, [1511.05980].

[116] ATLAS collaboration, M. Aaboud et al., *Measurement of top quark pair differential cross-sections in the dilepton channel in pp collisions at* $\sqrt{s} = 7$ *and 8 TeV with ATLAS*, *Phys. Rev. D* **94** (2016) 092003, [1607.07281].

[117] ATLAS collaboration, G. Aad et al., *Measurements of top-quark pair differential cross-sections in the lepton+jets channel in pp collisions at* $\sqrt{s} = 8$ *TeV using the ATLAS detector*, *Eur. Phys. J. C* **76** (2016) 538, [1511.04716].

[118] CMS collaboration, V. Khachatryan et al., *Observation of top quark pairs produced in association with a vector boson in pp collisions at $\sqrt{s} = 8$ TeV*, *JHEP* **01** (2016) 096, [1510.01131].

[119] CMS collaboration, V. Khachatryan et al., *Measurements of $t\bar{t}$ charge asymmetry using dilepton final states in pp collisions at $\sqrt{s} = 8$ TeV*, *Phys. Lett. B* **760** (2016) 365–386, [1603.06221].

[120] CMS collaboration, A. M. Sirunyan et al., *Measurement of the semileptonic $\mathrm{t\bar{t}}$ + γ production cross section in pp collisions at $\sqrt{s} = 8$ TeV*, *JHEP* **10** (2017) 006, [1706.08128].

[121] CMS collaboration, V. Khachatryan et al., *Search for s channel single top quark production in pp collisions at $\sqrt{s} = 7$ and 8 TeV*, *JHEP* **09** (2016) 027, [1603.02555].

[122] CMS collaboration, *Single top t-channel differential cross section at 8 TeV*, .

[123] CMS collaboration, V. Khachatryan et al., *Measurement of the t-channel single-top-quark production cross section and of the $| V_{tb} |$ CKM matrix element in pp collisions at $\sqrt{s}$= 8 TeV*, *JHEP* **06** (2014) 090, [1403.7366].

[124] CMS collaboration, S. Chatrchyan et al., *Observation of the associated production of a single top quark and a W boson in pp collisions at $\sqrt{s}$ =8 TeV*, *Phys. Rev. Lett.* **112** (2014) 231802, [1401.2942].

[125] CMS collaboration, A. M. Sirunyan et al., *Measurement of double-differential cross sections for top quark pair production in pp collisions at $\sqrt{s} = 8$ TeV and impact on parton distribution functions*, *Eur. Phys. J. C* **77** (2017) 459, [1703.01630].

[126] CMS collaboration, S. Chatrchyan et al., *Measurement of the $t\bar{t}$ production cross section in the dilepton channel in pp collisions at $\sqrt{s}$ = 8 TeV*, *JHEP* **02** (2014) 024, [1312.7582].

[127] CMS collaboration, V. Khachatryan et al., *Measurement of the differential cross section for top quark pair production in pp collisions at $\sqrt{s} = 8$ TeV*, *Eur. Phys. J. C* **75** (2015) 542, [1505.04480].

[128] CMS collaboration, V. Khachatryan et al., *Measurements of the $\mathrm{t\bar{t}}$ production cross section in lepton+jets final states in pp collisions at 8 TeV and ratio of 8 to 7 TeV cross sections*, *Eur. Phys. J. C* **77** (2017) 15, [1602.09024].

[129] ATLAS collaboration, M. Aaboud et al., *Measurement of the cross-section for producing a W boson in association with a single top quark in pp collisions at $\sqrt{s} = 13$ TeV with ATLAS*, *JHEP* **01** (2018) 063, [1612.07231].

[130] ATLAS collaboration, M. Aaboud et al., *Measurement of the production cross-section of a single top quark in association with a Z boson in proton–proton collisions at 13 TeV with the ATLAS detector*, *Phys. Lett. B* **780** (2018) 557–577, [1710.03659].

[131] ATLAS collaboration, M. Aaboud et al., *Measurement of the inclusive cross-sections of single top-quark and top-antiquark t-channel production in pp collisions at $\sqrt{s}$ = 13 TeV with the ATLAS detector*, *JHEP* **04** (2017) 086, [1609.03920].

[132] ATLAS collaboration, *Inclusive and differential measurement of the charge asymmetry in $t\bar{t}$ events at 13 TeV with the ATLAS detector*, .

[133] ATLAS collaboration, M. Aaboud et al., *Measurement of the $t\bar{t}Z$ and $t\bar{t}W$ cross sections in proton-proton collisions at $\sqrt{s} = 13$ TeV with the ATLAS detector*, *Phys. Rev. D* **99** (2019) 072009, [1901.03584].

[134] ATLAS collaboration, G. Aad et al., *Measurements of inclusive and differential cross-sections of combined $t\bar{t}\gamma$ and $tW\gamma$ production in the $e\mu$ channel at 13 TeV with the ATLAS detector*, *JHEP* **09** (2020) 049, [2007.06946].

[135] CMS collaboration, A. M. Sirunyan et al., *Measurement of the production cross section for single top quarks in association with W bosons in proton-proton collisions at $\sqrt{s} = 13$ TeV*, *JHEP* **10** (2018) 117, [1805.07399].

[136] CMS collaboration, A. M. Sirunyan et al., *Observation of Single Top Quark Production in Association with a Z Boson in Proton-Proton Collisions at $\sqrt{s}$ =13 TeV*, *Phys. Rev. Lett.* **122** (2019) 132003, [1812.05900].

[137] CMS collaboration, A. M. Sirunyan et al., *Measurement of differential cross sections and charge ratios for t-channel single top quark production in proton–proton collisions at $\sqrt{s} = 13$ TeV*, *Eur. Phys. J. C* **80** (2020) 370, [1907.08330].

[138] CMS collaboration, A. M. Sirunyan et al., *Measurement of the $\mathrm{t\bar{t}}$ production cross section, the top quark mass, and the strong coupling constant using dilepton events in pp collisions at $\sqrt{s} = 13$ TeV*, *Eur. Phys. J. C* **79** (2019) 368, [1812.10505].

[139] CMS collaboration, *Measurement of differential $\mathrm{t\bar{t}}$ production cross sections in the full kinematic range using lepton+jets events from pp collisions at $\sqrt{s} = 13$ TeV*, .

[140] CMS collaboration, A. M. Sirunyan et al., *Measurement of the cross section for top quark pair production in association with a W or Z boson in proton-proton collisions at $\sqrt{s} = 13$ TeV*, *JHEP* **08** (2018) 011, [1711.02547].

[141] CMS collaboration, A. M. Sirunyan et al., *Measurement of top quark pair production in association with a Z boson in proton-proton collisions at $\sqrt{s} =$ 13 TeV*, *JHEP* **03** (2020) 056, [1907.11270].

[142] A. M. Galda and M. Neubert, *ALP-LEFT Interference and the Muon $(g-2)$*, *JHEP* **11** (2023) 015, [2308.01338].

[143] E. E. Jenkins, A. V. Manohar and P. Stoffer, *Low-Energy Effective Field Theory below the Electroweak Scale: Operators and Matching*, *JHEP* **03** (2018) 016, [1709.04486].

[144] E. E. Jenkins, A. V. Manohar and P. Stoffer, *Low-Energy Effective Field Theory below the Electroweak Scale: Anomalous Dimensions*, *JHEP* **01** (2018) 084, [1711.05270].

[145] R. Aliberti et al., *The anomalous magnetic moment of the muon in the Standard Model: an update*, 2505.21476.

[146] J. Aebischer, W. Dekens, E. E. Jenkins, A. V. Manohar, D. Sengupta and P. Stoffer, *Effective field theory interpretation of lepton magnetic and electric dipole moments*, *JHEP* **07** (2021) 107, [2102.08954].

[147] T. Aoyama et al., *The anomalous magnetic moment of the muon in the Standard Model*, *Phys. Rept.* **887** (2020) 1–166, [2006.04822].

[148] S. M. Barr and A. Zee, *Electric Dipole Moment of the Electron and of the Neutron*, *Phys. Rev. Lett.* **65** (1990) 21–24.

[149] M. A. Buen-Abad, J. Fan, M. Reece and C. Sun, *Challenges for an axion explanation of the muon $g-2$ measurement*, *JHEP* **09** (2021) 101, [2104.03267].

[150] W. J. Marciano, A. Masiero, P. Paradisi and M. Passera, *Contributions of axionlike particles to lepton dipole moments*, *Phys. Rev. D* **94** (2016) 115033, [1607.01022].

[151] NA62 collaboration, E. Cortina Gil et al., *Observation of the $K^+ \to \pi^+ \nu\overline{\nu}$ decay and measurement of its branching ratio*, *JHEP* **02** (2025) 191, [2412.12015].

[152] D. J. Gross and F. Wilczek, *Ultraviolet Behavior of Nonabelian Gauge Theories*, *Phys. Rev. Lett.* **30** (1973) 1343–1346.

[153] H. D. Politzer, *Reliable Perturbative Results for Strong Interactions?*, *Phys. Rev. Lett.* **30** (1973) 1346–1349.

[154] S. Scherer, *Introduction to chiral perturbation theory*, *Adv. Nucl. Phys.* **27** (2003) 277, [hep-ph/0210398].

[155] C. Cornella, A. M. Galda, M. Neubert and D. Wyler, *$K^\pm \to \pi^\pm a$ at next-to-leading order in chiral perturbation theory and updated bounds on ALP couplings*, *JHEP* **06** (2024) 029, [2308.16903].

[156] C. Vafa and E. Witten, *Restrictions on Symmetry Breaking in Vector-Like Gauge Theories*, *Nucl. Phys. B* **234** (1984) 173–188.

[157] S. Coleman, *The Invariance of the Vacuum is the Invariance of the World*, *J. Math. Phys.* **7** (1966) 787.

[158] J. Goldstone, *Field Theories with Superconductor Solutions*, *Nuovo Cim.* **19** (1961) 154–164.

[159] J. Goldstone, A. Salam and S. Weinberg, *Broken Symmetries*, *Phys. Rev.* **127** (1962) 965–970.

[160] Flavour Lattice Averaging Group (FLAG) collaboration, Y. Aoki et al., *FLAG Review 2021*, *Eur. Phys. J. C* **82** (2022) 869, [2111.09849].

[161] J. Gasser and H. Leutwyler, *Chiral Perturbation Theory: Expansions in the Mass of the Strange Quark*, *Nucl. Phys. B* **250** (1985) 465–516.

[162] F. J. Gilman and M. B. Wise, *Effective Hamiltonian for Delta s = 1 Weak Nonleptonic Decays in the Six Quark Model*, *Phys. Rev. D* **20** (1979) 2392.

[163] J. A. Cronin, *Phenomenological model of strong and weak interactions in chiral U(3) x U(3)*, *Phys. Rev.* **161** (1967) 1483–1494.

[164] C. W. Bernard, T. Draper, A. Soni, H. D. Politzer and M. B. Wise, *Application of Chiral Perturbation Theory to K —> 2 pi Decays*, *Phys. Rev. D* **32** (1985) 2343–2347.

[165] M. Neubert and B. Stech, *A Consistent analysis of the Delta I = 1/2 rule in strange particle decays*, *Phys. Rev. D* **44** (1991) 775–793.

[166] V. Cirigliano, G. Ecker, H. Neufeld, A. Pich and J. Portolés, *Kaon decays in the standard model*, *Rev. Mod. Phys.* **84** (Mar, 2012) 399–447.

[167] R. J. Crewther, *Chiral Reduction of $K \to 2\pi$ Amplitudes*, *Nucl. Phys. B* **264** (1986) 277–291.

[168] J. Bijnens and G. Ecker, *Mesonic low-energy constants*, *Ann. Rev. Nucl. Part. Sci.* **64** (2014) 149–174, [1405.6488].

[169] R. J. Dowdall, C. T. H. Davies, G. P. Lepage and C. McNeile, *Vus from pi and K decay constants in full lattice QCD with physical u, d, s and c quarks*, *Phys. Rev. D* **88** (2013) 074504, [1303.1670].

[170] V. Cirigliano, G. Ecker, H. Neufeld and A. Pich, *Meson resonances, large N(c) and chiral symmetry*, *JHEP* **06** (2003) 012, [hep-ph/0305311].

[171] G. Ecker, J. Kambor and D. Wyler, *Resonances in the weak chiral Lagrangian*, *Nucl. Phys. B* **394** (1993) 101–138.

[172] J. Bijnens and F. Borg, *Isospin breaking in K —> 3 pi decays III: Bremsstrahlung and fit to experiment*, *Eur. Phys. J. C* **40** (2005) 383–394, [hep-ph/0501163].

[173] J. Bijnens, P. Dhonte and F. Borg, *K —> 3 pi decays in chiral perturbation theory*, *Nucl. Phys. B* **648** (2003) 317–344, [hep-ph/0205341].

[174] J. Kambor, J. H. Missimer and D. Wyler, *K —> 2 pi and K —> 3 pi decays in next-to-leading order chiral perturbation theory*, *Phys. Lett. B* **261** (1991) 496–503.

[175] A. Bilal, *Lectures on Anomalies*, *LPTENS-08-05* (2008) , [0802.0634].

[176] P. Herrera-Siklody, J. I. Latorre, P. Pascual and J. Taron, *Chiral effective Lagrangian in the large N(c) limit: The Nonet case*, *Nucl. Phys. B* **497** (1997) 345–386, [hep-ph/9610549].

[177] J. Kambor, J. H. Missimer and D. Wyler, *The Chiral Loop Expansion of the Nonleptonic Weak Interactions of Mesons*, *Nucl. Phys. B* **346** (1990) 17–64.

[178] NA62 collaboration, E. Cortina Gil et al., *Measurement of the very rare $K^+ \to \pi^+ \nu\bar{\nu}$ decay*, *JHEP* **06** (2021) 093, [2103.15389].

[179] NA62 collaboration, E. Cortina Gil et al., *Searches for hidden sectors using $K^+ \to \pi^+ X$ decays*, 2507.17286.

[180] M. Gorghetto, E. Hardy and G. Villadoro, *More axions from strings*, *SciPost Phys.* **10** (2021) 050, [2007.04990].

[181] C. O'Hare, "cajohare/axionlimits: Axionlimits." https://cajohare.github.io/AxionLimits/, July, 2020. 10.5281/zenodo.3932430.

[182] Particle Data Group collaboration, P. A. Zyla et al., *Review of Particle Physics*, *Progress of Theoretical and Experimental Physics* **2020** (08, 2020) 083C01.

[183] A. M. Galda and M. Neubert, *Saving or Destroying the Universe with Axion-Like Particles*, 2506.06426.

[184] A. Celis, J. Fuentes-Martin, A. Vicente and J. Virto, *DsixTools: The Standard Model Effective Field Theory Toolkit*, *Eur. Phys. J. C* **77** (2017) 405, [1704.04504].

[185] J. Fuentes-Martin, P. Ruiz-Femenia, A. Vicente and J. Virto, *DsixTools 2.0: The Effective Field Theory Toolkit*, *Eur. Phys. J. C* **81** (2021) 167, [2010.16341].

Chapter 7: Curriculum Vitae

Removed for privacy reasons.

Removed for privacy reasons.

Removed for privacy reasons.

Acknowledgments

Removed for privacy reasons.